Drought Characterization, Propagation, and Risk over Indian Region

Submitted in partial fulfilment of the requirements

for the award of the degree of

Doctor of Philosophy

by

Subhadarsini Das

Roll No. 718003

Supervisor

Prof. N. V. Umamahesh

DEPARTMENT OF CIVIL ENGINEERING

NATIONAL INSTITUTE OF TECHNOLOGY

WARANGAL - 506004 (T.S.) INDIA

JULY 2022

Drought Characterization, Propagation, and Risk over Indian Region

Submitted in partial fulfilment of the requirements

for the award of the degree of

Doctor of Philosophy

by

Subhadarsini Das

(Roll No: 718003)

Supervisor

Prof. N. V. Umamahesh

DEPARTMENT OF CIVIL ENGINEERING

NATIONAL INSTITUTE OF TECHNOLOGY

WARANGAL- 506004 (T.S.) INDIA

JULY 2022

NATIONAL INSTITUTE OF TECHNOLOGY

WARANGAL

CERTIFICATE

This is to certify that the thesis entitled **"Drought Characterization, Propagation, and Risk over Indian Region"** being submitted by **Ms. Subhadarsini Das** for the award of the degree of **Doctor of Philosophy** to the Faculty of Engineering and Technology of **National Institute of Technology Warangal** is a record of bonafide research work carried out by her under my supervision and it has not been submitted elsewhere for award of any degree.

Dr. N. V. Umamahesh
Thesis Supervisor
Professor
Department of Civil Engineering
National Institute of Technology
Warangal (T.S.) INDIA

Declaration

This is to certify that the work presented in the thesis entitled **"Drought Characterization, Propagation, and Risk over Indian Region"** is a bonafide work done by me under the supervision of **Prof. N. V. Umamahesh** and was not submitted elsewhere for the award of any degree.

I declare that this written submission represents my ideas in my own words and where others' ideas or words have been included, I have adequately cited and referenced the original sources. I also declare that I have adhered to all principles of academic honesty and integrity and have not misrepresented or fabricated or falsified any idea / data / fact / source in my submission. I understand that any violation of the above will be a cause for disciplinary action by the Institute and can also evoke penal action from the sources which have thus not been properly cited or from whom proper permission has not been taken when needed.

_____

(Name of the Student: **Subhadarsini Das**)

(Roll No. **718003**)

Date: _____

Abstract

According to the fourth assessment report of the Intergovernmental Panel on Climate Change (IPCC), a drought can be defined as a ‘deficiency of rainfall causing water shortage’ or ‘prolonged period of abnormally dry weather with scanty rainfall to cause a serious hydrological imbalance’. However, detection and quantification of drought events are complex as no universal definition of drought exists. In addition, the evolution of a type of drought to another type (e.g., meteorological to hydrological, hydrological to agricultural, agricultural to socio-economic drought) is not adequately understood. Furthermore, because of the effects of climatic variability and anthropogenic perturbations, it is postulated that the frequency of the drought hazard will be increased in the coming decades. At least once every three years, India is negatively impacted by drought conditions and is considered among the most vulnerable and drought-prone countries in the world. Hence, it is well understood that drought is likely to affect the overall economy of the country under the climate-sensitive economic sectors in India. For instance, it was reported that widespread drought is likely to impact the Indian economy by $100 billion.

This thesis delas with developing non-stationary drought indices, understanding the propagation from one drought to another drought, analysis the agricultural drought risk, identifying the future drought hotspot regions, and developing the seasonal Severity-Area-Frequency (SAF) relationship curve encompassing the uncertainty associate with Global Circulation/Climate Models (GCMs) and scenarios.

Initial part of the thesis is devoted to analyze the significance of the external factors in developing drought index. Therefore, to develop a new direction of drought identification and examine the drought properties, the non-stationary meteorological drought indices incorporating the large-scale climatic oscillations are carried out over Maharashtra. Two different drought indices, namely precipitation-based Standardized Precipitation Index (SPI) and precipitation and potential evapotranspiration (PET) based Reconnaissance Drought Index (RDI), are considered for the analysis. Large-scale climatic oscillations like Indian Summer Monsoon Index (ISMI), Southern Oscillation Index (SOI), Sea Surface Temperature

(SST), and Indian Ocean Dipole (IOD) are used as covariates. In the present study, to verify the best lag (between 0 and 12) and best large-scale climate oscillations at each grid point, we have used the Kendall correlation test at a significance level of 5%. The study is conducted for different time scales of drought events such as 3-, 6-, 9-, 12-, 24- month time scales. The non-stationary analysis is performed by varying the location parameter of the gamma and lognormal distributions of SPI and RDI drought indices, respectively. The outcomes from the analysis indicate that non-stationary modelling outperforms the stationary approach over the study area for different drought scales. In addition, notable differences are observed while comparing the different drought properties using stationary and non-stationary drought indices in the case of 3-, 6-, and 9- month time scales. ISMI is likely to influence the drought at smaller scale. However, IOD, SST, and SOI are expected to modulate the larger-scale drought events. A comparative study with respect to the historical drought assessment reveals that the presence of non-stationarity cannot be ignored for developing sustainable mitigation and adaptation strategy.

In the second part, drought properties of meteorological, hydrological and agricultural drought events are evaluated across India under non-stationary approach. Here, Standardized Precipitation Evapotranspiration Index (SPEI), Standardized Runoff Index (SRI), and Standardized Soil moisture Index (SSI) are used to characterize the meteorological, hydrological, and agricultural drought, respectively. The study is performed over 1170 grid points at a grid resolution of 0.5^{o} Lat x 0.5^{o} Lon over India. The runoff datasets are obtained from five different sources (ECMWF Reanalysis 5th Generation (ERA5), Famine Early Warning Systems Network Land Data Assimilation System (FLDAS), Global Land Data Assimilation System (GLDAS), Modern-Era Retrospective analysis for Research and Applications version 2 (MERRA-2), and National Centers for Environmental Prediction (NCEP)). Similarly, the soil moisture datasets are obtained from six diverse sources (Climate Prediction Center (CPC), ERA5, FLDAS, GLDAS, MERRA-2, and NCEP). In addition to meteorological, hydrological and agricultural droughts, socio-economic drought events are also computed. However, the socio-economic drought is evaluated based on the stationary approach. It is found from the analysis that the non-stationary model outperforms the stationary analysis for meteorological, hydrological and agricultural drought indices. The meteorological drought properties (drought events and duration) are more severe as compared

to the hydrological drought. The large duration and more severe hydrological droughts are observed mostly over southern and northern parts of India. The high agricultural drought duration and severity are observed over the northern parts and some patches of northeast and northwest regions of India. The high value of socio-economic drought severity is noticed over Punjab and Haryana.

Despite large spatio-temporal variability in droughts, the propagation time from one drought to another drought is not examined at local scale with the inclusion of external covariates over India. Third part of the thesis deals with examining the propagation time from meteorological to hydrological and from meteorological to agricultural drought. The drought propagation time is computed based on differences between the initiation to initiation (Δs), peak to peak (Δp) and termination to termination (Δe). In addition, the internal propagation of drought is estimated with the help of the variable motion relationship of speed-time process. The outcomes from meteorological to hydrological drought propagation show that the propagation time in case of Δs varies between 4 and 9 months with 62% of total area falling under 6 to 7 months followed by 20% of the total area under 7 to 8 months. In the case of Δp, the time of propagation varies from 9 to 12 months over 74% of the total area. About 70% of the total area, the time of propagation in Δe ranges from 15 to 20 months. The drought development and recovery duration are computed as 3.1 to 6 months over most of the areas. The internal propagation of hydrological drought ranges between the magnitude of 0.4 and 0.6 per month over most of the area in India. Similarly, the findings from meteorological to agricultural drought propagation indicate that the time to propagation in the case of Δs is found to be 5 to 6 months and 6 to 7 months over 39% and 53% of the total area, respectively. Similarly, the drought propagation over about 95% of the total area ranges from 9 to 15 months under Δp condition. The time to propagation varies between 10 to 15 months over 32% and 15 to 20 months over 65% of the total area in the case of Δe. The DDP range from 3.1 to 6 months is observed over about 65% of the total area. Similarly, the range between 3.1 to 6 months is evaluated over 84% of the total area in the case of DRP. The regions with high DDP are having high DRP across India.

In an agrarian country, the impact of hydro-meteorological variability has significant influence on agricultural productivity. In this study, the agricultural drought risk in terms of

the conditional probability of crop loss with respect to different drought severities is analysed. Different drought indices namely SPEI, SSI, Vegetation Condition Index (VCI) and Temperature Condition Index (TCI) are used to evaluate the conditional probability. The bivariate analysis using the copula theory is performed to understand the dependency structure between drought conditions and crop yield anomalies (cotton, groundnut, rice, and wheat) over the Maharashtra during 1998-2015. A total of five different copulas namely, Gaussian, Student's t-copula, Clayton, Gumbel, and Frank are used to analyse the bivariate joint dependence structure between yield anomalies and dominant drought indicator (SPEI, SSI, VCI, or TCI). From the analysis, it is observed that the agricultural productivity is significantly affected by the meteorological drought (SPEI). Under moderate drought conditions, Ahmednagar is found to be the most affected district due to the high probability of agricultural drought risk for cotton, groundnut, and wheat crops. With the increase in the drought severity, the conditional probability of agricultural drought risk is likely to increase. In addition, it is observed that the exclusion of non-stationarity will underestimate the agricultural risk, which will significantly affect the planning and management of agricultural sustainability over the study area.

Understanding the adverse consequences of drought events on various sectors, it is necessary to examine the future variability of drought under different climate change scenarios. Therefore, nineteen different GCMs from NEX-GDDP under Representative Concentration Pathway (RCP) 4.5 and 8.5 scenarios are used to characterise the future short (3-month scale) and long (12-month scale) term meteorological drought over Maharashtra. In addition, future meteorological drought hotspot regions are evaluated over the study area based on different drought properties. In order to identify the implications of temperature on drought SPEI drought index is chosen along with SPI index. The significant findings from the analysis point to the fact that with the increase in the monthly mean temperature and precipitation (more in case of RCP8.5 than RCP4.5), Maharashtra is likely to be wetting and warming during the 21st century except for Konkan region as compared to historical. The drought properties like peak and areal spread are expected to increase for both short and long-term drought conditions in most of the regions. The frequency of severe and extreme droughts is likely to increase in the short-term drought condition. Temperature plays an important role in

modulating the meteorological droughts. The number of hotspot regions decreases in long-term drought condition as compared to short-term drought condition.

In the last study, the seasonal SAF relationship curve for meteorological droughts is projected for five different seasons namely pre-monsoon, monsoon, post-monsoon, Kharif and Rabi. The uncertainty associated with GCMs, and scenarios is assessed using possibility theory. The SPEI drought index is used as an indicator of meteorological drought. The significant findings from the present analysis point to the fact that the precipitation magnitude is expected to increase in pre-monsoon, monsoon, and Kharif seasons over most of the areas in Maharashtra. Except for monsoon season, the potential evapotranspiration is projected to increase over 50% of the total area. The extreme drought condition during post-monsoon, pre-monsoon and Rabi seasons shows an increase in the frequency as compared to historical period. The SAF curve reveals that, in most of the cases, the percentage of drought-affected area is expected to increase for high magnitude of severity. In addition, the highest increment in the drought-affected area is observed during the Rabi season in future.

Contents

List of figures

List of tables

Nomenclature

The following list gives the notations used in chapters of the thesis.

μ	Location parameter in distribution
σ	Scale parameter in distribution
ξ	Shape parameter in distribution
Γ	Gamma function
P_k	Precipitation at kth month
PET_k	Potential evapotranspiration of kth month
α_o	ratio of precipitation to PET
$\Delta TVDP_i$	Change in total variability in development period in *i*th interval
$\Delta TVRP_i$	Change in total variability in recovery period in *i*th interval
$\overline{IDS(t_i)}$	Average Instantaneous Development Speed at t_i
$\overline{IRS(t_i)}$	Average Instantaneous Recovery Speed at t_i
T_{max}	Maximum temperature
T_{min}	Minimum temperature
$NDVI_{max}$	Maximum Normalized Difference Vegetation Index
$NDVI_{min}$	Minimum Normalized Difference Vegetation Index
$F_U(u)$	Marginal distribution on variable U
$F_V(v)$	Marginal distribution on variable V
$F_{UV}(u,v)$	Joint probability distribution of variables U and V
θ	Copula parameter
U_{sim}	Simulated yield
V_o	Observed meteorological variable
V_m	Modelled meteorological variable
F_o^{-1}	Inverse Cumulative Distribution Function of V_o
F_m	Cumulative Distribution Function of V_m
Ω	Universal set
$\Pi_X(x)$	Possibilistic value of variable X

Abbreviations

AIC	Akaike Information Criterion
AMO	Atlantic Multidecadal Oscillation
aSPI	Agricultural Standardized Precipitation Index
BT	Brightness Temperature
CDF	Cumulative Distribution Function
CORDEX	Coordinated Regional Climate Downscaling Experiment
CPC	Climate Prediction Center
DDP	Drought Development Period
DMI	Dipole Model Index
DRP	Drought Recovery Period
ECDF	Empirical Cumulative Distribution Function
ED	Extreme Drought
ENSO	El Niño–Southern Oscillation
ERA5	ECMWF Reanalysis 5th Generation
ESI	Evaporative Stress Index
ET	Evapotranspiration
EW	Extreme Wet
FLDAS	Famine Early Warning Systems Network Land Data Assimilation System
GAMLSS	Generalised Additive Model in Location, Scale and Shape
GCM	General Circulation/Climate Model
GLDAS	Global Land Data Assimilation System
IDS	Instantaneous Development Speed
IMD	India Meteorological Department
IOD	Indian Ocean Dipole
IPCC	Intergovernmental Panel on Climate Change
IRS	Instantaneous Recovery Speed
ISMI	Indian Summer Monsoon Index
LULC	Land Use Land Cover
MD	Moderate Drought
MEERA-2	Modern-Era Retrospective analysis for Research and Applications

	version 2
MLE	Maximum Likelihood Estimation
MMM	Multi Model Mean
MSDI	Multivariate Standardized Drought Index
MW	Moderate Wet
NAO	North Atlantic Oscillation
NCEP	National Centers for Environmental Prediction
NDVI	Normalized Difference Vegetation Index
NEX-GDDP	NASA Earth Exchange Global Daily Downscaled Projections
NN	Near Normal
NSE	Nash-Sutcliffe Efficiency
PDF	Probability Density Function
PDSI	Palmer Drought Severity Index
PET	Potential Evapotranspiration
PR	Precipitation
RCP	Representative Concentration Pathway
RDI	Reconnaissance Drought Index
RDI_N	Non-stationary Reconnaissance Drought Index
SAF	Severity-Area-Frequency
SD	Severe Drought
SOI	Southern Oscillation Index
SPEI	Standardized Precipitation Evapotranspiration Index
SPI	Standardized Precipitation Index
SPI_N	Non-stationary Standardized Precipitation Index
SRI	Standardized Runoff Index
SSI	Standardized Soil moisture Index
SST	Sea Surface Temperature
SSTA	Sea Surface Temperature Anomaly
SW	Severe Wet
TCI	Temperature Condition Index
TVDP	Total Variability in Development Period
TVRP	Total Variability in Recovery Period
VCI	Vegetation Condition Index

VHI	Vegetation Health Index

Chapter 1

Introduction

1.1 Climate change

*"Climate change is a '**huge threat'** to humanity and it is very important for governments to take action as quickly as possible"* said Giorgio Parisi after winning the Nobel Prize in Physics 2021. In addition, he stated that the change of extreme events is expected to increase very strongly due to the consequences of changing climate. According to the Intergovernmental Panel on Climate Change (IPCC), climate change refers to the change in the mean and/or the variability of its properties over an extended period usually decades or longer as a result of natural variability or anthropogenic interventions. However, the attribution of climate change reveals that anthropogenic induced warming is significantly larger than the natural influences. For instance, Figure 1.1 reveals that the observed warming during 1951 to 2010 is similar to the warming contributed due to anthropogenic forcings

(IPCC, 2014a). In addition, it can be noted that the warming range varies from 0.5°C to 1.3°C over the period 1951 to 2010 due to greenhouse gases (GHGs), a major forcing due to anthropogenic activities.

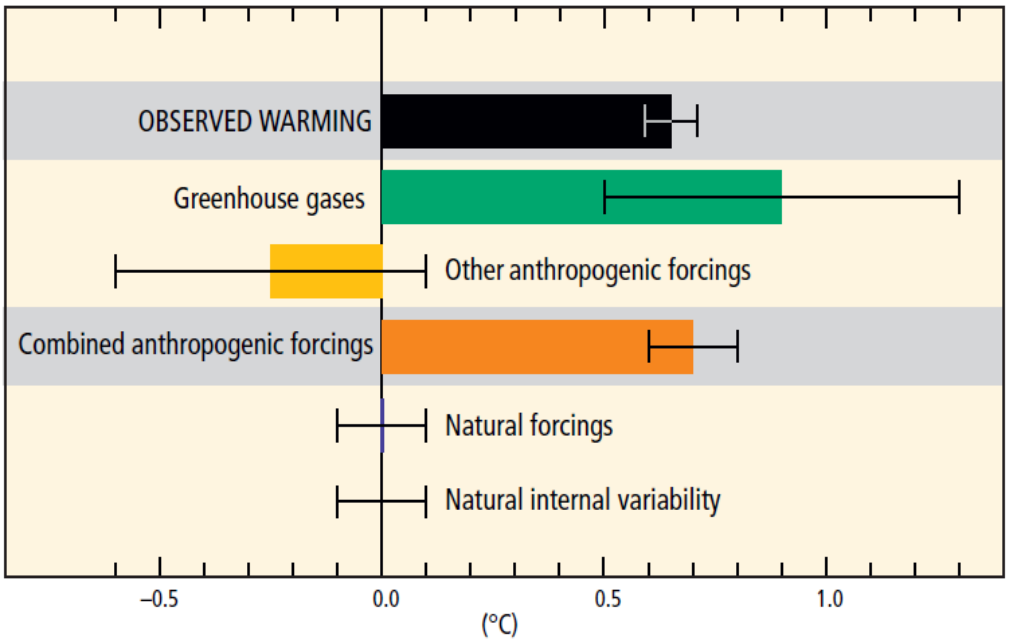

Figure 1.1: Attribution of global average surface temperature changes to the natural and anthropogenic forcing. (Source: IPCC 2014)

The feedback mechanism plays an important role in modulating the initial forcings resulting from the internal variations of different components of the earth's climate system. The feedback mechanism can either amplify (refers to positive feedback) or damp (refers to negative feedback) the initial forcings. For example, assuming fixed relative humidity, the atmospheric water vapour increases with increase in temperature following the Clausius–Clapeyron law. This increase in water vapour contributes further to the warming of the climate. According to Manabe and Wetherald (1967), this positive feedback loop amplifies a given forcing of the surface temperature by about a factor of two. In addition, the response time of the various components like atmosphere, land surface, ocean surface, vegetation, and sea ice to the external perturbations plays an important role in understanding the climate change impact. In particular, the response time of atmosphere, land surface, ocean surface, and vegetation are much lower (hours to years) than the response time (100 to 1000 years) of mountain glaciers, deep ocean, and ice sheets to the external perturbations.

In this sense, it is crucial to understand the impact of climate change to alleviate the adverse consequences through sustainable management plans. Figure 1.2 depicts the graphical representation of the causes, impact, and management practices of climate change. As discussed earlier, the natural variability (e.g., volcanic activity, changes in the orbit of the earth around the sun) and anthropogenic influences (e.g., urbanisation, GHGs emissions) are primary causes of climate change. However, the anthropogenic interventions have increased significantly imposing adverse effects on climate change as compared to the pre-industrial period (Masson-Delmotte et al., 2018). Focusing on the hydro-climatological components, the changing climate alters important variables like temperature, precipitation, and surface hydrology (e.g., runoff, soil moisture) (Douville et al., 2021). Subsequently, the changeability in these variables leads to the occurrences of extreme events such as drought, flood, extreme precipitation, and forest fire, among others that bring severe threat to the economy and ecosystem. Thus, it is indispensable to devise sustainable management practices in terms of prediction, risk assessment, mitigation, and development of social awareness regarding the implications of climate change.

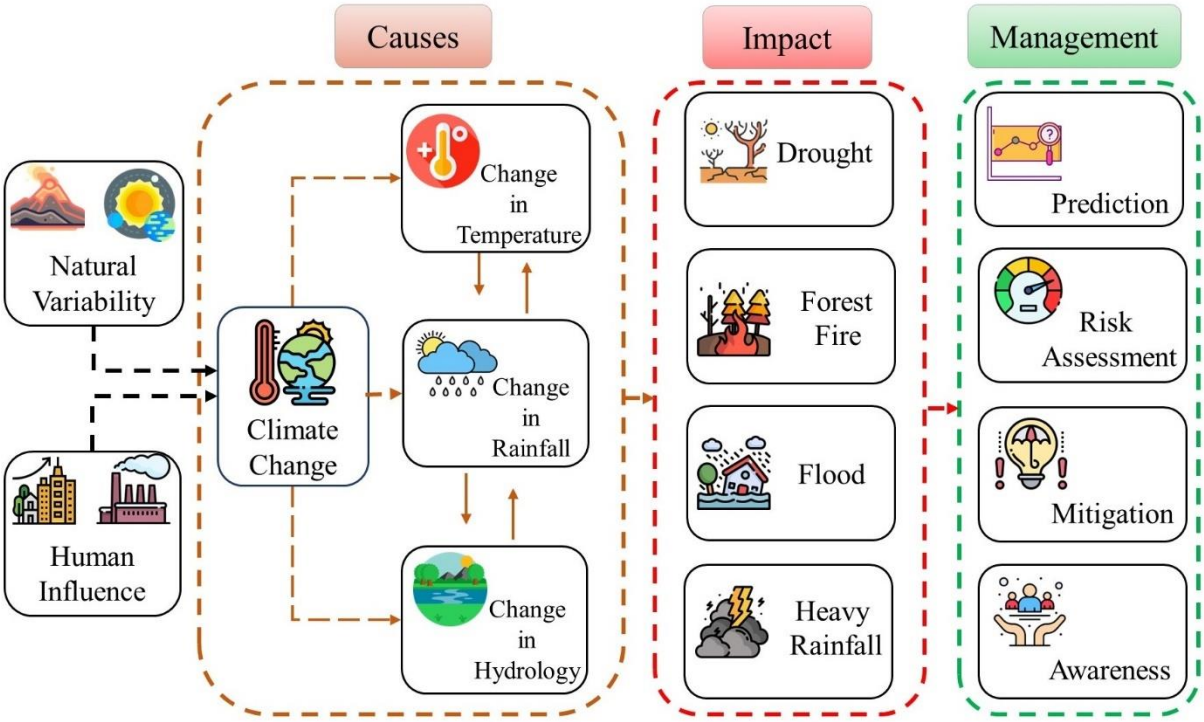

Figure 1.2: Graphical representation of causes, possible impact, and management practices under the scenario of changing climate

As a result of climate change, the extreme events are increasing and will become more frequent and severe. Subsequently, the adverse impacts will affect the economy substantially. Figure 1.3 depicts the number of disasters and associated economic losses across the globe. It is noticed that there is an increase in the number and economic loss from 1970 to 2019 (WMO, 2021). Surprisingly, the disaster losses are likely to increase significantly under the dual pressure of population growth and climate change. However, Figure 1.3 shows decrement in the number of disasters during 2010-2019 based on the reported number of disasters. Therefore, understanding the natural disasters under rapidly changing climate would help in formulating effective adaptation strategies.

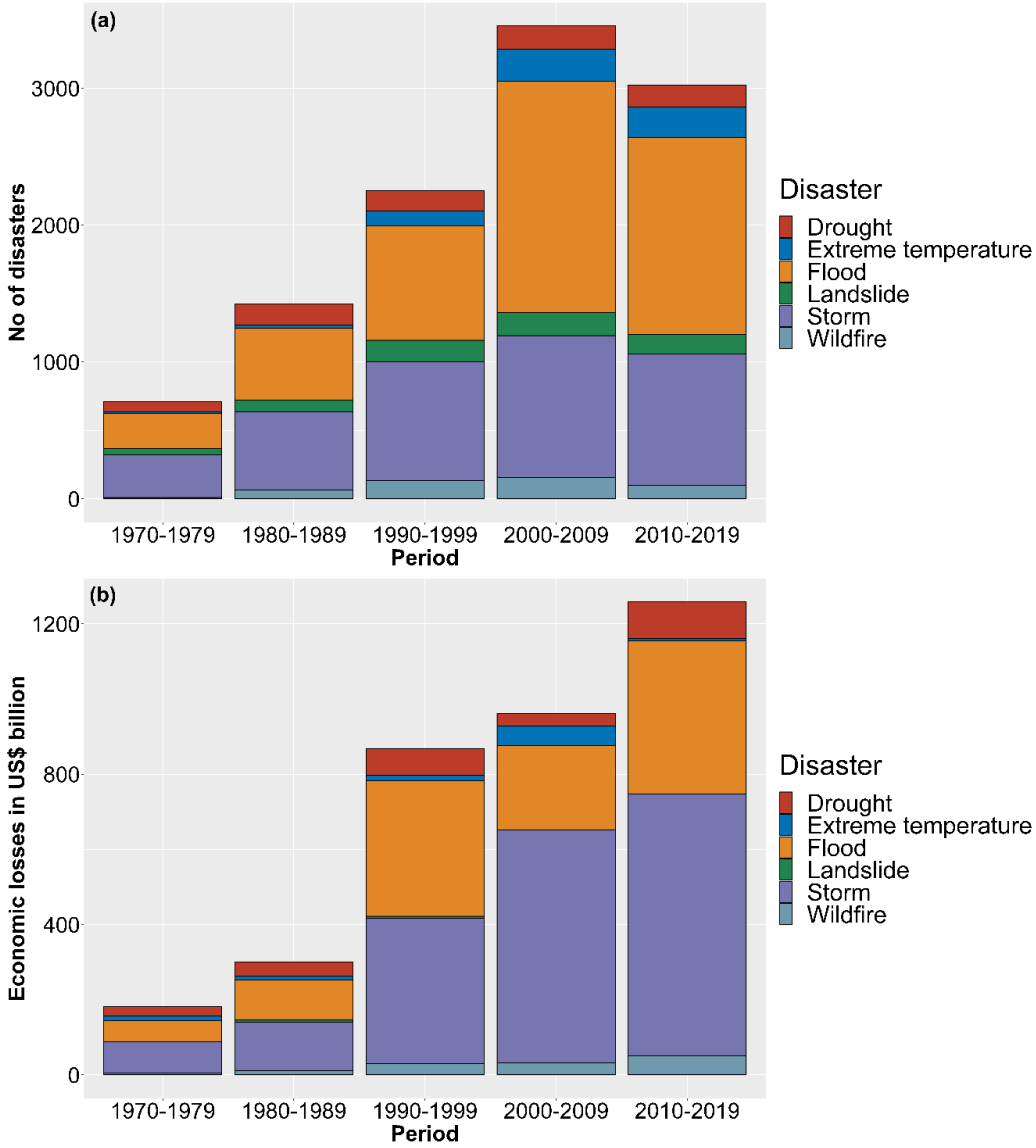

Figure 1.3: Distribution of (a) no of reported disaster and (b) economic losses by hazard type by decade across the globe (Data source: WMO (2021))

1.2 Climate change and water cycle

It is well understood that most of the adverse consequences of climate change are related to the qualitative and quantitative parameters of water. Therefore, it is necessary to understand the implication of climate change on water. Hydrology, as a multidisciplinary science that involves meteorology, climatology, geomorphology, and geology, among others, deals with the distribution and various manifestations of precipitation above and below the ground. Therefore, the climatological changes, anthropogenic influences, and variability in the ocean characteristics like temperature, and pressure affect the hydrological/water cycle. For instance, the changes in the GHGs concentration, and aerosols modify the global and regional variability of evaporation and precipitation (Douville et al., 2021). A warmer climate intensifies the moisture carrying capacity of the atmosphere, resulting in increased mean and extreme precipitation (Allan et al., 2020, 2014; Giorgi et al., 2019). The Asian monsoon is affected by the geographical variation in aerosols as it modulates the atmospheric circulation (Ganguly et al., 2012; Singh et al., 2019). The melting of snow under increasing temperature affects the seasonality of the river flows in snow-dominated basins (Allan et al., 2020). Likewise, direct human interventions like irrigation, land use land cover (LULC) changes, abstraction of surface and groundwater, and impoundment behind dams have substantial consequence on water cycle. For example, irrigation has significantly altered the regional water balance through increase in evapotranspiration (ET) and decrease in streamflow (Leng et al., 2016). The alteration of LULC (increasing rate of urbanization) affects ET, precipitation, runoff, and infiltration (Bosmans et al., 2017; Douville et al., 2021). In addition, greater and more extreme precipitation is likely to occur in the urban areas due to an increase in the sensible heat flux (Niyogi et al., 2017). Thus, all the components of the global water cycle have been modified due to the climatic and non-climatic drivers in recent decades, bringing new hydrological conditions (e.g., more frequent extreme conditions like floods and droughts) that were previously unfamiliar. The present thesis work is motivated to understand one of the extreme events i.e., drought in terms of its characteristics, propagation, and risk under the influence of climate change.

1.3 Droughts under changing climate

Due to the detrimental effect on various societal and economic factors, the research community has brought more attention towards the investigation of climate change impact on

climate hazards namely floods, droughts, heatwaves, etc. However, detection and quantification of drought events are complex as no universal definition of drought exists (Lloyd-Hughes, 2014). According to the fourth assessment report of IPCC, the drought can be defined as 'deficiency of rainfall causing water shortage' or 'prolonged period of abnormally dry weather with scanty rainfall to cause a serious hydrological imbalance'. Moreover, the drought can also be linked to the deficiency in the streamflow, soil moisture, agricultural productivity, and socio-economic conditions. As a result of climate change, the drought events have become more severe, and more frequent with longer duration across the globe (Toby, 2020). With varying properties, drought occurs over all hydro-climatological regions. Due to the increase in the carbon dioxide (CO_2) concentrations, the extra heat from global warming will increase the drying rate, establishing drought more quickly and with greater intensity (Trenberth et al., 2014). For instance, a warmer climate increases evaporation or evapotranspiration (with the availability of adequate moisture) that reduces the surface water and dries out soils and vegetation. The spatio-temporal variability of precipitation due to climate change results in increasing the period of both extreme precipitation and drought. In the context of climate change, within the "Atmosphere-Hydrology-Soil-Vegetation" system, the deficit in one hydro-meteorological variable propagates through the hydrological cycle and leads to the reduction in other hydro-meteorological variables. For example, the rainfall shortage for a longer period of time gives rise to the depletion in soil moisture, reservoir storage and streamflow etc. In this way, the deficit in precipitation (meteorological drought), soil moisture (agricultural drought) depletion and surface water shortage (hydrological drought) adversely affect the agricultural productivity, industrial activities and hydropower generation leading to socio-economic drought.

1.4 Non-stationary modelling of drought

In the absence of universal definition of drought, the monitoring of drought conditions is performed using different drought indices. For instance, but are not limited to, Standardized Precipitation Index (SPI) (Mckee et al., 1993) and Standardized Precipitation Evapotranspiration Index (SPEI) (Vicente-Serrano et al., 2010) for meteorological drought, Standardized Runoff Index (SRI) for hydrological drought (Shukla and Wood, 2008), Standardized Soil Moisture Index (SSI) for agricultural drought (Hao and AghaKouchak, 2013). These indices play important role in improving drought preparedness plans and effective risk management measures. Therefore, appropriate drought index identification has a

significant contribution to make to regional drought assessment. The traditional estimation of drought indices is based on the stationary probability distribution of one or more meteorological variables. However, owing to the dual pressure of climate change and anthropogenic interventions, the stationary assumption is no longer valid (Milly et al., 2008; Russo et al., 2013) and hence, the reliability and accuracy of the traditional approach to estimating droughts have been brought into question. Therefore, it is urgent to update the procedure for evaluating droughts to include the variabilities in the environmental conditions using nonstationary theory. The nonstationary approach makes it possible to introduce covariates as a linear/nonlinear function in the distribution parameters of climate variables. In addition, the significant development in the statistical theory (e.g., Extreme Value Theory (EVT)) enables us to model the complex phenomena of nature through physically based covariates. In this case, the covariates refer to the large or local scale variabilities that influence the drought conditions. For example, large-scale climatic oscillations like El Niño-Southern Oscillation (ENSO), Southern Oscillation Index (SOI), Indian Summer Monsoon Index (ISMI), Indian Ocean Dipole (IOD), among others and regional scale changeability in meteorological variables are considered. Therefore, the present study undertakes the non-stationary approach to understand the drought characteristics under changing climate.

1.5 Understanding drought propagation phenomena

As discussed earlier, the different drought conditions are interrelated through the "Atmosphere-Hydrology-Soil-Vegetation" system. Therefore, one drought can be translated to another drought condition. Primarily, the drought condition starts from the lack of available water i.e., deficit in precipitation amount. In the Indian context, the meteorological drought can be attributed to the weaker monsoon precipitation that occurs during the month from June to September. The prolonged deficits of meteorological drought can be translated into hydrological drought and the translation process is called as drought propagation. The time required to propagate from one drought to another is known as propagation time in which the accumulated deficits from one drought reflect in another drought (Apurv et al., 2017). In addition to the drought propagation, the internal propagation speed of drought events plays an important role. The internal propagation speed reflects the development and recovery speed of the development and recovery phases, respectively. The drought development is the phase between the drought initiation and peak. Similarly, the time period between peak and recovery is considered as the drought recovery phase. The climate and catchment characteristics play

an important role in drought propagation and are largely affected by climate change and anthropogenic interventions. However, under limited or no anthropogenic interventions, the drought propagation is controlled by climate and biophysical characteristics of the hydrographic basins (Van Loon, 2015). With this understanding, the propagation study under the influence of climate change provides important drought characteristics at local scale which can assist water managers and policy makers to devise sustainable management practices.

1.6 Drought projection, hotspot and risk assessment

As compared to the past drought events, the overall scenario of future long-term drought events is still incomplete. To devise drought mitigation strategies, it is important to evaluate the future drought conditions under different climate change scenarios. In order to project future scenarios, the outputs from the General Circulation Models/Global Climate Models (GCMs) are used as credible tools. According to IPCC, the GCMs that represent physical processes in the atmosphere, ocean, cryosphere and land surface are the most advanced tools for simulating the response of the climate system to increasing GHGs emission. In order to make projections for the future, fine resolution outputs are obtained from the coarser scale outputs from GCMs using the downscaling technique. Further, the associated biases are corrected through appropriate bias-corrected techniques. In the present day, the high-resolution outputs can be obtained directly by different agencies namely NASA Earth Exchange Global Daily Downscaled Projections (NEX-GDDP) and Coordinated Regional Climate Downscaling Experiment (CORDEX). Therefore, it is prudent to analyse the future drought characteristics under different climate change scenarios using the outputs from the GCMs. Moreover, considering the multiple GCMs will help in enveloping the associated uncertainties in future projections. The future projection of different drought properties will help in identifying drought hotspot regions and a comparative analysis can be performed with respect to the historical observations in order to enable the policymaker and government officials to propose sustainable drought management plans to combat the foreseen drought events. In addition to drought properties, the future projection of Severity-Area-Frequency (SAF) relationship curve can be used for providing quantitative information about drought by characterising various attributes of droughts like return period, areal extent, and severity. The SAF relationship has been used to understand the nature of spatio-temporal characteristics of drought at the regional scale. To formulate appropriate adaptation strategies, it is crucial to

assess the risk associated with the drought conditions. Moreover, the risk assessment related to the agricultural productivity due to the drought events is of paramount importance under the changing climate. Understanding of the agricultural risk is complex as it is modulated by various factors like meteorological, and hydrological variability. Thus, multivariate analysis can be used to overcome the issue. The copula theory has gained popularity among the researchers to analyse the joint return period of different drought properties. However, there is a limited application of multivariate analysis to examine the drought risk on rainfed agriculture. The outcomes will help the water and agricultural planners to formulate sustainable agricultural management plans.

1.7 Objectives of the study

The objectives of the study are listed as follows:

1. To perform the non-stationary analysis to examine the impact of external covariates in modelling the drought events.
2. To evaluate different drought characteristics with the use of meteorological, hydrological, agricultural, and socioeconomic drought indices.
3. To examine the spatio-temporal characteristics of drought propagation under the influence of external covariates.
4. To assess the agricultural drought risk on rainfed agriculture using the multivariate analysis.
5. To investigate the spatio-temporal characteristics of droughts through Severity-Area-Frequency (SAF) curve under different climate change scenarios and identify future drought hotspots based on the future variability of different drought properties.

It is worth noting that the objectives 1, 4, and 5 are performed over one of the drought provinces in India i.e., Maharashtra. However, the objectives 2, and 3 are carried out over entire India. The reasons behind choosing Maharashtra as the study area are: (i) during 1901-1998, 26 meteorological droughts are identified, and 11 out of 26 droughts affected more than 50% of the province (Gore and Ray, 2002); (ii) the probability of occurrence of drought during El Niño years is 55% over Maharashtra, and 59% over India (Gore and Ray 2002); (iii) 11,801 villages were affected by drought in 2013, and it is considered as the worst drought in the region in the last 40 years (Dandekar, 2013).

1.8 Contributions from the study

In a drought-vulnerable country like India, the analysis of drought in the context of a nonstationary approach is limited. Moreover, in connection with drought prone areas like Maharashtra, drought events under the influence of large-scale climatic oscillations have not been analyzed. Therefore, the first part of the study attempts to understand the variability in the drought properties with and without the inclusion of physical covariates in the computation over the Maharashtra state in India. The large-scale climatic oscillations like Indian Summer Monsoon Index (ISMI), Southern Oscillation Index (SOI), Sea Surface Temperature (SST), and Indian Ocean Dipole (IOD) are used as covariates. From the analysis it is found that non-stationary analysis is superior to the stationary analysis. In addition, notable differences are observed while comparing the different drought properties using stationary and non-stationary drought indexes. A comparative analysis of the historical drought that occurred in 2013 reveals that non-stationarity in the meteorological data sets cannot be ignored for developing a sustainable mitigation and adaptation strategy against drought hazard.

Understanding the importance of non-stationarity, the second part analyses different drought properties of meteorological, hydrological, and agricultural drought indices under non-stationary setting. The runoff datasets are obtained from five different sources (ECMWF Reanalysis 5th Generation (ERA5), Famine Early Warning Systems Network Land Data Assimilation System (FLDAS), Global Land Data Assimilation System (GLDAS), Modern-Era Retrospective analysis for Research and Applications version 2 (MERRA-2), and National Centers for Environmental Prediction (NCEP)). Similarly, the soil moisture datasets are obtained from six diverse sources (Climate Prediction Center (CPC), ERA5, FLDAS, GLDAS, MERRA-2, and NCEP). Here, Standardized Precipitation Evapotranspiration Index (SPEI), Standardized Runoff Index (SRI), and Standardized Soil moisture Index (SSI) are used to characterize the meteorological, hydrological, and agricultural drought, respectively. The non-stationary modelling of SRI and SSI is performed for each different data source. The drought properties using the ensemble mean are discussed for SRI and SSI indices. In addition to meteorological, hydrological and agricultural droughts, socio-economic drought events are also computed. The socio-economic drought is evaluated based on the water consumption and water availability. Here, water consumptions from six different sectors

namely domestic, electricity, irrigation, livestock, manufacturing, mining are used. Till date such type of study has not been carried out over entire India.

In spite of large spatio-temporal variability in droughts, the propagation time from one drought to another drought is not examined at local scale with the inclusion of external covariates over India. This part deals in examining the propagation time from meteorological to hydrological and from meteorological to agricultural drought. The drought propagation time is computed in 1170 grids blanketing the entire India based on differences between the initiation to initiation (Δs), peak to peak (Δp) and termination to termination (Δe). In addition, the internal propagation of drought is analyzed with the help of variable motion relationship of speed-time process. The drought indices developed using the external covariates are used for this analysis. Additionally, for each type of drought, instantaneous drought development speed and recovery speed are estimated to understand the rate at which drought develops and recovers.

In an agrarian country, the impact of hydro-meteorological variability has significant influence on agricultural productivity. Therefore, assessing the risk on agricultural system due to the effect of drought conditions is of paramount importance for agricultural sustainability. In this study, the agricultural drought risk in terms of conditional probability of crop loss with respect to different drought severities is analysed. Different drought indices namely SPEI, SSI, Vegetation Condition Index (VCI) and Temperature Condition Index (TCI) are used to evaluate the conditional probability. The bivariate analysis using the copula theory is performed to understand the dependence structure between drought conditions and crop yield anomalies (cotton, groundnut, rice, and wheat) over the Maharashtra province in India during 1998-2015. Total of five different copulas namely, Gaussian, Student's t-copula, Clayton, Gumbel, and Frank are used to analyse the bivariate joint dependence structure between yield anomalies and dominant drought indicator (SPEI, SSI, VCI, or TCI).

Finally, the future drought characteristics are projected for meteorological drought for short - and long-term durations incorporating the outputs from nineteen GCMs under Representative Concentration Pathway (RCP) 4.5 and 8.5 scenarios. The GCMs are obtained from NEX-GDDP data center. The relative changes in future projected drought properties with respect to recent past years are analysed. Based on the four properties i.e., affected area, frequency, severity and duration, the drought hotspot regions are identified under RCP 4.5 and 8.5

scenarios for future time series. Additionally, the seasonal SAF relationship curve for meteorological droughts is projected for five different seasons namely pre-monsoon, monsoon, post-monsoon, Kharif and Rabi. The uncertainty associated with GCMs, and scenarios is assessed using possibility theory.

1.9 Outline of the thesis

Literature relevant to climate change impact on drought, non-stationary analysis, drought propagation, agricultural risk, and multivariate analysis are concisely reviewed in Chapter 2.

Chapter 3 presents the non-stationary modelling of meteorological drought indices over Maharashtra. The large-scale climatic oscillations like ISMI, IOD, SOI, and SST are used as covariates for SPI and RDI drought indices. A comparative analysis of different drought properties is carried out using stationary and non-stationary approaches.

In Chapter 4, in addition to meteorological drought, the non-stationary analysis is carried out for hydrological and agricultural drought indices across entire India. In addition, the socio-economic drought analysis is performed based on gridded water demand and available water in terms of runoff.

Chapter 5 presents the drought propagation from meteorological to hydrological and meteorological to agricultural under the influence of external covariates. In addition, the internal propagation of each drought type is evaluated.

In Chapter 6, a probabilistic evaluation of agricultural drought risk is performed for four major crops (cotton, groundnut, rice, and wheat). In this study, both hydro-meteorological (SPEI and SSI) and remote sensing based (VCI and TCI) drought indices are considered.

Chapter 7 deals with the identification of future drought hotspot regions under short- and long-term drought conditions.

Chapter 8 presents the development of seasonal SAF relationship after analysing the uncertainty associated with GCMs and scenarios.

Chapter 9 presents the summary and conclusions of the work described in the thesis.

Chapter 2

Literature Review

2.1 Introduction

This chapter reviews the literature related to the non-stationarity in drought hazard to investigate the impact of climate change and its importance in the evaluation of drought characteristics, drought propagation and drought risk. Initially, literature related to the non-stationary analysis and its significance on drought assessment are discussed. Then, the characterizations of different types of droughts and their impacts across India are investigated. Subsequently, the behaviour of drought propagation between different types of droughts is reviewed. The significance of the evaluation of drought risk and its vulnerability on crop productivity, introduction of the multivariate analysis in drought risk analysis are examined afterwards.

2.2 Non-stationary Analysis

Since the second half of the 20th century, climate change has been addressed as the most important issue due to the increment in global warming. In past 30 years, the surface temperature has increased significantly as compared to any decade (IPCC, 2014, Qin and Thomas, 2014). In addition to the global climate change, the increasing interventions of anthropogenic activities like increasing rate of urbanization, increasing greenhouse gases, etc. act as catalyst for more severe and frequent extreme events. In past decades, the time-invariant or stationary approach is used for extreme hydro-climatic event analysis that assumes that the statistical properties of hydro-climatic variables do not change over time. However, as above said, the factors affecting the climatic variables no longer remain unaltered. Therefore, the inclusion of non-stationarity in the analysis of extreme hydro-climatic events deserves attention of the research community. In addition, due to the advancement in the computational facilities, the implementation of non-stationary to model the extreme events of the hydro-climatic variables has gained the popularity. With this understanding, the stationarity assumption in water resources risk management and planning is no longer valid (Milly et al., 2008; Sivapalan and Samuel, 2009; Villarini et al., 2010). Recent advances in understanding of ocean-atmosphere interactions demonstrate that there are well organized modes of interannual and interdecadal variability in climate which have significant influence on the hydro-meteorological extreme events. Therefore, recent studies focus on non-stationary analysis in evaluating different extreme events in changing climate. For example, Coles (2001) analysed various datasets such as maximum sea level, precipitation, and temperature under non-stationary setting. The covariates such as Southern Oscillation Index (SOI) and time are used to estimate the location and scale parameters of the selected distributions. The studies showed the applicability of the non-stationarity under the climate change scenario. Coles presented various methods for the successful use of the non-stationarity in the hydro-climatic extremes.

Katz et al. (2002) analysed the statistics of different extremes in hydrology considering time and large-scale climatic oscillations as covariates to estimate the distribution parameters. Authors used maximum likelihood estimation (MLE) to estimate in order to evaluate the parameters. They suggested to incorporate the trend in the analysis of hydrologic extremes due to the intensification of hydrological cycle as a result of climate change.

He et al. (2006) demonstrated the non-stationary analysis of extreme discharge implementing the Gumbel and Log-Pearson III distributions. They used three types of time dependent functions to introduce the non-stationarity. Through the non-stationary analysis, authors advocated that for more realistic and comprehensive outcomes a linkage should be established between the climate system and the distribution parameters.

Beguería et al. (2011) used non-stationary extreme value analysis for the daily precipitation series in northeast Spain. They used time as covariate in a generalised Pareto model. A log-likelihood ratio was used to analyse the significance of non-stationarity over stationary approach. At seasonal scale, the significance of non-stationary model was found for the event's intensity in winter and spring at a significance level of 5%.

Cheng & AghaKouchak (2014) modelled non-stationary Intensity Duration Frequency (IDF) curves from maximum extreme rainfall series at five stations in USA. Authors considered Generalized Extreme Value (GEV) distribution for annual maximum rainfall and time as a covariate in the distribution. From results, they found that 60% of extreme rainfall was underestimated by stationary model. This underestimation under stationary assumption increases flood risk and failure in infrastructure. Moreover, Bayesian approach was also carried out for uncertainty modelling for finding out the uncertainty in non-stationary return levels and the results indicated higher uncertainty in lower return level.

Li et al. (2015) developed Non-stationary Standardized Precipitation Index (NSPI) using non-stationary Gamma distribution. They used various climate indices as covariates for fitting the precipitation data. The performance of NSPI and traditional Standardized Precipitation Index (SPI) index was evaluated. It was found that NSPI is more robust than SPI as it incorporates the climate variations into account. In addition, different drought properties such as drought frequency, peak, severity, duration were computed for both NSPI and SPI. The study was performed over Luanhe River basin.

Cancelliere (2017) reviewed on the available methods for developing the non-stationary model for different hydrological processes. The diversification of these methods to evaluate the drought occurrences under the assumption of non-stationarity in hydro-meteorological variables was also explained. Author proposed a new methodology on four different precipitation time series having varying trends to characterise the drought length. Author suggested that the methods can be improved for incorporating the uncertainty associated with

the evaluation of non-stationarity in hydro-meteorological series and can be used for calculating other drought properties like severity, intensity etc.

Mukherjee et al., (2018) argued that the non-stationarity associated with climate change is expected to modulate the parameters of the distributions of input variables which is used to formulate different drought indices. Therefore, appropriate methodology should be formulated to incorporate the non-stationary information in order to characterize the drought under climate change. Subsequently, reliable information can be extracted for risk assessment and management of infrastructure.

Rashid and Beecham (2019) developed non-stationary SPI using Generalised additive model in Location, Scale and Shape (GAMLSS) modelling framework. Here, SOI, Sea Surface Temperature (SST), Pacific Decadal Oscillation (PDO), Southern Annular Mode (SAM) and Dipole Model Index (DMI) external covariates are incorporated for capturing the non-linear characteristics of precipitation in South Australia. The obtained results demonstrate the importance of non-stationary drought index for accurately capturing the drought characteristics in the changing climate.

Wang et al. (2020) used both climate driven and human induced indices are incorporated in non-stationary analysis of hydrological drought index i.e., Standardized Streamflow Index (SSI). The significant climate covariates and human induced indices were computed from correlation analysis and from Soil and Water Assessment Tool (SWAT) model respectively. A comparison analysis was conducted using Akaike information criterion (AIC) between Non-stationary SSI (NSSI) and SSI to examine the capability of NSSI. In conclusion, authors stated that the NSSI can give more reasonable and satisfactory results by accounting the non-stationarities in streamflow due to human activities and changing climate.

Das et. al (2020) used non-stationary Gamma distribution having climate indices in location parameter to incorporate climate variability in the computation of meteorological drought index. Authors compared the drought properties between the stationary and non-stationary analysis based on the statistical performances in two Himalayan states in India. Moreover, they performed bivariate analysis of different drought properties to provide a new concept for the effective management practices in the changing environment.

Bazrafshan et al. (2022) aimed to develop Non-stationary Standardized Precipitation Evapotranspiration Index (NSPEI) for robust quantification of drought characteristics. They varied the location parameter of the log-logistic distribution with multivariable function of time and climate indices. The study was performed over Iran using GAMLSS algorithm. They found that non-stationary modelling outperforms stationary modelling over 97% of total stations across the study area.

In the similar way, there are many studies which reveal the superiority of non-stationary analysis in different parts of the world while analysing the hydro-meteorological extremes. These include but are not limited to Olsen et al. (2010), Villarini et al. (2010), Gilroy and McCuen (2012), Salas and Obeysekera (2014), Mondal and Mujumdar (2015), Vasiliades et al. (2015), Gao et al. (2016), Song et al. (2020), Das and Umamahesh (2021), Zhang et al. (2021).

2.3 Drought characterization

Drought is the most unpredictable and least understood natural hazard (Hagman et al., 1984). The detection and quantification of drought events are complex as no universal definition of drought exists (Lloyd-Hughes, 2014). However, from hydrological point of view, drought occurs due to the less availability of water in a region for a significant period of time. It can be less in precipitation, reduction in soil moisture, low streamflow which are the primary reason behind the meteorological, agricultural, and hydrological drought, respectively. However, based on single variable, the drought condition can't be characterised for a particular region. It depends on multiple hydro-meteorological variables for capturing different aspects of drought conditions. Therefore, the use of different drought indices is the most common approach for drought characterisation. Drought indices can simplify the complex interrelationship of climate related parameters with different climatic condition. Therefore, in past studies, many researchers have introduced different drought indices for characterizing different types of droughts. For example

Despite the lack of a precise definition of drought, there are several indices to monitor the drought conditions (Li et al., 2015; Wilhite, 2017). To monitor the precipitation based meteorological drought, Palmer Drought Severity Index (PDSI; Palmer, 1965) and Standardized Precipitation Index (SPI; Mckee et al., 1993) are commonly used. Similarly, to

monitor runoff or streamflow based hydrological drought, the Standardized Runoff Index (SRI) is used (Shukla and Wood, 2008). Likewise, the Standardized Soil Moisture Index (SSI) and Agricultural Standardized Precipitation Index (aSPI) are widely used for agricultural drought (Hao and AghaKouchak, 2013; Tigkas et al., 2019). Many other drought indices have been proposed considering one or more climate variables such as the Standardized Precipitation Evapotranspiration Index (SPEI; Vicente-Serrano et al., 2010), Vegetation Drought Response Index (VegDRI; Brown et al., 2008), Reconnaissance Drought Index (RDI; Tsakiris and Vangelis, 2005), Multivariate Standardized Drought Index (MSDI; Hao and AghaKouchak 2014), and Evaporative Stress Index (ESI; Anderson et al. 2007).

González and Valdés (2006) developed a new index i.e., Drought Frequency Index (DFI) based on the purely probabilistic treatment. The drought index is developed on the basis of stochastic characterisation of extreme persistent deviation sequences. The performance of the index is examined and compared with respect to different issues such as magnitude selection, univariate versus multivariate, threshold selection and timescale issues. The newly developed index provides a consistent index for general drought characterization goals.

Santos et al. (2010) considered Standardized Precipitation Index (SPI) at different time scales to characterise drought events. They applied principal component analysis (PCA) and K-means clustering (KMC) to SPI series to evaluate spatial and temporal patterns of drought occurrences. From fast Fourier transform algorithm (FFT) of SPI pattern, authors found specific time period cycle at different region; for instance, 3.6-year cycle in the SPI pattern over south and 2.4-year and 13.4-year cycles in north of Portugal. They suggested the stronger influence of NAO in south Portugal because of which south portion experienced more frequent dry events.

Yang et al. (2017) evaluated seven meteorological drought indices namely Palmer Drought Severity Index (PDSI), modified PDSI (PDSI_CN), self-calibrating PDSI (scPDSI), Surface Wetness Index (SWI), SPI, SPEI and soil moisture simulation. Authors analysed the applicability of drought indices based on regional basis. They considered terrestrial water storage, observed streamflow and soil moisture for computing these indices. Authors concluded that the scPDSI is most appropriate for China. They showed some problems in PDSI and PDSI_CN in humid and arid areas, whereas the SPI and SPEI were more

appropriate for humid areas rather than arid and semiarid regions. Although the seven drought indices were able to detect the long-term trends of drought, there was a difference among the values of drought areas computed using the seven indices.

Zhao et al. (2019) worked on socio-economic drought characterisation on the basis of Multivariate Standardized Reliability and Resilience Index (MSRRI). They adopted cross wavelet analysis to examine the influence of meteorological driving factors on socio-economic droughts. From the outcomes it was observed that the MSRRI is effective for socio-economic drought evaluation. Moreover, the comprehensive effects of El Niño–Southern Oscillation (ENSO), East Asian Summer Monsoon (EASM) and Pacific North American (PNA) on socio-economic droughts were found.

Shah and Mishra (2020) developed integrated Drought Index (IDI) incorporating the responses from meteorological, agricultural, hydrological drought and accounting the ground water storage. Gaussian copula was used here to compute IDI by integrating SPI-1, Standardized Runoff Index (SRI-4), Standardized Soil moisture Index (SSI-1) and Standardized Ground water Index (SGI-1). Moreover, the required hydro-meteorological variables for evaluating the IDI were simulated from Variable Infiltration Capacity (VIC) model with SIMple Groundwater Model (VIC-SIMGM). Authors projected drought frequency based on IDI and showed its efficiency in the assessment of drought characteristics in both past and future climate in India.

For improvement in drought monitoring, to acquire better knowledge on its drivers and processes, Diaz et al. (2020) presented an approach to characterise the dynamics of drought. Based on SPEI, different drought characteristics like tracks, severity, duration, localisation, rotation of droughts were computed to identify drought. The outcomes from the study are used to build a model for the prediction of spatial drought tracks in India.

Agutu et al. (2020) considered three types of datasets such as remotely sensed data, in situ and model products for analysing drought behaviour in a complex topography region i.e., Upper Greater Horn of Africa. Precipitation, soil moisture, Vegetation Condition Index (VCI) and total water storage dataset were chosen for characterising drought and exploring the inconsistencies in areas. The inconsistencies were observed under extreme and moderate

droughts as compared to severe droughts. The obtained results indicated that the 3-month time scale sufficiently captured the agricultural drought and provided an indirect linkage with food security situation.

Javed et al. (2021) explored the spatiotemporal dynamics of meteorological and agricultural drought by utilising the remote sensing products and evaluated their linkage with winter wheat and summer corn yield losses. They derived the agricultural Standardized Precipitation Index (aSPI) for different time scales and Standardized Vegetation Supply Water Index (SVSWI) to explore the regional scale dynamics across China. From results, the increased frequency of drought events was found in most part of the country for 3-month aSPI. Moreover, a good correlation was observed between 3-month aSPI and SVSWI with winter wheat anomaly for some areas.

Similar to the above drought characterization studies, there are many studies related to different types of drought characterisation. These include, but are not limited to Ponce et al. (2000), González and Valdés (2003), Tsakiris et al. (2007), Yirdaw et al. (2008), Mishra and Singh (2010), Zargar et al. (2011), , Hao and Singh (2015), Ali et al. (2019), Ferreira et al. (2018), Zhang et al. (2019), Xu et al. (2021), Guo et al. (2022).

2.4 Drought propagation

In the context of causative mechanisms, the deficit in the precipitation and increasing evaporative demand propagate through the hydrologic cycle and subsequently develop into different drought events (Hellwig et al., 2020; J. Wu et al., 2020). In other words, from beginning to end, drought transition is encapsulated within the “Atmosphere-Hydrology-Soil-Vegetation” system (N. Chen et al., 2020). This transition from one form to another form of drought is known as drought propagation (Apurv et al., 2017; Haslinger et al., 2014). The understanding of drought propagation provides valuable information to improve the accuracy of drought analysis and prediction. In recent times, studies have been performed to analyse the drought propagation mechanisms and their controlling factors. For example

Peters et al. (2003) investigated the reason behind the transformation of droughts through groundwater system. In this study propagation from groundwater recharge to the discharge was evaluated. The propagation was examined by tracking a drought in recharge through a linear reservoir. The outcomes from the study revealed that the delay in groundwater system

caused the decrease in recharge from high-flow to low-flow period. The resulted in an increase in drought deficit for discharge compared with the drought deficit for recharge.

Van Loon et al. (2012)considered ten large scale models under both land-surface and global hydrological models to evaluate the simulations of drought propagation. They computed different types of drought characteristics, drought propagation features and hydrological drought typology. A clear reflectance of drought characteristics on drought propagation was found. From results, authors concluded that most of the drought propagation processes were well reproduced by the ensemble mean of large-scale models.

Jiefeng Wu et al. (2018) proposed a framework to determine the propagation speed through a variable motion relationship of speed-time process. They computed the Instantaneous Development Speed (IDS) and Instantaneous Recovery Speed (IRS) for each hydrological drought event by subdividing the individual propagation of into development and recovery phase. At last, the IDS and IRS values are cross validated for final outcomes. The results revealed that the variable motion method performed well in identifying the propagation period. They also found out that the sensitivity of IDS and IRS were correlated with external factors i.e., catchment characteristics, human activities and climate forcings.

Xu et al. (2019) used two drought indices i.e., SPI (for meteorological drought) and SRI (for hydrological drought) for investigating the drought propagation from meteorological to hydrological drought. Authors evaluated the correlation between two indices over three parts of the Luanhe river basin. They observed frequent occurrences of hydrological drought, whereas a little difference was observed in the meteorological drought characteristics between pre- and post-human disturbance period. The shorter propagation time i.e., 1-5 months was computed for grassland dominated subbasin. Whereas in case of forest dominated subbasin, it was 4-7 months during rainy season. However, in dry season, drought propagation time of 7-12 months was noticed over both grassland and forest dominated subbasins.

Apurv and Cai (2020) tried to understand the drought propagation mechanism through physical based hydrologic model. Authors considered multiple watersheds from different regions of contiguous United State to investigate about the controlling factors of drought propagation. From obtained results, similar spatial pattern was found between hydrological drought and climatic properties. Authors revealed the key watershed property i.e., storage-discharge relationship which controls the intensity of hydrological drought.

The interference of the construction of Three George Dam (TGD) in the modification of drought propagation was studied by Huang et al. (2021). They examined the impact of anthropogenic activity on meteorological drought to hydrological and agricultural drought propagation processes. Authors used trend and attribution analysis to explore the potential influence factors. They found significant impact of TGD which aggravate the drought propagation characteristics. Moreover, they observed that the meteorological to hydrological drought propagation speed was slowed down, whereas meteorological to soil moisture lag time became shorter.

The linkage among meteorological, agricultural and groundwater drought was investigated by H. Zhang et al. (2021) over humid and arid/semi-arid basins in China. They evaluated the correlation and propagation among these three types of droughts through Spearman rank correlation coefficient. SPI, SSI, and Groundwater drought index based on Gravity Recovery and Climate Experiment (GRACE) were considered to characterise meteorological, agricultural and groundwater drought, respectively. A strong linkage between meteorological and agricultural drought was found. Authors argued that the groundwater extraction could be the main factor for groundwater drought.

Ho et al. (2021) proposed a new approach to determine the drought propagation from meteorological to hydrological drought. They calculated the propagation time at a higher temporal resolution and considered high resolution remote-sensing data on a daily time step. The SPI, SRI, Standardized Evapotranspiration Deficit Index (SEDI) and Standardized Soil moisture Index (SSI) are considered. Index correlation method and temporal shift method are used for calculating drought propagation. The outcomes from the study suggested that the soil moisture drought showed a delayed response to the meteorological conditions. Whereas hydrological drought propagation is controlled by precipitation along with land cover, soil type, temperature and humidity.

Recently, Schumacher et al. (2022) worked on drought self-propagation behaviour. They considered last 40 largest recent droughts worldwide and used Lagrangian moisture tracking to examine the influence of soil moisture drought on precipitation. Authors found that the drylands were mostly prone to drought self-propagation due to the enhanced soil water stress and reduction in precipitation in these areas.

Likewise, propagation study has been carried out over Iberian Peninsula (Lorenzo-Lacruz et al., 2013), over China (Zeng et al., 2015; Wu et al., 2018; Xu et al., 2019; Ding et al., 2021), over United Kingdom (Barker et al., 2016), over South Korea (Jehanzaib and Kim, 2020; Sattar et al., 2020, 2019), Over Contiguous United States (Tijdeman et al., 2018), over Brazil (Bevacqua et al., 2021), over Spain (Barella-Ortiz and Quintana-Seguí, 2019), over South Africa (Botai et al., 2019), over India (Bhardwaj et al., 2020), among others.

2.5 Drought risk and vulnerability

Drought vulnerability refers to the degree of susceptibility of a region to drought, whereas drought risk is defined as the likelihood of potential losses caused by the combined effect of drought hazard, vulnerability and exposure. The dual effect of climate change and the rapid economic development have aggravated the drought risk condition. Meanwhile, rural communities are more susceptible to droughts as it has mostly agriculturally based economy which depends on climatic variability. Therefore, it is of great practical significance to assess the drought risk and effective utilisation of water resources for sustainable development of agricultural productivity. Over past years, researcher have focused on the evaluation of drought risk and its vulnerability.

Merabtene et al. (2002) determined the susceptibility of water supply system to droughts by using a decision support system (DSS) which was integrated with three fundamental modules: real time rainfall-runoff model, water demand forecast model and reservoir operation model. Based on genetic algorithm, they introduced two new features to minimize drought risk and to improve the convergence of the model to practical solutions. Authors considered reliability, resiliency, and vulnerability to formulate Drought Risk Index (DRI). They advocated that DSS as an efficient tool for evaluating water supply scenarios during drought conditions.

He et al. (2013) worked on the assessment of agricultural drought risk over China at 10 × 10 km grid scale. The drought risk was evaluated based on the natural disaster analysis theory. A clear southeast–northwest spatial pattern of agricultural drought risk was found. The drought risk was evaluated as the product of three components i.e., hazard, vulnerability and exposure. In addition, the study area was categorized based on the classifications of low, moderate, high and very high risk.

Borgomeo et al. (2015) proposed vulnerability-based approach to evaluate the water resources system vulnerability to hydrological drought condition using copula theory. From the generated synthetic streamflow series, the marginal distribution of streamflow for each month was produced by bootstrapping method, whereas the joint probability distribution for consecutive month was created by copula-based method. Applying the method to London water system, the obtained results indicated that the vulnerability of the water system is outside the range of past drought events. The vulnerability results along with climate model information were helpful for adopting water management options for long and severe drought.

Ahmadalipour and Moradkhani (2018) performed comprehensive assessment to evaluate the drought vulnerability in 46 African countries. Authors considered six different components (economy, energy, infrastructure, health, water resources, land use, society) and introduced a composite Drought Vulnerability Index (DVI) for each country. After checking the accuracy of DVI through various analysis, the regression models were fitted to the DVI for historical time series and were extrapolated for future time series to project DVI. The outcomes indicated an increase in the difference between low and highly vulnerable countries in future. Authors suggested that the DVIs can be used in long term drought risk analysis.

A regional based drought risk evaluation method was established in Heilongjiang in China to rank the drought risk. In this study, Liu et al. (2019) evaluated the drought risk based on remote sensing drought monitoring and uncertainty method.. They also used the most suitable drought monitoring model namely Temperature and vegetation polynomial model (TVPM). For introducing the uncertainty method, they applied statistical based interval weight determination of evaluation index method. Interval number sorting method was used to establish drought risk evaluation model.

Drought being the most serious disaster to cause severe agricultural damage has become a major threat to global food security. Therefore, Guo et al. (2021) attempted to simulate the growth of rice in future time period under different scenarios by using Environmental Policy Integrated Climate (EPIC) model. Authors used drought intensity and rice physical vulnerability curve to evaluate the global rice yield risk to drought. The results showed an average expected loss rate of 13.1% (± 0.4%) in global rice yield in future. Also, the fluctuation in rice drought risk and the area under rice yield risk will increase in future.

Li et al. (2022) focused on the rural areas for evaluating the drought risk and water resources allocation. Authors used SPEI drought index and computed drought duration, and severity based on run theory. They established the vulnerability curves based on loss data, and evaluated the risk of the cultivated areas, rural population and primary industry. From results, it was observed that the rapid increment in green areas increased the ecological water consumption. Subsequently, a high-risk level of drought was noticed in southern areas.

Similar to the above studies, there are many investigations on drought risk evaluation to help the policy makers, risk division and management. These include, but are not limited to Wu and Wilhite (2004), Pandey et al., (2010), Pulwarty and Sivakumar (2014), Blauhut et al. (2015), Chang et al. (2016), Tsakiris (2017), Frischen et al. (2020), Meza et al. (2020), Omer et al. (2021), Ma et al. (2022), Savari et al. (2022) .

2.6 Multivariate Analysis

Copula based multivariate analysis was developed by Sklar (1959). According to the Sklar's theorem, copula techniques are advantageous as they provide significant flexibility in modelling the dependence structure between two or more random variables having independent marginal distributions. There are two copula families: Elliptical family (Gaussian and Student's t-copula) and Archimedean family (Clayton, Gumbel, and Frank). In the realm of hydrology, the use of copula to analyse the hydrological extreme is extensive. For example

Favre et al. (2004) attempted to model multivariate extreme values based on copula theory. They tried on two different problems: first to find out the combined risk in the framework of frequency analysis; second to model peak flows and volume jointly. From results, they found copula as a promising way to apply in hydrology because of its applicability in wide range of correlation.

Kao and Govindaraju (2008) used trivariate copula for analysing extreme rainfall events. The trivariate copula family was applied to study the temporal distribution of extreme rainfall events in Indiana, USA. Subsequently, conditional probability of peak intensity, time to peak, percentage cumulative rainfall at 10% cumulative time increment were evaluated based on rainfall depth and duration. The obtained results suggested that the constant cross-product ratio theory can be applied to both discrete and continuous random variables.

Zhang et al. (2015) investigated the uncertainties in copula analysis resulted from the selection of marginal distribution and copula type. Thus, authors analysed hydrological drought events based on Bayesian approach in East River Basin, China. They evaluated the credible intervals of drought events with 20 years return period in terms of drought duration and severity. Moreover, it was found that stronger the heavy-tailed marginal distribution, greater the uncertainty.

In order to investigate the concurrent hydrological drought events to understand the inherent mechanism of hydrological extremes, Zhang et al. (2017) utilised copula functions. Here, authors selected the best suitable copula from Bayesian copula selection approach and the appropriate marginal distribution on the basis of AIC values. They evaluated the joint probability of concurrent drought between lake and river and observed the intensified concurrent drought occurrence in spring, summer and autumn.

A non-stationary frequency analysis of annual extreme rainfall using Archimedean copula was performed by Li et al. (2019) at four study regions in eastern coastal China. The rainfall volume and intensity were considered as two index variables. The time dependent copula function and GEV distribution were used model the joint and marginal distribution, respectively. From results, they observed the intensifying tendency of extreme rainfall volume and intensity.

Ballarin et al. (2021) compared univariate and multivariate approach to characterize extreme meteorological drought events for both past and future time series under different scenarios. They observed a significant increasing trend for temperature and intense drought events in future for both approaches. Authors found that the univariate approach could underestimate the risk associated with extreme events as it did not account the expected warming condition.

Likewise, there are many recent studies based on copula to examine the properties of droughts (J. Das et al., 2020a; Favre et al., 2004; Ganguli and Reddy, 2014; Hao and AghaKouchak, 2013; Kao and Govindaraju, 2010), and floods (Grimaldi and Serinaldi, 2006; Li and Zheng, 2016; Papaioannou et al., 2016; Tosunoglu et al., 2020). Apart from hydrologic extremes, copula has been used to model the characteristics of other extreme events such as heat waves (Mazdiyasni et al., 2019), concurrent occurrence of different climate extremes, known as compound extremes (Manning et al., 2018; Zscheischler and Seneviratne, 2017). However, the application of multivariate analysis in agrometeorological studies is relatively recent. For

instance, Bokusheva et al. (2016) and Madadgar et al. (2017) used joint distribution of rainfed agricultural crops and drought condition over Kazakhstan and Australia, respectively.

2.7 Future projection

The fact that the extreme weather events (e.g., extreme precipitation, heat waves) have become increasingly frequent all around the globe (Kundzewicz and Kaczmarek, 2000; Mazdiyasni et al., 2017), was well understood and witnessed during the latter part of the 20th century and early 21st century (IPCC, 2014). Among all the climate extremes, detection and quantification of drought events are complex. The analysis of drought can be carried out at short and long-term scales. The short-term forecast helps in providing the advisory to the farmers regarding the suitable crop cultivations and reallocation of water resources among the states (Bisht et al., 2019). In this light, numerous studies have been carried out around the globe in terms of different future drought characteristics. For example

Hanson and Weltzin (2000) discussed about the drought disturbances in future predicted drought conditions and their impacts on soil water availability to forests under climate change. They revealed several conclusions regarding the sensitivity of forests to future drought such as reduction in net primary production, mortality of stature plants etc. They also suggested that the regional scaled climate prediction along with higher temporal resolution and field-based experiments would be better for predicting the response of different forest regions to climate change.

Burke et al. (2010) evaluated the drought events during 20^{th} century and future time series to identify any potential future changes due to increased greenhouse gases. They computed precipitation indices and soil moisture index for different time scale. They considered outputs from Hadley Centre regional climate model (HadRM3) for future drought analysis. They found significant difference in soil moisture between model and reference data. Authors performed non-stationary extreme value theory to monthly indices to project future drought events. All drought indices showed an increment in drought occurrences in future time series.

Rajsekhar et al. (2015) conducted study on the possible changes in drought properties under the changing climate. They considered downscaled and bias-corrected data from five GCMs and a multivariate Drought Index to conduct the drought analysis in future time series.

Authors identified the spatial patterns of drought properties and the distribution of potential drought hazard areas. Drought vulnerability assessment and composite drought risk maps were also developed to achieve an effective drought mitigation strategy.

Lehner et al. (2017) investigated drought risk and aridity under the impact of climate change scenarios. They utilised a set of simulations from the Community Earth System Model targeting 1.5^{o}C and 2^{o}C. A small change in drought risk was found in U.S. Southwest and central plains, when warming was limited to 2^{o}C. However, a significant increase in drought risk was recognised in Mediterranean and central Europe under both 1.5^{o}C and 2^{o}C.

Martin (2018) used the outputs from 24 CMIP5 models to project duration and severity of drought events using 6-month SPI. More frequent, long lasting drought events are projected in dry regions. Projection of severe drought events and duration suggested an increasing trend over wetting region. Author stated that the projected drought characteristics has significant implications for planning and resilience.

Cook et al. (2020) analysed the drought condition incorporating future projections of precipitation, soil moisture and runoff from Phase Six of the Coupled Model Intercomparison Project (CMIP6). They found robust drying in the mean state in most of the parts by the end of 21st century based on multi-model ensemble. The regional hotspots with strong dryness were identified in western North America, Central America, Europe and the Mediterranean, China, Australia, southern Africa, Southeast Asia, Amazon. Moreover, some regions showed an increment in extreme drought risk by 200-300% compared to historical period. Authors also identified severe and extensive dryness in soil moisture and runoff compared to precipitation.

Prodhan et al. (2022) analysed the future drought and its impact on crop yield over South Asia based on ensemble machine learning approach. Authors considered CMIP6 global climate models and adopted SPEI drought index to characterise future drought. Moreover, they proposed non-linear ensemble of Random Forest (RF) and Gradient Boosting Machine (GBM) to evaluate the future risk of yield reduction under the impact of future drought. Results indicated high drought magnitude with longer duration, whereas high drought intensity with shorter duration. A high risk on yield loss under extreme drought condition in

future encounters 54.15%, 29.30% and 50.66% loss in rice, wheat, and maize crops respectively. Additionally, several past studies have examined the meteorological and hydrological droughts incorporating the future projections from GCMs under the Coupled Model Intercomparison Project 3 (CMIP3) and 5 (CMIP5) across the globe. For instance, over Europe (Spinoni et al., 2018; Thober et al., 2015), over United States (Ahmadalipour et al., 2017; Keellings and Engström, 2019), over China (Cao and Gao, 2019; Yao et al., 2020), over India (Bisht et al., 2019; Gupta and Jain, 2018), over Australia (Johnson and Sharma, 2015), over the globe (Spinoni et al., 2020; Ukkola et al., 2018).

2.8 Concluding remarks

This chapter presents an overview of non-stationary analysis, its importance in drought characterization, propagation, risk and drought projection under climate change. Based on the discussion regarding non-stationarity analysis, it is understood that the non-stationarity behaviour due to the changing climate cannot be ignored in the analysis of natural hazards. The literature are mostly based on the comparison between stationary and non-stationary analysis in different hydrological extremes. The comparative analysis comes up with the superiority of non-stationary analysis over stationary analysis in most of the regions in capturing the occurrences of extreme events appropriately. Non-stationary analysis can be conducted with the use of different statistical methods incorporating various physical covariates. Therefore, this thesis initially aims at examining the better model between stationary and non-stationary modelling in the study area for identifying the drought occurrences. Further, the literature focuses on the characterization of different droughts based on both univariate and multivariate indices. The significance of different drought indices for characterizing specific types of droughts are discussed for both stationary and non-stationary analysis. With this understanding the next part of the thesis examines the evaluation different drought properties like severity, duration, frequency for meteorological, hydrological, agricultural, and socio-economic drought in India.

Based on the literature regarding the drought propagation from one type to another along with internal drought propagation, it is crucial to understand the reason behind the transformation of drought through hydrological system. The literature suggests the reflectance of drought characteristics on drought propagation and about the significance of different controlling factors on drought propagation. Therefore, one part of thesis is assigned to the investigation of

drought propagation from meteorological to hydrological and agricultural drought along with internal drought propagation for each drought under both stationary and non-stationary approach. Literature based on drought risk and vulnerability suggest the necessity of evaluating the drought risk for adopting better drought management strategies. Specifically, the evaluation of agricultural drought risk which affects the global food security system is of paramount importance. Further, the studies on copula based multivariate analysis show its widespread application on hydrological system. Therefore, part of thesis is devoted to the computation of agricultural probabilistic drought risk for four major crops based on copula theory in the study area.

It is expected that drought risk is likely to increase in the twenty-first century. Additionally, literature related to the future projection of drought provide the evidence of the increment in drought occurrences in future time series under different climate change scenarios. Hence, the last part of thesis focuses on the evaluation of meteorological drought properties and identification of drought hotspot regions for different time scales under different climate change scenarios. Moreover, seasonal drought analysis for pre-monsoon, monsoon, post-monsoon, Kharif and Rabi is performed to evaluate severity-area-frequency relationship curve.

Chapter 3

Non-stationary modelling of drought

3.1 Introduction

As discussed in Chapter 1, the drought can be linked to the deficiency of the streamflow, soil moisture, agricultural productivity, and socio-economic conditions (Huang et al., 2016; A.K. Mishra and Singh, 2010; Wilhite and Glantz, 1985; X. Zhang et al., 2017). Different types of droughts (e.g., meteorological, hydrological, agricultural, and socio-economic) put enormous pressure on water availability, water demand, and agriculture. In this sense, the adverse consequences of drought affect socioeconomic status and subsequently increase economic risk and financial challenges. For instance, in an agrarian country like India, 50% of the total agricultural land (i.e., 68% of the total area) is highly susceptible to frequent severe drought conditions affecting about 50 million people annually (Dutta et al., 2013).

Due to the effects of climatic variability and anthropogenic perturbations, it is postulated that the frequency of drought hazard will increase in coming decades (Li et al., 2013a; Villarini et

al., 2011; Wang et al., 2015a). Most drought events in India are due to the low summer monsoon precipitation as a result of climate change or natural variability (Mishra et al., 2012; Roxy et al., 2015). While analyzing the relationships between droughts and natural variability like El Niño-Southern Oscillation (ENSO) during the period 1871–1999, WMO (1999) reported that 11 out of 21 drought events occurred during the El Niño years in the period 1871–1988. However, in the twenty-first century, the association between the two phenomena appears to have strengthened as three out of four El Niño years resulted in Indian droughts over the last 14 years (Saini and Gulati, 2014). Therefore, in India, comprehensive evaluation and periodic assessment of the characteristics and adverse impact of droughts is necessary for adaptation and mitigation (Aadhar and Mishra, 2017; Shah and Mishra, 2015).

Despite the lack of a precise definition of drought, several indexes exist for monitoring drought conditions (Li et al., 2015; WMO and GWP, 2016). The Palmer Drought Severity Index (PDSI) (Palmer 1965) and Standardized Precipitation Index (SPI) (Mckee et al. 1993) are commonly used to monitor precipitation-based meteorological droughts. Similarly, the Standardized Runoff Index (SRI) is used to monitor runoff- or streamflow-based hydrological droughts (Shukla and Wood 2008). Likewise, the Standardized Soil Moisture Index (SSI) and Agricultural Standardized Precipitation Index (aSPI) are widely used to monitor agricultural droughts (Hao and AghaKouchak, 2013; Tigkas et al., 2019). Many other drought indexes have been proposed that consider one or more climate variables, such as the Standardized Precipitation Evapotranspiration Index (SPEI) (Vicente-Serrano et al. 2010), Vegetation Drought Response Index (VegDRI) (Brown et al., 2008), Reconnaissance Drought Index (RDI) (Tsakiris and Vangelis, 2005), Multivariate Standardized Drought Index (MSDI) (Hao and AghaKouchak, 2014), and Evaporative Stress Index (ESI) (Anderson et al., 2007).

Understanding the importance of non-stationarity (as discussed in Chapter 1), the development of a non-stationary drought indices has gained significant momentum in recent years with the inclusion of various covariates in its computation. For example, large-scale climatic oscillations (Li et al., 2015; Rashid and Beecham, 2019), both large-scale climatic oscillations and human induced indexes (Wang et al., 2020b), and time (Bazrafshan and Hejabi, 2018; Park et al., 2019; Wang et al., 2015b) are used as covariates in modeling non-stationary droughts. However, the selected covariates and their selection procedure may vary. For instance, Li et al. (2015) selected large-scale climate indexes [e.g., Southern Oscillation Index (SOI), Atlantic Multidecadal Oscillation (AMO), North Atlantic Oscillation (NAO)]

based on a correlation analysis; Wang et al. (2020) computed the anthropogenic influence to incorporate as a covariate in the computation of non-stationary drought, based on the previous literature, and time was used as a covariate by Bazrafshan and Hejabi (2018).

The interannual and interdecadal variability in regional and global precipitation is closely linked to sea surface temperature (SST) and sea level pressure (Hu and Feng, 2001). Considering the time lag correlations between precipitation and climate oscillations, precipitation at monthly, seasonal, and annual scales can be predicted (He and Guan, 2013; Peng et al., 2014). Understanding the important linkage between large-scale climatic indexes and hydrometeorological variables, researchers analyzed the different drought indexes under the influence of climatic oscillations. For instance, Meza (2013) modeled the SPEI drought index using ENSO over Northern Chile; meteorological drought indexes like the SPI are modeled using different climatic oscillation indexes over the Luanhe River Basin in China (Li et al. 2015); non-stationary modeling of the RDI over Iran (Bazrafshan and Hejabi 2018) and the SSI drought index over the Luanhe River Basin (Wang et al. 2020).

In a drought-vulnerable country like India, the analysis of drought in the context of a non-stationary approach is limited (Ganguli and Reddy 2013; Salvi and Ghosh 2016). Moreover, to the best of the authors' knowledge, in connection with drought prone areas like Maharashtra, drought events under the influence of large-scale climatic oscillations have not been analyzed. Therefore, to develop a new approach to drought identification and examine drought properties, non-stationary meteorological drought indexes incorporating large-scale climatic oscillations are developed for Maharashtra. Two different drought indexes, SPI and RDI, are considered for the analysis. Large-scale climatic oscillations like the Indian Summer Monsoon Index (ISMI), the SOI, SST, and Indian Ocean Dipole (IOD) are used as covariates. The reason behind the selection of the climatic oscillations is discussed in the Section 3.2. The Generalized Additive Model in Location, Scale and Shape (GAMLSS) package in the R environment.

3.2 Study area and data used

3.2.1 Study area

To analyze and model non-stationary meteorological drought events at different time scales, Maharashtra is selected as the study area. Maharashtra lies between and 15° 61'E–22° 03'E

latitude and 72° 64'N–80° 90'N longitude. It covers an area of around 3,07,713 km^2 and is the third largest state in India. The state consists of six administrative divisions, namely Konkan, Pune, Nashik, Aurangabad, Amaravati, and Nagpur. The average elevation of the study area is 1,200 m above mean sea level. Annual precipitation over the study area varies between 512 and 3,765 mm, with an average of 1,133 mm during 1951–2013. In the period of 1901-1998, 26 meteorological droughts have been identified and 11 droughts out of those affected more than half of the state. Moreover, in 2013, 11801 villages were affected by a worst drought occurred in last 40 years in Maharashtra. The maximum temperature varies between 37°C and 46°C during summer and the minimum temperature between 3°C and 12°C during winter (1951–2013). Rainfed agricultural activity is the primary source of income for about 64% of the total population, and the state contributes about 15% of the country's gross domestic product (GDP) (P. D. Udmale et al., 2014). However, there exists a significant spatial variability of the precipitation from western (mostly wet) to eastern (mostly dry) parts of Maharashtra. A detailed representation of the study area is shown in Figure 3.1.

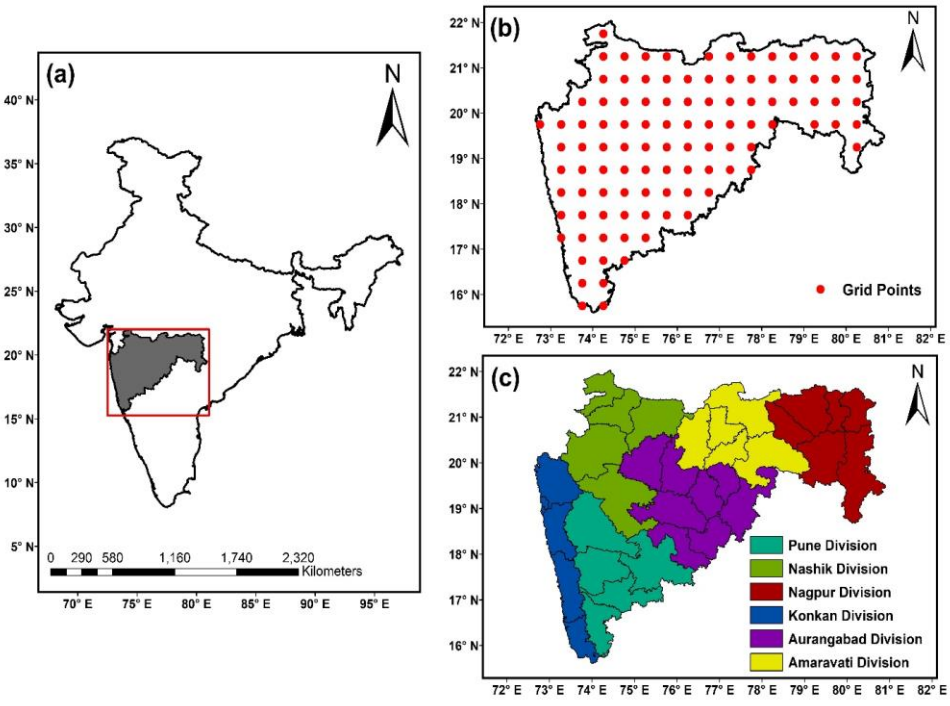

Figure 3.1: Description of the study area. (a) location map of Maharashtra superimposed over India map; (b) 103 grid points at a resolution of 0.5^o x 0.5^o over Maharashtra; (c) six different divisions of Maharashtra state

3.2.2 Observational datasets

The daily precipitation and temperature (maximum and minimum) data sets for this study are obtained from the India Meteorological Department (IMD), Pune, for the period 1951–2013. The original data are available at spatial resolution 0.25° × 0.25° and 1° × 1° for precipitation and temperature, respectively. The precipitation datasets are derived based on 6,955 rain gauge stations (Pai et al., 2014), and temperature data sets are prepared based on the 395 quality controlled temperature stations (Srivastava et al., 2009). The datasets can be obtained from https://www.imdpune.gov.in/Clim_Pred_LRF_New/Grided_Data_Download.html. To simplify the analysis and interpretation of the outcomes, the precipitation and temperature data sets are brought to a common grid point of 0.5° × 0.5° spatial resolution in this analysis. In addition to the precipitation and temperature data, wind speed, and cloud cover data are downloaded from the National Centers for Environmental Prediction (NCEP) reanalysis products (https://www.esrl.noaa.gov/psd/data/gridded/data.ncep.reanalysis.html). The spatial resolution of wind speed and cloud cover is brought to a common grid point as precipitation and temperature points using bilinear interpolation during 1951–2013. The bilinear interpolation is performed using the built-in function in "Raster" package in R environment. Here, the bilinear interpolation method is chosen among different interpolation methods as it is easy to use and apply when the source and destination grids are rectilinear (Jones, 1999). In addition, this method is suitable for continuous variables. In the bilinear method, the value at targeted grid point is interpolated from the values of the four nearest grid values. In other words, the weighted average of the four values corresponding to the four nearest grids is computed. The weights are determined by the distance between the target grid and other grids. The grid near to the target grid gets more weight and vice versa. The wind speed and cloud cover data sets are used to compute the potential evapotranspiration (PET) series, which will be further used to compute RDI at different time scales.

Table 3.1: Details of the datasets used in the present study

Dataset	Temporal Resolution	Spatial Resolution	Source
Precipitation	1951-2013 (Daily)	0.25° × 0.25°	IMD
Temperature	1951-2013 (Daily)	0.5° × 0.5°	IMD
Cloud cover	1951-2013 (Monthly)	2.5° × 2.5°	NCEP
Wind Speed	1951-2013 (Monthly)	2.5° × 2.5°	NCEP

3.2.3 Climate covariates and its association

3.2.3.1 Indian summer monsoon index (ISMI)

Most precipitation across India occurs during the monsoon season (i.e., June–September), which is modulated by the Asian summer monsoon and mainly due to the Indian summer monsoon. The Asian summer monsoon is one of the most energetic components of the Earth systems driven by convective (most important), radiative, and sensible heat sources/sinks (Wang et al., 2001). As a result of the boreal summer, two different convective regions are observed, one over the Bay of Bengal–India–Arabian Sea region and the other over the South China Sea and Philippine Sea region. The former is mainly responsible for the Indian summer monsoon, while the latter mostly accounts for the East Asia summer monsoon. In addition, previous studies found a possible connection between monsoon indexes with precipitation variability in China (Chang et al., 2019) and India (J. Das et al., 2020b). Therefore, the ISMI is a good indicator of the strength of monsoon precipitation over India, and the ISMI is used in a very limited way to analyze the characteristics of meteorological droughts. The ISMI is defined as the difference in the zonal winds at 850 hPa over (40°E–80°E, 5°N–15°N) and (70°E–90°E, 20°N–30°N). Because the wind variation at 850 hPa reflects the variation in convective heating compared to upper-level circulation, 850 hPa is used to compute the ISMI (Wang, 2000). In this context, the use of ISMI as a covariate for analyzing meteorological droughts is reasonable. ISMI dataset can be downloaded at http://apdrc.soest.hawaii.edu/projects/monsoon/seasonal-monidx.html.

3.2.3.2 Southern oscillation index (SOI)

The SOI is generally used to characterize the ENSO and is defined as the standardized sea-level pressure difference between Tahiti and Darwin, Australia (Cavazos and Rivas, 2004). The negative and positive values of SOI specify El Niño and La Niña episodes, respectively. These episodes exert a significant influence on the precipitation variability across the globe, so variations in the ENSO affect the perceptions about changes in drought (Gu et al., 2007; Hoerling et al., 2010; Trenberth, 2011; Trenberth et al., 2014). In particular, the ENSO phenomenon causes 6.3% of global precipitation variance and helps in explaining the variability in climate over the Northern Hemisphere (New et al., 2001). For instance, during El Niño episodes, there are major droughts over Southeast Asia, Australia, Brazil, Indonesia, and some parts of Africa (Trenberth et al. 2014). In India, because the summer monsoon is

largely affected by ENSO events (Roy, 2017; Turner et al., 2005), drought years are usually aligned with El Niño episodes while La Niña episodes bring excess precipitation to the country (Roy et al., 2019). Moreover, in a recent study, Agilan and Umamahesh (2018) identified the SOI as the suitable ENSO index to model extreme precipitation during monsoon and non-monsoon periods over India. Therefore, the SOI has been introduced as a climate covariate for modeling the non-stationarity in the different types of drought events (Li et al., 2015; Rashid and Beecham, 2019; Wang et al., 2020b). The monthly data of SOI can be downloaded from https://crudata.uea.ac.uk/cru/data/soi/.

3.2.3.3 Sea surface temperature (SST)

The variation in the SST, generally referred to as the SST anomaly (SSTA), has a pronounced effect on atmospheric climate (Mamalakis et al., 2017). In addition, Alexander et al. (2009) advocated that SSTA is considered one of the main ENSO indexes, and therefore, SSTA is likely to modify the precipitation and temperature variability around the globe. Many researchers have linked a precipitation anomaly with the SSTA, for example, in China (Yang et al., 2017b), the East Asian summer monsoon (Hu and Duan, 2015), the Indian summer monsoon (Chattopadhyay et al., 2015), and in Europe (Ionita et al., 2015). Likewise, it is well established that the SSTA is one of the major causes of the drought that prevails in many places around the world, for example, Canada (Shabbar and Skinner, 2004), the United States (McCabe et al., 2008), Europe (Ionita et al., 2012), and India (Niranjan Kumar et al., 2013). Therefore, selecting the SSTA as an explanatory variable in modeling the non-stationary drought index is reasonable . The monthly mean SSTA data sets as compared to 1981–2010 mean over NINO3.4 (17°E-120°W, 5°S-5°N) region can be downloaded from https://www.cpc.ncep.noaa.gov/data/indexes/.

3.2.3.4 Indian ocean dipole (IOD)

The IOD, in the tropical Indian Ocean, was just recently discovered and quantified with the Dipole Mode Index (DMI) (Saji et al., 1999). The IOD is characterized by the SST difference between the tropical western Indian Ocean (50°E–70°E, 10°S–10°N) and the tropical south-eastern Indian Ocean (90°E–110°E, 10°S–Equator) (Saji et al. 1999). The IOD is a coupled ocean–atmosphere phenomenon like ENSO, and the variability in the SST contributes to the variations in rainfall and storm activities of many countries surrounding the Indian Ocean (Paul and Rashid, 2017). In addition, studies show that the IOD makes a significant

contribution to modulating southwest (Ashok and Saji, 2007) and northeast (Geethalakshmi et al., 2009) monsoon precipitation. Some studies have indicated an association between the IOD and drought events across the globe (Forootan et al., 2019; Ummenhofer et al., 2011; Xiao et al., 2016). Moreover, a recent study postulates that with the increasing amount of greenhouse gases, the frequency of IOD events is likely to increase (Cai et al., 2014). Therefore, the IOD was selected as one of the covariates for non-stationary modeling of meteorological drought over Maharashtra. The DMI datasets are collected from https://psl.noaa.gov/gcos_wgsp/Timeseries/DMI/. It should be noted that the ISMI, SOI, SST, and IOD data sets were collected for the period 1951–2013.

Table 3.2: Details of the covariates used in the present study

Climate indices	Temporal Resolution	Sources
ISMI	Monthly	http://apdrc.soest.hawaii.edu/projects/monsoon/seasonal-monidx.html
SOI	Monthly	https://crudata.uea.ac.uk/cru/data/soi/
IOD	Monthly	https://www.cpc.ncep.noaa.gov/data/indexes/
SST	Monthly	https://psl.noaa.gov/gcos_wgsp/Timeseries/DMI/

3.3 Methodology

Initially, the monthly hydro-meteorological variables are cumulated according to different time scales. The large-scale oscillations are arranged based on different lag values. The Kendall tau correlation test is performed between the monthly cumulated hydro-meteorological variables and lag wise arranged climatic oscillations. The best lag is computed at a significance level of 5% at each grid point. Next, the suitable distribution is fitted with and without considering the oscillations values with selected lag. The best fit model is selected based on AIC value and the drought indices are computed by transforming the cumulative probability of fitted distribution to standard normal values.

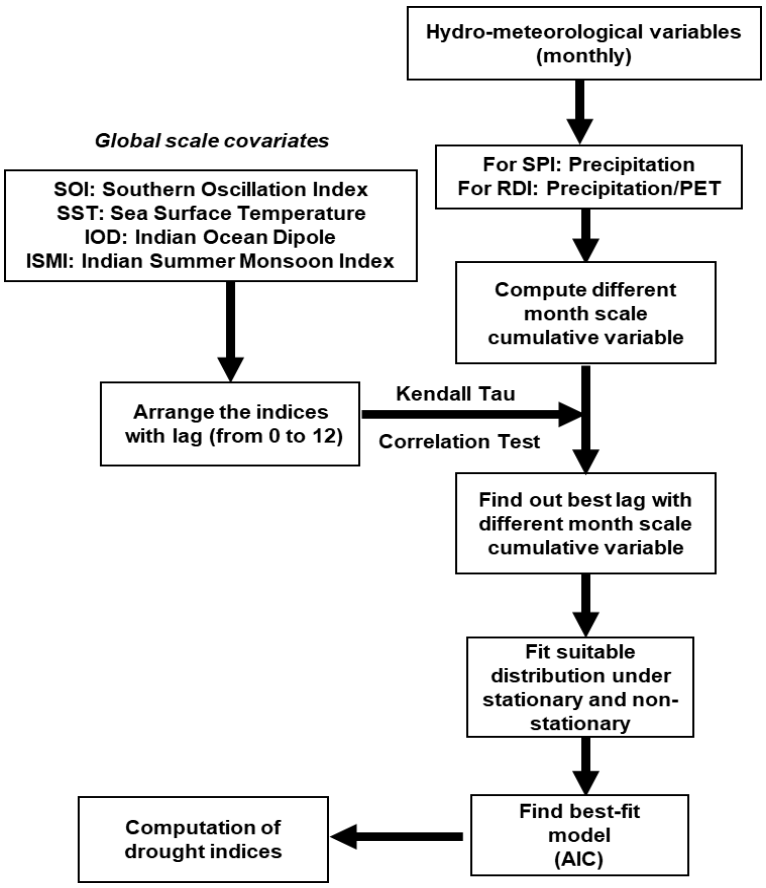

Figure 3.2: Methodological framework for the proposed study

3.3.1 Computation of SPI

The datasets discussed in Section 3.2 are collected for the period 1951-2013. At a spatial resolution of 0.5^o x 0.5^o, the number of grid points covering the state is 103 [Figure 3.1(b)]. At each grid point, the monthly precipitation series is extracted by accumulating the daily precipitation data and then the cumulative precipitation for different time periods (3-, 6-, 9-, 12-, 24- month time scales) is computed using Equation 3.1. Let, $x(t)$ represents monthly precipitation at time t, and for a time scale of m months, the cumulative precipitation $x_m(t)$ is presented as follows.

$$x_m(t) = \sum_{i=t-m+1}^{t} x(i) \tag{3.1}$$

The traditional SPI drought index is computed by fitting a two-parameter gamma distribution to the cumulative precipitation for different time periods and denoted as $x_m(t) \sim \text{gamma}(\mu,\sigma)$. The probability density function (PDF) of Gamma distribution is presented by

$$f(x_m(t) \mid \mu, \sigma) = \frac{1}{(\sigma^2 \mu)^{1/\sigma^2}} \frac{x_m(t)^{\frac{1}{\sigma^2}-1} \exp[-(x_m(t))/(\sigma^2 \mu)]}{\Gamma\left(1/\sigma^2\right)}; x_m(t) > 0, \mu > 0, \sigma > 0 \quad (3.2)$$

where, location and scale parameters are defined by μ, and σ, respectively, and Γ represents Gamma function. The cumulative probability of $x_m(t)$ is then transformed to standard normal values with mean 0 and standard deviation 1 (Abramowitz and Stegun, 1965). The transformed values are called as SPI for the particular series of precipitation. In this case, the distribution parameters are assumed to be stationary. However, to model/ incorporate the influence of climate change signals, the parameters of the distribution need to be time-variant (Russo et al., 2013) and hence, non-stationary modelling is necessary.

3.3.2 Computation of RDI

Unlike SPI, the computation of RDI involves two climate variables precipitation and potential evapotranspiration (PET). The PET is computed using the Penman-Monteith method (Penman, 1948) as it is regarded as the most suitable method to encompass climate change (Liu and Yang, 2010). The R package SPEI is used to evaluate PET at each grid point. The minimum climatic and geographical components required for the computation of PET in the above-said package are temperature, wind speed, cloud cover, latitude, and elevation at each grid point. The elevation at each grid point is extracted from the digital elevation map (DEM) at a spatial resolution of 90m from http://srtm.csi.cgiar.org/ (last accessed on 01st December 2019). Initially, the ratio of precipitation to PET accumulated for a given time window is evaluated. The ratio is called as the initial value (i.e., α_o) of RDI (Bazrafshan and Hejabi, 2018) and determined by,

$$\alpha_o(l) = \frac{\sum_{k=1}^{k=l} P_k}{\sum_{k=1}^{k=l} PET_k} \quad (3.3)$$

where $\alpha_o(l)$ represents RDI value for the aggregation time l, P_k and PET_k are the precipitation (in mm) and potential evapotranspiration (in mm) of the *kth* month of the year, l is the aggregation time window (in months and in the present case the aggregation time windows are 3-, 6-, 9-, 12-, and 24- months), k defines the month number over a time window.

Therefore, PET_k defines the cumulative PET from the month $k=1$ to $k=l$. For instance, if the starting month is June, then $k=1$ refers to the month of June. Then, the initial value is fitted with the lognormal distribution, and the PDF of the lognormal distribution is presented as

$$f(\alpha_o(l) \mid \mu, \sigma) = \frac{1}{\alpha_o(l)\sigma\sqrt{2\pi}} \exp\left[-\frac{1}{2\sigma^2} (\log(\alpha_o(l) - \mu)^2 \right]; \quad \alpha_o(l) > 0, \mu \sim (-\infty, +\infty), \sigma > 0 \tag{3.4}$$

where, location and scale parameters are defined by μ, and σ, respectively. The cumulative probability of $\alpha_0(l)$ is then transformed to standard normal values with mean 0 and standard deviation 1. The transformed values are called RDI for the particular series of initial values. However, for more extended period or in the context of climate change, the parameters of the probability distribution may vary with respect to time. Hence, drought characterisation under the influence on climatic variability is of paramount importance. The classification and the threshold values for drought identification according to SPI and RDI are presented in Table 1.

Table 3.3: Classifications and the associated ranges for SPI & RDI values (stationary and non-stationary)

Classification	Range	Category
Extreme Wet	SPI/RDI ≥ 2.00	EW
Severe Wet	1.5 ≤ SPI/RDI < 2.0	SW
Moderate Wet	1.0 ≤ SPI/RDI < 1.5	MW
Near Normal	-1.0 ≤ SPI/RDI < 1.0	NN
Moderate Drought	-1.5 ≤ SPI/RDI < -1.0	MD
Severe Drought	-2.0 ≤ SPI/RDI < -1.5	SD
Extreme Drought	SPI/RDI < -2	ED

3.3.3 Non-stationary modelling of drought indices

3.3.3.1 Selection of large-scale climate oscillations

In this study, four large-scale climate indexes (ISMI, SST, SOI, and IOD) are selected to indicate climate anomalies. The measurements of the climate indexes usually exhibit sporadic disturbances (Wang et al., 2020). Therefore, it is necessary to smooth the data series through

moving average by continuously averaging over n samples. Moreover, the moving average will minimize the effect of outliers in the statistical models and reduce the monthly random variability. In the present study, the n value corresponds to the time scale of droughts, i.e., 3, 6, 9, 12, and 24 months. After smoothing the series at various n values, the large-scale climate indexes are arranged according to different lags. It should be noted that the lag varies from 0 to 12. Next, a correlation analysis is carried out between the arranged large-scale climate indexes (for all lags) and the obtained cumulative precipitation using Equation 3.1. Generally, Kendall and Spearman correlation tests are used to examine the possible teleconnection among the hydrological variables and climate patterns (McCormick et al., 2009; Niu et al., 2014). In this study, to verify the best lag and best large-scale climate indexes at each grid point, the Kendall correlation test was used at a significance level of 5%. For a more detailed description of the Kendall test, interested readers are advised to consult (Kendall, 1955). The obtained appropriate large-scale climate indexes and their best lag at each grid point are considered as a covariate for that grid point. It is worth mentioning that the correlation analysis is performed for both the SPI and RDI at all 103 grid points.

3.3.3.2 Computation of non-stationary drought indices

In this study, to perform a non-stationary analysis of SPI and RDI, a GAMLSS package (Rigby and Stasinopoulos, 2005a) is used. This package is extensively used in a non-stationarity framework in hydrological applications (Villarini et al., 2010). Moreover, in comparison with other methods, like maximum likelihood (ML) and a two-stage method based on weighted least squares (TSWLS), it is found that GAMLSS outperforms these two methods in terms of flexibility and superior treatment of non-stationarity (Debele et al., 2017). GAMLSS is a semiparametric regression-type model that enables the user to introduce explanatory variables or random effects (i.e., covariates in this study) as a linear or nonlinear function with different statistical parameters (i.e., location, scale, and shape). For a detailed description of GAMLSS, the reader may consult Rigby and Stasinopoulos (2005) and Stasinopoulos and Rigby (2007). However, a brief description of the GAMLSS theory is presented here.

In this analysis, the datasets (x_i *for* $i = 1,\ 2,\ 3, ..., n-1,\ n$) are assumed to be independent and fitted with a distribution function as $F_x(x_i \mid \theta^i, where\ \theta^i = (\theta_{1i}, \theta_{2i}, \theta_{3i}, \theta_{4i}))$. For instance, in case of SPI, the accumulated precipitation series for different time scales are considered as

x_i. The matrix θ represents the parameters of the probability distribution, such as location, scale, shape, and kurtosis parameters. Hence, to find out the *kth* parameter (k=1, 2, 3, 4 for μ, σ, ν, τ, respectively) of a distribution associated with the explanatory variables/covariates through the monotonic link $g_k(\bullet)$ functions are defined as

$$g_k(\theta_k) = \eta_k = X_k \beta_k + \sum_{j=1}^{J_k} Z_{jk}(\gamma_{jk}) \tag{3.5}$$

where θ_k is the vector of length of dataset, β_k is the parameter vector of length J_k, the matrix of X_k is $n \times J_k$ and Z_{jk} is the non-parametric additive function of γ_{jk}. It is worth mentioning that the selected covariates for different aggregate time scales are varied linearly in the parameter of the selected distribution. Initially, the aggregated precipitation series at different time scales are fitted with the stationary gamma distribution separately for all the grid points. Next, the location parameter of the gamma distribution is described as a linear function of the selected covariates for all the grid points over Maharashtra. Similarly, in the case of RDI, the analysis is performed with the lognormal distribution. The selection of the best among stationary and non-stationary approaches is evaluated using Akaike information criterion (AIC) (Akaike, 1974). The minimum value of AIC corresponds to the optimal model. Therefore, the non-stationary model can be defined as follows:

For non-stationary SPI (SPI_N): $x_m(t) \sim Gamma(\mu_t, \sigma)$ (3.6)

For non-stationary RDI (RDI_N): $\alpha_o(t) \sim \log normal(\mu_t, \sigma)$ (3.7)

$$\mu_t = b_o + b_1 C_1(t) + b_2 C_2(t) + b_3 C_3(t) + ... + b_m C_m(t) \tag{3.8}$$

where, b_0, b_1, b_2, b_3, ……, b_m are regression constants and C_1, C_2, ……., C_m are the associated covariates. In GAMLSS, there are two algorithms for fitting the models, namely the CG algorithm (named after Cole and Green, 1992) and the RS algorithm (named after Rigby and Stasinopoulos, 1996). However, in the present study, the RS algorithm is used because it does not require an initial value of parameters to confirm convergence and the method is faster for large data sets. The cumulative probability of the gamma distribution (the same will hold for lognormal distribution) obtained after the non-stationary analysis is transformed into a standard normal variate to obtain the non-stationary SPI (SPI_N). The

classifications of the stationary and non-stationary drought indexes are presented in Table 3.1. In this study, -1 is considered as the threshold below which all events will be referred to as a drought. Therefore, the drought properties discussed in the next section are estimated based on the selected threshold.

3.3.4 Identification of drought properties

Several methods exist for identifying drought properties, such as the discrete Markov process, percentile method, run analysis, and others. Because run analysis (Yevjevich, 1967) has been generally used for this purpose (Mishra et al., 2009; Reddy and Ganguli, 2012), it will be applied in this study. In a run analysis, it is assumed that a drought is the sequence of values below a threshold. Here, three different drought properties, severity, duration, and peak, are analyzed using a threshold value of -1 for both SPI and RDI. A graphical representation of the different drought properties is depicted in Figure 3.3. From the figure, the duration is computed from the start of a drought event to the termination of the event. Therefore, in this case, the minimum length of the duration is 1 month. Subsequently, severity is computed as the cumulative magnitude of SPI during the particular duration. The minimum value of the SPI (and similarly in the case of the RDI) during the given duration is defined as the peak.

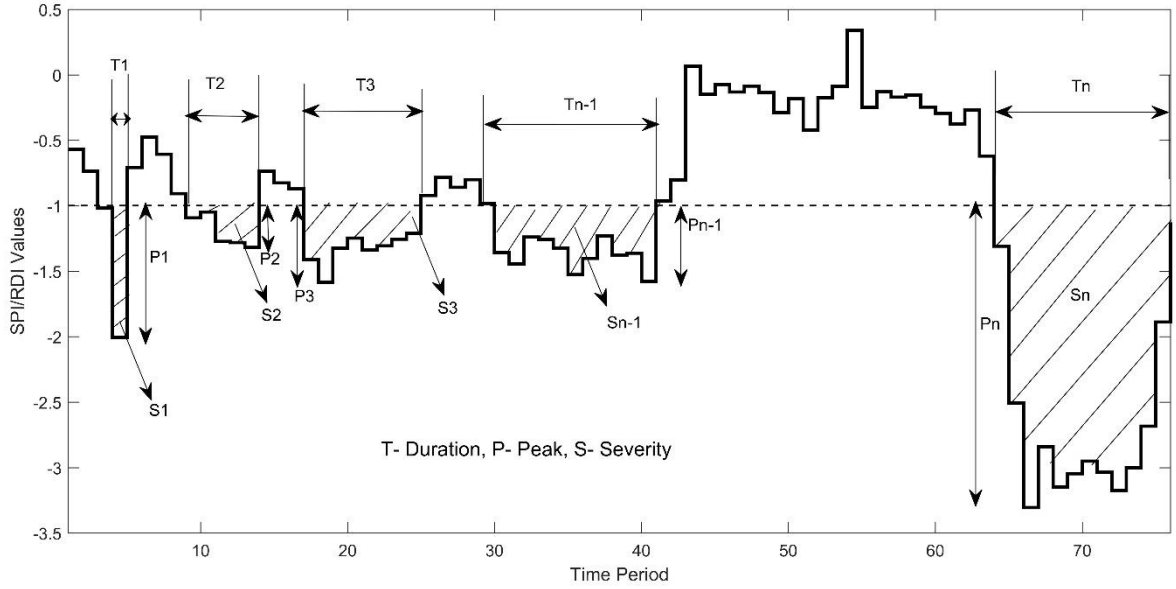

Figure 3.3: Graphical representation of the different drought properties such as Severity, Duration, and Peak. The dotted line represents the truncation level

3.4 Results

3.4.1 Spatio-temporal variability of meteorological variables

The spatiotemporal variabilities of meteorological variables, such as precipitation, mean temperature, and PET, are analyzed over the study area. The monthly mean during 1951–2013 is computed for all variables at each grid point. The spatial variability of each variable is plotted for each month, as shown in Figure 3.3, for monthly mean precipitation over the study area. Similarly, the spatio-temporal variability of average temperature and PET are depicted in Figure 3.4 and Figure 3.5, respectively.

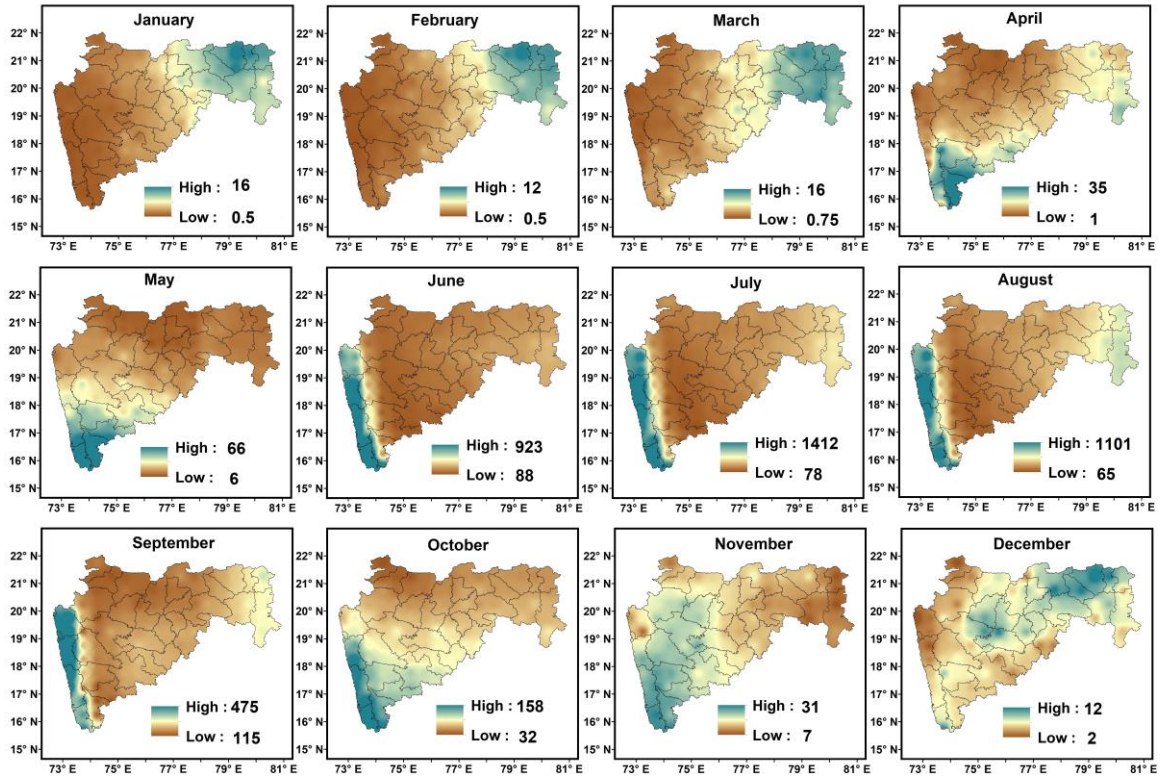

Figure 3.4: Spatio-temporal variability of mean monthly precipitation (in mm)

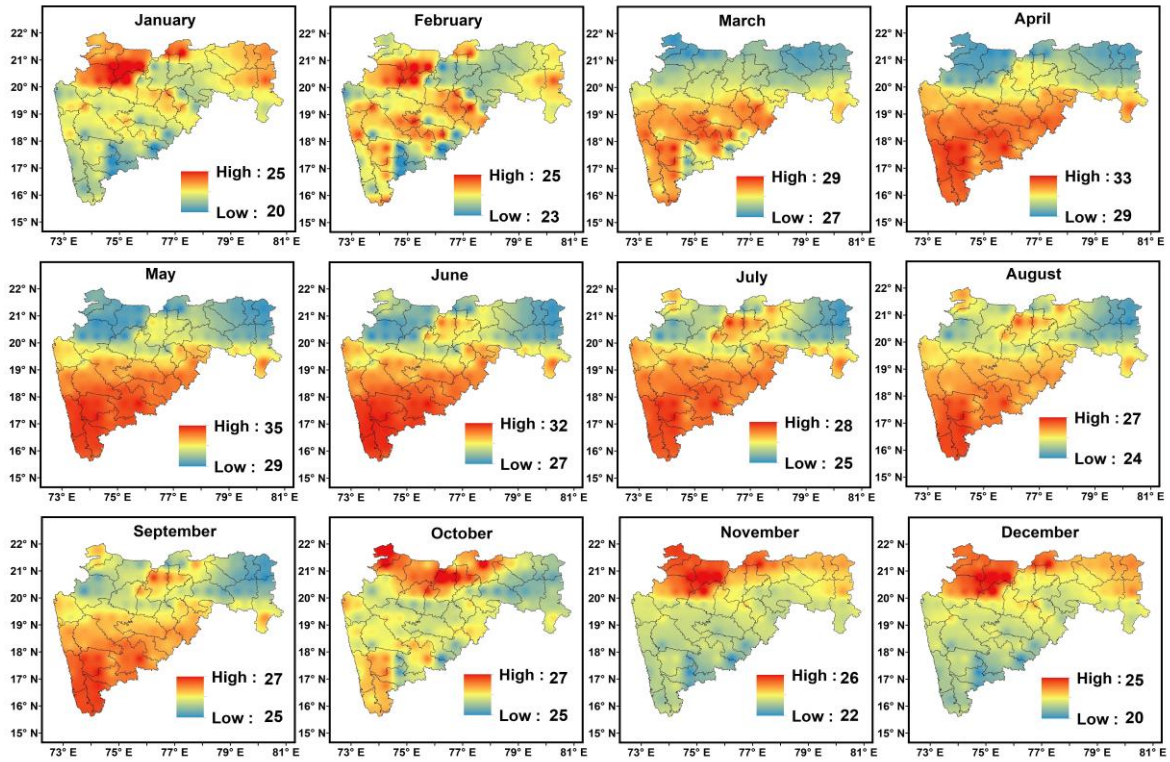

Figure 3.5: Spatio-temporal variability of mean monthly temperature (in ^{o}C)

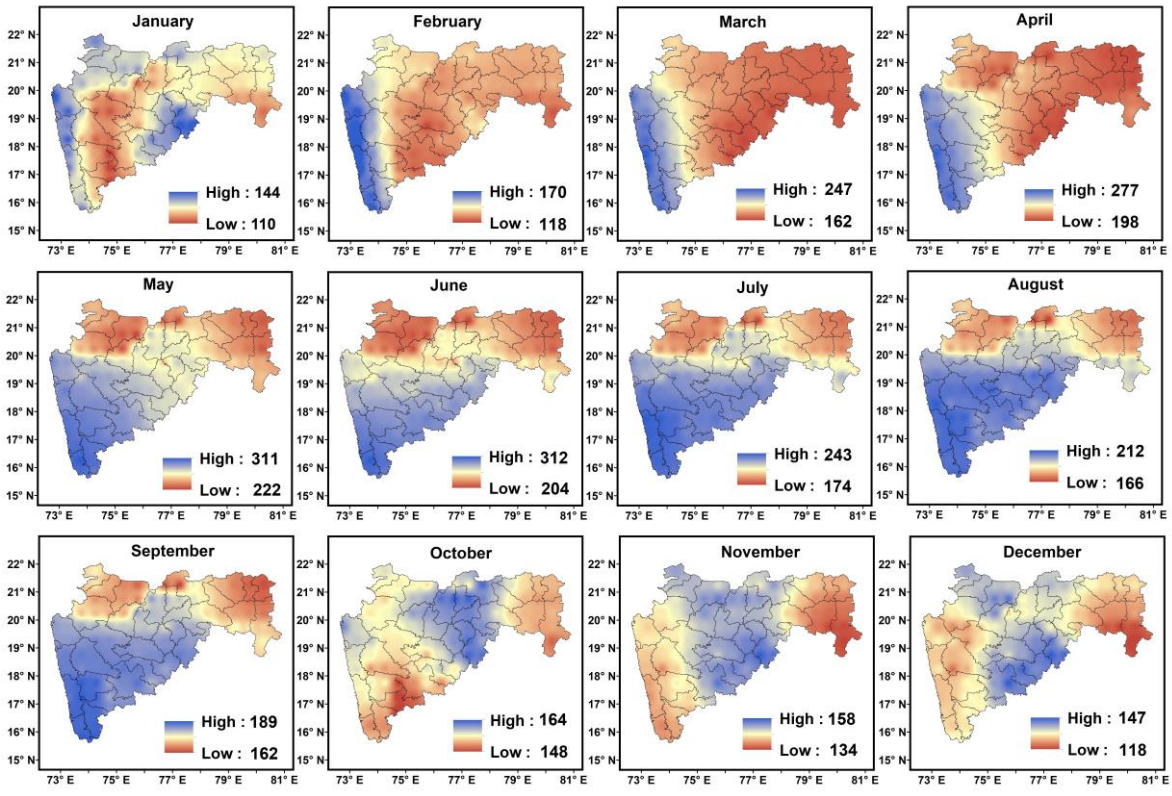

Figure 3.6: Spatio-temporal variability of mean monthly PET (in mm)

It can be observed from Figure 3.3 that during the monsoon season (i.e., June, July, August, and September) the Konkan division receives a high level of precipitation, while the central part of the Maharashtra state, such as the Nashik and Aurangabad divisions, receive much less rainfall. The results are similar to those obtained by Subash et al. (2011). The mean temperature variability over the study area (Figure 3.4) exhibits higher average temperature for 8 out of 12 months over Konkan, Pune, and Aurangabad divisions. Similarly, the average PET (Figure 3.5) over Konkan, Pune, and Aurangabad divisions is high from May to September. However, during November and December, a higher PET is observed over the Aurangabad division. Also note that in most cases, the mean temperature and PET trends are similar, suggesting the sensitivity of PET to temperature.

3.4.2 Comparison between non-stationary and stationary modeling

The non-stationary model is developed by linearly varying the climatic oscillations at the location parameter of the gamma (for SPI) and lognormal (for RDI) distributions. To develop the stationary model, the parameters are kept constant for the chosen distributions. To check the goodness of fit and to avoid model overfitting, the AIC is applied. The suitable lag of large-scale climatic oscillations is assessed using a Kendall correlation test at a significance level of 5%. The analysis is performed for all 103 grid points and different time scales. Since there are many grid points in the study, one grid point (i.e., 20.25 latitude, 75.25 longitude) is considered for further explanation. However, for the selected single grid point, the significant lags are presented in Table 3.2.

Table 3.4: Significant lag of different climatic-oscillations for different time scales at the reference point for non-stationary modelling of SPI & RDI

Climate Oscillations	*ISMI*	*SOI*	*SST*	*IOD*
Time scale	**SPI**			
3-month scale	0	-	-	12
6-month scale	0	-	-	-
9-month scale	0	-	7	-
12-month scale	0	9	8	10
24-month scale	0	-	5	12

Time scale	RDI			
3-month scale	0	-	-	12
6-month scale	0	-	-	-
9-month scale	0	-	8	-
12-month scale	0	9	8	9
24-month scale	0	0	6	12

It is observed from the analysis that for almost all grid points, the ISMI has a significant correlation at lag zero, i.e., the current year ISMI affects the precipitation of that particular year. The dash in the table denotes that there is no significant correlation for that particular time scale and those climatic oscillations. Then the different climatic oscillations corresponding to the identified significant time lags are selected as covariates to estimate location parameter of the frequency distribution fitted for the reference grid point. The AIC value is used as a comparative measure between the stationary and non-stationary analyses. Table 3.3 gives the AIC values obtained for the SPI and RDI on different time scales for the reference grid point.

Table 3.5: The computed AIC values at the reference point for both stationary and non-stationary approaches in case of SPI & RDI

Time scales	SPI		RDI	
	Non-stationary	Stationary	Non-stationary	Stationary
3-month scale	8221.64	9041.16	-1294.49	-431.89
6-month scale	9699.02	10401.52	-539.05	217.14
9-month scale	9831.50	10291.63	-1062.95	-504.98
12-month scale	9937.53	10043.23	-1433.54	-1307.20
24-month scale	10452.01	10513.71	-1836.60	-1671.78

From the AIC values obtained for all the grid points for stationary and non-stationary analysis, it is concluded that the non-stationary approach outperforms the stationary approach over all 103 grid points in the Maharashtra study region in India.

3.4.3 Analyzing drought characteristics

According to the classification of the SPI and RDI values (Table 3.1), the occurrence frequencies of different drought events are evaluated for both the stationary and non-stationary approaches. The comparison is carried out for the drought categories moderate drought (MD), severe drought (SD), and extreme drought (ED) (refer to Table 3.1). Here, for simplicity of presentation, the occurrence frequency of different droughts is presented for the reference point in Figure 3.6. It should be noted that the results are presented for both the SPI and RDI

For the SPI, there is a higher frequency of SD on 3-, 12- and 24- month scales, ED on a 6-month scale, and MD on 9-, 12-, and 24-month scales in the case of SPI_N as compared to the stationary SPI. Otherwise, the stationary SPI has a higher frequency than SPI_N. Similarly, for RDI the frequency of occurrence on all time scales is higher for the MD categories using RDI_N compared to RDI. In addition, the increase in the frequency for SD is observed for 12- and 24-month scales using RDI_N and for ED on the 3-month scale. Moreover, on 9-, 12-, and 24-month scales, the pattern of change in the drought frequency is similar for both SPI and RDI with or without the influence of large-scale climatic oscillations. It is worth mentioning that at other grid points, the results obtained by the SPI and SPI_N are not consistent. Therefore, it can be postulated that the large-scale climatic oscillations could cause different effects on the drought evaluation and frequency across Maharashtra. Similar results are obtained by Li et al. (2015) while analyzing the association of large-scale climate oscillations with meteorological drought over the Luanhe River Basin.

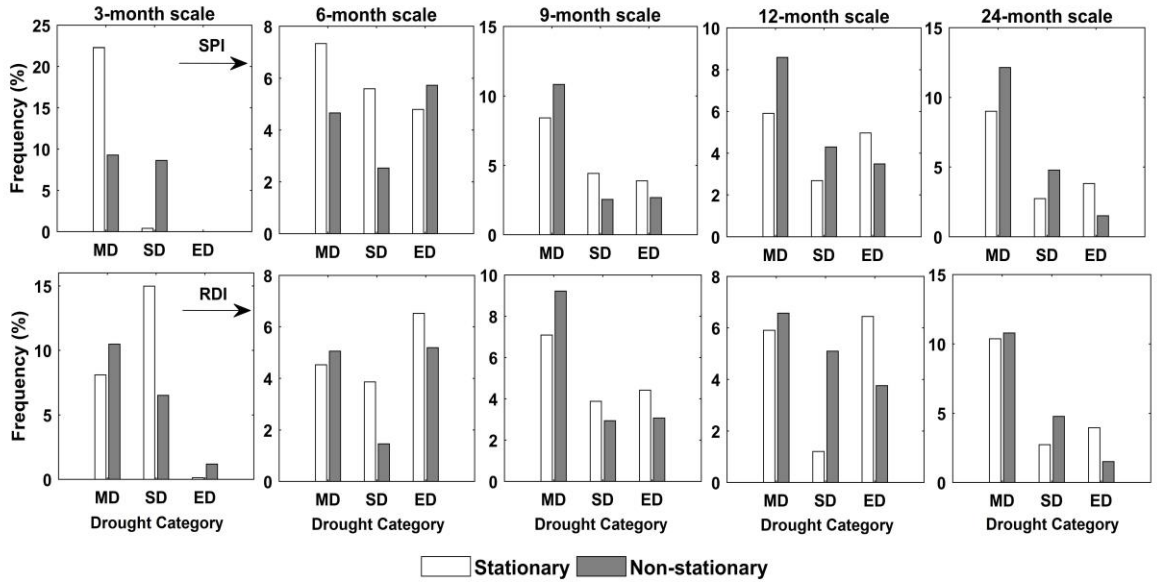

Figure 3.7: Comparison of frequency of occurrence of droughts of different categories under stationary and non-stationary approaches for the reference grid point. The upper (lower) panel represents the SPI (RDI) drought index

3.4.4 Analyzing drought properties

Drought properties, i.e., severity, duration, and peak, are analyzed using non-stationary and stationary approaches. In addition, the counts of MD, SD, and ED drought events are also examined. For comparison, the empirical probability density function for all the drought properties across the study area are determined. The density plot of the drought properties and number of events of different drought types are presented in Figure 3.7 and Figure 3.8, respectively, for the SPI. In the case of the RDI, the outcomes are similar to the SPI value and hence, the plots are not shown for the brevity. It is worth mentioning that in the case of severity and peak, only the magnitude is considered.

It can be noticed from Figure 3.7 that there are noticeable differences in the density plots of the results obtained based on the stationary and non-stationary approaches for 3-, 6-, and 9-month scales. For example, for drought duration the PDFs on 3- and 6-month scales appear to have shifted to the right for the stationary case. Conversely, for drought peak, the distribution appears to have shifted markedly to the right for the non-stationary approach. Moreover, the differences in the referenced PDFs decrease gradually as the time scale increases. These results show that the association of large-scale climatic oscillations likely alter the drought

properties. Similar observations are made when analyzing the number of events of different drought types (Figure 3.8). Considering the ISMI as a covariate and its variability on an intra-annual scale may be one reason for the large variabilities on smaller time scales. In addition, the influence of SOI, SST, and IOD on precipitation is mostly noticed on an interannual scale (J. Das et al., 2020b); hence, the inclusion of such indexes may influence drought properties on 12- and 24-month scales. Therefore, incorporating climatic oscillations in modeling droughts can be a feasible alternative in a changing environment.

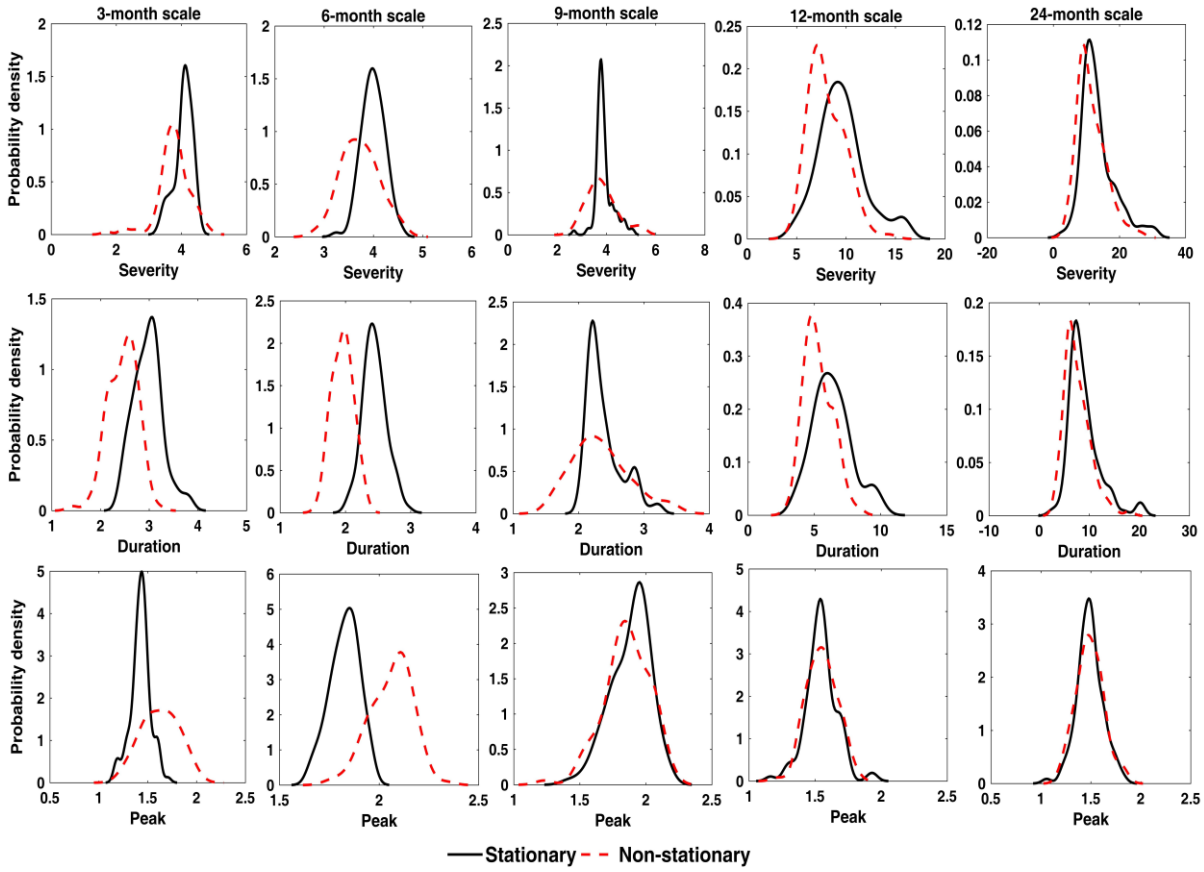

Figure 3.8: Probability density plot of drought properties computed for SPI at different time scales

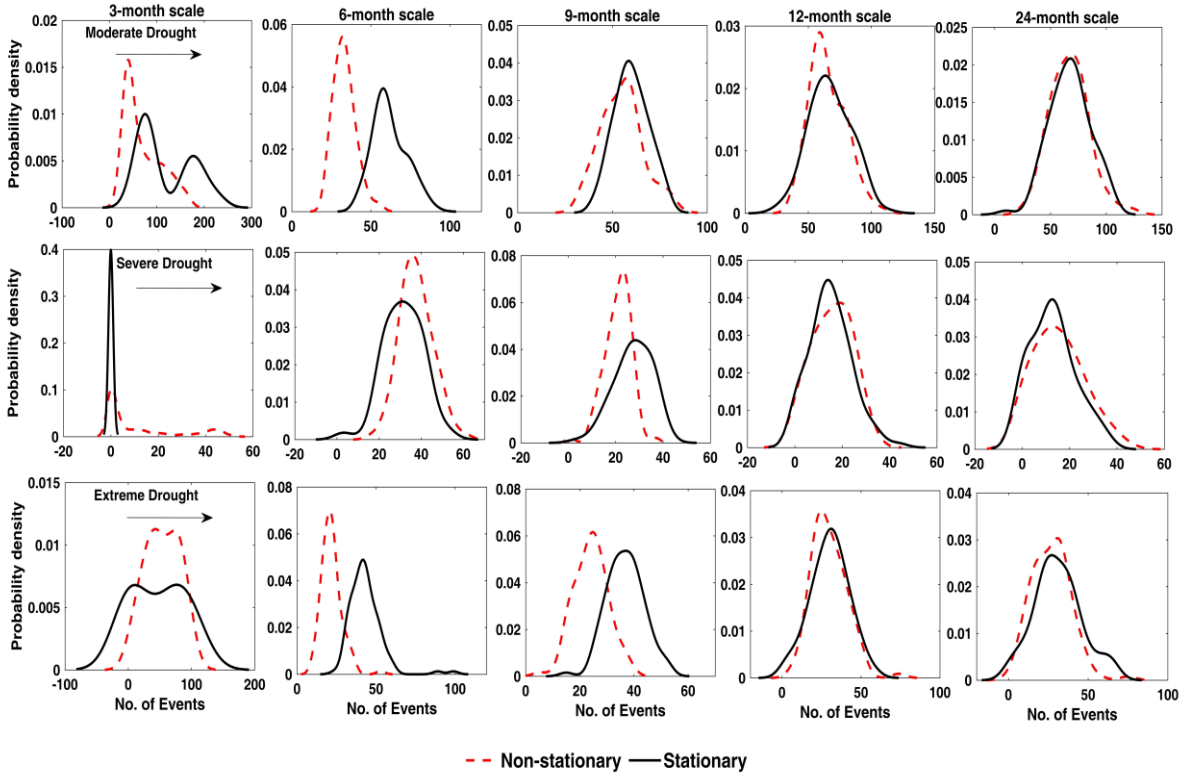

Figure 3.9: Probability density plot of no. of drought events computed for the SPI drought index at different time scales

3.4.5 Comparison with historical drought event

The central part of Maharashtra is a semiarid region owing to the very low precipitation and high PET and is considered a drought prone area (Gore and Ray, 2002). Moreover, the 2013 drought was the region's worst drought in the last 40 years and severely affected the central part of Maharashtra. The reduced precipitation in 2012 is considered one of the reasons for the 2013 drought. Therefore, this study considered the Aurangabad division (popularly known as the Marathwada region) for a comparison of stationary and non-stationary drought indexes on a 12-month scale. To this end, stationary and non-stationary SPI and RDI are spatially plotted for the monsoon months over the Aurangabad division. The SPI and RDI plots are presented in Figure 3.9 and Figure 3.10, respectively. Note that, though there is evidence of drought conditions in the Aurangabad division, severe drought conditions were not identified using the stationary approach. Moreover, the area under drought is larger under non-stationary conditions compared to the stationary approach during monsoon months. Similar results are observed in the case of the RDI. Moreover, when more than one meteorological variable is

included, the non-stationary RDI captures more drought-affected areas compared to the non-stationary SPI during the months of June and July.

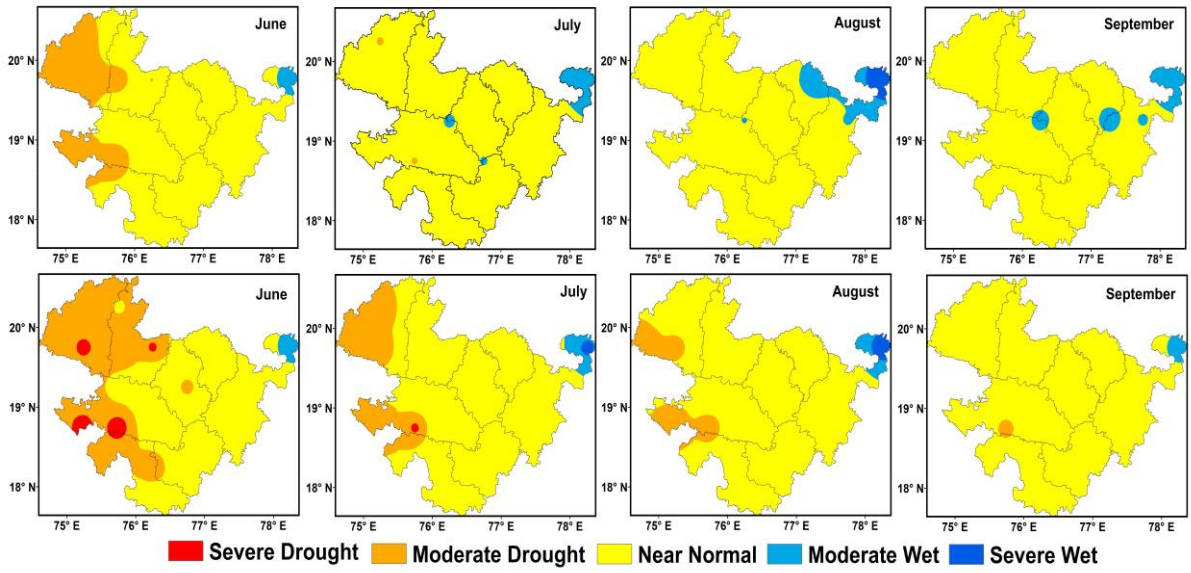

Figure 3.10: Regional demonstration of stationary and non-stationary SPI at 12-month scale during the year 2013 over Aurangabad division. The upper panel shows the stationary and the lower panel shows the non-stationary approach

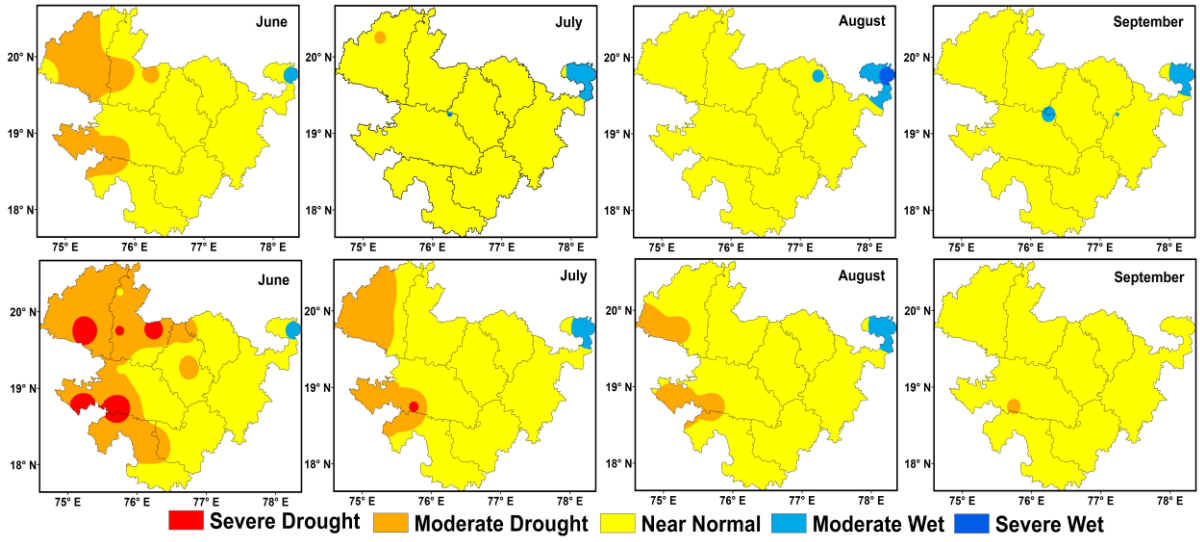

Figure 3.11: Regional demonstration of stationary and non-stationary RDI at 12-month scale during the year 2013 Aurangabad division. The upper panel shows the stationary and the lower panel shows the non-stationary approach

3.5 Discussion and summary

The research reported in this chapter attempts to develop non-stationary meteorological drought indices incorporating large-scale climatic oscillations as covariates for estimating the location parameter of the gamma (for SPI) and lognormal (for RDI) distributions. In general, precipitation is the major leading factor for the occurrence of meteorological drought (Zargar et al., 2011), whereas hydrological drought is associated with human interventions along with climate anomalies (Zhang et al., 2012). In the future, meteorological drought conditions are likely to be modulated by large-scale oscillations, so the temporal lag association of climatic oscillation and meteorological variables can produce reliable information for drought management (Li et al. 2015). The non-stationary approach enables the introduction of climatic oscillations with a lag time varying from 0 to 12 months and yields fairly good results compared with the stationary drought index.

In the case of the non-stationary drought indexes, their time varying nature is incorporated through covariates like the ISMI, SOI, SST, and IOD, which exert a direct or indirect influence on precipitation series (Mishra and Singh 2010). Moreover, the non-stationary estimation of drought indexes can incorporate the development of meteorological variables in a changing environment. More precisely, the time-varying PDFs of meteorological variables are updated with time, providing a robust and suitable drought assessment. In addition, because the stationarity-based drought index is sensitive to the reference periods, evaluation of the frequencies of extreme over other reference periods is difficult (Salvi and Ghosh, 2016). In this sense, the non-stationarity based indices are capable of capturing extreme events because they are insensitive to the reference periods due to their time-varying nature

The variability of monthly precipitation across Maharashtra shows higher precipitation levels across the Konkan division and minimum precipitation in central regions of Maharashtra, such as Nashik and Aurangabad. The regional precipitation variability over India is regulated by large-scale climatic oscillations like the ISMI, SST, IOD, and SOI (J. Das et al., 2020b; Maity and Kumar, 2007); however, one of the reasons for the precipitation variability across central Maharashtra can be attributed to its geographical location. Because of its location on the leeward side of Western Ghats, central Maharashtra receives much less rainfall. It is observed that the sensitivity of PET variability is regulated by temperature in most regions, which is in line with the findings of Guo et al. (2017). The percentage changes in the

frequency of drought types under stationary and non-stationary approaches vary considerably, suggesting that large-scale climatic oscillations modulate the frequency of occurrence of drought across the study area. A similar kind of observation was made by Li et al. (2015) while analyzing non-stationary drought in the Luanhe River Basin. The variability in the drought properties and occurrence of different drought categories were found to be significant on small time scales (e.g., 3-, 6-, and 9-month scales) than on larger scales in comparisons between the stationary and non-stationary approaches. In this sense, it is worth mentioning that under drought mitigation practices in the context of agricultural practices (Parsons et al., 2019), small- and medium-scale water resource management will be affected in the changing scenario of climate change. In addition, the inclusion of large-scale climatic oscillations in the computation of drought indexes appears to be more appropriate over the study area, and a similar conclusion was drawn by Li et al. (2015) while studying the Luanhe River Basin. Owing to intra-annual variability, the ISMI is responsible for modulating droughts on smaller time scales. However, SST, IOD, and SOI are likely to affect drought events on larger scales as the variability of these climatic oscillations is observed on interannual scales.

In the context of climate change, in addition to precipitation, other meteorological variables, such as evaporation, relative humidity, and temperature, have profound effects on drought occurrence (Núñez et al., 2014; Zarch et al., 2015a). For instance, in semiarid regions, instead of considering a single meteorological variable, multiple variables play a dominant role in drought occurrence and effective drought monitoring (Bazrafshan, 2017). Therefore, in a changing climate, the joint behaviour of multiple meteorological variables and the increasing or decreasing trend of each variable may significantly influence the estimation of drought indexes. For instance, an increase in temperature may result in the same amount of precipitation; however, an increase in evapotranspiration can affect drought severity (Li et al. 2015). Because this type of drought index (RDI in this study) is more sensitive to changing environmental conditions, introducing large-scale climatic oscillations as a covariate can provide a robust way of estimating drought properties.

Summarising the findings, it is found that the non-stationary model outperforms the stationary approach over all time scales. The ISMI is likely to influence droughts on smaller scales. However, the IOD, SST, and SOI are expected to modulate larger-scale drought events. Comparative study of the probability plots of drought properties reveals that, though there are noticeable variabilities between the stationary and non-stationary conditions on all time

scales, a significant difference is noticed on the 3-, 6-, and 9-month time scales. A comparative study with respect to historical drought assessments reveals that the presence of non-stationarity cannot be ignored for developing sustainable mitigation and adaptation strategy. Hence, next chapter deals with examining the different types of droughts (meteorological, hydrological, and agricultural) and their properties under the influence of external covariates.

Chapter 4

Analysing the drought properties under different drought conditions

4.1 Introduction

From Chapter 3, it is found that the non-stationary approach outperforms the stationary approach with the inclusion of external covariates at regional scale. Therefore, the present chapter deals with the non-stationarity analysis of meteorological, hydrological, and agricultural drought events across India. In case of meteorological drought, the historical background and development of the drought index is discussed in Chapter 3. Likewise, the present chapter presents a brief background related to the hydrological, and agricultural drought indices under non-stationary approach.

As discussed in the earlier chapters, the global climate has changes remarkably over the last century. Therefore, the hydrological cycle and its available water resources are greatly varied

under the changing climate scenarios. For instance, increase in the evapotranspiration without enhancement of precipitation has heightened the intensity and frequency of hydrological drought (A. Dai, 2013; Sheffield et al., 2012). McCabe and Wolock (2011) concluded that the variability of streamflow is highly sensitive to the precipitation after examining the independent effects of temperature and precipitation in the United states. In Alpine river, climate change is responsible for 85% decrease in the streamflow (Saidi et al., 2018). Similarly, several studies argued that the streamflow is modulated by the climatic variability over Indian river basins (Islam et al., 2012; Mishra and Lilhare, 2016; Panda et al., 2013; Setti et al., 2020). In this sense, researchers have attempted to link the variability of climate change to hydrological drought to develop robust drought index (Jehanzaib et al., 2020; Wang et al., 2022; Zou et al., 2018). However, there is a dearth in studying the non-stationary hydrological drought in India.

In addition to the meteorological and hydrological drought events, the variability in the climate affects the agricultural drought. The soil moisture variability can be considered in order to develop and evaluate the agricultural drought (Ajaz et al., 2019; Fang et al., 2021; Zhou et al., 2021). In the absence of irrigation, soil moisture drought affects crop production and food security in India (Mishra et al., 2017, 2014a). Therefore, the agricultural drought analysis under non-stationary approach is necessary to devise sustainable drought management plans. Till date, there is no study that incorporates the non-stationarity to understand the agricultural drought. Thus, the present chapter analyses the non-stationarity in meteorological, hydrological, and agricultural droughts across India.

With increase in global population, the direct and indirect consumption of water also increases. It brings more challenges to deal with water security associated with different sectors such as irrigation, infrastructure, mining etc. Therefore, when the available water fails to meet the water demand of a specific area, the socio-economic condition is significantly affected over that area. This situation can be named as socio-economic drought. Therefore, in this study, for the analysis of socio-economic drought occurrences, the gridded water consumption data is collected for six different sectors i.e., domestic, electricity, irrigation, livestock, manufacturing, mining during 1970-2010. It should be noted that the meteorological, hydrological, and agricultural droughts are analysed during 1982 to 2015.

4.2 Data used

4.2.1 Runoff, soil moisture, and water consumption datasets

In the present study, the grid-wise analysis is carried out at a resolution of 0.5^{o} Lat x 0.5^{o} Lon over India that includes 1170 grid points (Figure 4.1). The annual precipitation variability over different states in India ranges between 250mm and 3000mm. Similarly, the average temperature during winter is around 10^{o}-25^{o}C and during summer is around 32^{o}-40^{o}C. The meteorological datasets used in the present study are discussed in Chapter 3. In addition to the mentioned meteorological data, soil temperature dataset is obtained from NCEP reanalysis data.

It is well understood that the different datasets with different uncertainties would result in different outcomes. In order to incorporate the variability among the datasets, the runoff datasets are obtained from five different sources (ERA5, FLDAS, GLDAS, MERRA-2, and NCEP). Another important reason for choosing the datasets is due to inconsistencies in the continuous available observed streamflow data and difficulty in obtaining the streamflow data over the river basins that share the international boundary with neighbouring countries. The above-said runoff datasets are obtained at 0.25^{o} Lat x 0.25^{o} Lon for ERA5 (for abbreviation refer to Chapter 1) (Hersbach et al., 2020), 0.1^{o} Lat x 0.1^{o} Lon for FLDAS (McNally, 2018), 1^{o} Lat x 1^{o} Lon for GLDAS (Rodell et al., 2004), 0.5^{o} Lat x 0.65^{o} Lon for MERRA-2 (Gelaro et al., 2017), and 1.915^{o} Lat x 1.875^{o} Lon for NCEP (Kanamitsu et al., 2002). Similarly, the soil moisture datasets are obtained from six diverse sources (CPC, ERA5, FLDAS, GLDAS, MERRA-2, and NCEP). The CPC soil moisture dataset is obtained at a grid resolution of 0.5^{o} Lat x 0.5^{o} Lon (Fan and van den Dool, 2004). The reliability of above mentioned runoff and soil moisture datasets on drought parameters are verified by various researchers across the globe (Bai et al., 2016; N. Chen et al., 2020; McNally et al., 2017; Spennemann et al., 2015; Zaussinger et al., 2018) It should be noted that the runoff datasets from all the sources are extracted at a common resolution of 0.5^{o} Lat x 0.5^{o} Lon to maintain the consistency with the meteorological datasets. The gridded water consumption data is collected for six different sectors i.e., domestic, electricity, irrigation, livestock, manufacturing, mining during 1970-2010. The links to the datasets are provided at the end of the present chapter.

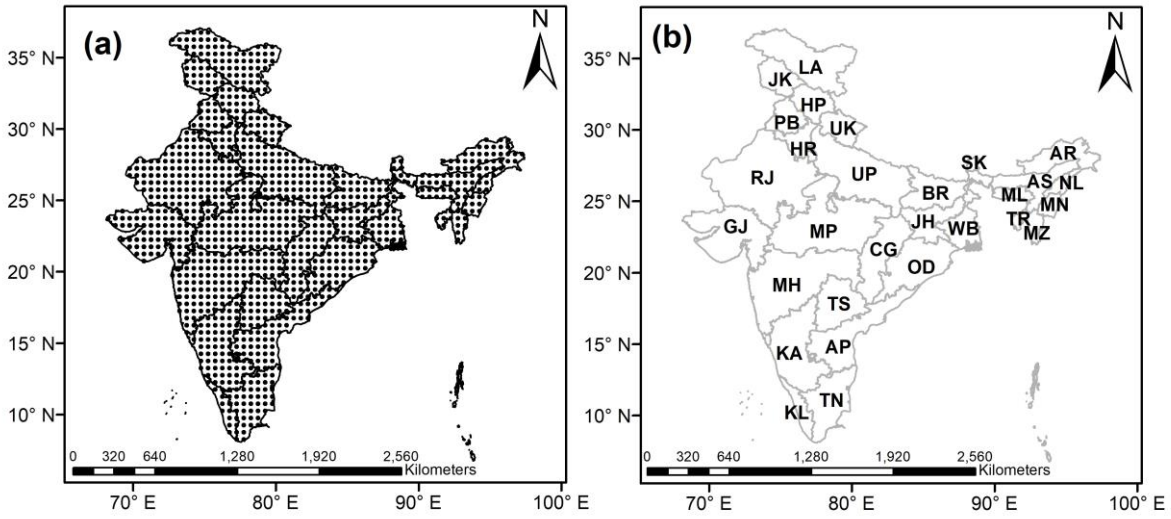

Province	ID	Province	ID
Andhra Pradesh	AP	Mizoram	MZ
Arunachal Pradesh	AR	Nagaland	NL
Assam	AS	Odisha	OD
Bihar	BR	Punjab	PB
Chhattisgarh	CG	Rajasthan	RJ
Gujarat	GJ	Sikkim	SK
Haryana	HR	Tamil Nadu	TN
Himachal Pradesh	HP	Telangana	TS
Jharkhand	JH	Tripura	TR
Karnataka	KA	Uttar Pradesh	UP
Kerala	KL	Uttarakhand	UK
Madhya Pradesh	MP	West Bengal	WB
Maharashtra	MH	Ladakh*	LA
Manipur	MN	Jammu and Kashmir*	JK
Meghalaya	ML		

*Selected Union territory as the areal coverage is more

Figure 4.1: (a) represents the gridded locations at a resolution of 0.5^{o} x 0.5^{o} over India; (b) shows different provinces/states in India

Table 4.1: Details of runoff and soil moisture datasets

Soil moisture and Runoff Datasets	Spatial Resolution	Temporal Resolution	Source
ERA5	0.25°× 0.25°	Monthly	https://cds.climate.copernicus.eu/cdsapp#!/dataset/reanalysis-era5-land-monthly-means?tab=overview
FLDAS	0.1° × 0.1°	Monthly	https://disc.gsfc.nasa.gov/datasets/FLDAS_NOAH01_C_GL_M_001/summary
GLDAS	0.1°× 0.1°	Monthly	https://disc.gsfc.nasa.gov/datasets/GLDAS_NOAH10_M_2.0/summary?keywords=GLDAS

MERRA2	0.5°× 0.65°	Monthly	https://disc.gsfc.nasa.gov/datasets/M2TMNXLND_5.12.4/summary?keywords=MERRA-2
NCEP	1.915° × 1.875°	Monthly	https://psl.noaa.gov/data/gridded/data.ncep.reanalysis2.html
CPC	0.5°× 0.5°	Monthly	https://www.cpc.ncep.noaa.gov/products/Soilmst_Monitoring/US/Soilmst/Soilmst.shtml

4.3 Methodology

4.3.1 Computation of different non-stationary drought indices

As the indicator of meteorological drought, Standardized Precipitation Evapotranspiration Index (SPEI) is used that represents the simplified form of the water balance using precipitation minus potential evapotranspiration (PET) value at each month (Vicente-Serrano et al., 2010). The present study uses Standardized Runoff Index (SRI) to represent the hydrological drought. Similarly, Standardized Soil moisture Index (SSI) is adopted to represent the agricultural drought. The parametric distribution namely Log-logistic is fitted to the precipitation minus PET to estimate SPEI at all the grid points. However, in case of runoff and soil moisture datasets different types of distributions (Gamma, Exponential, Logistic, Lognormal, Normal, and Weibull) are examined and the best suitable distribution is considered (according to Akaike Information Criteria (AIC) value) at each grid point to compute SRI. The cumulative distribution functions obtained by fitting the selected distributions are mapped onto the Normal distribution using the inverse of cumulative standard normal Gaussian function to develop dimensionless index (Mishra et al., 2016). In this procedure, the parameter of the selected distribution is not conditioned with external factors (also known as covariate) and can be called as stationary approach. The SPEI and SRI indices can be evaluated at multiple accumulation period in order to provide the drought condition at seasonal (1-3 month), annual (12-month), or longer time-scales (Bhardwaj et al., 2020). In the present study, 1-month scale of SPEI and SRI is considered to analyse the drought propagation as the larger time scale might overlook the drought propagation at short time scale.

In order to analyse the influence of large-scale climatic indices on the meteorological drought, non-stationary analysis is carried out. Here, the framework proposed by Das et al. (2020b) and Chapter 3 is used to perform the non-stationary modelling of SPEI drought index. Initially, the large-scale climatic indices are arranged in a lagged fashion from no lag to 12-lag and the

suitable lag is chosen based on the Kendall correlation analysis (Kendall, 1955) between PR minus PET series and arranged large-scale climatic indices at a significance level of 5% . Next, the climatic indices with selected lag are considered as covariates to develop the non-stationary model. This analysis is performed over all the grid points individually. It should be noted that the non-stationary modelling is performed by introducing the covariates in the estimation of location parameter of the selected distribution in case of SPEI, SRI and SSI drought indices.

However, in case of SRI index, only the meteorological variables (precipitation, PET, relative humidity, and wind speed) are considered as covariates for non-stationary modelling. In case of agricultural drought index, the meteorological variables such as precipitation, air temperature, and soil temperature are considered as covariates. In case of SRI, fifteen (tabulated in Table 4.1) different models and for SSI seven (tabulated in Table 4.2) models are designed by considering the various combinations of meteorological variables and the optimum model is selected based on the lowest AIC value among the models. Similarly, the selection between stationary and non-stationary models is performed using the AIC value. The entire analysis is carried out using the Generalized Additive Model in Location, Scale and Shape (GAMLSS) package in R platform developed by Rigby and Stasinopoulos (2005).

Table 4.2: Different combination of covariates in the location parameter of the selected model for the development of the non-stationary SRI

Model	**Precipitation**	**PET**	**Relative humidity**	**Wind speed**
Model 1	✓	-	-	-
Model 2	-	✓	-	-
Model 3	-	-	✓	-
Model 4	-	-	-	✓
Model 5	✓	✓	-	-
Model 6	✓	-	✓	-
Model 7	✓	-	-	✓
Model 8	-	✓	✓	-
Model 9	-	✓	-	✓
Model 10	-	-	✓	✓

Model 11	✓	✓	✓	-
Model 12	-	✓	✓	✓
Model 13	✓	-	✓	✓
Model 14	✓	✓	-	✓
Model 15	✓	✓	✓	✓

Table 4.3: Different combination of covariates in the location parameter of the selected model for the development of the non-stationary SSI

Model	**Precipitation**	**Air temperature**	**Soil temperature**
Model 1	✓	-	-
Model 2	-	✓	-
Model 3	-	-	✓
Model 4	✓	✓	-
Model 5	✓	-	✓
Model 6	-	✓	✓
Model 7	✓	✓	✓

4.3.2 Computation of socio-economic drought index

The graphical representation to evaluate the socio-economic drought is presented in Figure 4.2. Initially, the threshold value of water consumption is determined as the maximum amount of water consumption among six different sectors grid wise. Then, the water scarcity condition is identified when the available runoff of a grid point is not sufficient to meet the threshold value of water consumption at that grid point. This is computed by differencing the threshold value of water consumption from the runoff value for different sources. The negative value indicates the socio-economic drought condition whereas the positive value indicates the sufficient availability of water to meet the water demand from each sector. A socio-economic drought event initiates at the point when the difference between runoff and threshold water demand is negative and continues up to the condition when runoff is more than the threshold value of water demand. Subsequently, different drought properties i.e., drought severity, duration and no of droughts are also calculated. Drought severity is in the form of water scarcity amount which is computed as the cumulative summation of required water during a drought event, whereas the drought duration is the number of months under socio-economic drought occurrences.

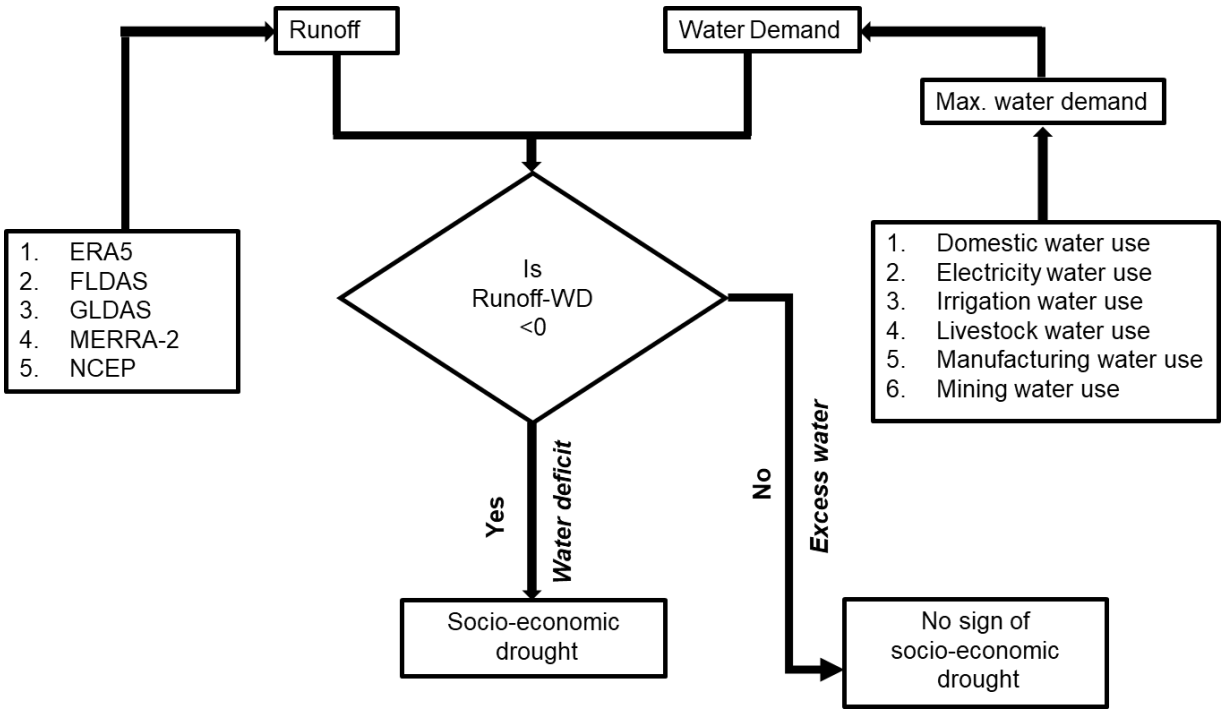

Figure 4.2: Graphical representation of adopted methodology to identify the socio-economic drought conditions

4.4 Results

4.4.1 Drought properties

From the analysis it is found that the non-stationary analysis outperforms the stationary analysis at each grid point for meteorological (SPEI), hydrological (SRI) and agricultural (SSI) drought conditions. For instance, the comparison between stationary and non-stationary analysis is provided based on the AIC values for different indices (Table 4.4). For the brevity, grid locations from different parts of India are chosen. The meteorological drought properties are presented in Figure 4.3. Mostly, the high values of drought duration and severity are observed over the southern parts of India (e.g., Karnataka (KA), Kerala (KL), and Tamil Nadu (TN)). The regions with high value of drought duration show high value of severity. However, the number of drought events are higher mostly over Madhya Pradesh (MP) in central India, parts of Maharashtra (MH), Gujarat (GJ) and Rajasthan (RJ) in western parts of India, Uttar Pradesh (UP), Uttarakhand (UK) in northern parts, and Chhattisgarh (CG), and parts of Odisha (OD) in eastern parts of India.

Table 4.4: The computed AIC values for the covariate (AICw) and without (AICw/o) covariate for different drought indices

Grid	SPEI		SRI		SSI	
	$AIC_{w/o}$	AIC_{w}	$AIC_{w/o}$	AIC_{w}	$AIC_{w/o}$	AIC_{w}
76.25, 33.75 (North)	9037.0	8870.2	454.5	-897.2	1910.0	1572.0
71.25,23.25 (West)	9383.6	9119.7	-254.7	-1136.1	2578.2	2209.6
91.75,25.75 (East)	10399.5	10033.8	1787.7	1059.0	2715.4	2258.7
77.75,10.75 (South)	9000.8	8647.3	-1134.0	-2000.9	2774.9	2416.8
76.75,22.75 (Central)	10034.8	9547.8	-145.1	-1130.6	3085.6	2543.4
82.25,20.75 (Central)	9998.6	9451.6	321.2	-908.7	3234.4	2760.4

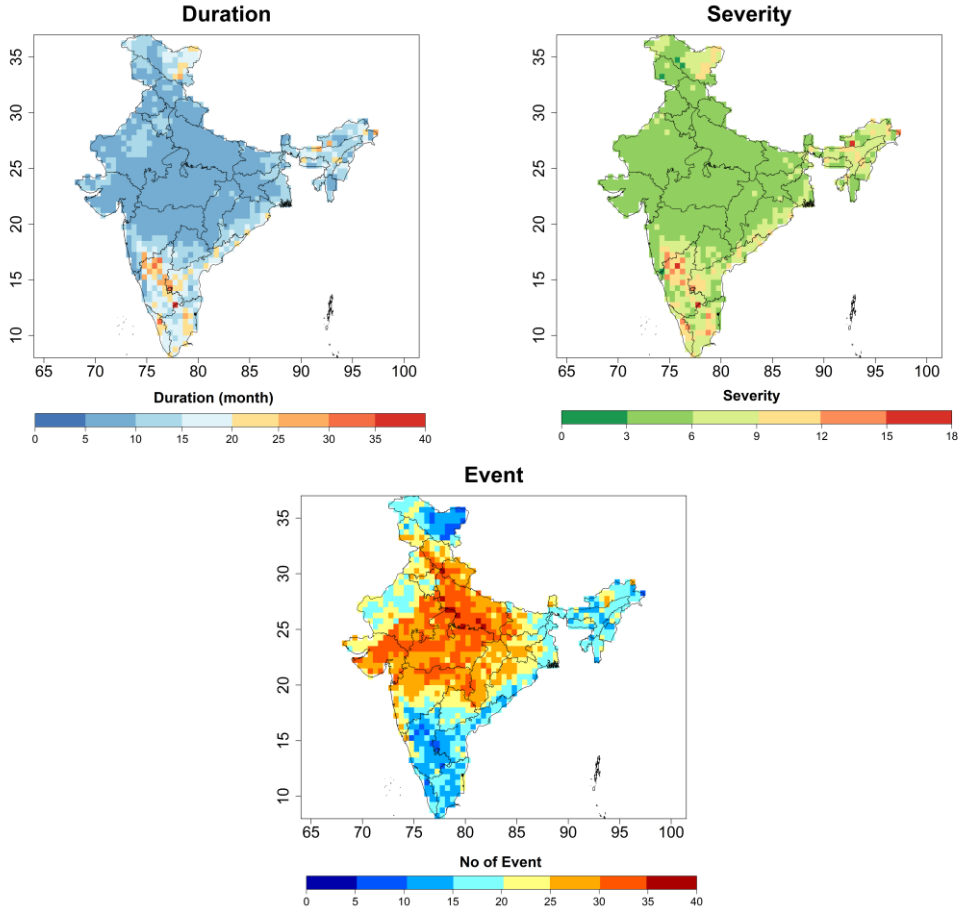

Figure 4.3: Different drought properties using SPEI drought index

About 94% of total area comes under the drought duration ranging between 6 and 20 months with the highest value of 57% in the case of drought duration between 6 and 10 months. Similarly, the severity magnitude of 3 to 9 occupies about 91% of the total area with highest

(72%) in case of magnitude from 3 to 6. During the study period, the number of drought events between 10 and 35 is noticed over 97% of the total area.

The duration, severity, and frequency of hydrological drought events discerned from different datasets are presented in Figure 4.4, Figure 4.5, and Figure 4.6, respectively during 1982-2015. From Figure 4.4, it can be noticed that maximum percentage of area i.e., 36% in ERA5, 43% in FLDAS, and 40% in NCEP is observed for the drought duration ranging from 10 months to 15 months. However, in the case of GLDAS and MERRA2, the maximum percentage of area (i.e., 79% and 68%, respectively) is noticed for 5 months to 10 months drought duration. Considering the SRI values from all the models, it is observed that more than 85% of the total area has come under the drought duration of 5 months to 20 months. The high value of drought duration is observed over small parts in northern region for SRI values from ERA5, FLDAS, NCEP and southern region from NCEP.

In case of severity value ranging from 5 to 10 (Figure 4.5), the highest percentage of area is computed as 53% in ERA5, 75% in GLDAS, 71% in MERRA2, and 52% in NCEP. The regions under the high values of drought severity are similar as drought duration. As compared to drought duration and severity, the intermodal variability is high in case of number of drought events as presented in Figure 4.6. It can be observed from the figure that more than 40% of the total area is under the influence of high no of drought event i.e., between 25 and 35 in the case of GLDAS and MERRA2. However, the spatial distribution of the drought event is different between these models. For instance, the high drought events are zoned over most parts in India except some parts in northern, northwest, and southern regions in case of GLDAS. Conversely, mostly the western parts of the country are affected by the large number of drought events as observed in MERRA2.

The hydrological drought properties obtained from the ensemble average of all the runoff datasets (Figure 4.7) reveal that the higher value of duration and severity is observed mostly over the southern and northern parts of India. Conversely, the low magnitude of duration and severity is noticed over the western and northeast parts of India. The number. of drought events are between 20 and 25 during the study period over most of the regions in India.

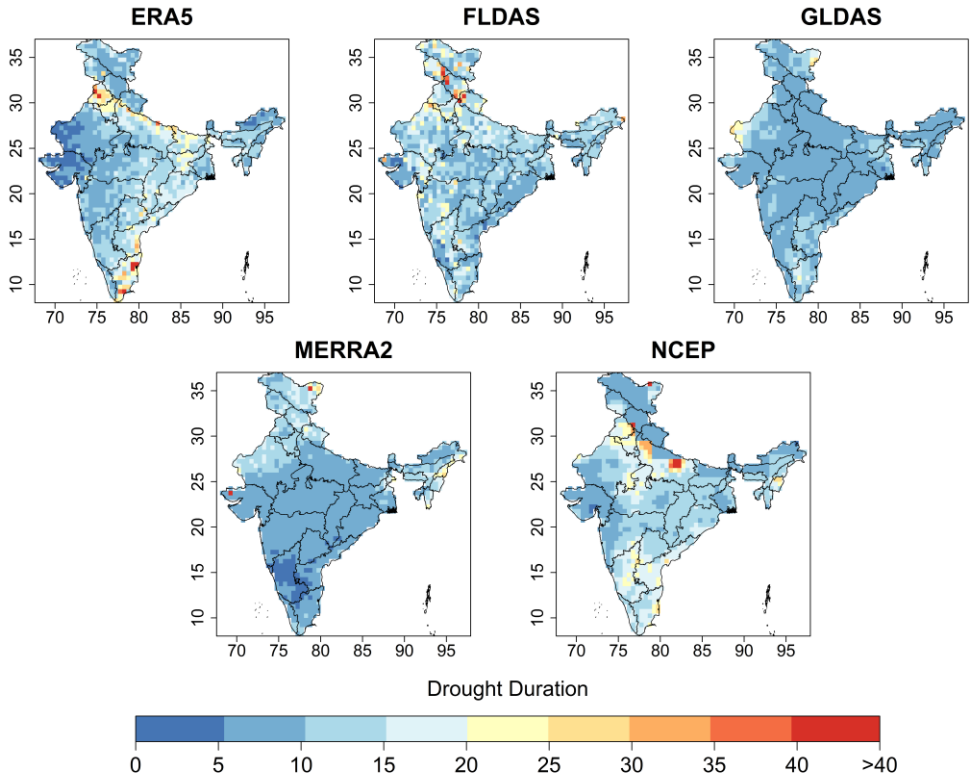

Figure 4.4: Drought duration (in months) computed from different runoff datasets

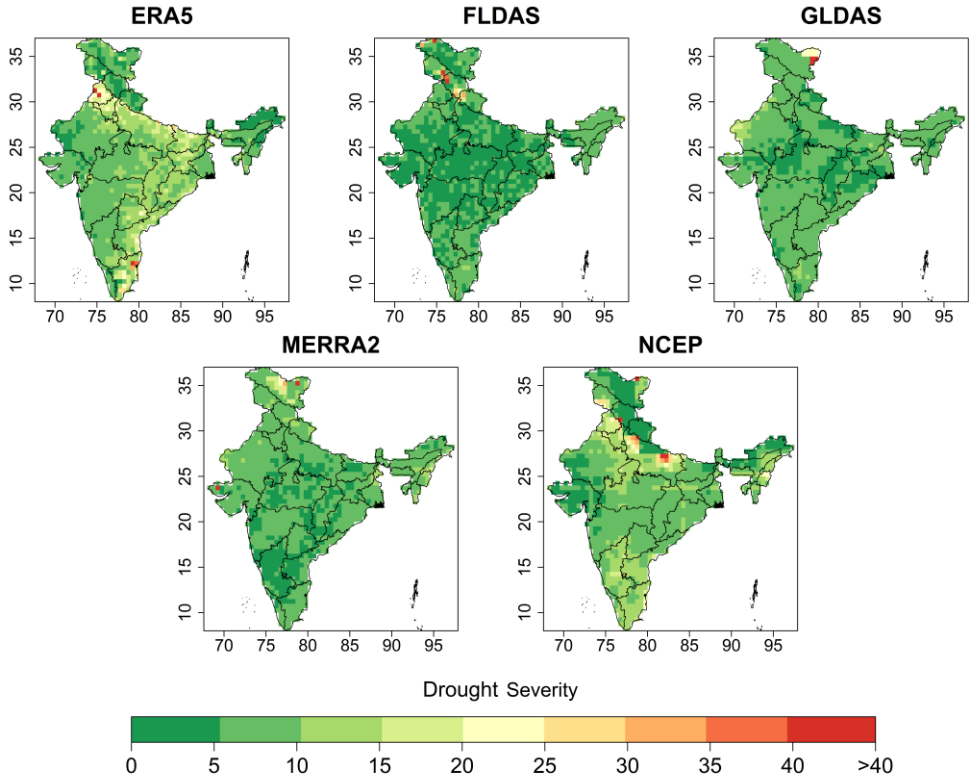

Figure 4.5: Drought severity computed from different runoff datasets

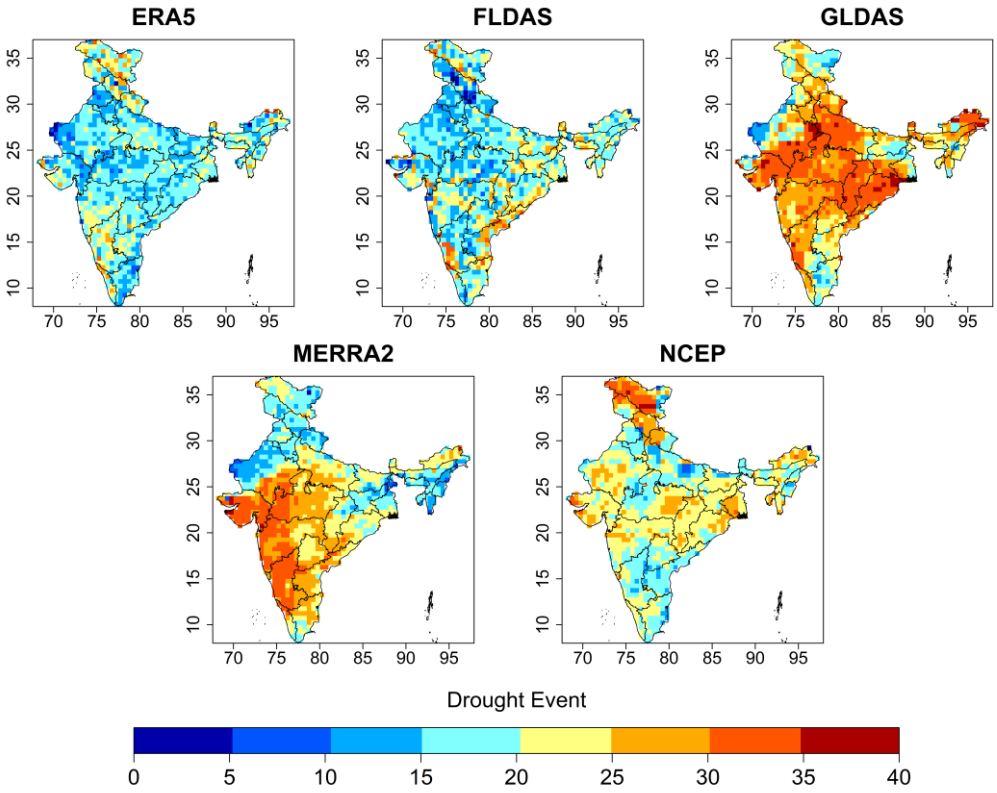

Figure 4.6: Number of drought events computed from different runoff datasets

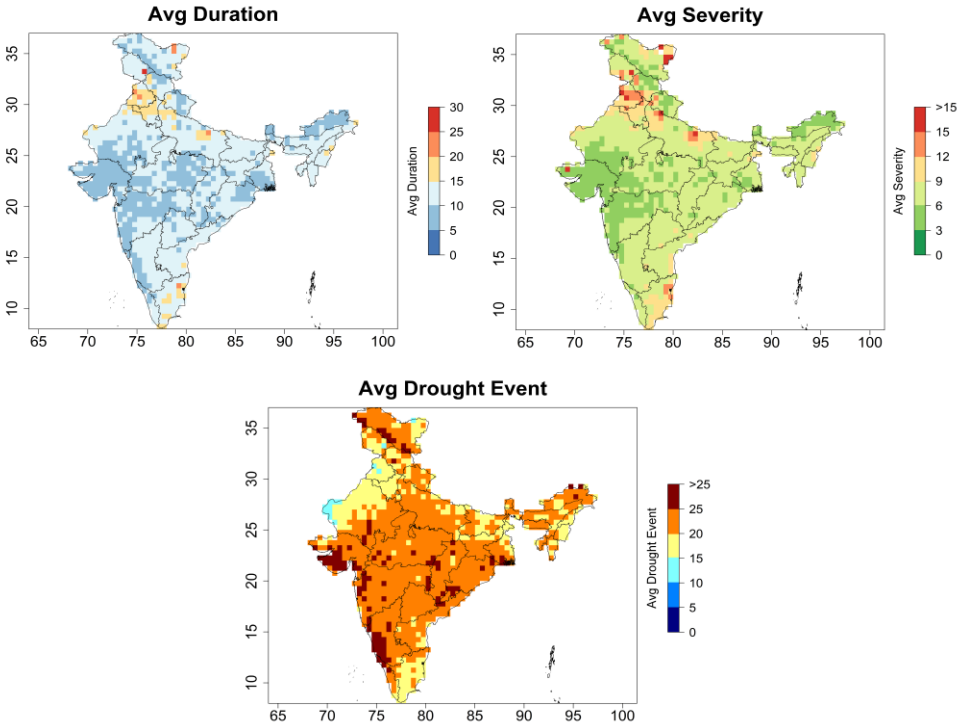

Figure 4.7: Different drought properties obtained from the ensemble average of all the runoff datasets

The duration, severity, and frequency of agricultural drought events obtained from different soil moisture datasets are presented in Figure 4.8, Figure 4.9, and Figure 4.10, respectively. It can be noted from Figure 4.8 that the drought duration varies from 11 to 15 months for ERA5, FLDAS, GLDAS, and MERRA2 over 60%, 50%, 48%, and 56% of the total area. However, in the cases of CPC and NCEP, the ranges of drought duration vary from 6 to 10 months over 43% and 59% of total area. Over more than 95% of the total area of India, the agricultural drought duration ranges between 6 and 20 months based on the threshold value (i.e., zero) chosen in the present study. Figure 4.9 describes the spatial variability of agricultural drought magnitude/severity across India during 1982-2015. It is observed that 70% to 93% of total area come under the severity range from 5.1 to 10 while considering all the soil moisture datasets. Unlike the drought duration, the spatial distribution of drought severity is uniform across the India for all the data sources. The drought event numbers are plotted in Figure 4.10. Though there is significant variability in the drought occurrences across different data sources, the high occurrence of agricultural drought is noticed over the western parts of India in case of all the datasets. The drought occurrence range between 20 to 25 is observed over 30% of area in CPC, 48% in ERA5, 42% in FLDAS, 45% in GLDAS, 36% in MERRA-2 and 47% in NCEP dataset.

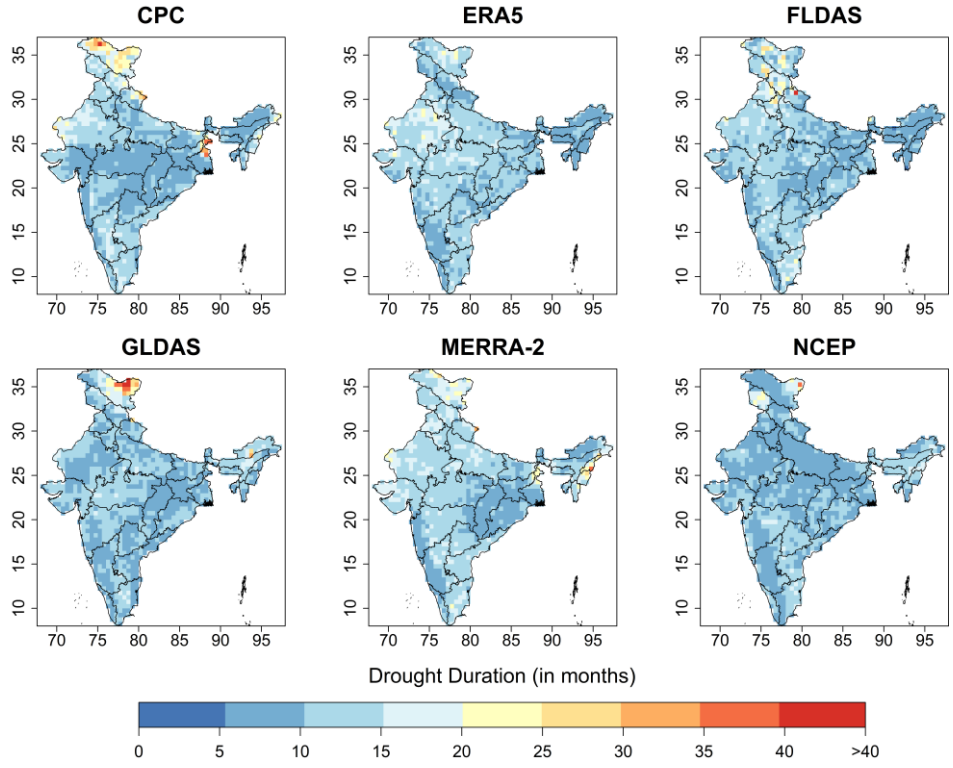

Figure 4.8: Drought duration (in months) computed from different soil moisture datasets

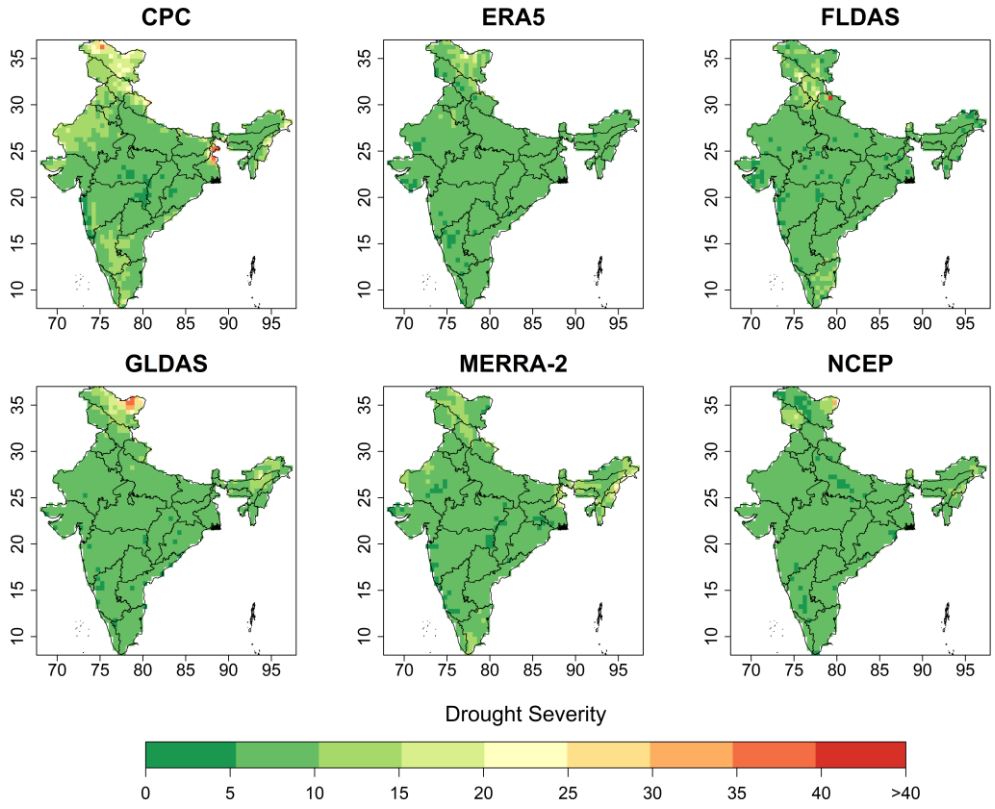

Figure 4.9: Drought severity computed from different soil moisture datasets

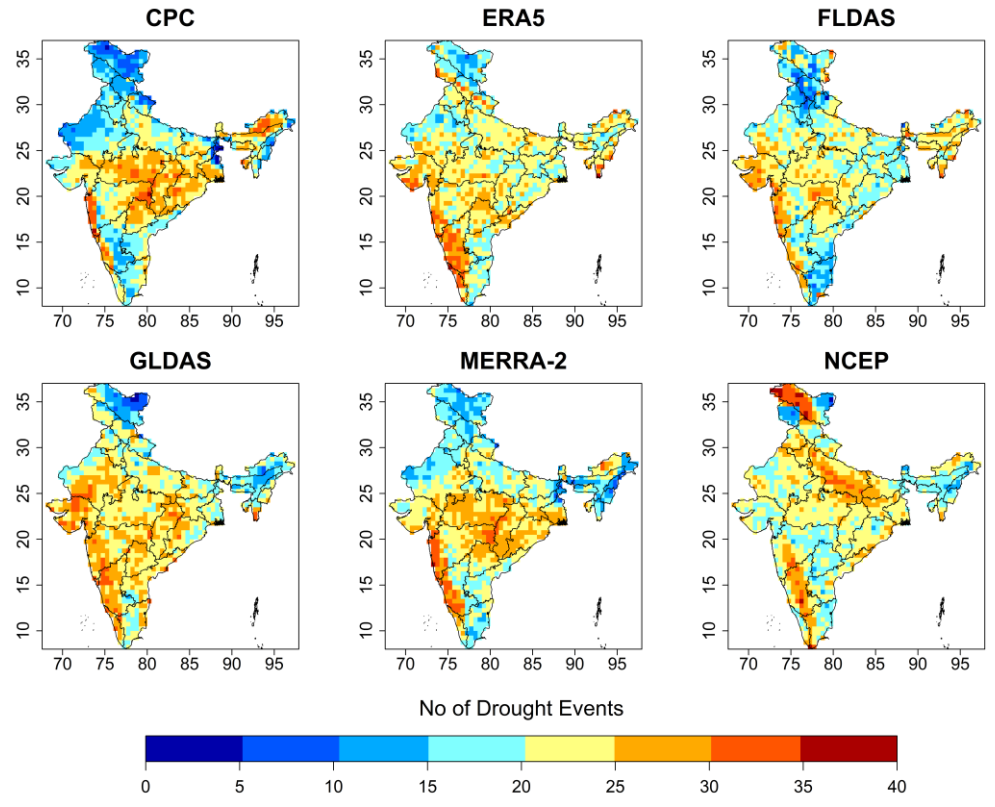

Figure 4.10: Number of drought event computed from different soil moisture datasets

The ensemble average of all the datasets for different agricultural drought properties is presented in Figure 4.11. It can be noted that high drought duration and severity are observed over the northern parts and some patches of northeast and northwest regions of India. About 69% of the total area comes under the drought duration ranging from 11 to 15 months. Similarly, the severity values from 6.1 to 9 are noticed over 77% of the total area. The ensemble average of number of drought events reveals that the agricultural drought occurrence along the west coast and some parts in the central India is high (i.e., more than twenty-five occurrences during the study period). Whereas the number of drought events ranges between 21 to 25 are evident over 61% of the total area.

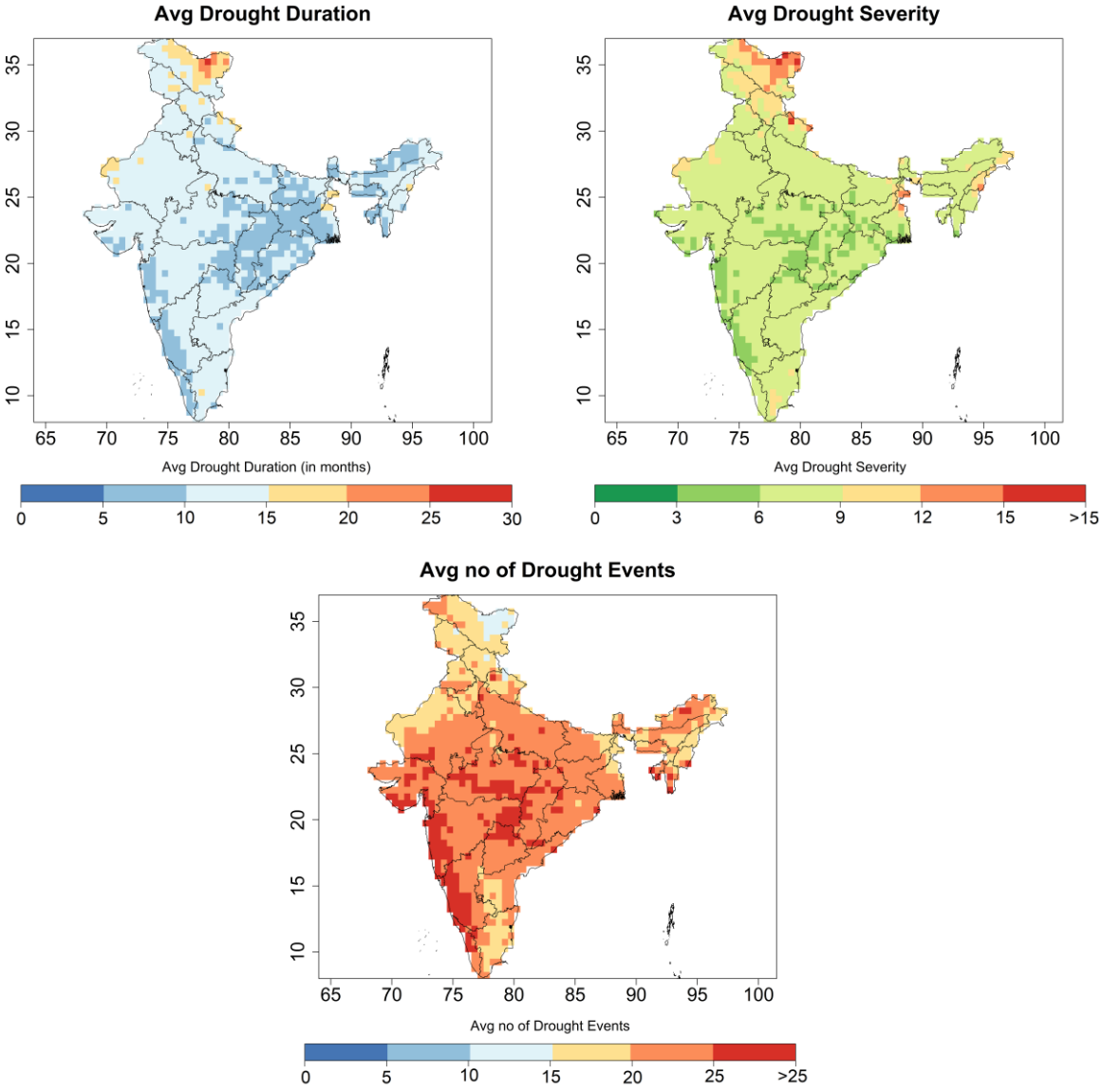

Figure 4.11: Different agricultural drought properties obtained from the ensemble mean of six different soil moisture datasets during 1982-2015

Different drought properties related to the socio-economic drought are computed for various runoff datasets. The duration, severity (or water shortage in this case), and frequency of socio-economic drought events obtained from different runoff datasets are presented in Figure 4.12, Figure 4.13, and Figure 4.14, respectively. It can be noted from Figure 4.12 that the drought duration up to 20 months is observed for ERA5, FLDAS, MEERA-2 and NCEP over about 31% of the total area. However, in case of GLDAS, the percentage of area is about 24%. For the duration between 200 to 350 months, the percentage of area is computed as 34%, 28%, 52%, 26% and 24% for ERA5, FLDAS, GLDAS, MEERA-2 and NCEP, respectively. The spatial variability of socio-economic drought duration is found to be similar for most of the runoff datasets. The severity (Figure 4.13) in terms of water shortage varies up to 3 meter over 71%, 75%, 61%, 75% and 78% of area for ERA5, FLDAS, GLDAS, MEERA-2 and NCEP, respectively. The drought event numbers are plotted in Figure 4.14. It is found that 59%, 53%, 69%, 51%, and 58% of total area is covered in case of the drought occurrences up to 10 for ERA5, FLDAS, GLDAS, MEERA-2 and NCEP, respectively.

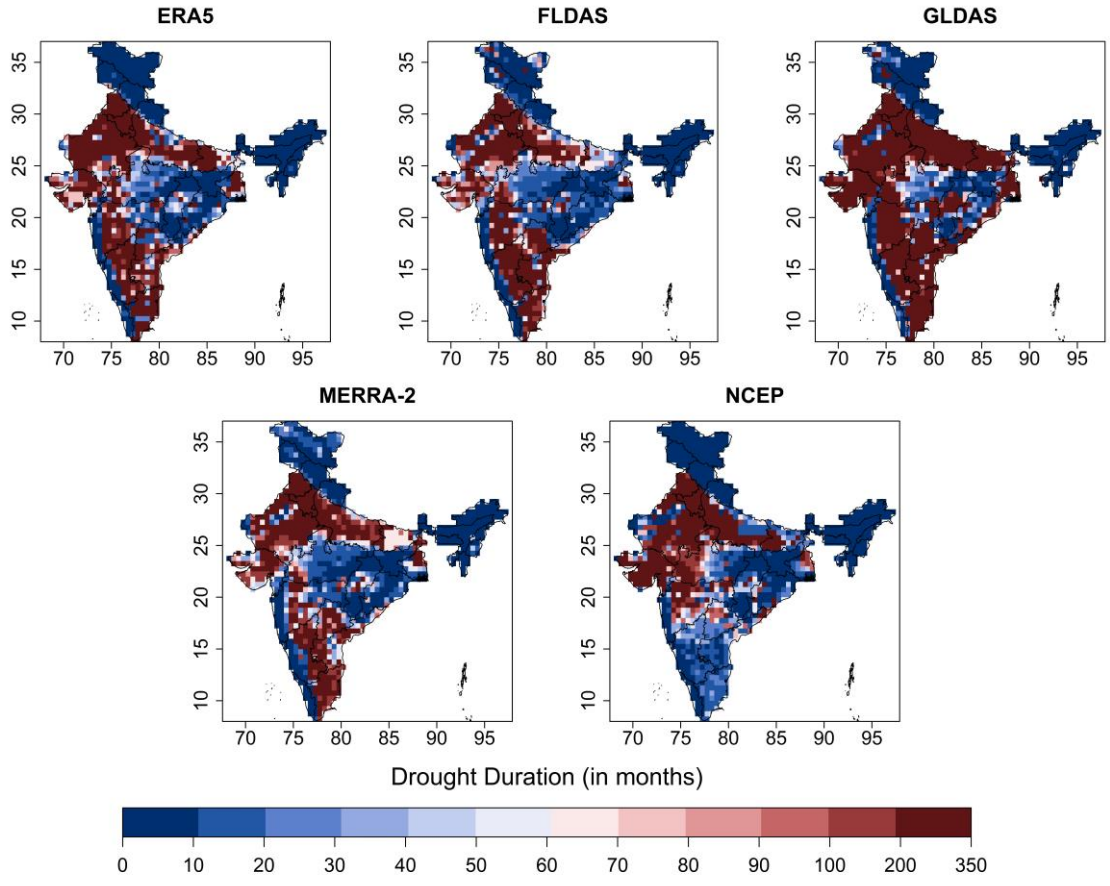

Figure 4.12: Socio-economic drought duration determined using different runoff datasets

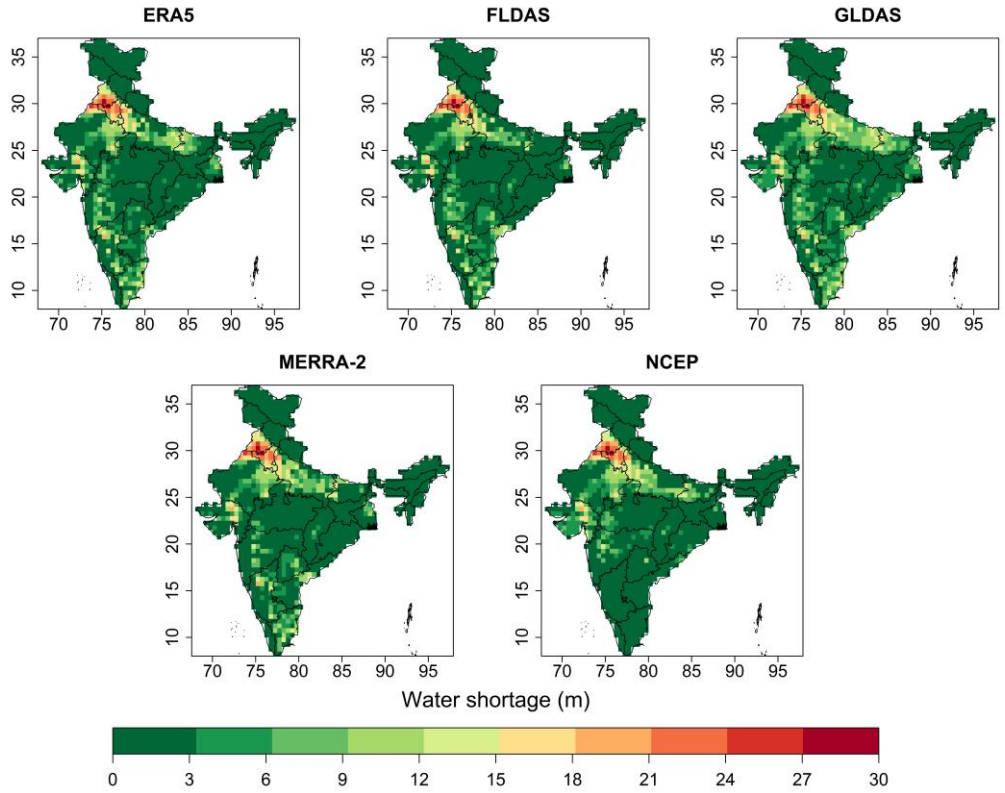

Figure 4.13: Socio-economic drought severity determined using different runoff datasets

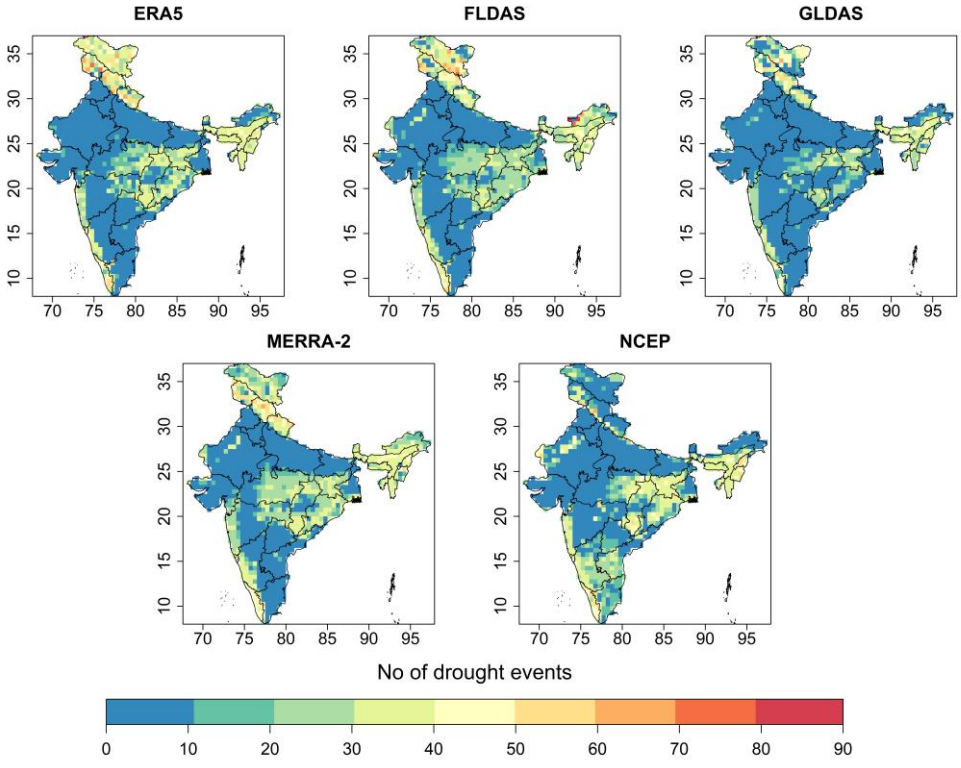

Figure 4.14: Number of socio-economic drought events determined using different runoff datasets

The ensemble average of all the datasets of different socio-economic properties is presented in Figure 4.15. It can be noted that 50% of the total area is under the drought duration between 100 and 350 months. Most of the regions such as Rajasthan, Punjab, Haryana, Gujarat, some part of Maharashtra, Tamil Nadu, some portion of Andhra Pradesh and Telangana suffer from longer drought duration ranging from 90 to 350 months. Furthermore, in case of drought severity, around 0 to 3m of water scarcity occurs in 71% of total area. The highest water scarcity is observed over most portions of Punjab and Haryana.

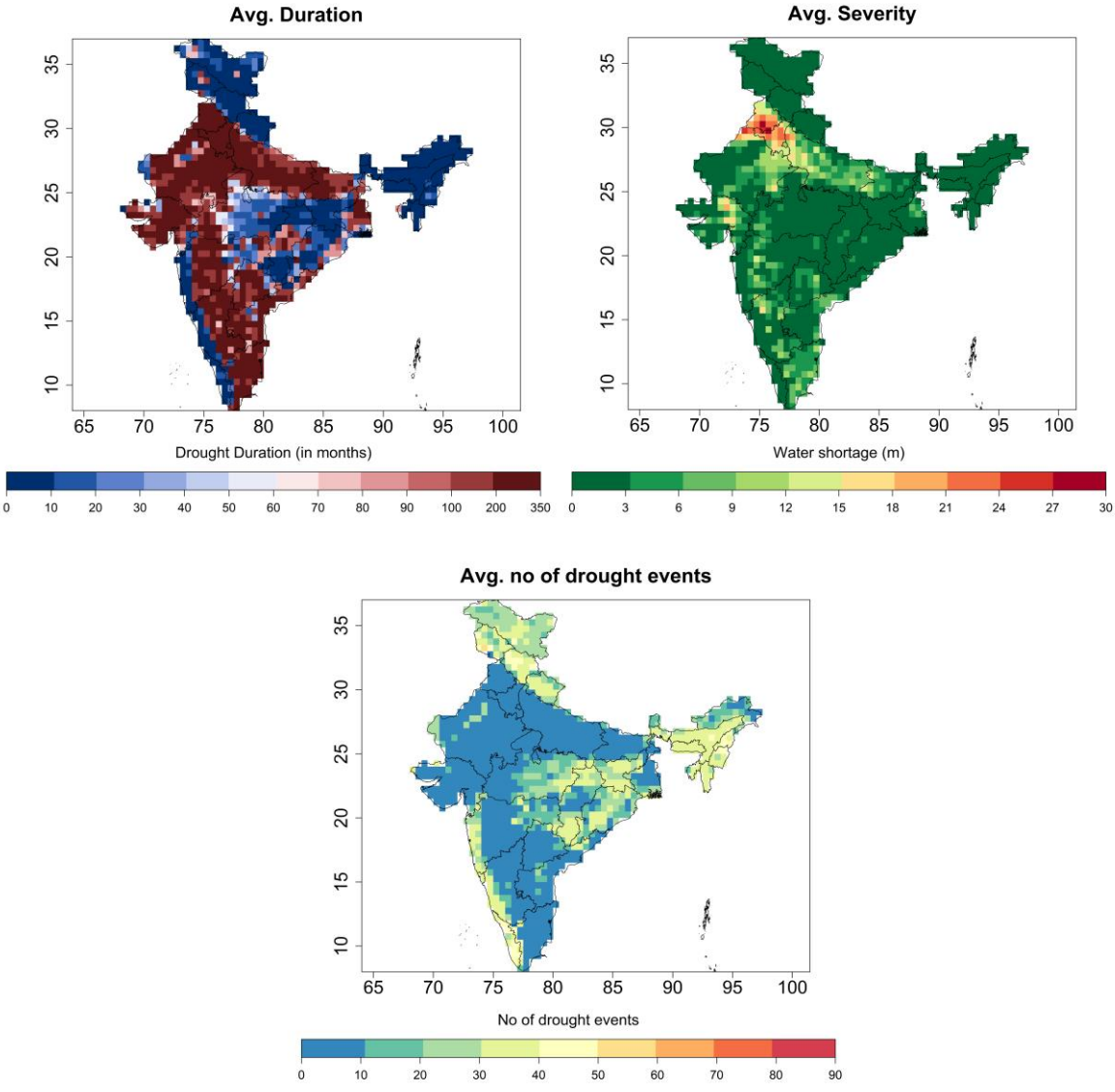

Figure 4.15: Different socio-economic drought properties obtained from the ensemble mean of different runoff datasets during 1982-2010

4.5 Discussion and summary

The research reported in this chapter attempts to develop non-stationary meteorological, hydrological, and agricultural drought indices incorporating external large-scale climatic oscillations and regional hydro-meteorological variabilities as covariates in estimating the location parameter of the suitable distributions. As entire India is considered for the study, it is cumbersome to set up a hydrological model for the entire India due to the significant alterations in the streamflow as a result of anthropogenic activities (e.g., influence of dam) and inconsistencies in the continuous available observed streamflow data. Thus, available gridded runoff datasets at a resolution of 0.5^{o} Lat x 0.5^{o} Lon is considered. Five different gridded runoff datasets are considered to encompass the associated uncertainties with the datasets. Similarly, six soil moisture datasets are also collected. In addition, the drought characteristics extracted from ensemble mean of all the datasets are analysed. To provide a unified outcome from all the runoff and soil moisture datasets, the ensemble mean is considered. In other words, the average prediction performance of all contributing members in the ensemble is chosen to extract the important findings from the analysis. Combining the multiple datasets in order to solve one problem and focusing on their consistency may obtain the results closer to the truth (N. Chen et al., 2020).

In the changing environmental condition, the lag structure of large-scale climate indices provide vital information about meteorological drought management (Li et al., 2015). Similarly, the regional climatological variability influences the hydrological drought characteristics. The precipitation variability as a leading factor of meteorological drought is modulated by the large-scale climate indices (A.K. Mishra and Singh, 2010). Conversely, the hydrological drought is linked with climate anomalies and human interventions (Zhang et al., 2012). The agricultural productivity is sensitive to the short- and long-term climate change and under the warming climate scenario it is challenging to identify the agricultural droughts due to the complex interaction between precipitation and temperature (Mishra et al., 2014a). Therefore, inclusion of regional precipitation and temperature variability in developing the agricultural drought index enables to accommodate the interaction between the precipitation and temperature. Thus, present study develops the non-stationary meteorological, hydrological and agricultural drought indices incorporating the large-scale climate indices and regional hydro-meteorological variability. In line with the past studies (Cheng and Aghakouchak, 2014; J. Das et al., 2020a; Jehanzaib et al., 2021; Vasiliades et al., 2015), it is

observed that the non-stationary analysis outperforms the stationary analysis. The inclusion of non-stationarity helps in capturing the evolution of drought events under the changing environment condition and provides valuable information about drought management (Li et al., 2015).

The variability in meteorological and hydrological components influence the drought properties (Núñez et al., 2014; Zarch et al., 2015b). It is observed that with increase in drought duration, the drought severity has increased under meteorological and hydrological drought indices. The present findings are in line with the previous studies carried out over different parts of the world (Adhyani et al., 2017; Cavus and Aksoy, 2020; Satish Kumar et al., 2021; Spinoni et al., 2014). In case of meteorological drought, it is observed that the drought event with short duration and low severity has high frequency, while long duration and high severity has low frequency characteristics. The similar observations are noticed by Ge et al. (2016) while analysing the spatiotemporal pattern of droughts in the continental United States. The southern parts of India experience the high magnitude of drought duration and severity. In line with the present outcomes, Mallya et al. (2015) and Mishra et al. (2021) also identified the severe drought conditions over south India. Mishra et al. (2021) attributed it to the deficit northeast monsoonal rainfall over consecutive years that contributes about 40% of total rainfall in southern India. In addition, Jain et al. (2019) advocated that the dryness during the monsoon period as a result of negative IOD and warm SST bring the exceptional drought condition over south India. In general, the meteorological drought properties are more severe than hydrological drought properties. Like meteorological drought, the agricultural drought events with lower duration and severity are more in numbers and vice versa. In case of socio-economic drought, comparing the number of drought events and drought duration, it is observed that the regions having high drought duration are associated with lesser number of drought events. It can be concluded that in those portions, a single drought event takes more time to recover from the water scarcity condition.

Summarising the findings, it is found that the non-stationary model outperforms the stationary analysis for meteorological, hydrological and agricultural drought indices. It is found that the meteorological drought properties (drought events and duration) are more severe as compared to the hydrological drought. The large duration and more severe hydrological droughts are observed mostly over southern and northern parts of India. The high agricultural drought duration and severity are observed over the northern parts and some patches of northeast and

northwest regions of India. About 69% of the total area comes under the drought duration ranging from 11 to 15 months. Similarly, the severity values from 6.1 to 9 are noticed over 77% of the total area. The high value of socio-economic drought severity is noticed over Punjab and Haryana. With this understanding, the next chapter deals with the investigation of drought propagation from meteorological to hydrological and meteorological to agricultural incorporating the non-stationary drought indices developed in the present study.

Chapter 5

Drought propagation under the influence of external covariates

5.1 Introduction

Droughts are different from other natural disasters as the development is usually slow and have significant impact on agriculture (Gupta et al., 2020; Lobell et al., 2020), water resources (AghaKouchak et al., 2015; Pokhrel et al., 2021; Qiu et al., 2021), ecosystem (X. Feng et al., 2021; Fu et al., 2021; Y. Zhang et al., 2021), and economic sectors (Frame et al., 2020; Naumann et al., 2021). In addition, the recovery period after a drought event can be lengthy and affects the ecosystem resilience and stability (L. Liu et al., 2019). Under the background of climate change, the frequency and intensity of drought events are expected to increase (Spinoni et al., 2018). With increasing number of drought events, regions with long recovery time are likely to suffer a new drought event before full recovery. Moreover, the industry and agricultural sectors have high demand for water resources with increasing rate of human

population and development (J. Das et al., 2020c). Therefore, it is necessary to understand the drought occurrence, and mechanism at regional scale to improve its monitoring, management, and prediction.

In the context of causative mechanisms, the deficit in the precipitation and increasing evaporative demand propagate through the hydrologic cycle and subsequently developing into a hydrological drought (Han et al., 2019; Hellwig et al., 2020; Van Loon, 2015). In other words, from beginning to the end, drought transition is encapsulated within the "Atmosphere-Hydrology-Soil-Vegetation" system (N. Chen et al., 2020). This transition from one form to another form of drought is known as drought propagation (Apurv et al., 2017; Haslinger et al., 2014). The understanding of drought propagation provides valuable information to improve the accuracy of drought analysis and prediction. Due to the dual effect of climate change and population growth, it is difficult to analyse the spatio-temporal evolution of drought. However, under the limited or no anthropogenic interventions, drought propagation is primarily controlled by the climatic factors and biophysical characteristics of the study area (Van Lanen et al., 2013; Van Loon, 2015).

In recent times, studies have been performed to analyse the drought propagation mechanisms and their controlling factors (Apurv and Cai, 2020; J. Wu et al., 2021). The drought propagation studies have been carried out across the globe (Barker et al., 2016; Bevacqua et al., 2021; Bhardwaj et al., 2020; Botai et al., 2019; Jehanzaib et al., 2020; Tijdeman et al., 2018; Y. Xu et al., 2019). It is found that the propagation time from meteorological to hydrological drought varies with respect to the study area. For instance, Bhardwaj et al. (2020) found four to five months for the majority of locations in India and Xu et al. (2019) noticed that the time of propagation in grassland and forest dominated subbasins varies between one to five months and four to seven months in northern China, respectively. In addition, the factors (e.g., temperature, catchment characteristics, climate type, climate change) influencing the drought propagation are studied globally (Gevaert et al., 2018; Peña-Gallardo et al., 2019; Van Loon and Laaha, 2015). The above-said studies did not include the large-scale climate indices and regional hydro-meteorological variability in developing the drought indices which would affect the drought propagation. Therefore, there is a dearth in understanding the influence of large-scale climate indices, and regional hydro-meteorological variables in modulating the drought events and subsequently the propagation.

The agricultural sector in India is the mainstay of country's economy as it contributes to the large share of the Gross Domestic Product (GDP), provides employment to the large portion of population, and responsible for overall development in other sectors (J. Das et al., 2020c). India has great variations in the climate zone with different terrains and elevations. In India, about 56% of the net cultivated area is rainfed accounting 44% of food production. The future climate change analysis reveals that the drought risk in India is likely to increase under different climate change scenarios (Bisht et al., 2019; Gupta and Jain, 2018). Thus, it is crucial to understand the mechanisms of drought propagation in India. Recently, scholars have started investigating the drought propagation from meteorological to agricultural drought (N. Chen et al., 2020; Ding et al., 2021a; Du et al., 2021; Wang et al., 2021; Zhu et al., 2021). However, there is a lack of study regarding the propagation mechanism from meteorological to agricultural drought over the agrarian country like India.

With this understanding, this chapter presents the drought propagation study that includes from meteorological to hydrological and meteorological to agricultural drought conditions over India. From Chapter 4, it is found that the non-stationary drought index enables to incorporate the large-scale climatic oscillations and regional variability. In addition, the non-stationary drought analysis outperforms the stationary analysis. Thus, meteorological, hydrological, and agricultural drought indices used in the present study are taken from Chapter 4. The important research questions addressed in this study are as follows: (i) What is the time of propagation from meteorological to hydrological and agricultural drought according to the drought initiation (Δs), peak (Δp), and termination (Δe); (ii) How the meteorological, hydrological, and agricultural drought development and recovery period varies over India; and (iii) What is the spatial variability of speed of hydrological, and agricultural drought development and recovery across India? The outcomes will provide a basis for the study of different droughts at regional scale and are useful to inform future early warning and monitoring systems.

5.2 Methodology

It should be noted that the details of the hydro-meteorological datasets and large-scale climatic oscillations used to develop the drought indices are presented in Chapter 3 and Chapter 4. In addition, Chapter 4 describes the implementation of non-stationarity in the computation of different drought indices. The developed indices are used here to understand

the influence of external factors in drought propagation study. In this chapter, the concept of drought propagation is introduced. Here, drought propagation from meteorological to hydrological and agricultural drought is presented. In addition, the drought development period (DDP) and drought recovery period (DRP) are analysed. The rate of change of cumulative drought deficit for development and recovery phases are computed to evaluate the Instantaneous Development Speed (IDS) and Instantaneous Recovery Speed (IRS), respectively. The methodological development is similar for both the cases. Therefore, the entire methodology is explained with respect to the propagation from meteorological to hydrological drought. The graphical representation of drought propagation is presented in Figure 5.1.

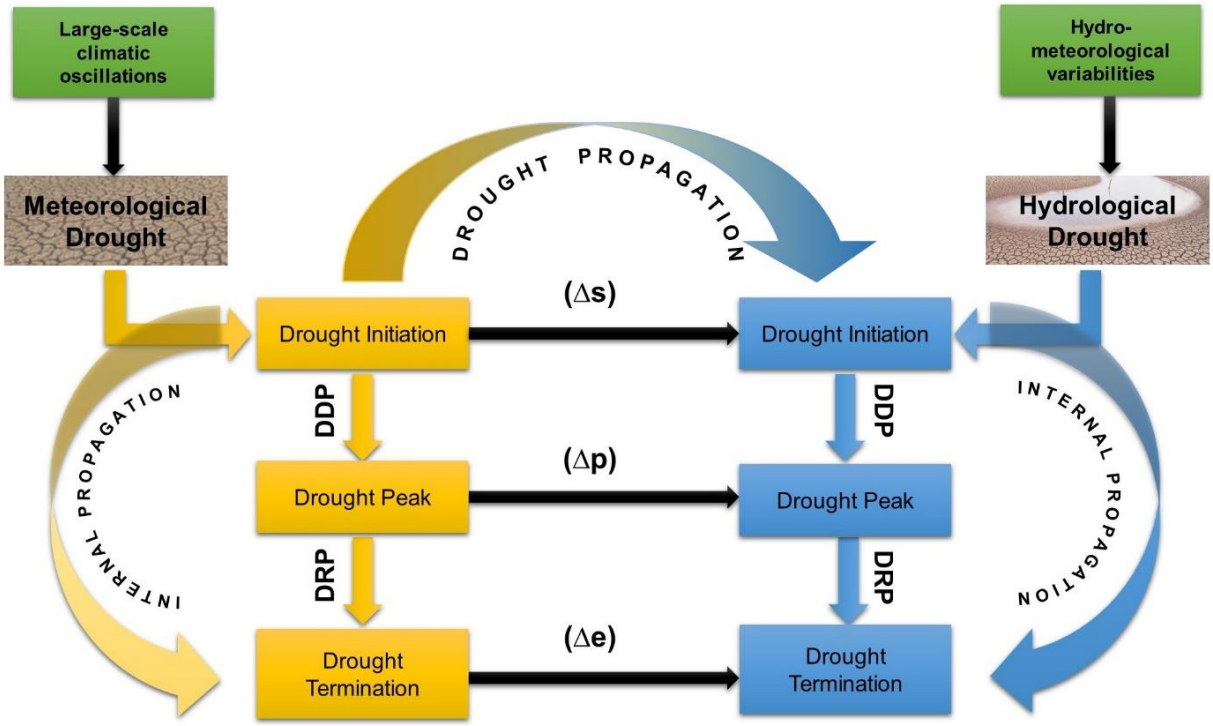

Figure 5.1: Graphical abstract representing different components of drought propagation

It can be seen from the figure that the drought indices developed using the non-stationary approach is used to evaluate the drought propagation. The inter and intra propagation of drought is known as drought propagation and internal propagation, respectively. The period from initiation to peak is known as DDP and period from peak to termination is termed as DRP. The drought propagation is studied for three different cases i.e., for Δs, Δp and Δe. It should be noted that the entire analysis is carried out for all the grid points over India (refer to Figure 4.1 in Chapter 4).

5.2.1 Propagation of meteorological to hydrological drought

The propagation time is the period during which the deficit in the meteorological variable reflects as a deficit in the hydrological variable (Huang et al., 2017). In the present study, the propagation time from SPEI to SRI is estimated based on the three different ways i.e., difference between the initiation to initiation, peak to peak, and termination to termination of meteorological and hydrological drought spell (Figure 5.2).

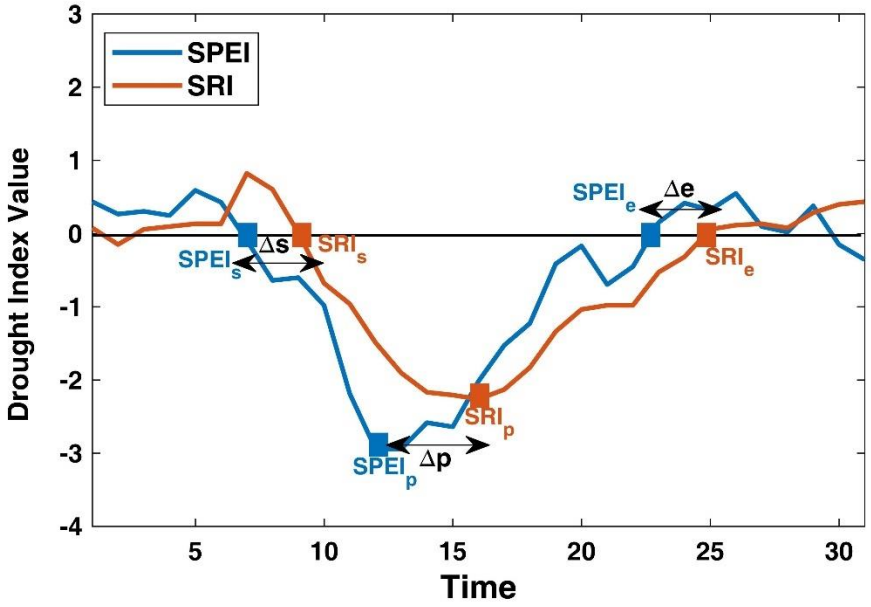

Figure 5.2: Graphical presentation of different drought propagation criteria (initiation to initiation, peak to peak, and termination to termination) used in the present study

The threshold for considering an event as drought is set to zero (Jingwen Wu et al., 2018) below which all the values are considered as drought condition. In this study, the drought spell is defined when the SPEI and SRI values are below zero for more than and equal to three months, consecutively. In the same way the initiation of a meteorological (hydrological) drought event is defined if the 1-month SPEI (SRI) is below the threshold for three or more consecutive months. Likewise, the termination of meteorological (hydrological) drought event is considered when the 1-month SPEI (SRI) is above the threshold for three or more consecutive months. Here, an extended period of the meteorological drought that starts twelve months prior to the initiation of hydrological drought is considered to account the lag that might exist between meteorological and hydrological drought. Subsequently, the difference between the initiation to initiation (Δs), peak to peak (Δp) and termination to termination (Δe)

of hydrological and the nearest meteorological drought event for each drought spell is computed to identify the accumulation period of meteorological drought that translates to hydrological drought using the 1-month SPEI and SRI. Lastly, the mean of the propagation time at different drought spells is computed for three different conditions at each grid point. Due to high seasonality in the precipitation, the correlation-based analysis is not suitable over Indian region in order to identify the drought propagation (Bhardwaj et al., 2020). It is worth mentioning that the drought propagation is computed for the SRI values obtained from different runoff data sources. It should be noted that the same methodology is applied for the propagation from meteorological to agricultural drought. In case of agricultural drought, SSI is used.

5.2.2 Hydrologic drought development and recovery

In this section, an important aspect of hydrological drought propagation is analysed that focuses on the time required for drought development and drought recovery (Figure 5.3). In other words, it defines the internal processes of drought propagation that occurs between the development and recovery of hydrological drought (Bonsal et al., 2011; Thomas et al., 2014). In this study, the methodology proposed by Wu et al. (2018) is used to evaluate the propagation speeds using the variable motion relationship which incorporates the non-uniform rates of internal drought propagation. The development phase (DP) of drought is defined as the time difference between the initiation and peak point (Δs-p) and the recovery phase (RP) is the time difference between the peak and termination point (Δp-e). The rate of change of SRI from initiation (peak) to peak (termination) can be characterized by development speed (recovery speed) (Parry et al., 2016a, 2016b). Here, rate of change of cumulative drought deficit for development and recovery phases are computed to evaluate the Instantaneous Development Speed (IDS) and Instantaneous Recovery Speed (IRS), respectively.

The Total Variability in Development Period (TVDP) and Total Variability in Recovery Period (TVRP) are computed as the cumulative of SRI values during the development phase and recovery phase, respectively for each identified drought spell. To compute the IDS and IRS, the development and recovery phases are divided into intervals (i=1, 2… n-1, n) as presented in Eqs. 5.1 and 5.2. Subsequently, the average of IDS and IRS is estimated with the help of Eqs. 5.3 to 5.4. It should be noted that the temporary drought recovery events in the development phase and drought development in the recovery phase are not included.

Therefore, the IDS (or IRS) at at t_i using the $\Delta TVDP_i$ (or $\Delta TVRP_i$), which is equal to $TVDP_i - TVDP_{i-1}$ (or $TVRP_i - TVRP_{i-1}$), can be computed as follows:

$$IDS(t_i) = \frac{\Delta TVDP_i}{\Delta t_i} \ (i = 1, 2, ..., n) \tag{5.1}$$

$$IRS(t_i) = \frac{\Delta TVRP_i}{\Delta t_i} \ (i = 1, 2, ..., n) \tag{5.2}$$

The average of IDS (or IRS) for a certain period of drought event can be computed as follows:

$$\overline{IDS} = \frac{\sum_{t_1}^{t_n} \Delta TVDP_i}{\sum_{t_1}^{t_n} \Delta t_i} (i = 1, 2, ..., n) \tag{5.3}$$

$$\overline{IRS} = \frac{\sum_{t_1}^{t_n} \Delta TVRP_i}{\sum_{t_1}^{t_n} \Delta t_i} (i = 1, 2, ..., n) \tag{5.4}$$

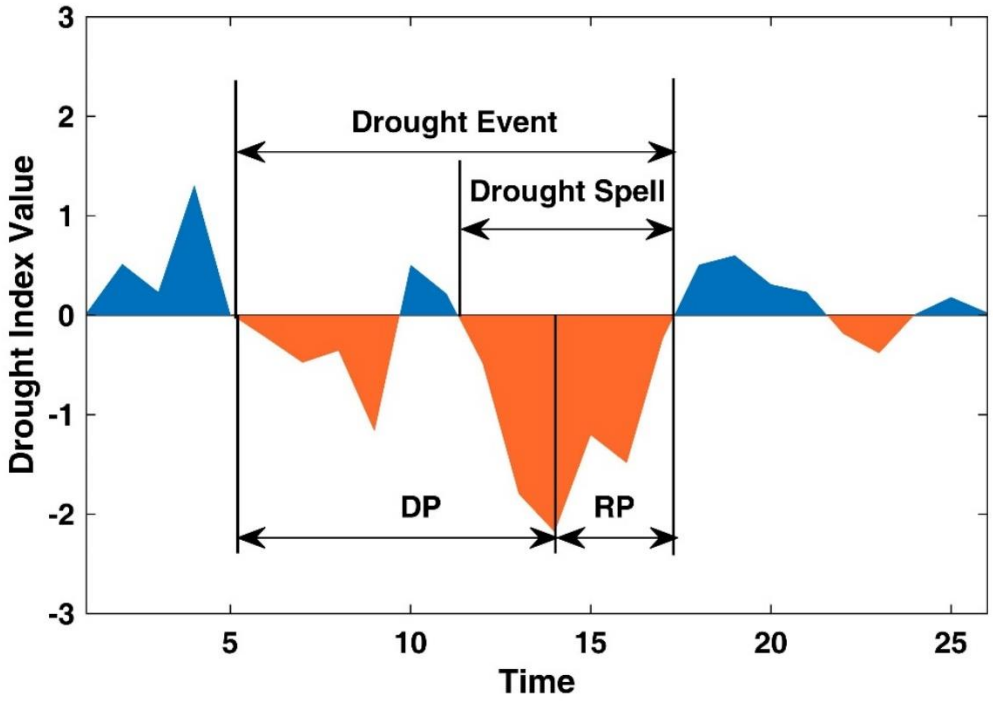

Figure 5.3: Graphical presentation of drought event, drought spell, development period (DP), and recovery period (RP)

5.3 Results

5.3.1 Drought development and recovery period

The duration of DP and RP is known as drought development period (DDP) and drought recovery period (DRP), respectively. The average DDP and DRP of all the runoff datasets are presented in Figure 5.4 and Figure 5.5, respectively. The inter-model variability of DDP and DRP is significantly large among the models. For instance, MEERA2 indicates about 65% of the total area with DDP below 3 months. Whereas GLDAS shows about 64% of total area having DDP between 3.1 to 6 months. Similarly, the percentage area varies from 40% to 71% for DRP between 3.1 to 6 months among the models. The spatial variability is similar in the cases of ERA5, FLDAS, and NCEP for the corresponding high values of DDP and DRP.

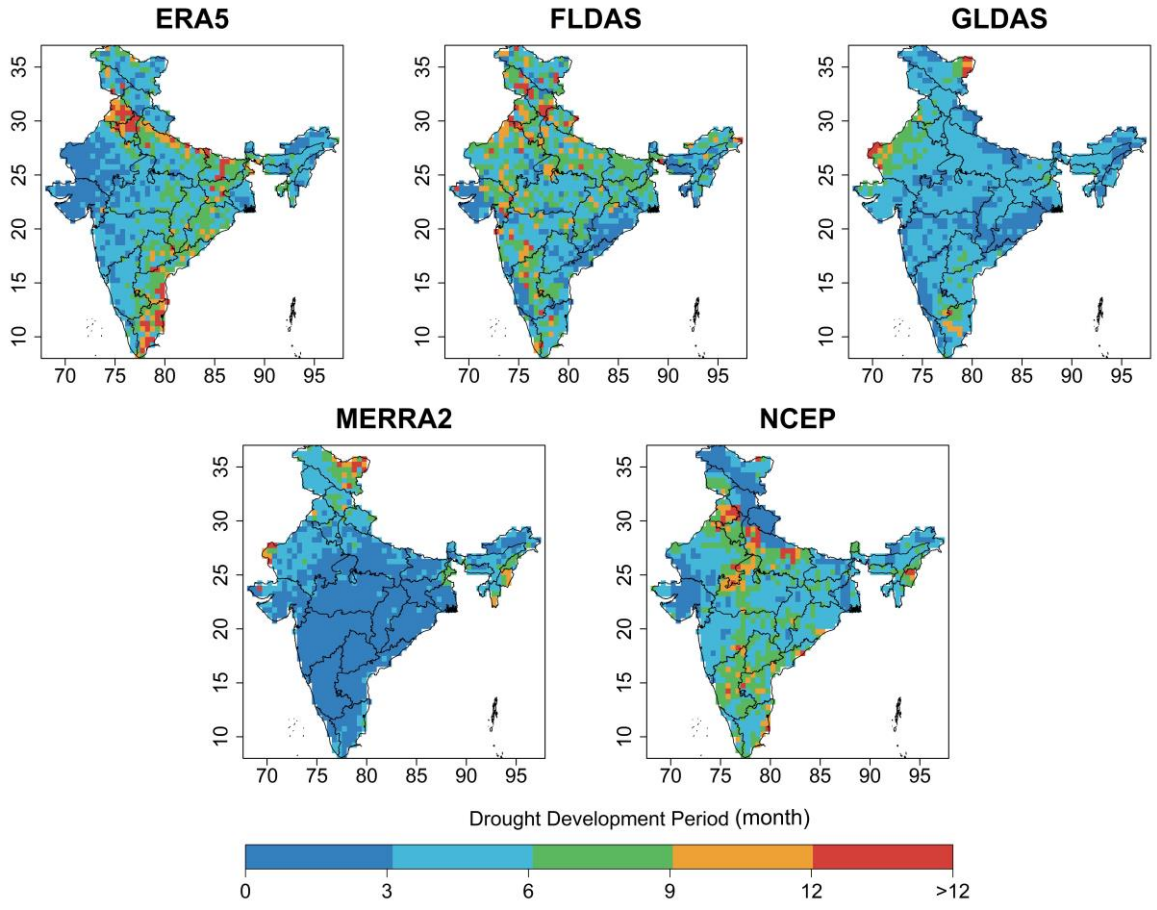

Figure 5.4: Average drought development period computed from different runoff datasets

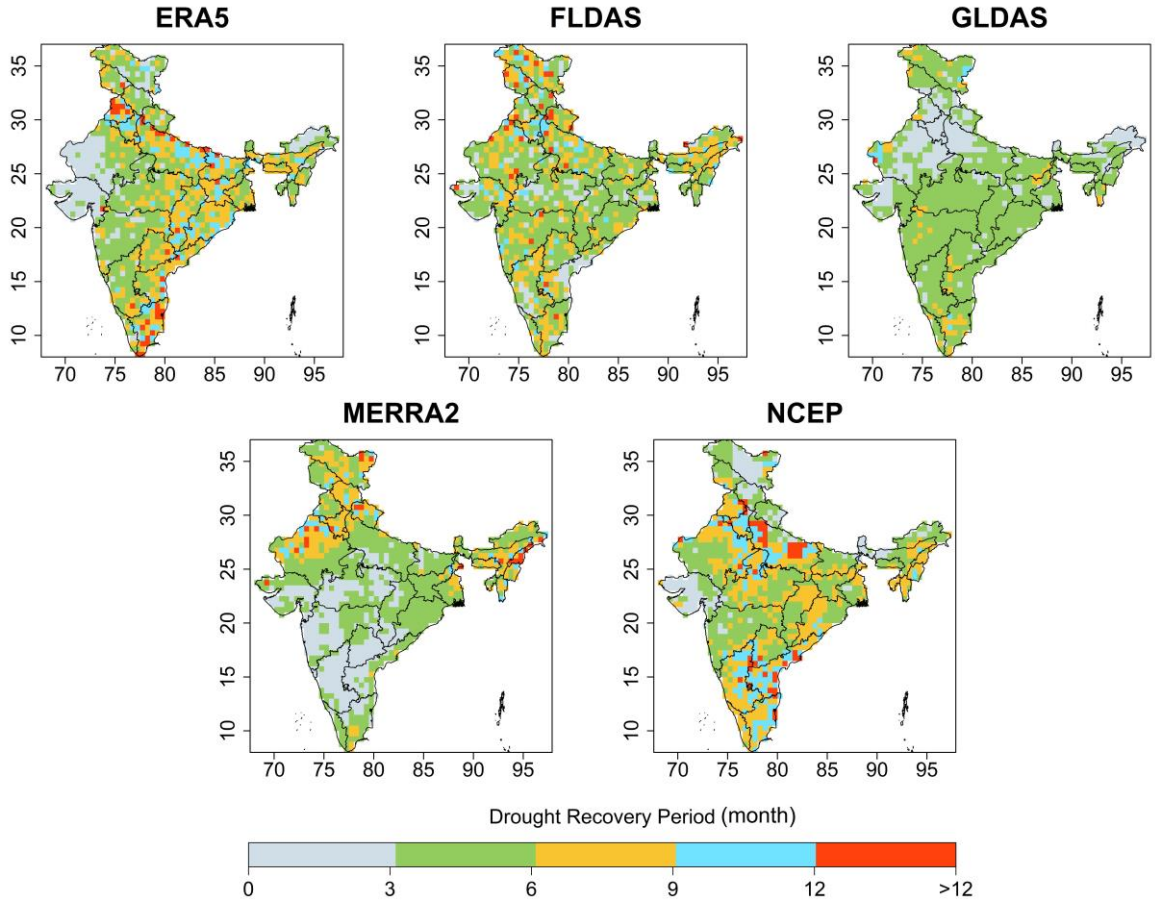

Figure 5.5: Average drought recovery period computed from different runoff datasets

The agricultural drought development period (DDP) and drought recovery period (DRP) are presented in Figure 5.6 and Figure 5.7, respectively. From Figure 5.6, it can be noted that there is spatial variability among different datasets regarding DDP. However, the range of DDP is 3.1 to 9 months over more than 80% of the total area as computed from the SSI index of all models. The higher DDP is observed over the northern parts of India in the cases of CPC, FLDAS, and GLDAS datasets. Whereas high DDP over north-western parts of India is noticed for CPC, ERA5, and MERRA-2 models' datasets. It is observed from Figure 5.7 that in case of DRP value ranging from 3.1 to 6 months, the highest percentage of area is computed as 50% in CPC, 63% in ERA5, 65% in FLDAS, 66% in GLDAS, 52% in MERRA-2, and 76% in NCEP. The grids with high value of DDP are also associated with high value of DRP.

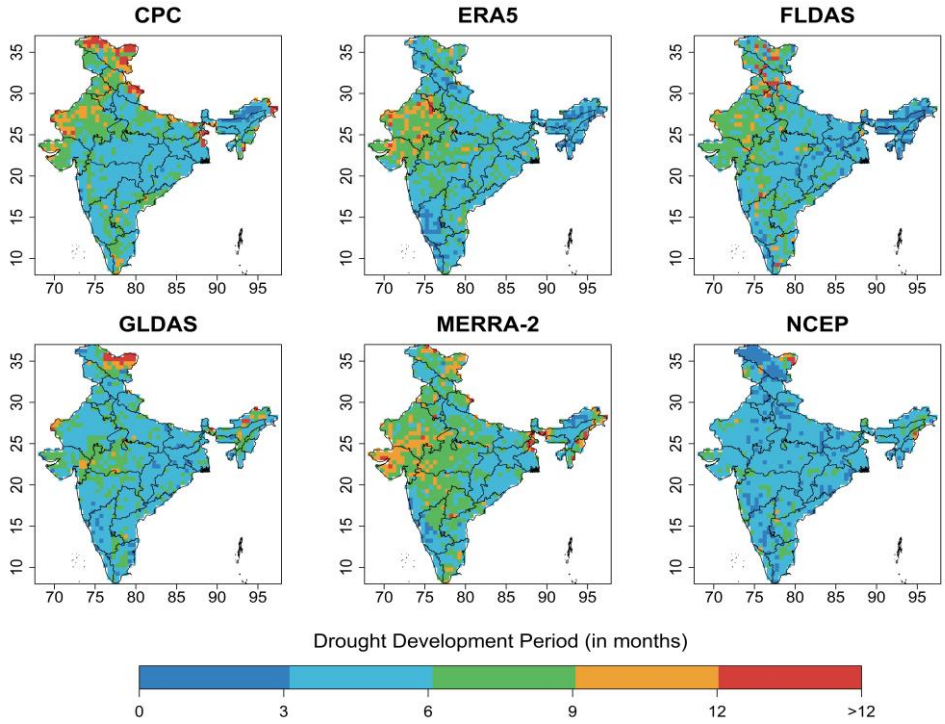

Figure 5.6: Average drought development period computed from different soil moisture datasets

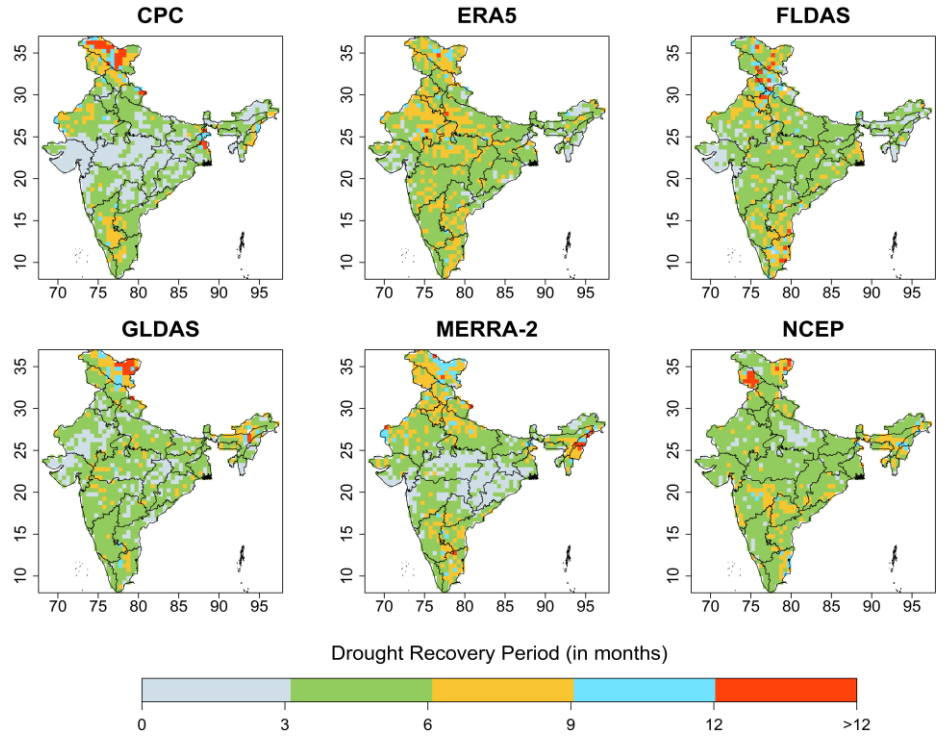

Figure 5.7: Average drought recovery period computed from different soil moisture datasets

Likewise, it is found that locations with the high value (greater than 10 months) of DDP are also having high value of DRP for meteorological drought index (Figure 5.8). These regions are mostly located over southern and northern parts of India. It is computed that the highest areal coverage of DDP and DRP of about 59% and 46% of the total area respectively for the time period of 3.1 to 6 months. The high DDP and DRP is noticed over some parts of Karnataka (KA), Tamilnadu (TN), Kerala (KL), and Ladakh (LA). The ensemble mean of DDP and DRP incorporating all runoff datasets is presented in Figure 5.9. It can be noted from the figure that the DDP and DRP of 3.1 to 6 months is observed over most of the areas i.e., about 78% in DDP and 67% in DRP. In addition, only 1% of the area with DDP and DRP more than 12 months is noticed during the study period. Figure 5.10 presents the ensemble mean of DDP and DRP considering all the soil moisture datasets. The DDP range from 3.1 to 6 months is observed over about 65% of total area. Similarly, the range between 3.1 to 6 months is evaluated over 84% of the total area. The regions with high DDP are having high DRP across India.

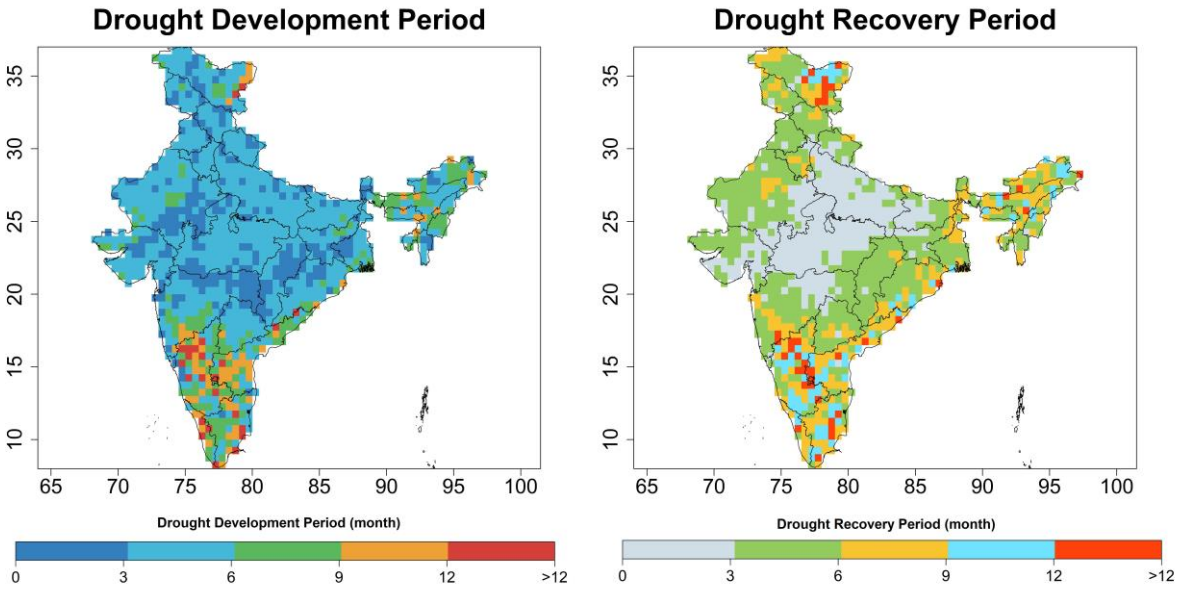

Figure 5.8: The DDP and DRP of meteorological drought using IMD data over India during 1982-2015

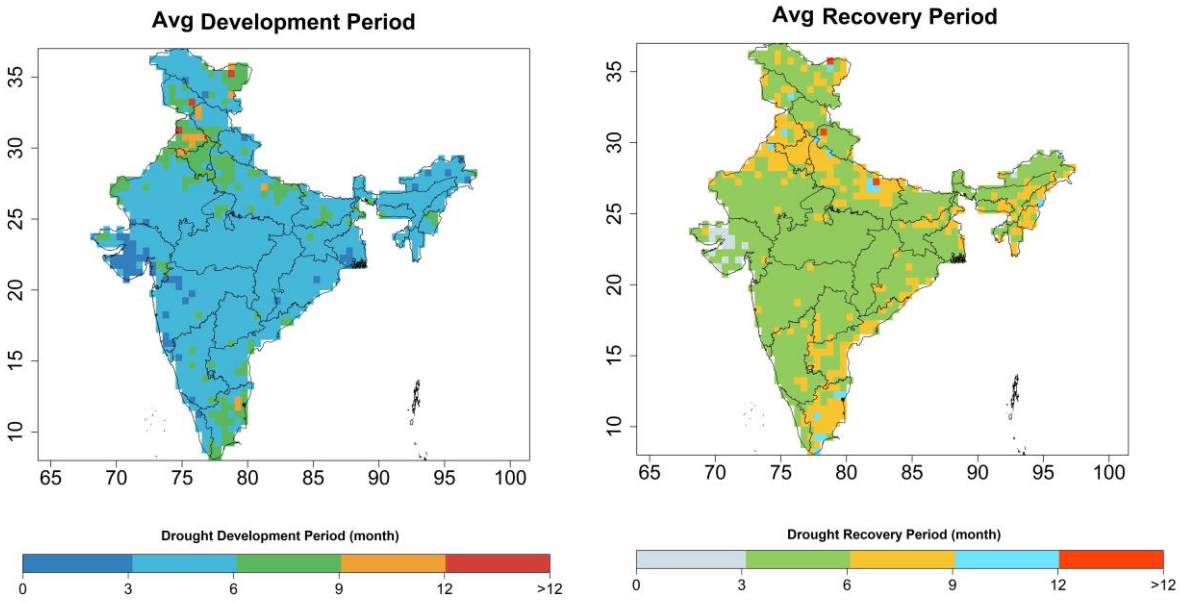

Figure 5.9: The ensemble mean DDP and DRP of hydrological drought over India during 1982-2015

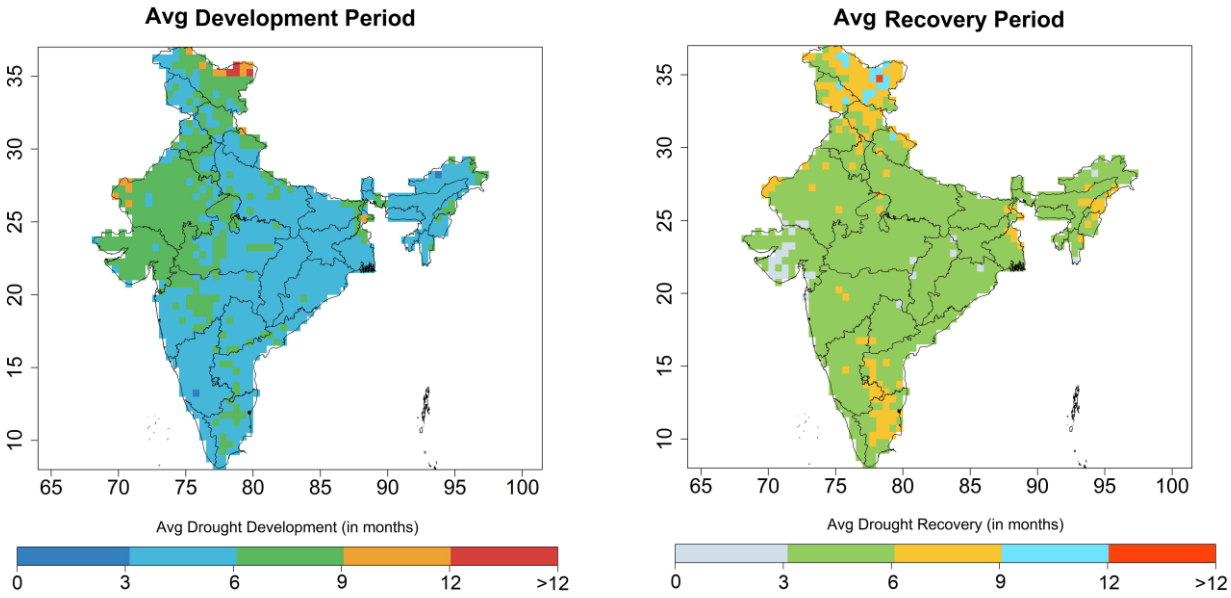

Figure 5.10: The ensemble mean DDP and DRP of agricultural drought over India during 1982-2015

5.3.2 Instantaneous drought development and recovery speed

Next, the internal propagation of droughts is examined using the concept of IDS and IRS. Here, the rate of internal drought propagation is characterised by the instantaneous

propagation speed. It is worth noting that high value of IDS demands quick and efficient drought management practices. Similarly, the low value of IDS suggests that there is more time to prepare against a developing drought. The understanding of development and recovery rate of internal drought propagation enables water managers in proposing efficient water management strategies. The IDS and IRS of hydrological drought computed using the five different runoff datasets are depicted in Figure 5.11 and Figure 5.12, respectively. From Figure 5.11, information is discerned on the highest percentage of area observed with the IDS values between 0.40 and 0.60 per month for ERA5 (57%), GLDAS (56%), MEERA2 (48%), and NCEP (49%) and between 0.20 and 0.40 per month for FLDAS (42%). However, all the runoff datasets agree with the highest percentage of area for the IRS values from 0.40 to 0.60 per month (Figure 5.12).

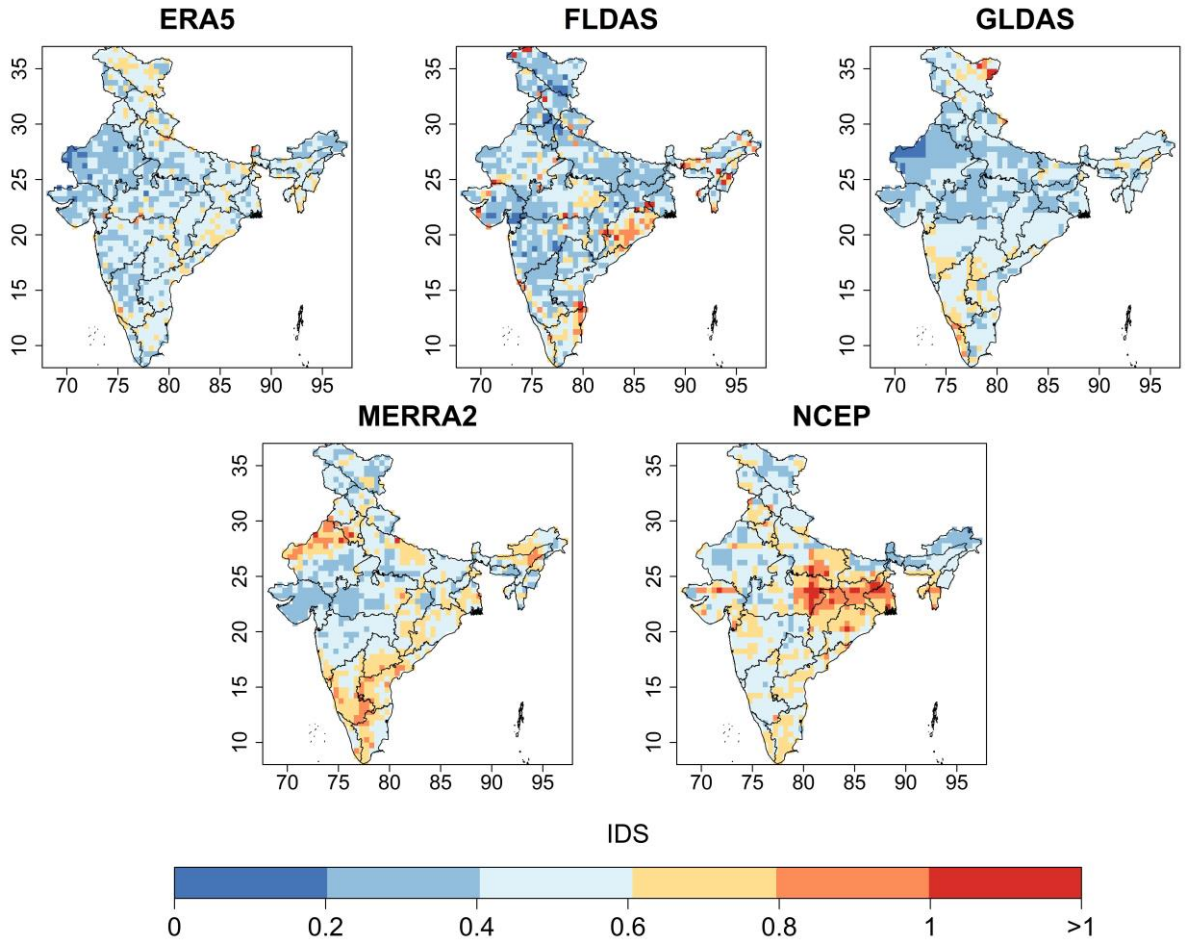

Figure 5.11: Average instantaneous development speed computed from different runoff datasets during 1982-2015

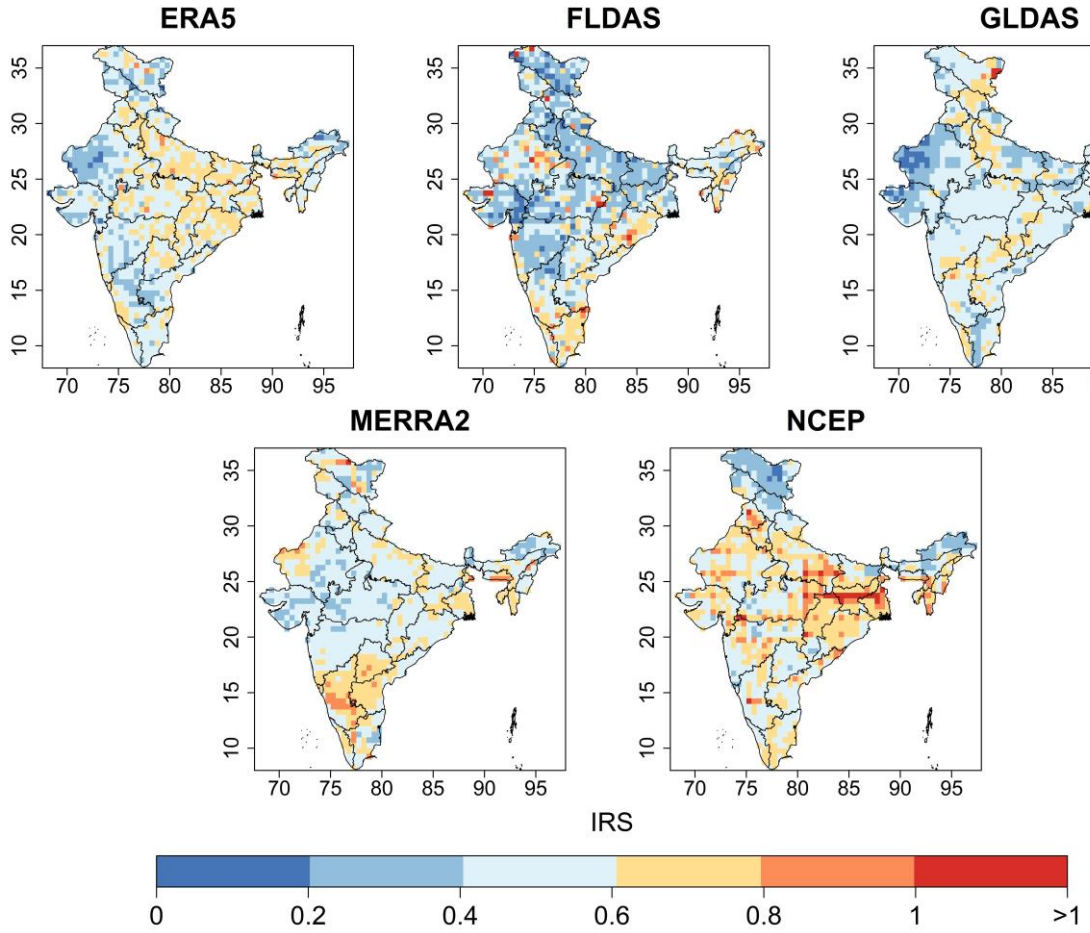

Figure 5.12: Average instantaneous recovery speed computed from different runoff datasets during 1982-2015

The IDS and IRS of agricultural drought evaluated using six different datasets are presented in Figure 5.13 and Figure 5.14, respectively. From Figure 5.13, it can be noted that the percentage of area in range of 0.41 to 0.60 per month for IDS is more across all the models (48% in CPC, 46% in ERA5, 57% in FLDAS, 54% in GLDAS, 46% in MEERA-2, and 70% in NCEP). Moreover, the IDS range between 0.20 and 0.60 per month is noticed for more than 80% of total area in all the datasets. The similar observation is made in case of IRS (Figure 5.14). The highest percentage of area under IRS value from 0.41 to 0.60 is observed in the cases of CPC, FLDAS, GLDAS and NCEP. However, in ERA5 and MEERA-2 datasets, the highest percentage of area is computed in the IRS range between 0.20 and 0.40 per month. The IDS and IRS of meteorological drought is presented in Figure 5.15 using the IMD dataset. It can be noted that about 53% and 47% of the total area comes under the range between 0.4 and 0.6 per month in the case of IDS and IRS, respectively.

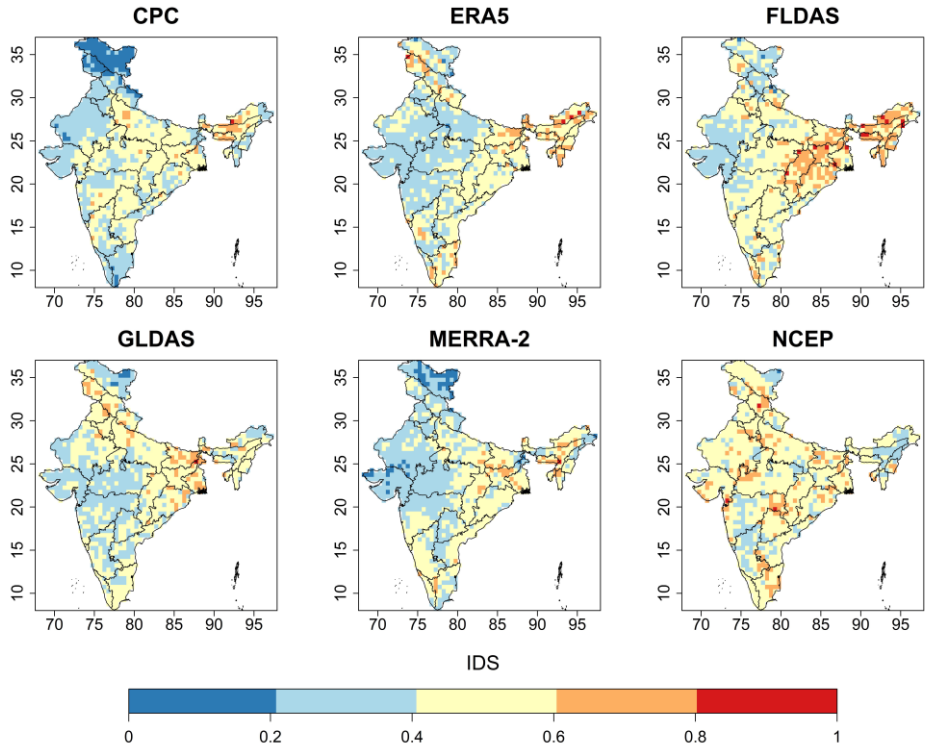

Figure 5.13: Average instantaneous development speed computed from different soil moisture datasets

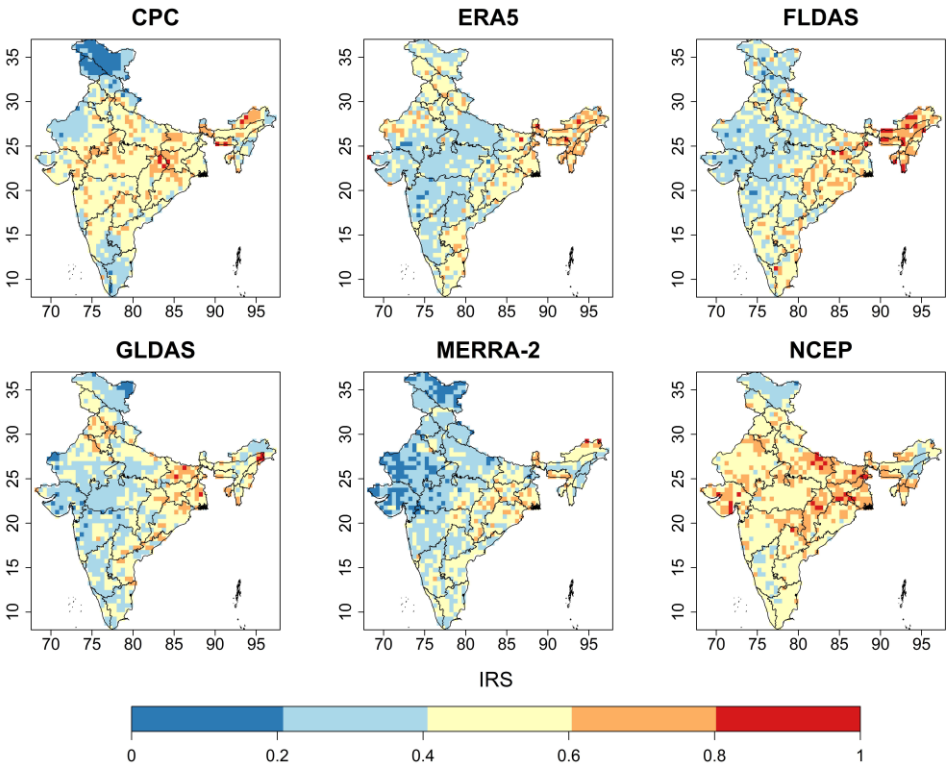

Figure 5.14: Average instantaneous recovery speed computed from different soil moisture datasets

The ensemble average of IDS and IRS for hydrological drought events is plotted in Figure 5.16. It is clear from the figure that most of the area in India has the IDS and IRS values between 0.40 and 0.60 per month. In about 82% of total area the IDS and IRS values vary between 0.40 and 0.60 per month. Interestingly, the high values (0.60 to 0.80 per month) of IDS and IRS are observed mostly in the eastern and southern parts of India. Conversely, the low values (0.20 to 0.40) of IDS and IRS are noticed mostly over western and northern parts of India.

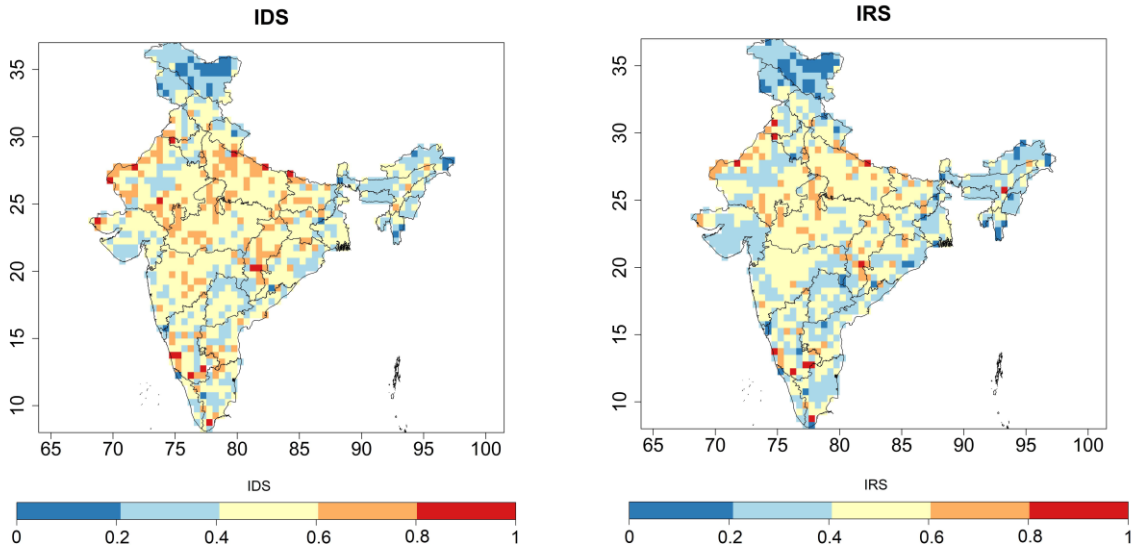

Figure 5.15: The IDS and IRS computed for the meteorological drought events

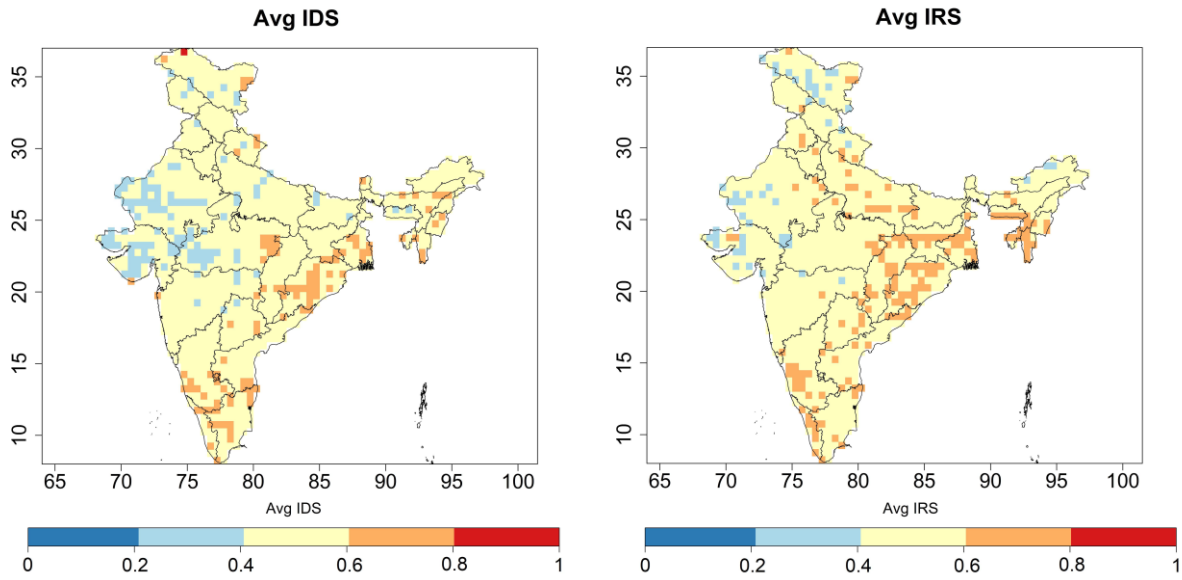

Figure 5.16: The ensemble mean IDS and IRS computed for the hydrological drought events

The ensemble average of IDS and IRS for agricultural drought considering the six different datasets are presented in Figure 5.17. It is evident from the figure that most of the area in India has the IDS and IRS values between 0.20 and 0.60 per month. Precisely, the percentage of total area in the cases of IDS and IRS is computed as 71% and 66% for the range between 0.41 and 0.6 per month, respectively. The low values of IDS and IRS are observed over northern and northwest regions in India. However, high values are noticed over eastern and northeast regions over India.

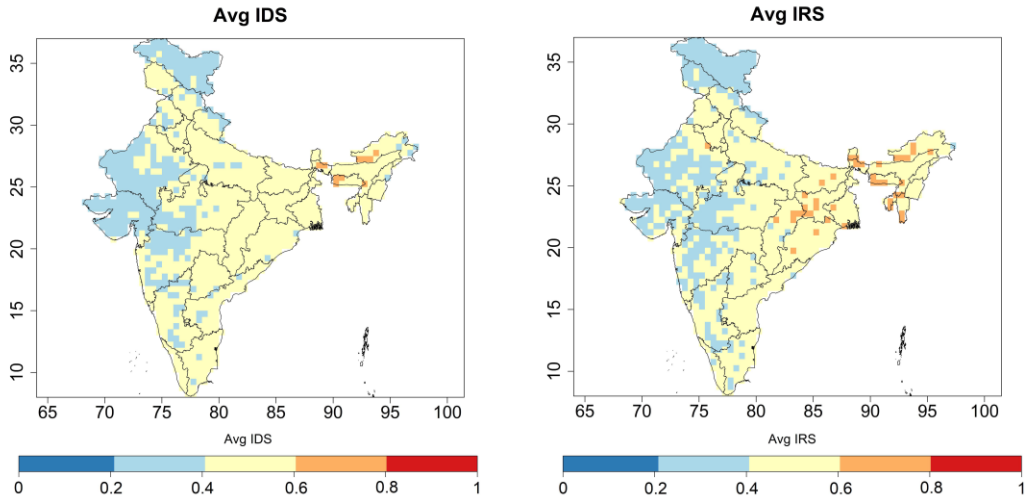

Figure 5.17: The ensemble mean IDS and IRS computed for the agricultural drought events

5.3.2 Drought propagation time

In this section, the important findings related to drought propagation (meteorological to hydrological and meteorological to agricultural) are presented. The drought propagation from meteorological to hydrological with respect to Δs, Δp, and Δe using the five different runoff datasets are presented in Figure 5.18, Figure 5.19, and Figure 5.20, respectively. In the case of Δs, the drought propagation is computed as 6 to 8 months over most of area (55% to 64%) considering all the runoff datasets. It is found that the drought propagation in Δs varies between 4 to 8 months over more than 90% of the study area as observed in the cases of ERA5, FLDAS, GLDAS, and MERRA2. Three out of five datasets are in line with the outcomes that the highest percentage of area with propagation time corresponding to Δp is 9 to 12 months (Figure 5.19). Whereas the time to propagation is computed as 6 to 9 months over 65% of area for MERRA2 dataset. It is observed that the propagation time within the range of 6 to 15 months is observed over 81 to 97% of total area considering the outputs from all the datasets. The propagation time of meteorological to hydrological drought determined

using Δe is more when compared with Δs and Δp (Figure 5.20). It is noticed that the range of the drought propagation time over 86 to 98% of total area varies from 10 to 25 months in the case of Δe.

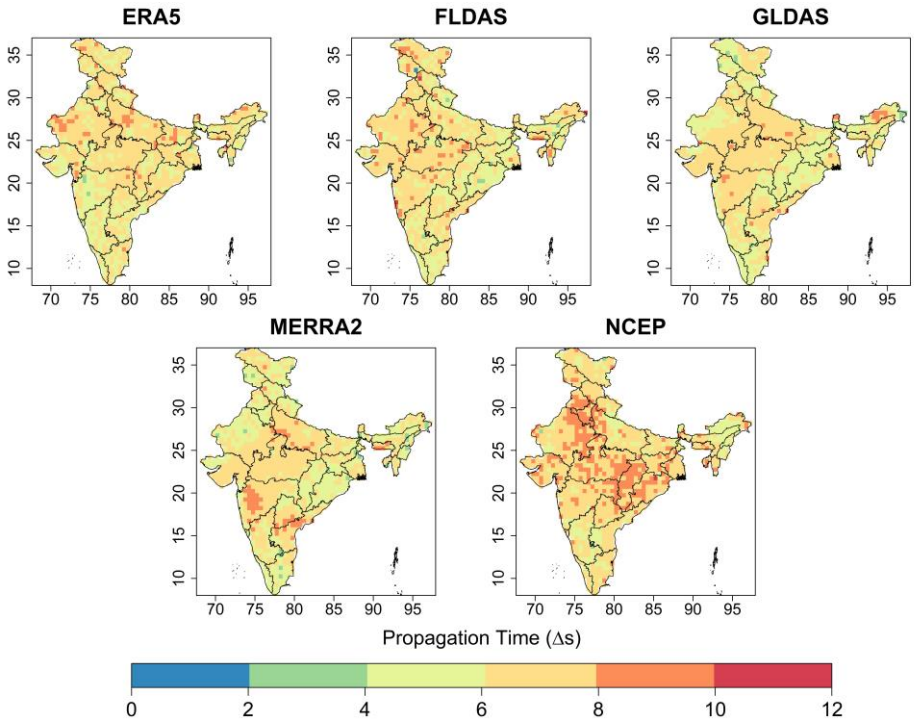

Figure 5.18: Propagation time (in months) computed from different runoff datasets for Δs

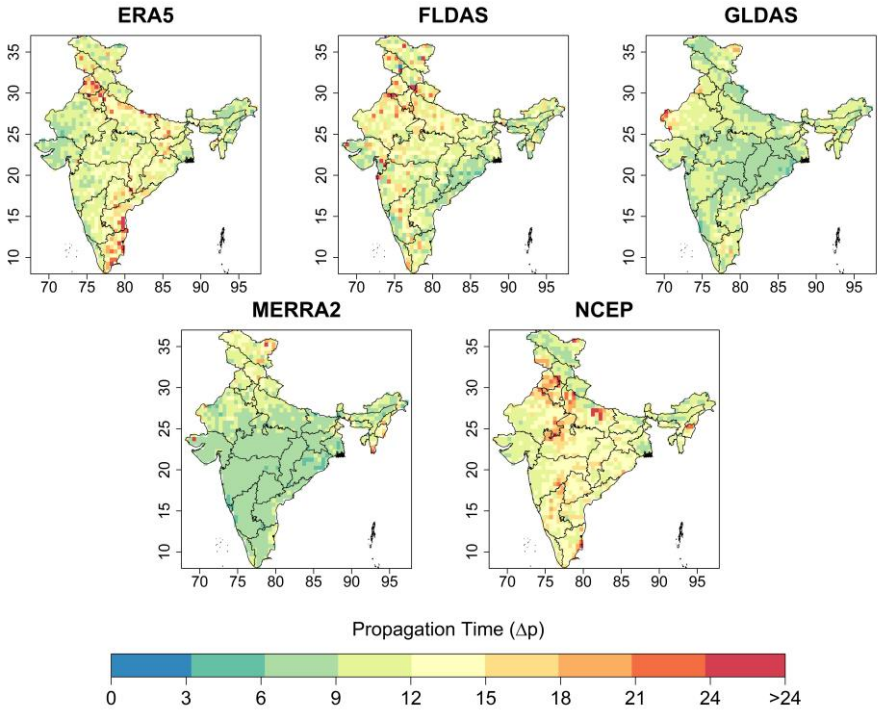

Figure 5.19: Propagation time (in months) computed from different runoff datasets for Δp

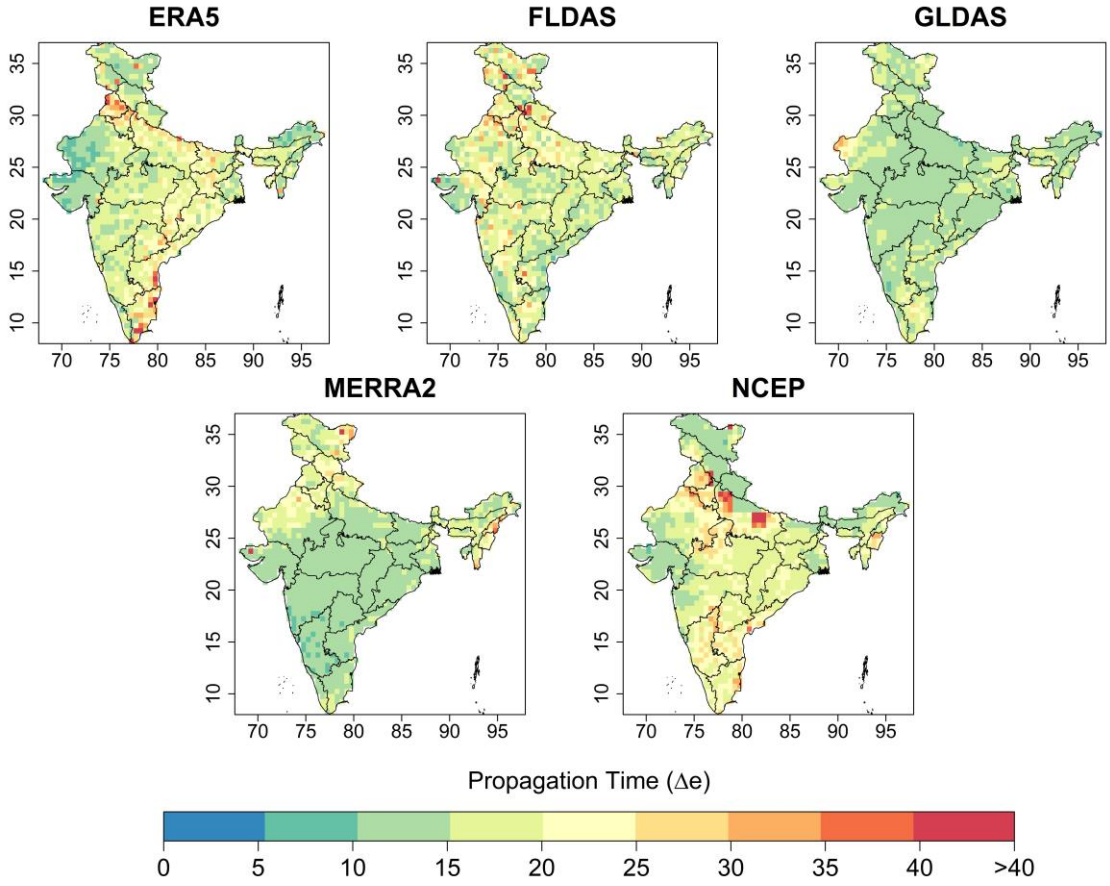

Figure 5.20: Propagation time (in months) computed from different runoff datasets for Δe

Similarly, the drought propagation with respect to initiation, peak and termination using the six different soil moisture datasets (i.e., agricultural drought) are presented in Figure 5.21, Figure 5.22, and Figure 5.23, respectively. The drought propagation period is evaluated as 4 to 8 months (Figure 5.21) over more than 85% of the total area in the case of Δs considering all the soil moisture datasets. More than 50% of the area comes under the propagation period between 6 to 8 months for ERA5, FLDAS, GLDAS, and NCEP and 4 to 6 months for CPC, and MERRA-2 datasets. In case of Δp (Figure 5.22), time to propagation is computed as 6 to 9 months over 80% of area for CPC, 9 to 12 months over 50%, 51%, 58%, and 57% for ERA5, FLDAS, GLDAS, and NCEP, respectively. The propagation time of meteorological to agricultural drought in Δe is more as compared to Δs and Δp (Figure 5.23). The propagation period is computed as 15 to 20 months over 51 to 58% of total area in case of all the datasets except for CPC. In case of CPC, it is noticed that 88% of the total area comes under the propagation period from 5 to 10 months.

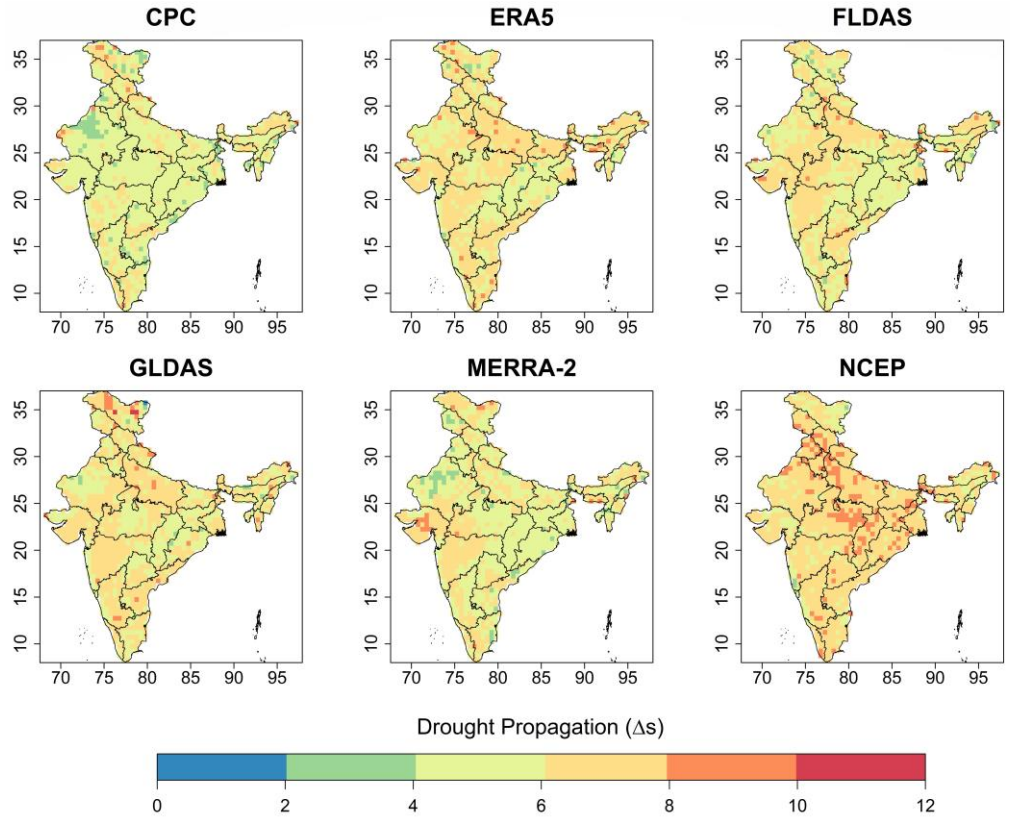

Figure 5.21: Propagation time (in months) from different soil moisture datasets for Δs

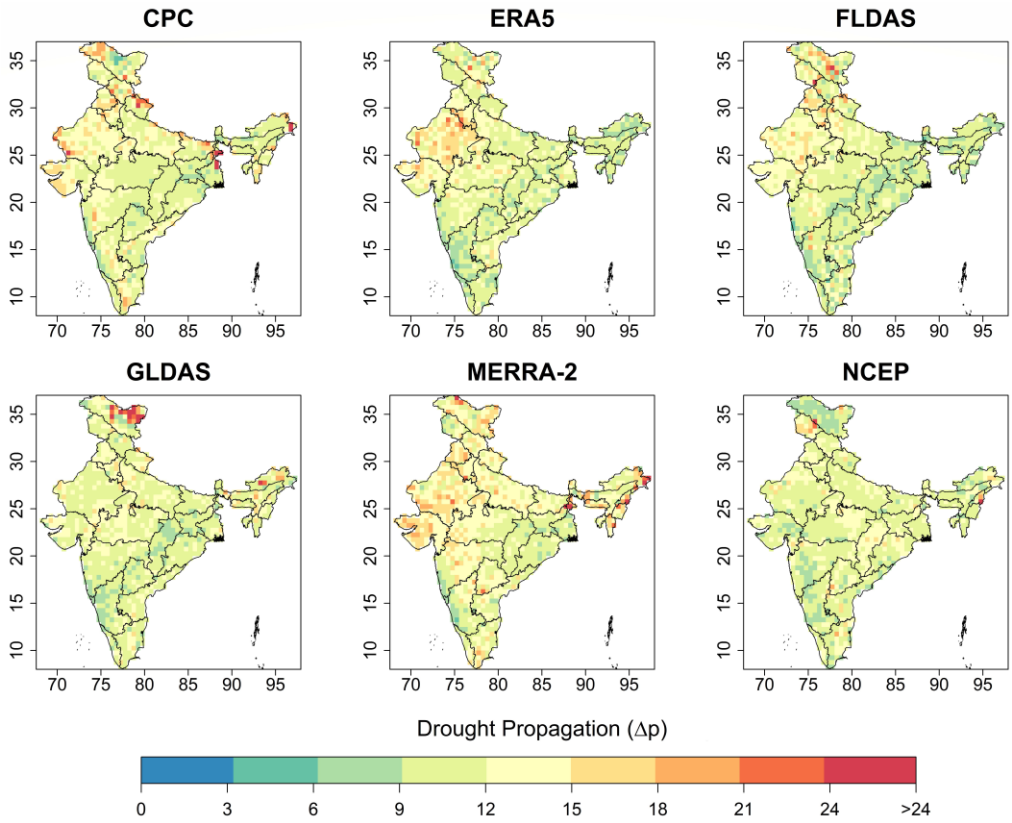

Figure 5.22: Propagation time (in months) from different soil moisture datasets for Δp

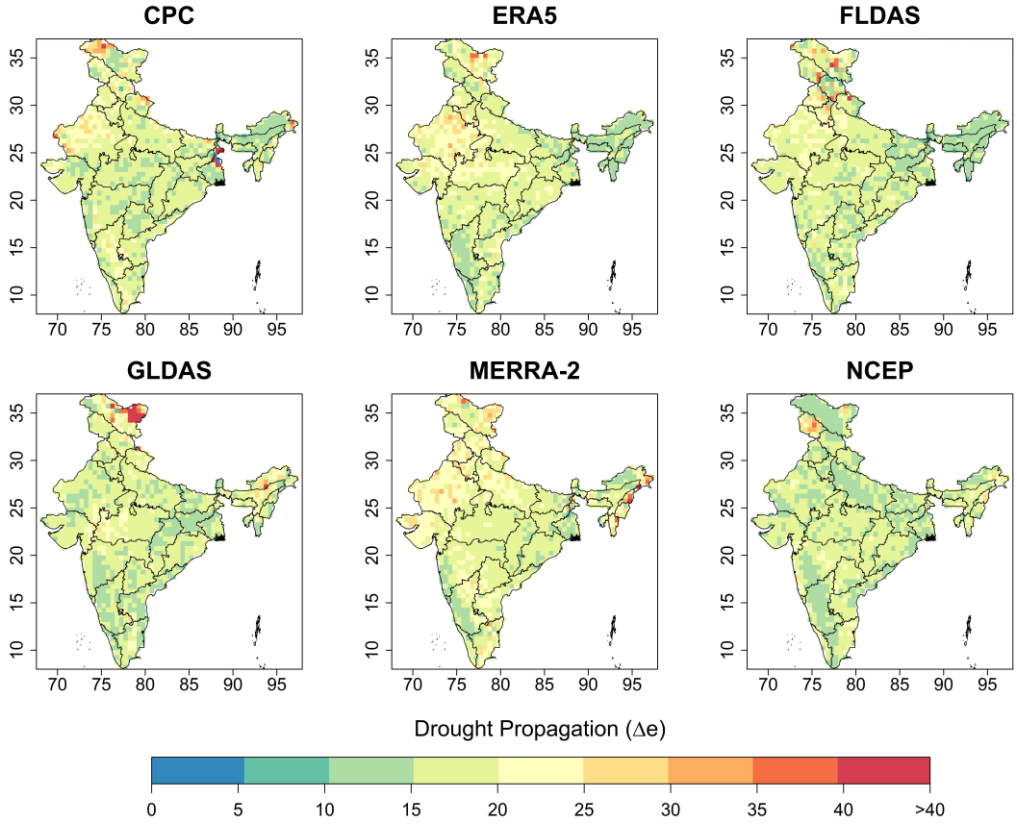

Figure 5.23: Propagation time (in months) from different soil moisture datasets for Δe

The ensemble mean of drought propagation time from meteorological to hydrological at three different cases are presented in Figure 5.24. The propagation time in case of Δs varies between 4 and 9 months with 62% of total area falls under 6 to 7 months followed by 20% of total area under 7 to 8 months. The propagation time over southern, parts of eastern, parts of northeast, and parts of northern regions is less as compared to the central parts of India. In the case of Δp, the time of propagation varies from 9 to 12 months over 74% of the total area. About 70% of total area, the time of propagation in Δe ranges from 15 to 20 months. The ensemble mean of drought propagation time from meteorological to agricultural in different cases are presented in Figure 5.25. The time to propagation in case of Δs is found to be 5 to 6 months and 6 to 7 months over 39% and 53% of the total area, respectively. Similarly, the drought propagation over about 95% of total area ranges from 9 to 15 months under Δp condition. The time to propagation varies between 10 to 15 months over 32% and 15 to 20 months over 65% of total area in case of Δe.

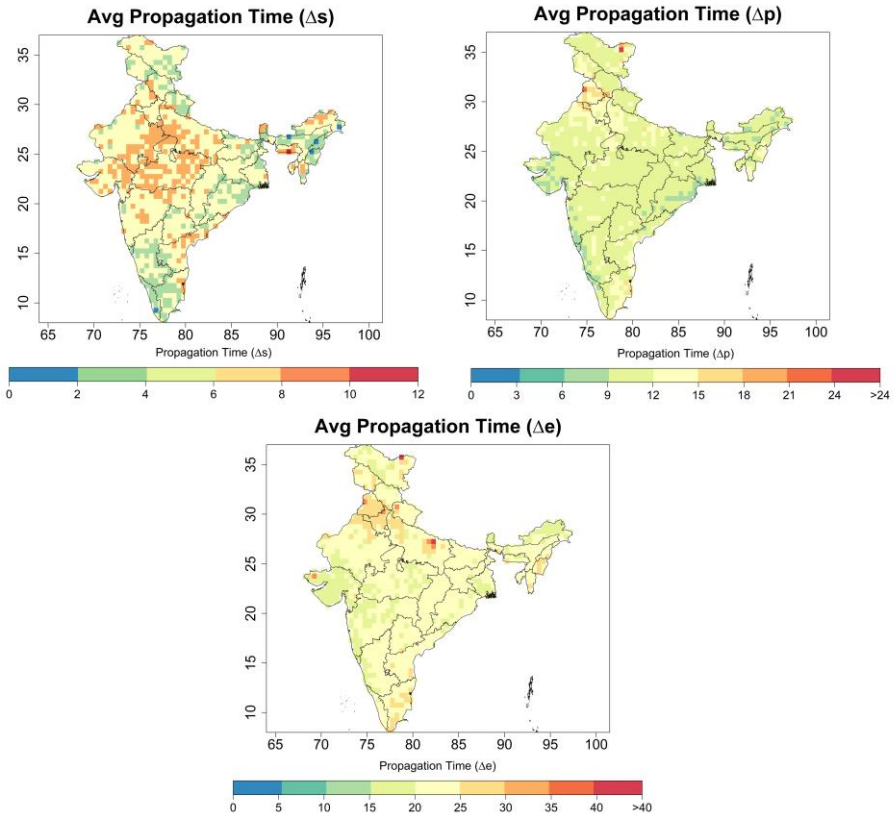

Figure 5.24: Average propagation time from meteorological to hydrological drought

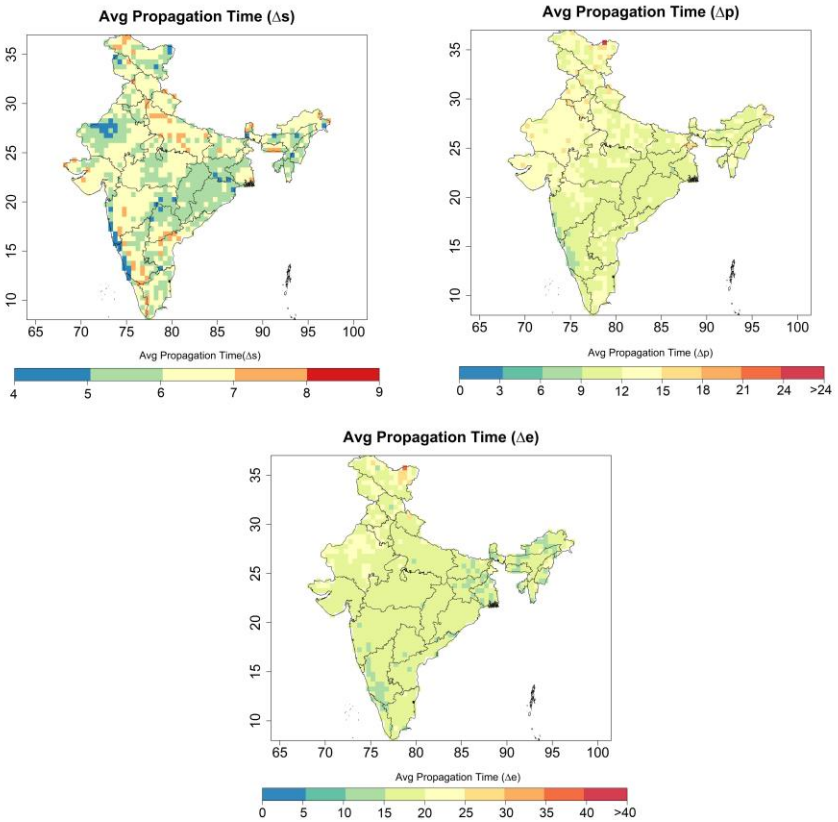

Figure 5.25: Average propagation time from meteorological to agricultural drought

5.3.3 Influence of external drivers on drought propagation

To find out the influence of external drivers/covariates on drought propagation, a comparison between the drought propagation with and without external drivers is examined. To do so, the percentage changes in IDS, IRS, DDP, DRP, Δs, Δp and Δe are computed with respect to the hydrological drought index computed without external covariates. Figure 5.26 presents the change in percentage of above-said drought propagation characteristics. It should be noted that the ensemble average of five different runoff datasets are considered for the analysis. It can be noted from the figure that except for drought propagation time in Δs, the drought propagation characteristics are underestimated when computed neglecting the external covariates. For instance, over 75% of area in IDS, 87% of area in IRS, 73% of area in DDP, 53% of area in DRP, 61% of area in Δp, and 66% of area in Δe are underestimated when compared incorporating the influence of external covariates. In the case of Δs, the percentage of change mostly varies between the ranges of -20% and 20%. The magnitude of change in case of IDS, IRS, DDP, and DRP is higher than time to propagation. In addition, the state-wise average percentage of change is computed. In the case of IDS, it is observed that the highest and lowest value of percentage change (absolute) is observed over Rajasthan (RJ) and Odisha (OD), respectively. Similarly, the highest and lowest absolute percentage is noticed over Gujarat (GJ) and Ladakh (LA) in case of IRS, over Manipur (MN) and Ladakh (LA) in case of DDP, over Mizoram (MZ) and Himachal Pradesh (HP) in case of DRP, over Manipur (MN) and Punjab (PB) in case of Δs, over Punjab (PB) and Odisha (OD) in case of Δp, and over Manipur (MN) and Andhra Pradesh (AP) in case of Δe.

In case of agricultural drought, over 96% of area in IDS, over 82% area in IRS, over 98% area in DDP, over 99% area in DRP, over 64% of area in Δp, and over 98% area in Δe are underestimated when compared with the values calculated in absence of covariates (Figure 5.27). It is found that the magnitude of change is higher in case of internal drought variability (within the drought event) as compared to inter drought variability (between meteorological and agricultural drought event). The highest and lowest value of mean absolute percentage change is observed over Gujarat (GJ) and Tamilnadu (TN) in the case of IDS, respectively. Likewise, the highest and lowest absolute percentage is noticed over Gujarat (GJ) and Tamilnadu (TN) in the case of IRS, over Tamilnadu (TN) and Ladakh (LA) in the case of DDP, over Madhya Pradesh (MP) and Ladakh (LA) in the case of DRP, over Arunachala

Pradesh (AR) and Himachal Pradesh (HP) in case of Δs, over Ladakh (LA) and Andhra Pradesh in case of Δp, and over Madhya Pradesh (MN) and Ladakh (LA) in case of Δe.

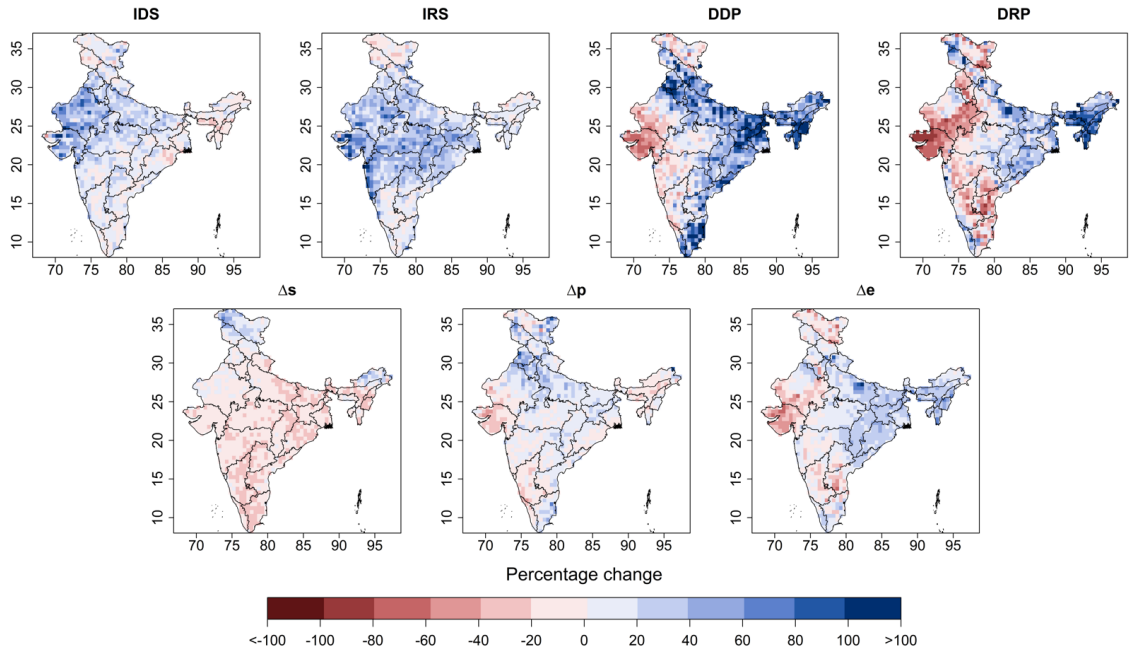

Figure 5.26: The percentage change of different drought propagation characteristics with respect to the hydrological drought computed excluding the external drivers

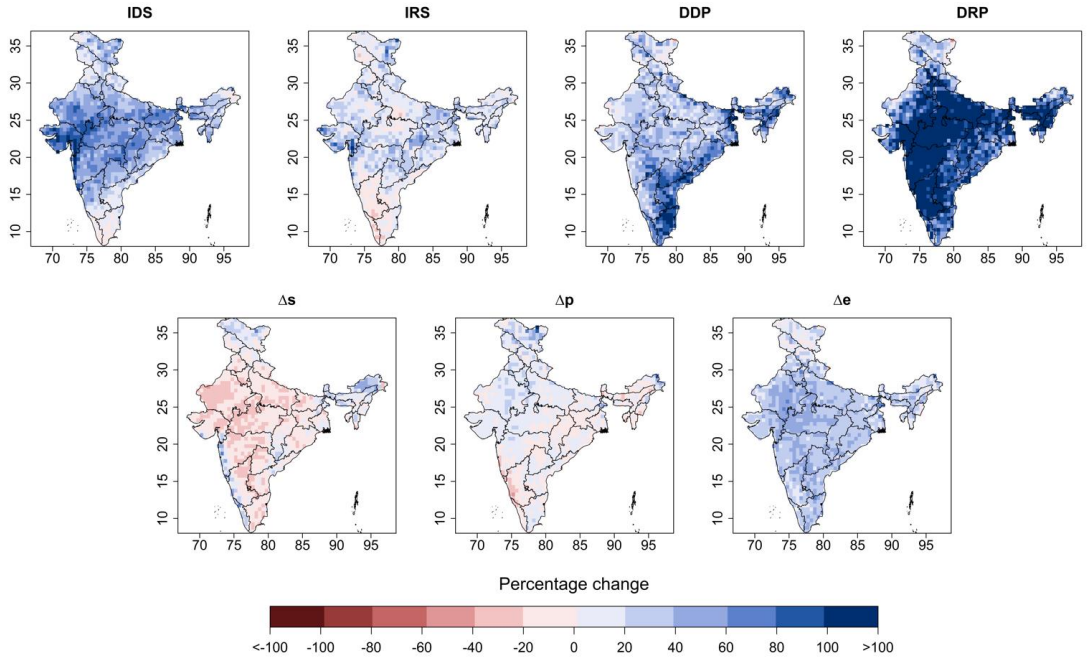

Figure 5.27: The percentage change of different drought propagation characteristics with respect to the agricultural drought computed excluding the external drivers

5.4 Discussion and summary

The prime motive of the present study is to investigate the propagation time from meteorological to hydrological and agricultural drought at gridded scale which is crucial for drought management and warning system (Huang et al., 2017). Moreover, the grid-wise evaluation of time to propagation enables to provide useful information for the local drought early warning and mitigation (N. Chen et al., 2020). As entire India is considered for the study, it is cumbersome to set up a hydrological model for the entire India due to the significant alterations in the streamflow as a result of anthropogenic activities (e.g., influence of dam) and inconsistencies in the continuous available observed streamflow data. Similarly, availability of in situ soil moisture datasets at regional scale covering entire India is not possible. Thus, available gridded runoff and soil moisture datasets at a resolution of 0.5^{o} Lat x 0.5^{o} Lon are considered. Five different gridded runoff and six different soil moisture datasets are considered to encompass the associated uncertainties with the datasets. In addition, the drought characteristics extracted from ensemble mean of all the datasets are analysed. To provide unified outcomes from all the runoff and soil moisture datasets, the ensemble mean is considered. In other words, the average prediction performance of all contributing members in the ensemble is chosen to extract the important findings from the analysis. Combining the multiple datasets in order to solve one problem and focusing on their consistency may obtain the results closer to the truth (N. Chen et al., 2020).

The analysis of DDP and DRP suggests that the grids where the period of drought (meteorological and hydrological) development is more (less) also have a high (low) recovery period. The present finding is in line with the outcomes of Bhardwaj et al. (2020) and Wu et al., (2018) where they considered hydrological drought events. Incorporating the variable motion relationship of speed-time process, hydrological drought propagation can be identified. Traditionally, the propagation of drought is expressed as transformation of one drought type to another type. However, the same drought type experiences the internal propagation (Parry et al., 2016b; Thomas et al., 2014). The concept of IDS and IRS represents the internal variability of drought events and provides crucial feedback about requisite policy changes based on different phases of drought (Bandyopadhyay et al., 2020; Wilhite et al., 2014). Unfortunately, the current policies do not consider the internal drought propagation in formulating the strategies. Moreover, at local scale the combined information of IDS and IRS can strengthen the drought prediction and early warning system. In the case of hydrological

drought, southern and eastern parts of India show high IDS and IRS values suggesting that the drought would develop rapidly and reach its peak and recover quickly to the normal condition. Therefore, these shorter duration droughts need prompt and efficient drought management practices. In the present study, the application of irrigation (as an anthropogenic intervention) is not incorporated and assumed that the variability of soil moisture depends on the precipitation. Because the agricultural drought depends on the precipitation variability and availability of soil moisture that counters water loss due to evapotranspiration (Sheffield et al., 2004). The IDS and IRS defines the speed at which the internal development and recovery of drought occurs. Therefore, prompt, and efficient actions should be taken for high values of IDS.

The propagation time from meteorological to hydrological and meteorological to agricultural drought is computed at each grid point across India. The propagation time depends completely on method being used (Bevacqua et al., 2021) and hence, the present analysis includes three different approaches to examine the propagation time. The propagation time with respect to Δs is shorter than Δp and Δe. In addition, the Δs is not sensitive as compared to others and provide lowest and most smoothed out values for propagation time (Bevacqua et al., 2021). It is observed that the concurrent meteorological drought events during the phase of hydrological and agricultural drought development and recovery periods increase the entire length of hydrological and agricultural events. For instance, a hydrological drought event with duration of 45 months encompasses 3 concurrent meteorological drought events with duration varying from 8 to 10 months. A comparative analysis (in case of Δs only) of the present outcomes with Bhardwaj et al. (2020) reveals that there is a difference in the time range of drought propagation. For instance, the present study evaluates that the propagation period ranges between 4 and 9 months. Whereas Bhardwaj et al. (2020) computed that the propagation period varies between 0 and 5 months. However, it is noticed that the spatial distribution of low and high propagation period between two studies is similar. The variability in the magnitude of propagation time might have resulted due to the inclusion of large-scale climatic indices and regional hydro-meteorological variability in the computation of drought indices. The present analysis at regional scale would provide efficient water management strategies at local scale whereas the findings by Bhardwaj et al. (2020) help at the sub-basin scale.

Summarising the findings, it is found that locations with the high value of DDP are also having high value of DRP in both the cases (hydrological and agricultural). In case of

hydrological drought, most of the area in India has the IDS and IRS values between 0.40 and 0.60 per month. However, the same varies between 0.20 and 0.60 per month in the case of agricultural drought. The meteorological to hydrological propagation time in case of Δs varies between 4 and 9 months with 62% of total area falling under 6 to 7 months followed by 20% of total area under 7 to 8 months. In the case of Δp, the time of propagation varies from 9 to 12 months over 74% of the total area. For about 70% of total area, the time of propagation in Δe ranges from 15 to 20 months. In case of Δs, the propagation from meteorological to agricultural drought is found to be 5 to 6 months and 6 to 7 months over 39% and 53% of the total area, respectively. Similarly, the drought propagation over about 95% of total area ranges from 9 to 15 months under Δp condition. The time to propagation varies between 10 to 15 months over 32% and 15 to 20 months over 65% of total area in case of Δe. It is found that the drought propagation and its characteristics are underestimated over most of the regions in India when computed without the external drivers. In addition to drought propagation, it is necessary to evaluate the agricultural risk associated with drought events. As an agrarian country, India's economy largely depends on agricultural productivity. Therefore, it is of utmost importance to examine the agricultural drought risk for different crops. In this sense, the next chapter deals with the evaluating the agricultural drought risk on rainfed agriculture using the multivariate analysis.

Chapter 6

Copula-based agricultural drought risk analysis

6.1 Introduction

The agricultural drought is considered as complex natural hazard (Dai, 2011a). The nexus between meteorology, soil, and crop systems makes agricultural drought more cumbersome to understand (Liu et al., 2020). It measures the vulnerability in terms of crop productivity which is sensitive to both hydrological and meteorological conditions (Tsakiris et al., 2013). The agricultural drought, because of insufficient soil moisture in the root zone due to lack of precipitation (Liu et al., 2018), reduces the crop productivity (Shen et al., 2019). Over arid and semi-arid regions, the crop productivity is highly vulnerable to the seasonal variations in hydro-meteorological variables like precipitation, soil moisture, temperature, and evapotranspiration (Gidey et al., 2018). As a result, the balance between the food supply and demand is affected greatly under the dual pressure of climate change and population growth.

Globally, the overall crop productivity is likely to be affected profoundly due to the changeability in climate as it explains about 60% of the yield variability (Matiu et al., 2017; Ray et al., 2015). Moreover, the rainfed agriculture is highly susceptible to such kind of climatic changeability that results in extreme weather events like droughts, heatwaves, and heavy precipitation (Ribeiro et al., 2019; Zampieri et al., 2017). It is estimated that the extreme weather events are responsible for 18-43% global yield variability for maize, spring wheat, rice, and soybeans (Vogel et al., 2019). In India, the agriculture is considered as the mainstay of economy as it contributes significantly to Gross Domestic Product (GDP), employment and overall development of other sectors. The studies have shown downward trends in the yield of major crops such as rice, maize, and wheat due to changing climate over India (Gupta et al., 2017; Pathak et al., 2003; Rupa Kumar et al., 2002). The failure of crop under the influence of extreme weather conditions entails significant economic losses and hence, the evaluation of the risk associated with the agricultural productivity due to the extreme conditions is of paramount importance (Madadgar et al., 2017; Xie et al., 2018).

The occurrence mechanism of agricultural drought is complex as it is modulated by the natural, social, and economic factors (X. Liu et al., 2019b). Thus, many drought evaluation indices are proposed to characterize the drought quantitatively. However, most of the evaluation indices cannot integrate all the factors affecting the occurrence of drought suggesting insufficient mechanism to describe drought occurrence. Therefore, it is required to combine single index factors to evaluate the agricultural drought risk incorporating the multivariate statistical analysis (Liu et al., 2019). The copula as a multivariate analysis is being used widely. According to the Sklar's theorem (Sklar, 1959), copula techniques are advantageous as they provide significant flexibility in modelling the dependence structure between two or more random variables.

Recently, the application of copula theory in drought analysis has gained popularity among the researchers. The bivariate analysis is successfully applied in the cases of meteorological (J. Das et al., 2020a), hydrological (Borgomeo et al., 2015; K. Feng et al., 2021), and agricultural (Bokusheva et al., 2016; Madadgar et al., 2017; Vergni et al., 2015; H. Wu et al., 2021) drought conditions. In case of agricultural drought, the copula theory is generally used to examine the joint return period of different drought properties (Dai et al., 2020; Poonia et al., 2021; Vergni et al., 2015), to predict the agricultural drought (H. Wu et al., 2021; Wu et al., 2022), and to develop multivariate agricultural drought index (Bateni et al., 2018; P. K.

Das et al., 2020). In some studies, researchers established the bivariate relationship to analyse the sensitivity between drought indicators and crop yield (Bokusheva et al., 2016; Madadgar et al., 2017). However, the risk associated with the crop yield due to the drought conditions is not examined in the context of changing climate. In addition, over agrarian country like India, it is of paramount interest to examine the agricultural drought risk for multiple crops.

Besides the hydro-meteorological drought indices, various remote sensing-based indices are proposed due to the recent advancement in the satellite technology. These indices provide accurate, flexible, and reliable findings related to agricultural drought and thus have attracted the attention of various agriculturalists, hydrologists, meteorologists, and environmentalists (Gidey et al., 2018). The credibility of remote sensing-based indices lies in detecting the spatial and temporal drought occurrence which can be effectively utilised for alleviating the risk that arises from drought. In addition, the satellite-based observations overcome some limitations of station-based observations providing spatially explicit and dynamic large-scale drought monitoring (Zhang et al., 2016). In this sense, the remote sensing-based indices such as Vegetation Health Index (VHI), Vegetation Condition Index (VCI), Temperature Condition Index (TCI) based on Normalized Difference Vegetation Index (NDVI) and Brightness Temperature (BT) have been successfully applied in modelling crop productivity (Bokusheva et al., 2016; Dalezios et al., 2014; Kogan et al., 2015). Liu and Kogan (1996) advocated that NDVI images provide a useful tool to understand the large-scale climatic variability while VCI Images enable to evaluate the severity of a regional drought. The TCI conditions are estimated with respect to the max/min's temperature envelope and the modified formula of TCI reflect different response of vegetation to temperature.

Under this background, the present study aims to examine the agricultural drought risk under stationary and non-stationary drought conditions. In this study, the agricultural drought risk is defined as the conditional probability of crop losses under drought conditions. Here, two hydro-meteorological drought (Standardized Precipitation Evapotranspiration Index (SPEI) and Standardized Soil moisture Index (SSI)) and two remote sensing-based drought indices (VCI and TCI) are considered. Based on satellite-based and station-based information, drought conditions are evaluated and then linked with crop yield anomalies with the use of appropriate copula functions. The primary objectives of the present study are (i) to evaluate the dependency between yield anomalies and different drought conditions using copula, (ii) to examine the agricultural drought risk by preserving the joint dependence, and (iii) to analyse

the agricultural drought risk under stationary and non-stationary settings. The conditional probability of non-exceedance of crop loss threshold is used to estimate the agricultural drought risk that ranges from 0 (low risk) to 1 (high risk). In this study, the analysis is carried out on four different types of rainfed crops (rice, wheat, groundnut, cotton) during their respective cropping seasons. To the best of the authors' knowledge, the present study is the first of its kind to be carried out over Indian region. It is evident from Chapter 4 that the non-stationary analysis outperforms the stationary analysis while analysing the drought conditions Moreover, most of the applications of copula in non-stationary drought conditions are carried out to evaluate the joint return period of different drought properties. However, there is dearth in application of both non-stationary and copula-based approach to analyse the agricultural risk. In addition, a comparative study of agricultural risk under stationary and non-stationary conditions can provide valuable information regarding risk associated with climate hazard. The outcomes from the analysis would be helpful in monitoring and mitigating agricultural drought risk.

6.2 Description of different datasets

6.2.1 Crop yield data

The different crop yield datasets are collected over Maharashtra which is chosen as the study area in the present analysis. Figure 6.1(a) represents the different administrative divisions in Maharashtra province. In this study, four major crops namely cotton (cash crop) Figure 6.1(b), groundnut (oilseed) Figure 6.1(c), and rice Figure 6.1(d) and wheat (cereals) Figure 6.1(e) have been selected to analyse the agricultural drought risk. It should be noted that these crops can be cultivated in any season based on the availability of irrigation requirements. However, in this analysis, the seasons when the cultivations of crops depend on the rainfall are considered to examine the conditional probability of non-exceedance of crop loss events with the changing climatic conditions. Thus, for rice, Kharif (June to December) season; for wheat, Rabi season (October to March); for groundnut, Kharif season (June to October); and for cotton, Kharif season (July to December) have been considered. The annual values of crop yield data (i.e., the ratio of crop production (t) to harvested area (ha)) for respective seasons are collected during the period of 1998-2018 (for rice and wheat) and for the period of 1999-2018 (for groundnut and cotton) in Maharashtra. It is worth mentioning that all the selected crop datasets are not available for all the districts in Maharashtra. In this way, 25 districts

contribute wheat production during Rabi season, 21 districts contribute rice production during Kharif, whereas 18 and 21 districts involve in groundnut and cotton production during Kharif season, respectively. The different crop datasets over the study area are collected from https://www.aps.dac.gov.in/APY/Public_Report1.aspx. Regarding the hydro-meteorological datasets and external covariates to develop non-stationary index, the descriptions are already provided in Chapter 4. In the present analysis the soil moisture data is downloaded from Climate Prediction Center (CPC) global monthly soil moisture data (Fan and van den Dool, 2004). The CPC dataset is a reanalysis product that uses records from 30,000 sites managed by international agencies and the records are quality controlled, along with concurrent radar/satellite observations and numerical model forecasts (M. Li et al., 2020).

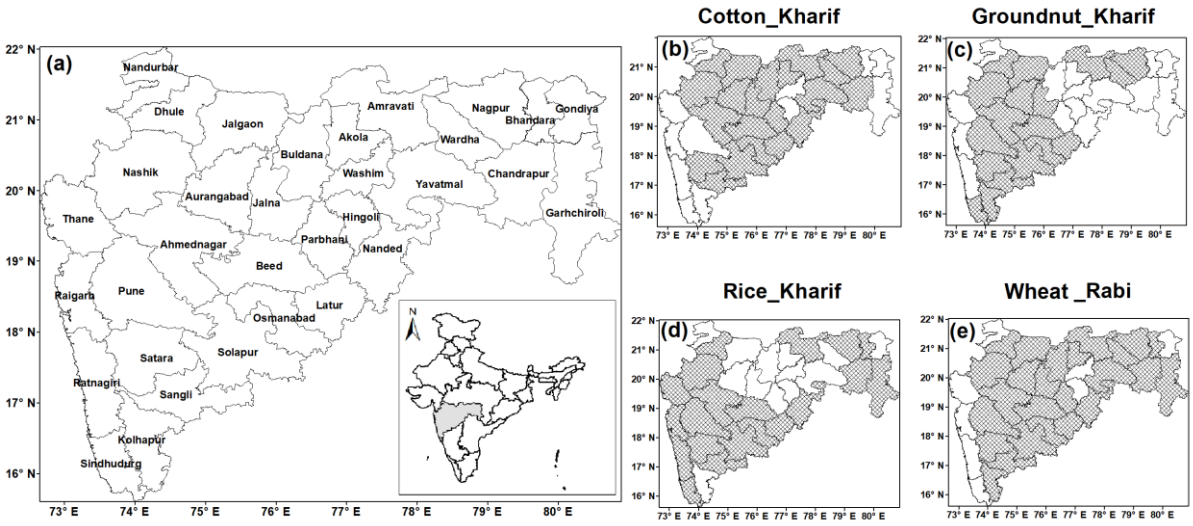

Figure 6.1(a) Map of Maharashtra with districts and its location in India; (b) Districts showing available crop data for cotton; (c) Districts showing available crop data for groundnut; (d) Districts showing available crop data for rice; (e) Districts showing avail crop data for wheat

6.2.2 Remote sensing indices

In the present analysis, two remote sensing-based indices are used namely Vegetation Condition Index (VCI) and Temperature Condition Index (TCI). These indices are based on both NDVI and Brightness Temperature (BT). Therefore, they have the ability of examining the changes in ecosystem in terms of its fluctuation within its minimum and maximum value of BT and NDVI. The VCI identifies the vegetation stress due to the lack of moisture content whereas TCI signifies the vegetation stress due to the high temperature. The detailed description of the calculation of VCI and TCI were first provided by Kogan (1995, 1990). The

range of the values of both VCI and TCI varies between 0 to 100, where the values less than 40 indicate the occurrence of drought conditions (Kogan, 2002). Therefore, for the evaluation of the response of crop yield to different conditions of drought hazard, the weekly global map of VCI and TCI are retrieved at 4 km spatial resolution scale from NOAA's ftp server (ftp://ftp.star.nesdis.noaa.gov/pub/corp/scsb/wguo/data/VHP_4km/geo_TIFF/) for the period of 1997 to 2018. Here, the reason behind the addition of weekly data for 1997 is because the sowing period of some seasonal crops harvested in 1998 starts in Kharif season of the previous year. The VCI and TCI are obtained by the equations as following:

$$VCI = \frac{\left(NDVI - NDVI_{\min}\right)}{\left(NDVI_{\max} - NDVI_{\min}\right)} \times 100 \tag{6.1}$$

$$TCI = \frac{\left(T_{\max} - T\right)}{\left(T_{\max} - T_{\min}\right)} \times 100 \tag{6.2}$$

where, $NDVI$, $NDVI_{min}$, and $NDVI_{max}$ are the smoothed weekly NDVI, its multi-year absolute maximum, and minimum, respectively. Similarly, T, T_{max}, and T_{min} are the smoothed weekly temperature, its multi-year maximum, and minimum, respectively.

Comprising the major crop life cycle moments, the involved weeks have been selected for different crops on seasonal basis. In detail, the analysis of this study has been performed between week 22 (approximately in the beginning of June) and week 52 (ending of December) for rice in Kharif, between week 40 (the beginning of October of the year n-1) and week 13 (approximately the ending of March of the year n) for wheat in Rabi, between week 22 (beginning of June) and week 44 (end of October) for groundnut in Kharif and between week 26 (in the beginning of July) and week 52 (end of December) for cotton in Kharif.

6.3 Methodology

The graphical representation of the adopted methodology for the analysis is presented in the form of flow chart in Figure 6.2. Initially, the SPEI and SSI drought indices are computed by using the hydro-meteorological datasets at each grid point. Next, the non-stationary analysis is carried out for SPEI and SSI using different climate oscillations and regional hydrological conditions at each grid point, respectively. A comparison between stationary and non-stationary drought indices is carried out based on Akaike Information Criteria (AIC). The crop loss threshold is then obtained for different crops and districts using detrend crop yield

series. The dominant drought indicator in explaining the variability of each crop time series is selected for each district. Subsequently, copula-based risk analysis is carried out incorporating the crop loss threshold, crop yield anomaly, and dominant indicator at each district. In addition, comparison of risk analysis under stationary and non-stationary settings is performed where SPEI or SSI are selected as dominant drought indicators. Here, the methodologies related to crop loss threshold, identification of dominant indicator, and copula-based risk analysis are discussed, as non-stationary analysis is already explained in Chapter 4.

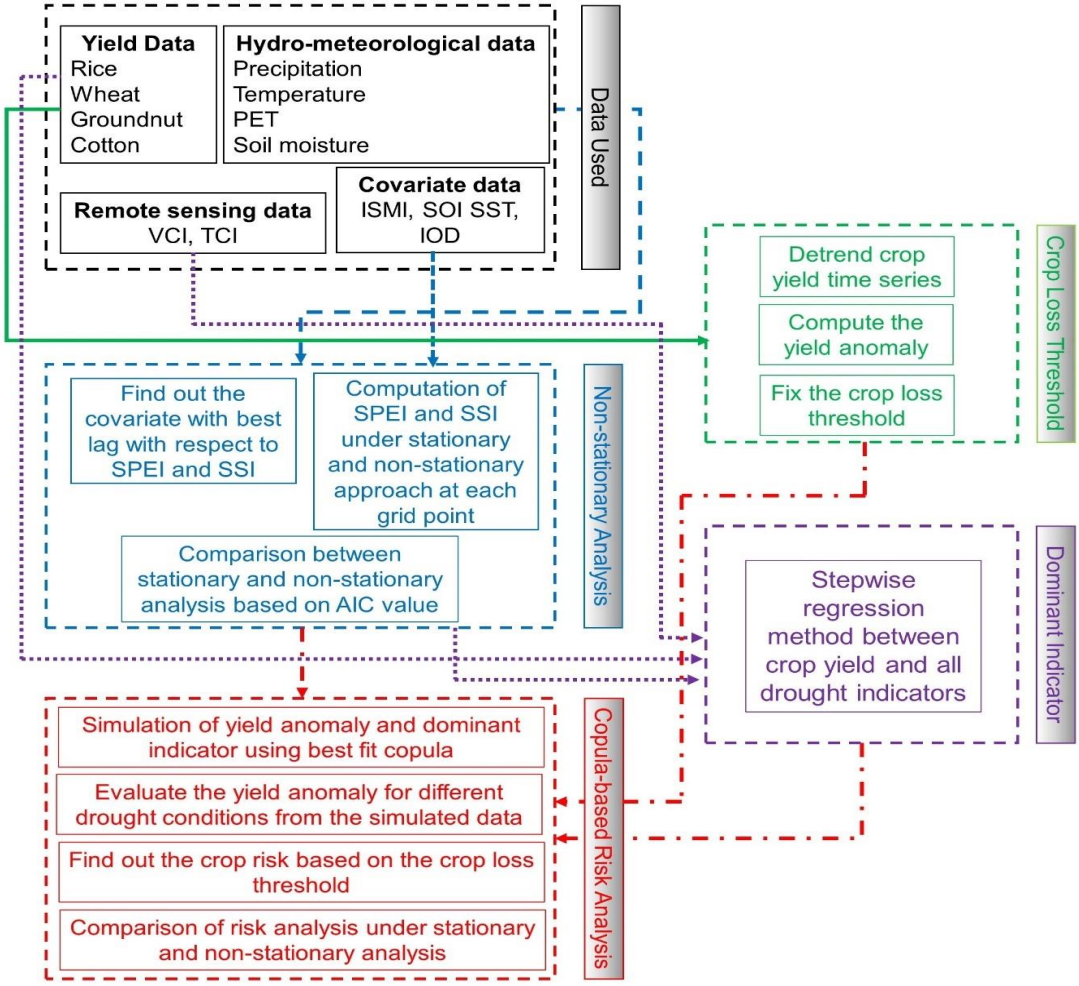

Figure 6.2: Proposed flow chart of the present study

6.3.1 Calculation of crop loss threshold

The annual crop yield values of rice, wheat, groundnut, and cotton are computed as the ratio between total annual crop production and cultivated area during the period of 1998-2018. The

yield anomalies are computed after removing the non-climatic factors. This is performed by removing the linear trend from the yield (Páscoa et al., 2017). In the present study, the crop loss events are marked when the yield anomalies are below the minus one (-1) standard deviation of the data series of annual crop yield anomalies. The motive is to focus on the expected chance that the negative yield anomalies will not exceed the crop loss threshold of different crops in each district. The annual crop loss threshold (t/ha) is computed for all the selected crops over different districts in Maharashtra and presented in Figure 6.3.

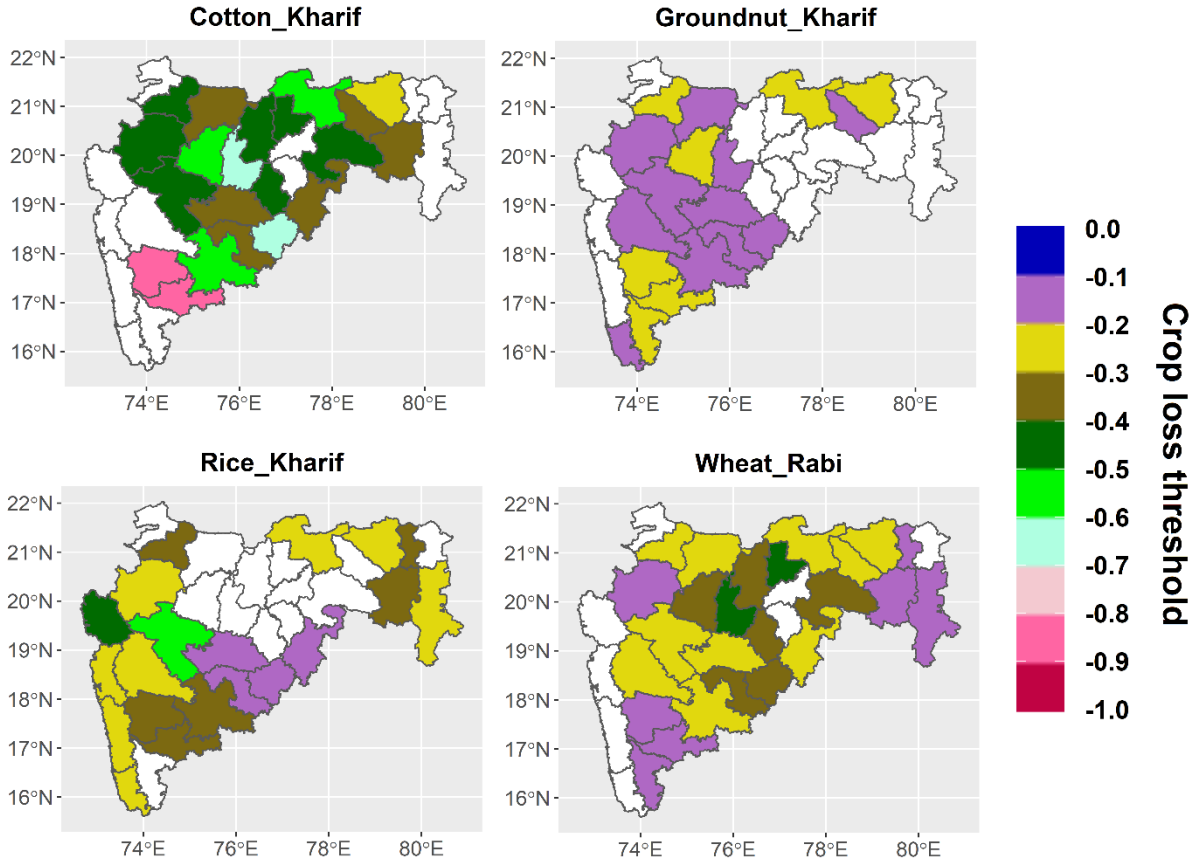

Figure 6.3: The crop loss threshold computed as -1 standard deviation of crop yield anomaly (t/ha) for each district. The districts with no yield data are coloured in white

It can be noted from Figure 3 that the range of crop loss threshold varies between -0.9 and -0.2 for cotton, -0.3 and -0.1 for groundnut, -0.6 and -0.1 for rice, -0.5 and -0.1 for wheat crop. The relatively low value of standard deviation suggests that the crop loss thresholds correspond to the values slightly below normal. Therefore, the difference between the maximum and minimum annual yield values is small.

6.3.2 Selection of dominant drought indicator

To find out the dominant predictor that significantly impacts the crop production based on different levels of drought severity, both the hydro-meteorological (SPEI and SSI) and remote sensing-based drought indicators (VCI and TCI) are used. The selection of the dominant indicator is carried out by considering the 182 drought indicators in case of rice in Kharif (31 -week intervals of VCI, 31-week intervals of TCI, and 5-month by 12-time scales intervals of SPEI and SSI). Similarly, there are total of 142, 174, and 172 drought indicators for groundnut in Kharif, cotton in Kharif, and wheat in Rabi season, respectively. A stepwise linear regression is employed to select the best subset of drought indicators at 95% confidence level. Subsequently, the district-wise best dominant predictor is picked up for each seasonal crop on the basis of the largest absolute value of regression coefficients. In addition, to evaluate the contribution of each dominant drought indicator to its respective crop yield variability, partial correlation analysis has been conducted. A dominant indicator is selected through stepwise regression, where the dominant indicator can estimate the variance that is not explained by other indicators. This variance can be computed using the squared partial correlation coefficient.

6.3.3 Copula-based risk analysis

The joint behaviour of yield anomalies and dominant drought indicator for each crop is estimated using bivariate copula function. The copula constructs the multivariate joint distribution for two or more correlated variables having independent marginal distributions. Mathematically, given two correlated variables U and V with marginal distributions $F_U(u)$ and $F_V(v)$, the joint probability distribution $F_{UV}(u,v)$ using copula function C can be defined as

$$F_{UV}(u,v) = C(F_U(u), F_V(v)) \tag{6.3}$$

In the present study a total of five different copulas namely, Gaussian, Student's t-copula, Clayton, Gumbel, and Frank are used to analyse the bivariate joint dependence structure between yield anomalies and dominant drought indicator (SPEI, SSI, VCI, or TCI). The Gaussian and Student's t-copula come under Elliptical family. Similarly, Archimedean family includes Clayton, Gumbel, and Frank copulas. The Archimedean copulas are more popular due to their ability in capturing the wider variety of joint dependence structure. The

asymmetrical tail behaviour with greater dependence in lower and upper tail is described by Clayton and Gumbel copulas, respectively. The symmetric dependence with and without tail dependence is captured by Student's t-copula and Frank copula, respectively. The mathematical description, and parameter range of the above-said copula functions are presented in Table 6.1. It should be noted that these formulations might not be unique. Therefore, it is advised to refer to the associated reference in Table 6.1.

Table 6.1: Different copulas, their mathematical description, parameter range, and suitable references

Name	Mathematical Description	Parameter Range
Gaussian (Li et al., 2013b)	$\int_{-\infty}^{\phi^{-1}(u)}\int_{-\infty}^{\phi^{-1}(v)}\frac{1}{2\pi\sqrt{\left(1-\theta^2\right)}}\exp\left(-\frac{u^2+v^2-2\theta uv}{2\left(1-\theta^2\right)}\right)dudv$	$\theta\in[-1,1]$
t (Li et al., 2013b)	$\int_{-\infty}^{t_{\theta_2}^{-1}(u)}\int_{-\infty}^{t_{\theta_2}^{-1}(v)}\frac{\Gamma\left(\left(\theta_2+2\right)/2\right)}{\Gamma\left(\theta_2/2\right)\pi\theta_2\sqrt{\left(1-\theta_1^2\right)}}\left(1+\frac{u^2-2\theta_1uv+v^2}{\theta_2}\right)^{(\theta_2+2)/2}dudv$	$\theta_1\in[-1,1]$ *and* $\theta_2\in(0,\infty)$
Clayton (Clayton, 1978)	$\max\left(u^{-\theta}+v^{-\theta}-1,0\right)^{-1/\theta}$	$\theta\in[-1,\infty)\setminus 0$
Frank (Li et al., 2013b)	$-\frac{1}{\theta}\ln\left[1+\frac{\left(\exp\left(-\theta u\right)-1\right)\left(\exp\left(-\theta v\right)-1\right)}{\exp\left(-\theta\right)-1}\right]$	$\theta\in\mathbb{R}\setminus 0$
Gumbel (Li et al., 2013b)	$\exp\left\{-\left[\left(-\ln\left(u\right)\right)^{\theta}+\left(-\ln\left(v\right)\right)^{\theta}\right]^{1/\theta}\right\}$	$\theta\in[1,\infty)$

Prior to the application of copula function, the marginal distributions of yield anomalies and dominant drought indicator are transformed to uniformly distributed values between 0 and 1. This is performed by using Canonical Maximum Likelihood (CML) method (Genest et al., 1995), where the kernel density estimator of cumulative distribution function (CDF) is used to transform the marginal to uniform distribution. The estimation of marginal distributions is performed non-parametrically and the suitable copula parameters are computed using copula functions by means of maximum likelihood. In case of small sample size, the heavy assumption about the marginal distribution can be avoided using the semi-parametric approach. In addition, the use of semi-parametric method preserves the important source of information corresponding to the climatic variables. In the present study the selection of

appropriate copula function is carried out using the VineCopula package in R programming (https://cran.r-project.org/web/packages/VineCopula/index.html).

After fitting the bivariate joint dependence between the yield anomalies *(U)* and dominant drought indicator *(V)*, 1000 pairs of simulated yield anomalies $(F_{Usim}(u))$ and drought indicator $(F_{Vsim}(v))$ are computed based on the appropriate copula function and its parameter. The simulated datasets are in the range [0, 1]. Subsequently, the simulated values are transformed back to the original scale using the kernel estimations of the inverse CDF. The data points among simulated yield anomalies (U_{sim}) which correspond to a particular drought condition (v^*) (no drought, or moderate drought, or extreme drought conditions) among the simulated drought indicator values (V_{sim}) are selected such that

$$U_{sim^*}(u,v) = U_{sim}(u \mid v < v^*) \tag{6.4}$$

The drought condition according to the severity is presented in Table 6.2. By using the joint distribution, the conditional probability of yield anomalies with respect to different drought conditions $F_{U_{sim^*}}$ preserves the dependence between the marginal distributions of yield anomalies and dominant drought indicator. The agricultural drought risk is evaluated in terms of conditional probability of non-exceedance of crop loss threshold for each seasonal crop over different districts and defined as

$$F_{U_{sim^*}}(-U_{std}) = Pr(U_{sim^*} \leq -U_{std}) \tag{6.5}$$

where, $-U_{std}$ represents crop loss threshold value for different crops and districts.

Table 6.2: Classification of drought severity for SPEI, SSI, VCI, and TCI

SPEI and SSI	VCI and TCI	Drought Class
Greater than -0.84	Greater than 40	No Drought
Between -0.84 and -1.28	Between 40 and 20	Moderate Drought
Less than and equal to -1.28	Less than and equal to 20	Extreme Drought

6.4 Results

6.4.1 Identification of dominant drought indicator for different crops

The drought condition for each crop over each district is characterised by one dominant drought indicator which is obtained from the stepwise regression analysis. Figure 6.4 presents the district wise dominant drought indicator for different crops.

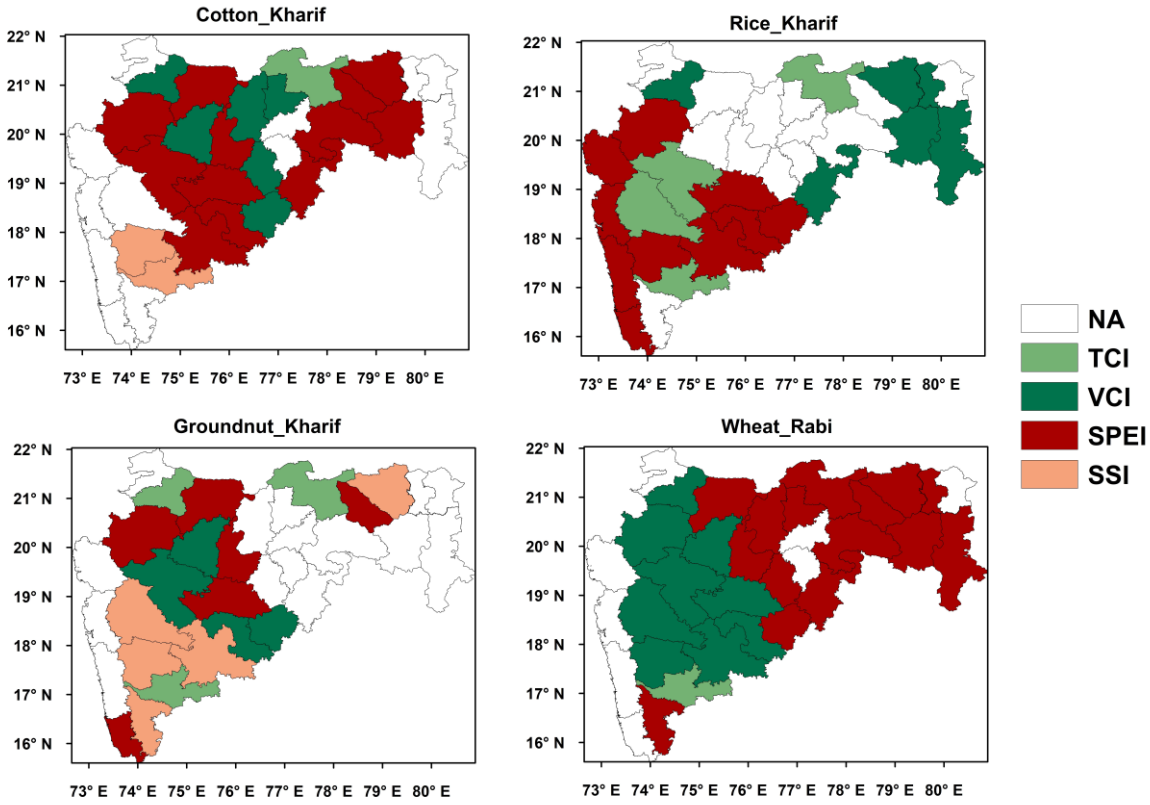

Figure 6.4: The selected dominant drought indicator for different districts and crops

It can be noticed from the figure that for cotton (12 out of 21 districts), groundnut (6 out of 18 districts), rice (10 out of 21 districts), and wheat (15 out of 25 districts) crops, SPEI is found to be the dominant indicator for most of the districts that implies the significance of meteorological variables on crop production in those districts. SPEI is dominant over eastern part of Maharashtra for wheat crop during Rabi season and western and south part of Maharashtra for rice crop during Kharif season. However, in case of cotton, SPEI is dominant over central part and small area from eastern part of Maharashtra. SSI as a dominating drought indicator is observed for cotton (over 2 districts), and groundnut (over 5 districts) crops only. The dominance of VCI is more as compared to TCI for all the crops. For wheat

crop, the dominance of VCI is noticed over the western part of the study area. However, for rice, mostly the eastern part of Maharashtra is dominated by VCI drought index. In case of cotton and groundnut, the crop productivity is affected due to VCI over central part of Maharashtra. The TCI as least dominated drought index is found for all the selected crops in the study area. Table 6.3 represents the list of dominant drought indicators with selected week in case of TCI and VCI or time scale and month in case of SPEI and SSI for each crop and district. For instance, the correspondent drought conditions are characterised by the SPEI (August with 2-month time scale) in the case of cotton and by the VCI (week 41, middle of October) in the case of groundnut.

Table 6.3: Dominant drought indicator for each district and crop type

District	Cotton_Kharif	Groundnut_Kharif	Rice_Kharif	Winter_Rabi
Ahmednagar	SPEI-2-8	VCI-41	TCI-32	VCI-40
Akola	VCI-38	----	----	SPEI-3-3
Amaravati	TCI-52	TCI-30	TCI-33	SPEI-6-11
Aurangabad	VCI-39	VCI-40	----	VCI-40
Beed	SPEI-3-9	SPEI-12-8	SPEI-3-8	VCI-9
Bhandara	----	----	VCI-52	SPEI-7-11
Buldana	VCI-38	----	----	SPEI-3-3
Chandrapur	SPEI-3-9	----	VCI-52	SPEI-7-11
Dhule	VCI-38	TCI-36	VCI-33	VCI-8
Garhchiroli	----	----	VCI-51	SPEI-1-1
Gondiya	----	----	----	----
Hingoli	----	----	----	----
Jalgaon	SPEI-3-9	SPEI-1-7	----	SPEI-1-1
Jalna	SPEI-8-10	SPEI-1-7	----	SPEI-4-12
Kolhapur	----	SSI-4-10	----	SPEI-1-1
Latur	VCI-37	VCI-37	SPEI-8-8	SPEI-2-12
Nagpur	SPEI-1-12	SSI-1-10	VCI-51	SPEI-4-3
Nanded	SPEI-1-12	----	VCI-35	SPEI-4-3
Nandurbar	----	----	----	----
Nashik	SPEI-6-9	SPEI-3-9	SPEI-2-9	VCI-7
Osmanabad	SPEI-4-8	VCI-39	SPEI-5-8	VCI-46
Parbhani	VCI-39	----	----	SPEI-4-1
Pune	----	SSI-3-8	TCI-33	VCI-41
Raigarh	----	----	SPEI-4-10	----
Ratnagiri	----	----	SPEI-3-8	----
Sangli	SSI-11-12	TCI-44	TCI-22	TCI-11

Satara	SSI-2-8	SSI-6-8	SPEI-5-10	VCI-5
Sindhudurg	----	SPEI-7-10	SPEI-5-9	----
Solapur	SPEI-8-8	SSI-3-8	SPEI-2-10	VCI-42
Thane	----	----	SPEI-6-10	----
Wardha	SPEI-6-12	SPEI-2-7	----	SPEI-3-2
Washim	----	----	----	----
Yavatmal	SPEI-8-8	----	----	SPEI-4-1

Figure 6.5 depicts the percentage of variance explained by the dominant indicator for different crops. According to the figure, more than 50% of the cotton crop variability is explained by the selected dominant drought indicator over Amaravati (50.89%), Chandrapur (57.07%), Dhule (61.25%), Jalgaon (52.52%), Nagpur (66.83%), and Satara (63.58%) districts. Over Kolhapur, Osmanabad, and Solapur districts, more than 50% of the groundnut yield variability is described by the selected dominant drought indicators. In case of rice, the highest crop yield variance is explained over Bhandara district (73.31%) followed by Dhule (61.61%) and Raigarh (60.70%) districts by the dominant drought indicators. Similarly, the districts Jalgaon, Parbhani, and Jalna show a percentage of explained variance higher than 70% in the case of wheat.

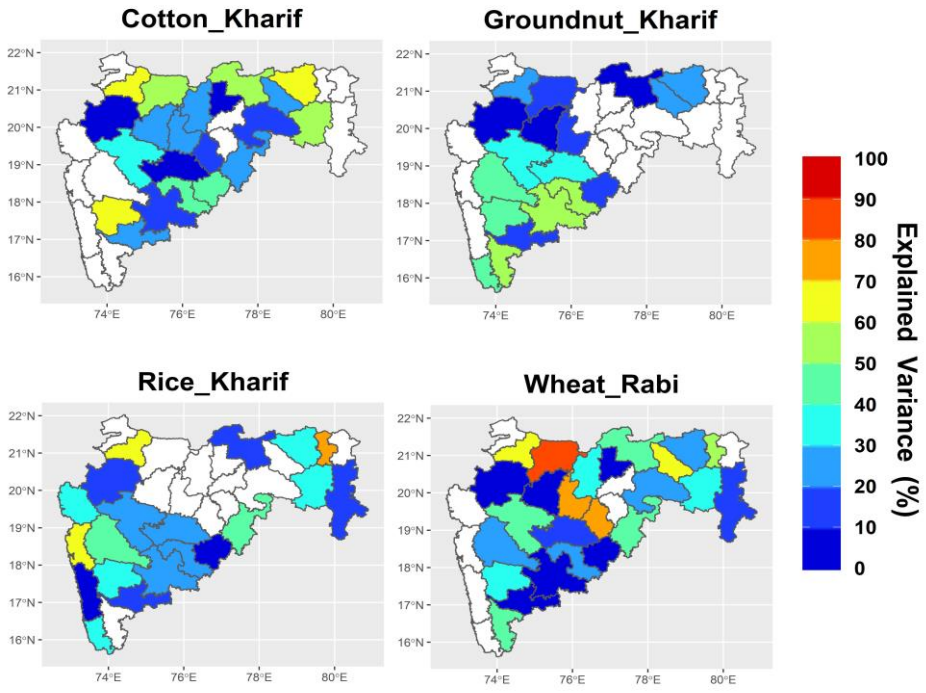

Figure 6.5: The percentage variance of each crop variability explained by the selected dominant drought indicator

6.4.2 Identification of suitable copula for different crop types

The copula analysis is carried out using different copula functions (refer to Table 6.1) for each pair of crop yield anomaly and drought indicator. Figure 6.6 presents the selected copula based on the lowest AIC value for different crops and Figure 6.7 depicts the grouped bar plots which incorporates the number of districts adopting each copula type for different type of dominant drought indicators. It can be noted from Figure 6.6 that Frank copula is the most selected copula type of all the crops (12 districts in case of cotton, 9 districts in case of groundnut, 11 districts in case of rice, and 12 districts in case of wheat). Followed by Frank copula, Clayton copula is found to be suitable for groundnut (6 districts), rice (9 districts), and wheat (9 districts) crops. The Student's t and Gumbel copulas are not found suitable for any of the selected crops and rice crop, respectively. The Gaussian copula is selected as best fit copula over 5 districts in case of cotton, 2 districts in case of groundnut, 1 district in case of rice, and 3 districts in case of wheat crop.

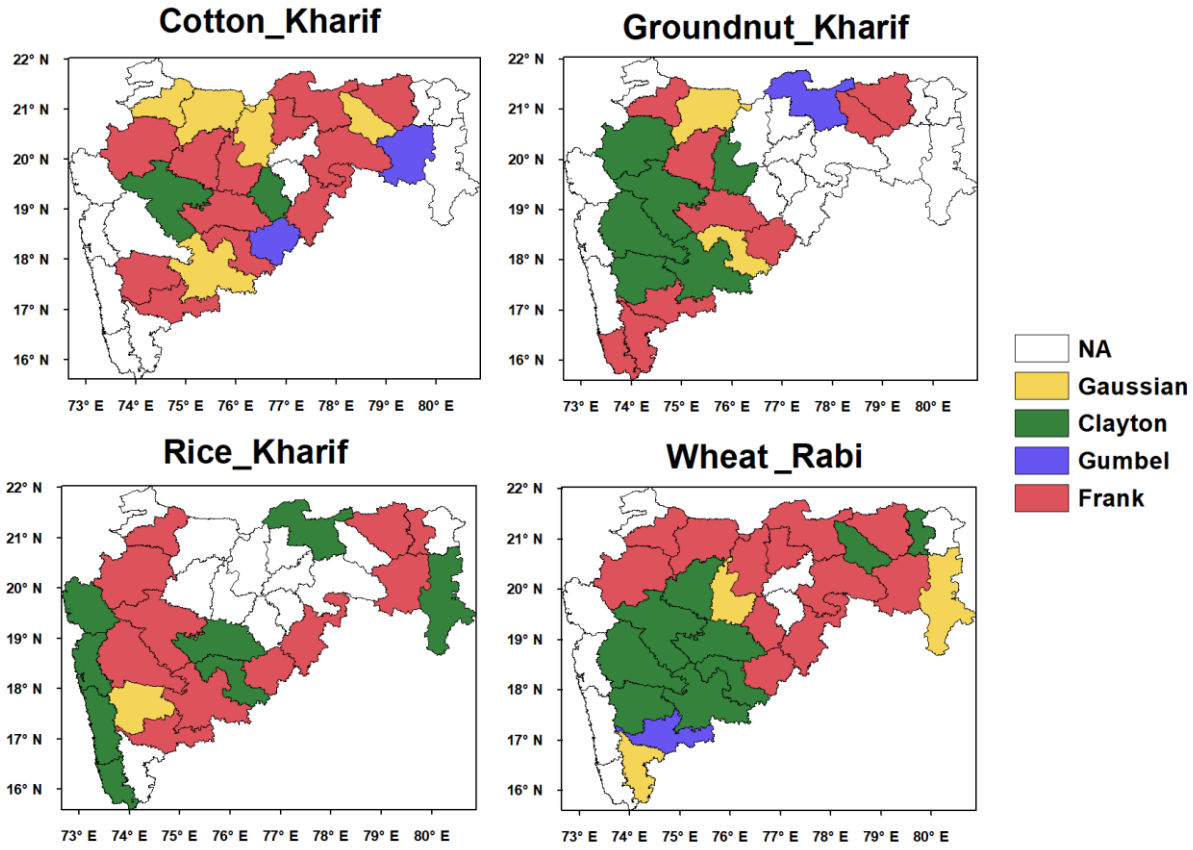

Figure 6.6: The selected copula function for each district and crop type

From Figure 6.7, it is noticed that most of the districts whose drought conditions are characterised by SPEI follow Frank copula (for cotton, groundnut, and wheat) and Clayton copula (for rice). The joint probability of SSI and crop yield anomaly is better modelled using the Frank copula for cotton (2 districts) and using both Clayton (3 districts) and Frank (2 districts) copulas for groundnut. The districts which are dominated by VCI are found to be fitted using Clayton, Frank, Gaussian, and Gumbel copulas for cotton crops. Similarly, Frank and Gumbel copulas for groundnut, Clayton and Frank for Rice, and Gumbel alone for wheat are used to model the dependence structure of VCI and crop yield anomalies. Likewise, the Gumbel and Frank Copulas can capture the joint probability between TCI and crop yield anomalies of wheat and cotton crops, respectively. Whereas Frank (2 districts) and Gumbel (1 district) copulas for groundnut and Clayton (1 district) and Frank (3 districts) copulas for rice crop are selected to model the joint dependency.

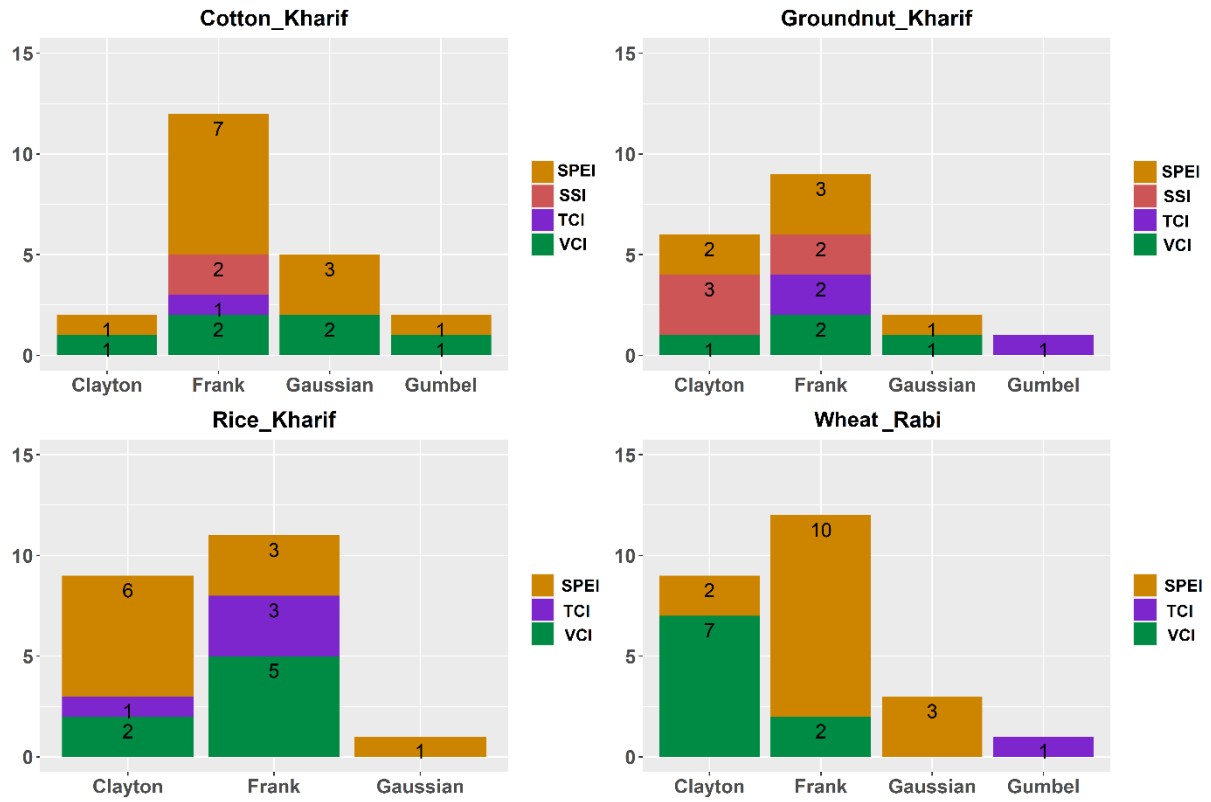

Figure 6.7: Bar plot to describe number of districts under different copula functions for each crop

6.4.3 Analysis of agricultural drought risk for different crops

After establishing the joint dependency using copula functions, the subsequent generated simulations are used to evaluate the conditional distributions of crop yield anomalies under no drought, moderate drought, and extreme drought conditions. Figure 6.8 presents the conditional probability of crop loss under no drought condition according to the crop loss threshold mapped in Figure 6.3. It can be noted that the conditional probability is considerably low in the case of all crops during no drought condition. For instance, the agricultural risk is found to be ranging from 0% to 20% chance of non-exceedance for all the selected crop loss thresholds. Likewise, Figure 6.9 depicts the conditional probability of agricultural drought risk during moderate drought condition. It should be noted that the districts which are shaded in grey colour indicate the absence of moderate drought condition. The chance of non-exceedance of cotton crop loss threshold is found to be more than 95% over Ahmednagar district. In addition, over Aurangabad, and Akola districts, the chance of non-exceedance of agricultural drought risk with respect to cotton crop loss threshold is computed as 32% and 26%, respectively. In the case of groundnut, the agricultural drought risk over Ahmednagar, Jalna, Aurangabad, and Beed is evaluated as 88%, 62%, 29%, and 23% chance of non-exceedance, respectively. Under moderate drought condition, it is computed as 81% for Beed district, 67% for Satara district, 50% for Latur district, 44% for Osmanabad district, and 29% for Nagpur district. The agricultural drought risk for the wheat crop is considerably high i.e., more than 70% over Ahmednagar, Aurangabad, Beed, Osmanabad, Pune, Satara, and Solapur districts. The affected districts are less in number in case of extreme drought condition as compared to the no drought and moderate drought conditions (Figure 6.10). Only two districts namely Ahmednagar and Ratnagiri are having very high conditional probability for cotton and rice crops, respectively.

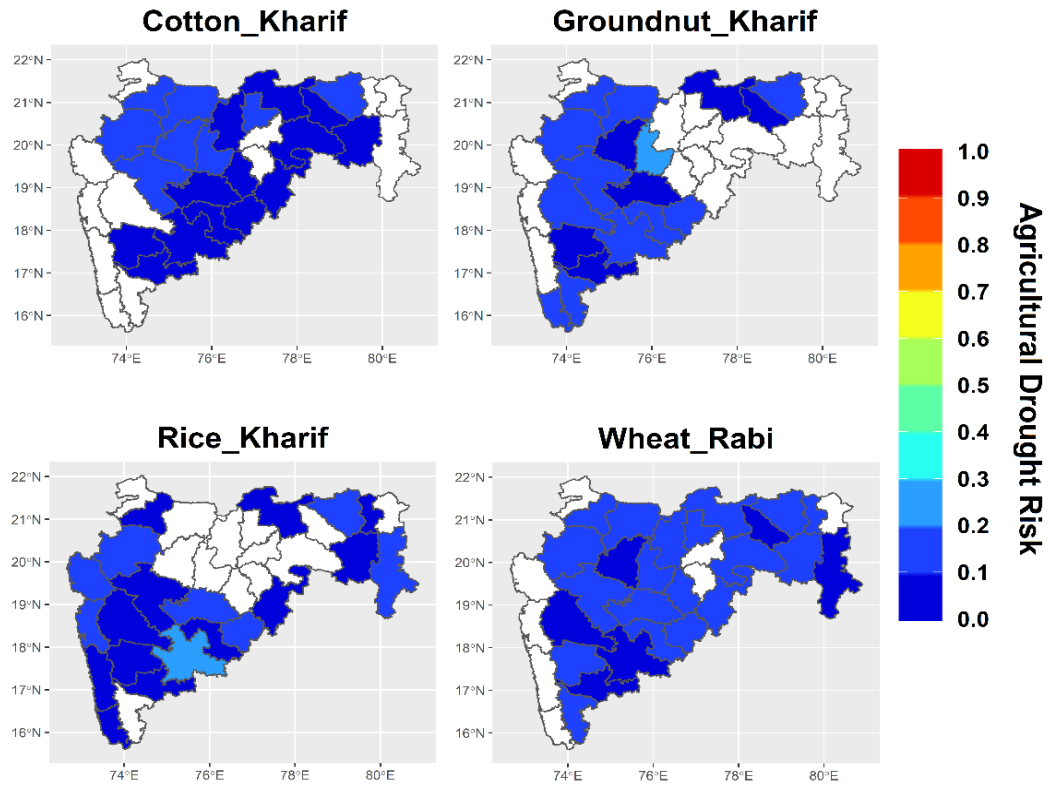

Figure 6.8: Agricultural drought risk under no drought condition for each crop

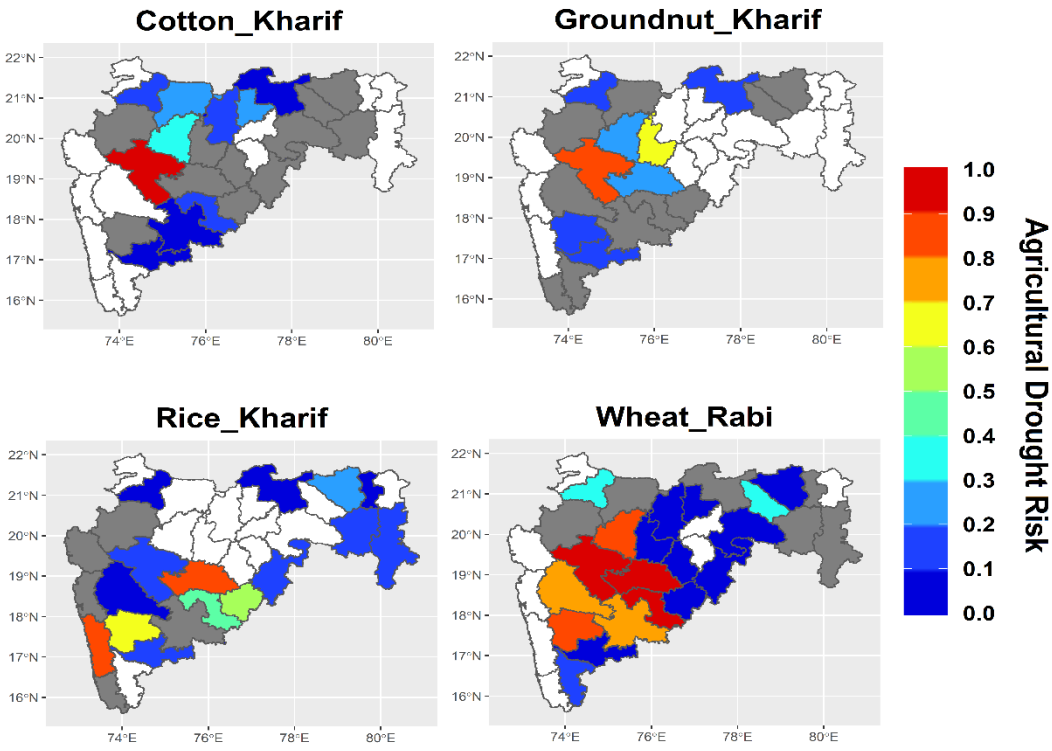

Figure 6.9: Agricultural drought risk under moderate drought condition for each crop. The grey shaded area represents that the no moderate drought condition is observed

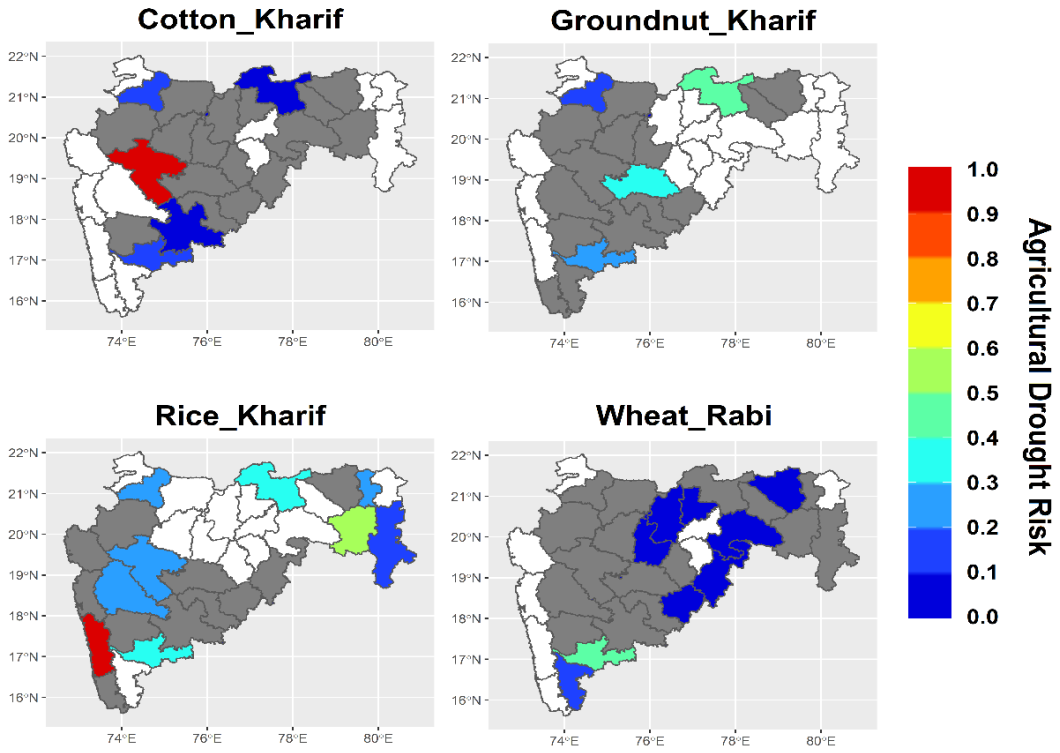

Figure 6.10: Agricultural drought risk under extreme drought condition for each crop. The grey shaded area represents that no extreme drought condition is observed

6.4.4 Comparison of risk under stationary and non-stationary approaches

The comparative study of agricultural risk between stationary and non-stationary approaches is performed by considering the districts where SPEI or SSI is selected as dominant drought indicator. Figure 6.11 presents the comparison between stationary and non-stationary drought risk for cotton crop. It should be noted that the upper and lower panel present the stationary and non-stationary cases, respectively. The map of districts which are affected only by SPEI or SSI is embedded in the upper left corner map. The number of districts affected by the moderate and extreme drought condition as a result of SPEI or SSI are more in non-stationary case than stationary case. For instance, Ahmednagar, Jalgaon, and Osmanabad districts in case of moderate drought and Ahmednagar district in case of extreme drought are not captured by the stationary condition. In addition, the non-stationary conditional probability of agricultural drought risk is high as compared to stationary approach.

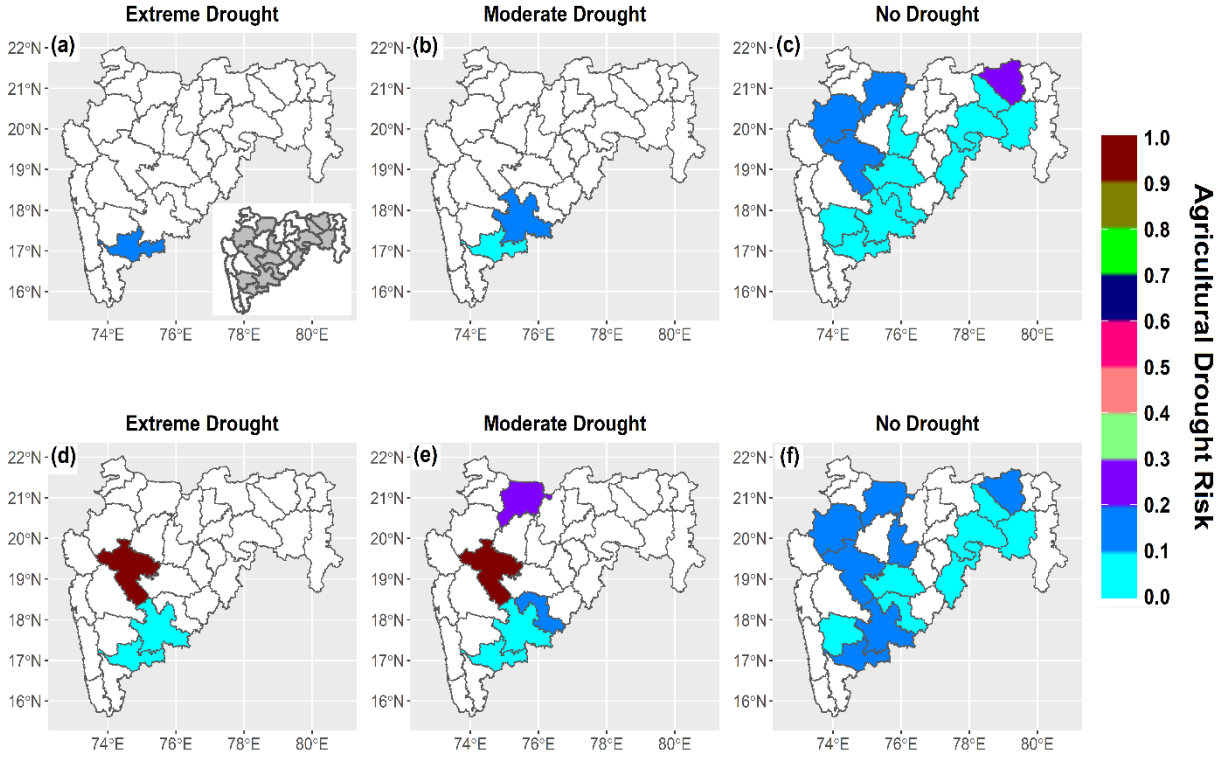

Figure 6.11: Stationary (a-c) and non-stationary (d-f) comparison of agricultural drought risk for cotton crop. The grey shaded map (upper left corner) shows the districts where SPEI or SSI is selected as dominant drought indicator

Similarly, Figure 6.12 depicts the comparison of agricultural drought risk for groundnut crop. Unlike the cotton crop, significant difference is not observed between stationary and non-stationary analysis for extreme and no drought conditions. However, Beed and Jalna districts show high conditional probability of agricultural drought risk in the case of moderate drought condition. In the case of rice (Figure 6.13), no moderate and extreme drought conditions are observed under stationary condition. However, under non-stationary condition, some of the districts (Beed, Latur, Osmanabad, Ratnagiri, and Satara) in moderate, and Ratnagiri district in extreme drought condition exhibit high conditional probability of agricultural drought risk. Likewise, for wheat (Figure 6.14), the significant difference of drought risk between stationary and non-stationary drought is noticed for moderate and extreme drought conditions over one (Wardha) and four (Akola, Buldana, Nagpur, and Nanded) districts, respectively.

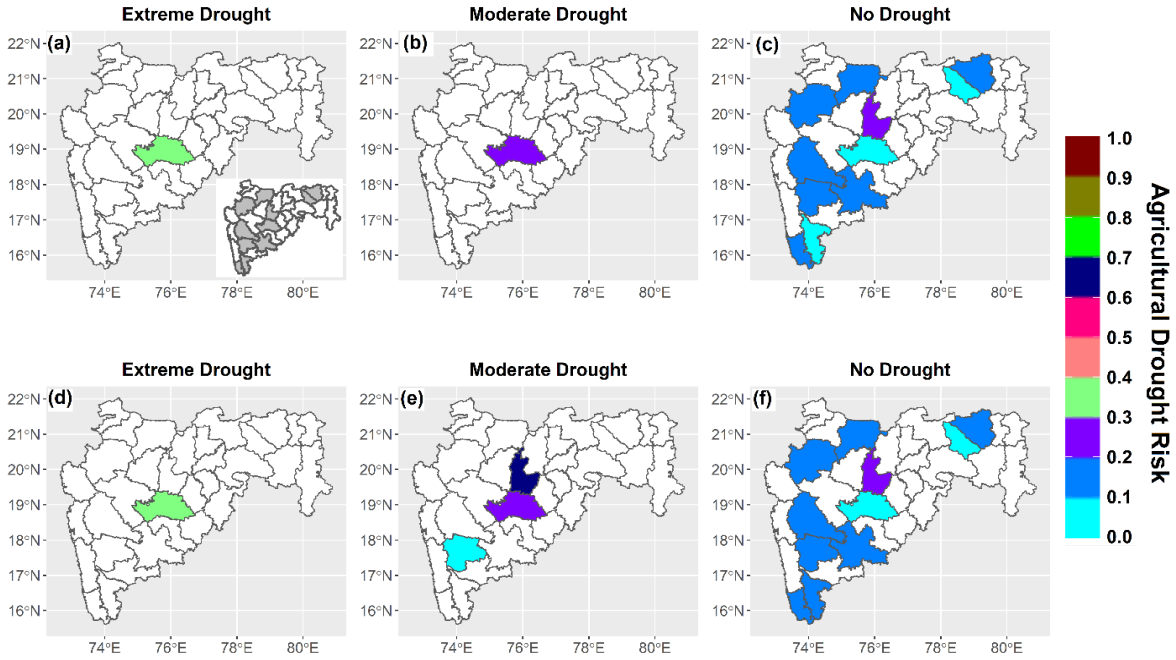

Figure 6.12: Stationary (a-c) and non-stationary (d-f) comparison of agricultural drought risk for groundnut crop. The grey shaded map (upper left corner) shows the districts where SPEI or SSI is selected as dominant drought indicator

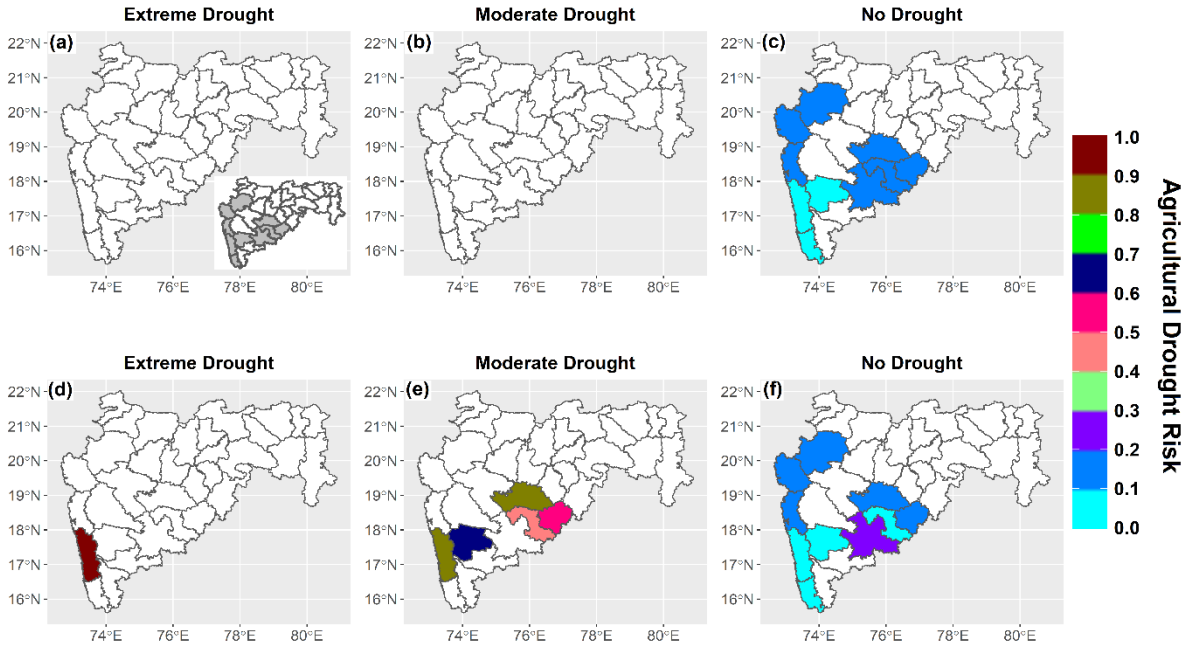

Figure 6.13: Stationary (a-c) and non-stationary (d-f) comparison of agricultural drought risk for rice crop. The grey shaded map (upper left corner) shows the districts where SPEI or SSI is selected as dominant drought indicator

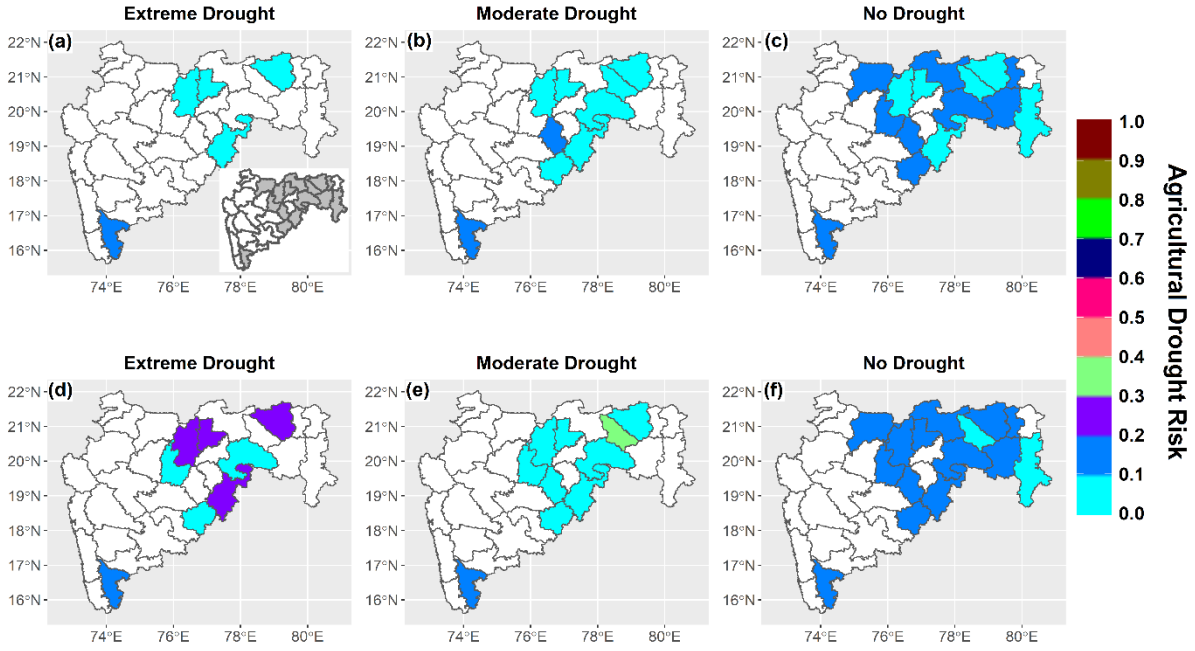

Figure 6.14: Stationary (a-c) and non-stationary (d-f) comparison of agricultural drought risk for wheat crop. The grey shaded map (upper left corner) shows the districts where SPEI or SSI is selected as dominant drought indicator

6.5 Discussion and summary

The present study aims at analysing the dependence structure between crop yield anomalies and drought conditions using the copula-based approach. Based on the obtained dependency structures, the agricultural drought risk is evaluated over the study area which is proposed in terms of conditional probability of non-exceedance of crop loss threshold under three different types of drought conditions. In addition, the agricultural drought risk is characterised combining the advantages of both hydro-meteorological (SPEI, and SSI) and remote sensing-based (VCI, and TCI) drought conditions. In case of hydro-meteorological drought condition, the agricultural risk is computed and compared for stationary and non-stationary conditions.

In general, SPEI is found as significant drought indicator (Figure 6.4) over the maximum number of districts in all the crops, suggesting the climatic factors have significant influence on the agricultural productivity over the study area. Similar kind of finding is observed by Kelkar et al. (2020) while analysing the impact of climate variability on crop production in Maharashtra. However, the districts with higher explained variance do not necessarily coincide with the selection of SPEI. For instance, the districts with higher variance explained

is shared by all the drought indicators for cotton, by SSI for groundnut, mostly by VCI in the case of rice, and by SPEI for wheat. A west-east gradient of suitability of SPEI is observed in the case of rice (western districts) and wheat (eastern districts) crops. However, the yield variability over eastern districts over rice and western districts over wheat is mostly explained by VCI.

The most selected type of copula in all the crops is found to be Frank copula, suggesting equal level of dependency in both the tails between drought indicators and yield anomalies. In most of the cases of Frank models, the dominant drought condition is characterised by SPEI index. The Clayton copula over selected districts suggest stronger dependence between the lower tail values of dominant drought indicators and yield anomalies. Most often, the drought conditions for Clayton models are dominated by SPEI and VCI in the cases of rice and wheat, respectively. On the other hand, the districts with Gumbel models are characterised by VCI and SPEI for cotton, and TCI for both groundnut and wheat crops, suggesting high values of the drought indicators promote positive crop yield anomalies.

In most of the cases (16 out of 23 instances), the higher probability of drought risk under moderate and extreme drought conditions are modelled by Clayton copula. Under moderate drought condition, the higher probability of agricultural drought risk for wheat crop is characterised by VCI only and modelled by Clayton copula. It suggests that the higher severity of VCI results in higher agricultural drought risk for wheat crop. Likewise, for cotton and groundnut, the higher agricultural drought risk is modelled by Clayton copula. In spite of different dominant drought indicators, the dependency structure between the moderate drought condition and crop yield anomaly is similar for cotton, groundnut, and wheat crops. In the case of rice, higher agricultural drought risk is modelled by SPEI drought indicator. Under moderate drought condition, Ahmednagar is found to be the most affected district due to the high probability of agricultural drought risk for cotton, groundnut, and wheat crops. The number of cases is significantly less under extreme drought condition as compared to moderate drought condition. However, the probability of crop loss has increased with drought severity (from moderate to extreme). In most of the cases (considering both moderate and extreme drought conditions), the higher probability agricultural drought risk is modelled with SPEI or VCI as dominant drought indicator.

From the stationary and non-stationary analysis, it is observed that the number of affected districts is more under non-stationary approach for all the crops. In the case of cotton crop,

Ahmednagar and Jalgaon districts are not captured under stationary analysis for both moderate and extreme drought conditions. It is found from the analysis that the stationary approach will underestimate agricultural drought risk due to the ignorance of large-scale oscillations and regional hydrological variability in the computation. Subsequently, this will significantly affect the planning and management of agricultural sustainability over the study area.

In summary, the significant findings from the present analysis point to the fact that the drought hazard is primarily characterised by SPEI drought indicator in all the crops. The higher probability of drought risk under moderate and extreme drought conditions are modelled by Clayton copula suggesting greater probabilities of joint extreme low values. With increase in the drought severity the conditional probability of agricultural drought risk is likely to increase. In addition, it is observed that the exclusion of non-stationarity will underestimate the agricultural risk, which will significantly affect the planning and management of agricultural sustainability over the study area. The findings from the study aim to contribute to device effective decision-making procedure in agricultural practices. Understanding the adverse consequences of drought events on various sectors, it is necessary to examine the future variability of drought under different climate change scenarios. Therefore, next chapter deals with projecting the future changes in the drought event using multiple General Circulation Models/Global Climate Models (GCMs) under different climate change scenarios. In addition, identification of future drought hotspots is carried out in the next chapter.

Chapter 7

Identification of future meteorological drought hotspots

7.1 Introduction

The fact that the extreme weather events (e.g., extreme precipitation, heat waves) have become increasingly frequent all around the globe (Kundzewicz and Kaczmarek, 2000; Mazdiyasni et al., 2017), was well understood and witnessed during the latter part of the 20th century and early 21st century (IPCC, 2014). Among all the climate extremes, detection and quantification of drought events are complex as no universal definition of drought exists (Lloyd-Hughes, 2014). In addition, the drought is often mentioned as 'creeping disaster' (Wilhite, 2016) that develops slowly and often unnoticed and has widespread indirect consequences (Van Loon, 2015). Therefore, the drought as a climate hazard and its manifold aspects have become paramount importance in the changing and warming world (A. G. Dai,

2013) and has evolved as a “hot topic” in hydro-climatology research arena (Trenberth et al., 2014).

The analysis of drought can be carried out at short- and long-term scales. The short-term forecast helps in providing the advisory to the farmers regarding the suitable crop cultivations and reallocation of water resources among the states (Bisht et al., 2019). In this light, numerous studies have been carried out around the globe in terms of different drought characteristics like duration, severity, peak, areal extent, etc. Trenberth et al. (2014) advocated that the frequency and intensity of the natural droughts are likely to increase significantly. Similarly, during 1950- 2008, the global dry areas and extreme conditions have increased by 1.74% and 1.27% per decade for the global land, respectively (Dai, 2011b).

As compared to the past drought events, the overall scenario of future long-term drought events is still incomplete (Spinoni et al., 2019). Several past studies have examined the meteorological and hydrological droughts incorporating the future projections from GCMs under the Coupled Model Intercomparison Project 3 (CMIP3) and 5 (CMIP5) across the globe. For instance, over Europe (Spinoni et al., 2018; Thober et al., 2015), over United States (Ahmadalipour et al., 2017; Keellings and Engström, 2019), over China (Cao and Gao, 2019; Yao et al., 2020), over India (Bisht et al., 2019; Gupta and Jain, 2018), over Australia (Johnson and Sharma, 2015), over the globe (Spinoni et al., 2020; Ukkola et al., 2018). Nevertheless, most of the projections are performed at medium scale spatial resolution and incorporating a limited number of simulations. Due to such limitations, the future projections are associated with larger uncertainties (A. G. Dai, 2013; Lu et al., 2019).

The studies, as mentioned above, except a few, employed Standardized Precipitation Index (SPI) as a meteorological drought indicator to characterise the drought under the future climate change scenarios. According to the definition, SPI accounts only precipitation to describe the drought. However, in the present climate change scenario, it is expected that with constant relative humidity, the moisture content in the atmosphere roughly increases by 6-7% per 1^{o}C warming rise in the lower tropospheric temperature (Willett et al., 2007). Therefore, water holding capacity of the atmosphere is increased under the warming climate, which directly affects the intensity and occurrence of the precipitation events over time (Cheng and Aghakouchak, 2014).

To evaluate the future short and long-term drought condition over the Indian region, it is inevitable to examine the current status of meteorological drought projection by various researchers. Ojha et al. (2013) examined the meteorological drought frequency using SPI as drought indicator and outputs from seventeen GCMs under CMIP3 multi-model dataset and showed an increasing trend of drought frequency over India. Future changeability of soil moisture drought over India was analysed by Mishra et al. (2014) using outputs from the seven GCMs from CMIP5 experiment. They revealed that the frequency and areal extents of soil moisture drought are likely to be increased. Aadhar and Mishra (2018) analysed the impact of climate change on meteorological drought frequency with the help of Standardized Precipitation Evapotranspiration Index (SPEI) as a drought index. In their study, they incorporated meteorological variables from five CMIP5 GCMs and observed an increasing drought frequency. Gupta and Jain (2018) used meteorological outputs from seven Regional Climate Models (RCMs) to investigate the spatio-temporal drought projections over India. Similarly, Bisht et al. (2019) adopted nine GCMs from the CMIP5 project to evaluate the future drought characteristics using the SPEI index over India. All the above-said studies have incorporated the meteorological inputs from the GCMs or RCMs. In addition, the studies have focused on entire India and the identification of the drought hotspot regions are not performed. Therefore, based on the past studies, identification of various drought properties and drought hotspot at a regional scale using newly developed high-resolution outputs from NASA Earth Exchange Global Daily Downscaled Projections (NEX-GDDP) would provide useful inference to the sustainable water resources management practices.

With this understanding, this chapter attempts to identify future meteorological drought hotspots incorporating different drought properties over a drought prone province in India, i.e., Maharashtra. To the best of our knowledge, no such multifaceted effort has been conducted over the Maharashtra province so far. In addition, this chapter includes the outputs from nineteen different GCMs from NEX-GDDP for the first time to characterise the future short (3-month scale) and long (12-month scale) term meteorological drought. In the light of the discussion made above, the present study is motivated to find out possible answers to the following questions, (i) whether the future projected climate change would bring frequent and severe drought condition during the 21st century over a region, (ii) what are the possible implications on future meteorological drought events due to the projected temperature? (iii) How the future drought hotspots are likely to change?

7.2 Data used

7.2.1 NEX-GDDP historical and future datasets

The description of the study area and historical meteorological datasets are already discussed in Chapter 3. To project the future meteorological droughts (i.e., SPI and SPEI), the future projections of meteorological datasets (precipitation, maximum (Tmax) and minimum (Tmin) temperature) are obtained from NEX-GDDP data, which is released in June 2015 by NASA (R. Xu et al., 2019). The spatial resolution of the datasets is 0.25^o Lat and 0.25^o Lon and available at daily time scale. The NEX-GDDP datasets incorporate simulations from twenty one GCMs from the CMIP5 experiment and are downscaled to the high resolution using bias correction spatial disaggregation (BCSD) based downscaling methodology (Thrasher et al., 2013). The period of the historical and future projected datasets can be obtained during 1950-2005 and 2006-2100, respectively. The future projections of the datasets are available for two emission scenarios, i.e., RCP 4.5 and 8.5. Recently, NEX-GDDP datasets are successfully used in various studies over different parts of the world (Singh et al., 2019; Xu et al., 2019). In the present study, nineteen GCMs are used from NEX-GDDP experiment based on the complete availability of the datasets. The details of the GCMs and their respective institutions are presented in Table 7.1.

7.2.2 Spatial resolution and time period used for analysis

In order to simplify the analysis and for meaningful interpretation of the outcomes, the meteorological datasets (both historical and future) are extracted from the NEX-GDDP projections using the grid point locations that blanket the study area at a spatial resolution of 0.5^o Lat ×0.5^o Lon. Due to the present spatial resolution of IMD meteorological data, authors could not use the NEX-GDDP datasets at 0.25^o Lat ×0.25^o Lon. The grid points (the total count is 103) covering the study area are presented in Figure 1(c). It should be noted that the NEX-GDDP datasets are bias-corrected using the historical meteorological data sets from the Terrestrial Hydrology Research Group at Princeton University (Sheffield et al., 2006). However, it is observed that the NEX-GDDP datasets, while compared with IMD observations, are not capturing the extreme precipitation and temperature events at the regional scale (more discussion is presented in Section 7.4). Therefore, bias-correction is again carried out over 103 grid points. For bias correction, 1951-2005 is chosen as

reference/baseline period (precipitation, maximum and minimum temperature) as historical GCMs' datasets are available up to 2005 and the IMD temperature datasets are available from 1951. For the comparison of future meteorological drought indices, the future time span is divided into three equal lengths of 26 years, i.e., 2022-2047, 2048-2073, and 2074-2099. Moreover, the drought indices and their properties for the recent past, i.e., 1993-2018 is used as historical period and compared with three segments of the future period.

Table 7.1: List of the GCMs with their respective institution used for the present study

Sl. No.	Model	Institution
1	ACCESS1-0	Commonwealth Scientific and Industrial Research Organization and Bureau of Meteorology, Australia
2	BCC-CSM1-1	Beijing Climate Center, China
3	CanESM2	Canadian Centre for Climate Modelling and Analysis, Canada
4	CCSM4	National Center for Atmospheric Research, America
5	CESM1-BGC	National Center for Atmospheric Research, America
6	CNRM-CM5	Centre National de Recherches Meteorologiques, Centre Europeen de Recherche et Formation Avancees en Calcul Scientifique, France
7	CSIRO-Mk3-6-0	Commonwealth Scientific and Industrial Research Organization/Queensland Climate Change Centre of Excellence, Australia
8	GFDL-CM3	Geophysical Fluid Dynamics Laboratory, America
9	GFDL-ESM2G	Geophysical Fluid Dynamics Laboratory, America
10	GFDL-ESM2M	Geophysical Fluid Dynamics Laboratory, America
11	INMCM4	Institute of Numerical Calculation, Russia
12	IPSL-CM5A-LR	Institut Pierre-Simon Laplace, France
13	IPSL-CM5A-MR	Institut Pierre-Simon Laplace, France
14	MIROC-ESM	Atmosphere and Ocean Research Institute, Japan
15	MIROC-ESM-CHEM	Atmosphere and Ocean Research Institute, Japan
16	MPI-ESM-LR	Max Planck Institute for Meteorology, Germany
17	MPI-ESM-MR	Max Planck Institute for Meteorology, Germany
18	MRI-CGCM3	Max Planck Institute for Meteorology, Germany
19	NorESM1-M	Norway Consumer Council, Norway

7.3 Research methodology

7.3.1 Bias correction of meteorological datasets

Initially, the bias correction of the daily meteorological datasets is performed at 103 grid points over the study area using the IMD datasets as a reference during 1951-2005 for selected 19 GCMs. In the context of future projection, it assumes stationarity of both the scale relationship and internal errors from the GCM (Hewitson et al., 2014). In other words, the correction factor for the present or historical period is valid for future conditions. In the present study, the quantile mapping method is used to correct the bias in precipitation and temperature datasets. Based on a comparative study among different bias correction methods, Gudmundsson et al. (2012) suggested that non-parametric quantile mapping has the best skill in reducing the bias as no specific distribution is assumed for the distribution of datasets and is presented as follows.

$$V_o = F_o^{-1}(F_m(V_m)) \tag{7.1}$$

where, V_o and V_m are observed and modelled meteorological variables (here, precipitation and temperature), F_m is the cumulative distribution function (CDF) of V_m and F_o^{-1} is the inverse CDF corresponds to V_o. The computation is performed by using the "qmap" package in R developed by Gudmundsson (2016) and can be downloaded from https://cran.r-project.org/web/packages/qmap/index.html.

7.3.2 Drought indices computation: SPI and SPEI

For each realisation (i.e., simulation from each GCM), the bias-corrected daily precipitation and temperature (maximum and minimum) datasets are converted into monthly series. In order to isolate the effect of temperature on future projections of meteorological drought, both SPI and SPEI are chosen in the present study. In the warming climate, though the precipitation may increase, the atmospheric evaporative demand may be more than the increase in rainfall (Spinoni et al., 2019). Therefore, the influence of temperature on meteorological drought is considered through the changes in Potential Evapotranspiration (PET), which is used in the computation of meteorological drought such as SPEI.

For each future simulation, future scenario, GCM, and grid point, the series SPI and SPEI values are computed. Following the methodology proposed by Mckee et al. (1993) for SPI

and by Vicente-Serrano et al. (2010) for SPEI, the precipitation and water balance component (i.e., the difference between precipitation and PET) are fitted with Gamma and log-logistic distribution, respectively. It is worth mentioning that for the comparison of 3-time segments during the future with historical, the transformation obtained during the baseline period from 1951 to 2005 is used for computation of SPI and SPEI for the accumulation period of 3, and 12 months in future and historical period (i.e., between 1993 and 2018). The computation is performed using the "SCI" package in R developed by Gudmundsson and Stagge (2015) and can be found at https://cran.r-project.org/web/packages/SCI/index.html. The computation of SPI and SPEI is presented in Chapter 3 and Chapter 4, respectively. However, in the present case, PET is computed using the Hargreaves method. For estimation of PET using the Penman-Monteith's method, other meteorological variables like cloud cover, wind speed, relative humidity, sunshine hour are required along with the precipitation and temperature data. Though all the variables described above are available for the past, unfortunately, such variables at high resolution are not available in the NEX-GDDP experiment. Moreover, it is found that Hargreaves method is superior to the Thornthwaite method (Aadhar and Mishra, 2020; Bandyopadhyay et al., 2012) and study revealed the similarity between the Hargreaves method and Penman-Monteith's method in estimating PET (Kingston et al., 2009). The classification of drought is similar to the classification as presented in Chapter 3.

7.3.3 Drought frequency, severity, duration, peak and areal spread

Different drought properties are evaluated following Das et al. (2020), i.e., with the help of "run theory" developed by Yevjevich (1967). In the present study, the events below -1 are considered as drought events. Therefore, a drought event is explained as the length between when an event falls down the pre-define truncation level (i.e., -1) and joins back to the truncation level. The graphical representation of different drought properties using run theory is presented in Chapter 3 (Figure 3.2).

With this understanding, the frequency of the drought is defined as the count of drought event for a given duration. The duration of drought is defined as the temporal length of a drought event, and the minimum length is one month. Similarly, the severity of a drought event is estimated as the absolute cumulative sum of the SPI/SPEI series for that particular drought duration. Therefore, drought duration and drought severity are strongly correlated. The minimum value of SPI/SPEI for a particular drought event is referred to as peak. In order to analyse the areal spread of the drought event, the maximum areal spread at each year is

chosen to find out the inter-annual variability. The areal spread is computed based on the fraction of area under drought (based on the grid points which are affected by drought).

It should be noted that the analysis is carried out over each division (kindly refer to Chapter 3) over the entire Maharashtra. Initially, the weight of each grid point corresponding to any division shapefile is computed. The weight represents the percentage of the area of any grid point falling within the division shapefile. For instance, if the weight value of a grid is 1 (0.6), then the complete grid (60% of the area) comes inside the shapefile. It is worth mentioning that, for the comparison purpose, the historical period (i.e., 1993-2018) is denoted as "T0" and similarly, 2022-2047, 2048-2073, and 2074-2099 segments are represented as "T1", "T2", and "T3", respectively.

7.4 Results

7.4.1 Bias correction: NEX-GDDP simulations versus IMD observation

Before using the nineteen GDDP simulations to project the two different meteorological droughts and analyse different drought properties, the correctness of the meteorological variables like precipitation, Tmax, and Tmin are evaluated using IMD observations during the baseline period. As discussed in the Section 7.3.1, the bias correction is carried out using the quantile mapping technique.

Bias correction relies on the reference or baseline data (Maraun et al., 2017). The NEX-GDDP simulation datasets were bias-corrected using the historical meteorological data sets from the Terrestrial Hydrology Research Group at Princeton University (Sheffield et al., 2006). Although the NEX-GDDP data have been bias-corrected during their generation process, it further needs bias-correction using the datasets available for the region (S. Chen et al., 2020) as the number of observation gauges over the area may be more as compared to the historical datasets used to correct initial bias in NEX-GDDP data. In this sense, while examining the IMD and NEX-GDDP datasets, Jain et al. (2019) noticed variability in the daily scale datasets of NEX-GDDP as compared to IMD dataset. Presently, while comparing with different quantiles of the IMD observational datasets, it is observed that most of the models show discrepancy at higher quantiles. In this sense, the NEX-GDDP model outputs are bias-corrected based on the IMD observations. For the brevity, a comparison between the before and after bias correction of precipitation for the grid point (75.375 long, 20.125 lat) is

presented in Figure 7.1. Moreover, for maximum and minimum temperature, the comparison plots are depicted in Figure 7.2

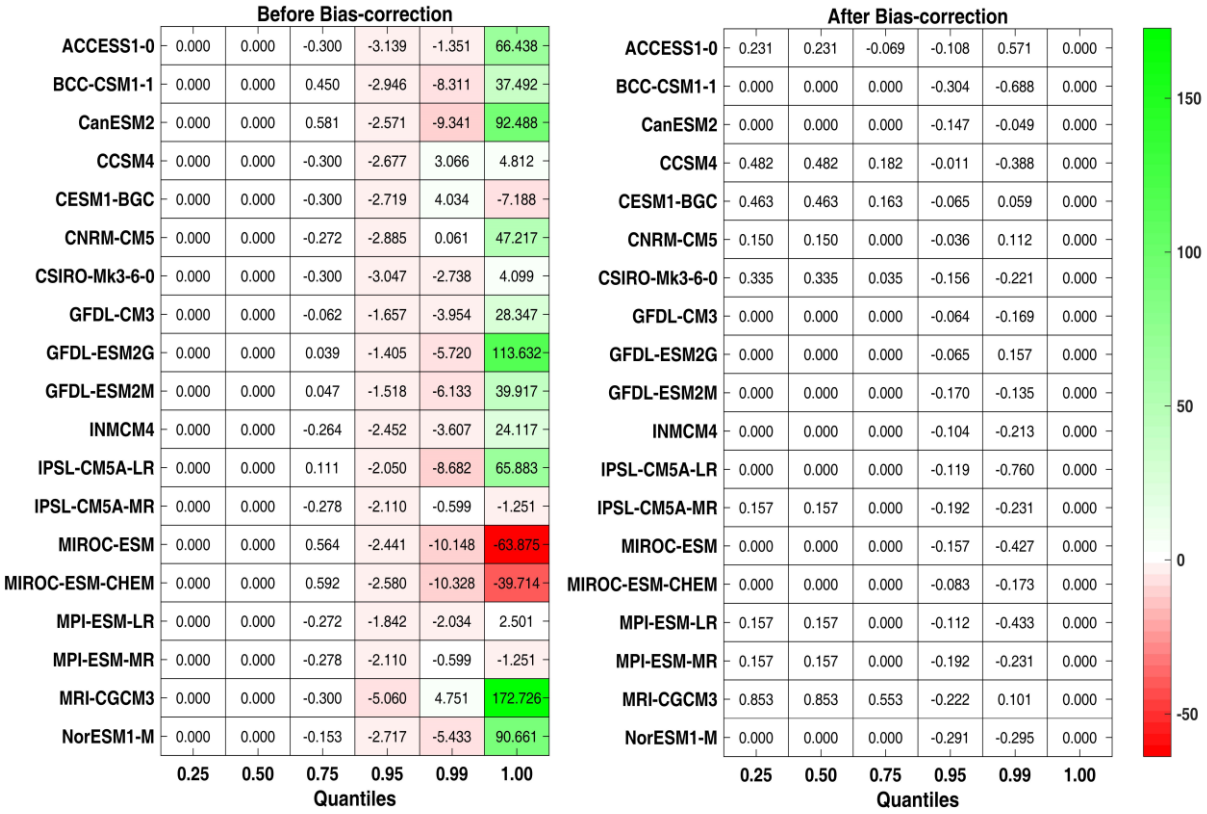

Figure 7.1: Heatmaps of before and after bias-correction of precipitation. The unit of colorbar is in mm

The units in Figure 7.1 and Figure 7.2 are mm and degree Celsius, respectively. The values represent the deviation from the observed data for each model and selected quantile. It can be noted from Figure 7.1 that the bias correction has improved the modelled outcomes for the higher quantiles (mostly the values at 95th, 99th, and 100th quantiles). However, in case of maximum and minimum temperature datasets, the bias is adjusted over the entire series. For maximum and minimum temperature series, the difference is high in case of minimum temperature than maximum temperature. It should be noted that the difference values are different at different grid points over the study area. The future projected values of precipitation, maximum and minimum temperature are corrected based on the correction during the baseline period.

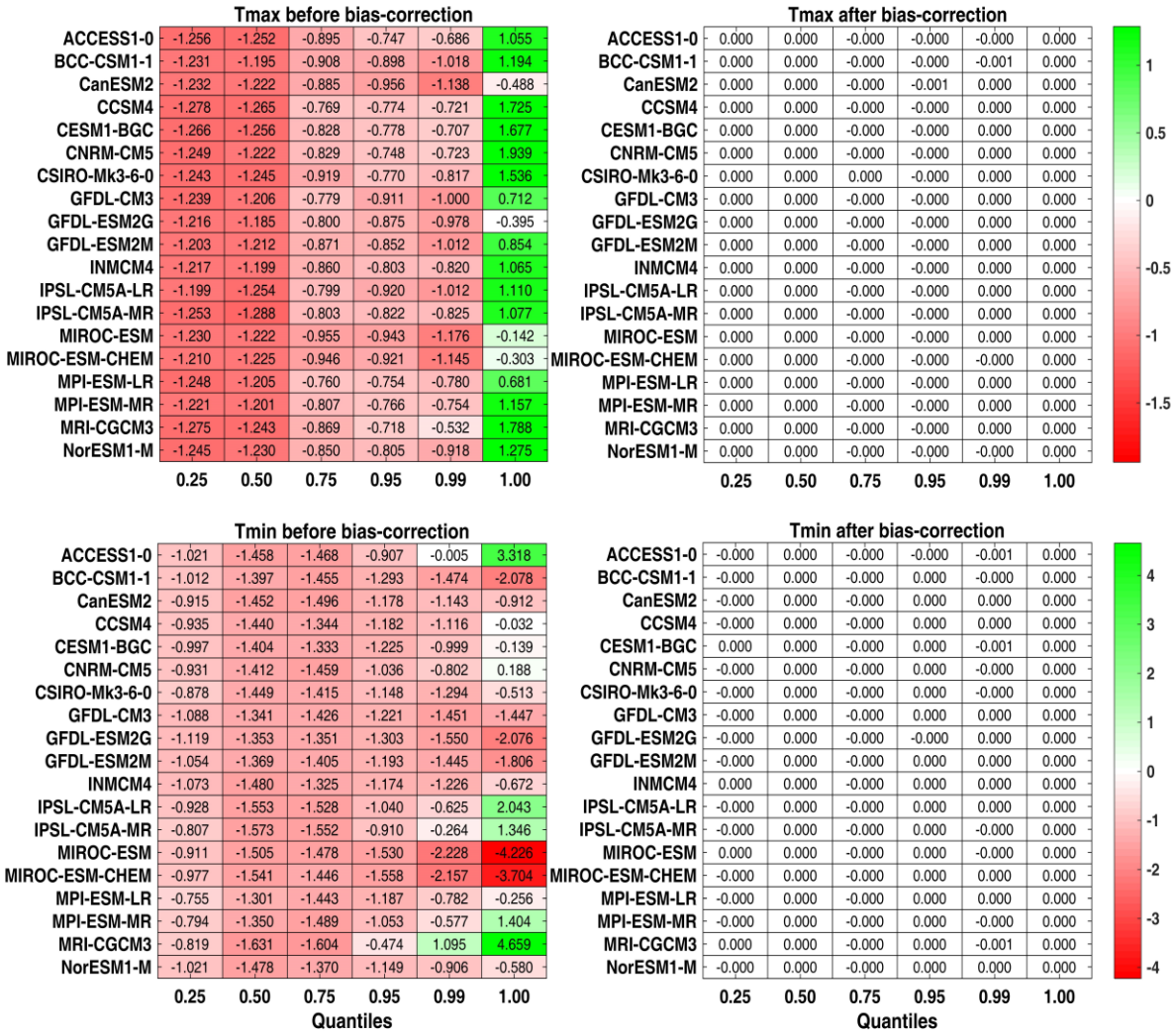

Figure 7.2: Heatmaps of before and after bias-correction of maximum and minimum temperature. The unit of colorbar is in degree C

7.4.2 Projection during the 21st century: wetting or drying warming?

To analyse the projected climatological conditions during the 21st century over the study area under RCP4.5 and 8.5 scenarios, the precipitation, Tmax, Tmin, and PET for T1, T2, and T3 segments are compared with T0 period. Figure 7.3 shows the change in the Multi Model Mean (MMM) of precipitation between 3 different future segments and historical period. The upper (lower) panels show the monthly precipitation variations over Amaravati, Aurangabad, and Konkan (Nagpur, Nashik, and Pune) regions under both the RCP scenarios. For Tmax, Tmin and PET the monthly MMMs are presented in Figure 7.4, Figure 7.5, and Figure 7.6, respectively.

It can be noted from Figure 7.3 that the monthly precipitation during T0 is high over Konkan as compared to the other regions as Konkan region is situated in the Western Ghats, a high precipitation zone due to its geographical aspects. Similarly, Aurangabad and Nashik regions receive less precipitation (within 120-160mm) during the monsoon period with comparison to other regions during T0. During 2022-2099, the precipitation during the monsoon period is likely to increase overall the regions except Konkan. The future projected monthly precipitation pattern during 2022-2099 over Konkan shows no significant change under both the scenarios. The increase in the monthly precipitation (mostly during monsoon) is higher under RCP8.5 than RCP4.5. In particular, the monsoon precipitation is projected to increase over Amaravati by 15-27% for RCP4.5 and 20-40% for RCP8.5, over Aurangabad by 21-34% for RCP4.5 and 21-44% for RCP8.5, over Nagpur by 7-19% for RCP4.5 and 17-34% for RCP8.5, over Nashik by 14-25% for RCP4.5 and 13-34% for RCP8.5, and over Pune by 10-19% for RCP4.5 and 13-33% for RCP8.5 during 2022-2099. Moreover, monthly precipitation is likely to increase from T1 to T3, i.e., T1<T2<T3. In general, a wetting tendency is observed during the 21st century under both the scenarios except Konkan.

The future projections of Tmax and Tmin are presented in Figure 7.4 and Figure 7.5, respectively. It can be noticed from both the figures that the MMM of monthly maximum and minimum temperature are projected to increase as compared to the historical period in both the scenarios over all the regions. However, the increase is more in case of RCP8.5 than RCP4.5 with the same pattern as precipitation, i.e., T1<T2<T3. The average temperature is projected to increase over Amaravati by 0.58-3.4^{o}C for RCP4.5 and 1.66-4.5^{o}C for RCP8.5, over Aurangabad by 0.43-3.3^{o}C for RCP4.5 and 1.46-4.4^{o}C for RCP8.5, over Konkan by 0.43-3.3^{o}C for RCP4.5 and 1.37-3.2^{o}C for RCP8.5, over Nagpur by 0.46-3.3^{o}C for RCP4.5 and 1.43-4.4^{o}C for RCP8.5, over Nashik by 0.57-3.1^{o}C for RCP4.5 and 1.47-4.1^{o}C for RCP8.5, and over Pune by 0.72-2.6^{o}C for RCP4.5 and 1.54-3.5^{o}C for RCP8.5 during 2022-2099. The projected temperature changes are in line with the latest report of the Intergovernmental Panel on Climate Change (IPCC, 2014) based on the CMIP5 simulations. Therefore, in a broader sense, the projected climatology over Maharashtra is likely to be wetting and warming during the 21st century except for Konkan region as compared to historical. In the Konkan region, the warmer climatology is likely to prevail with no significant change in the monthly precipitation variability.

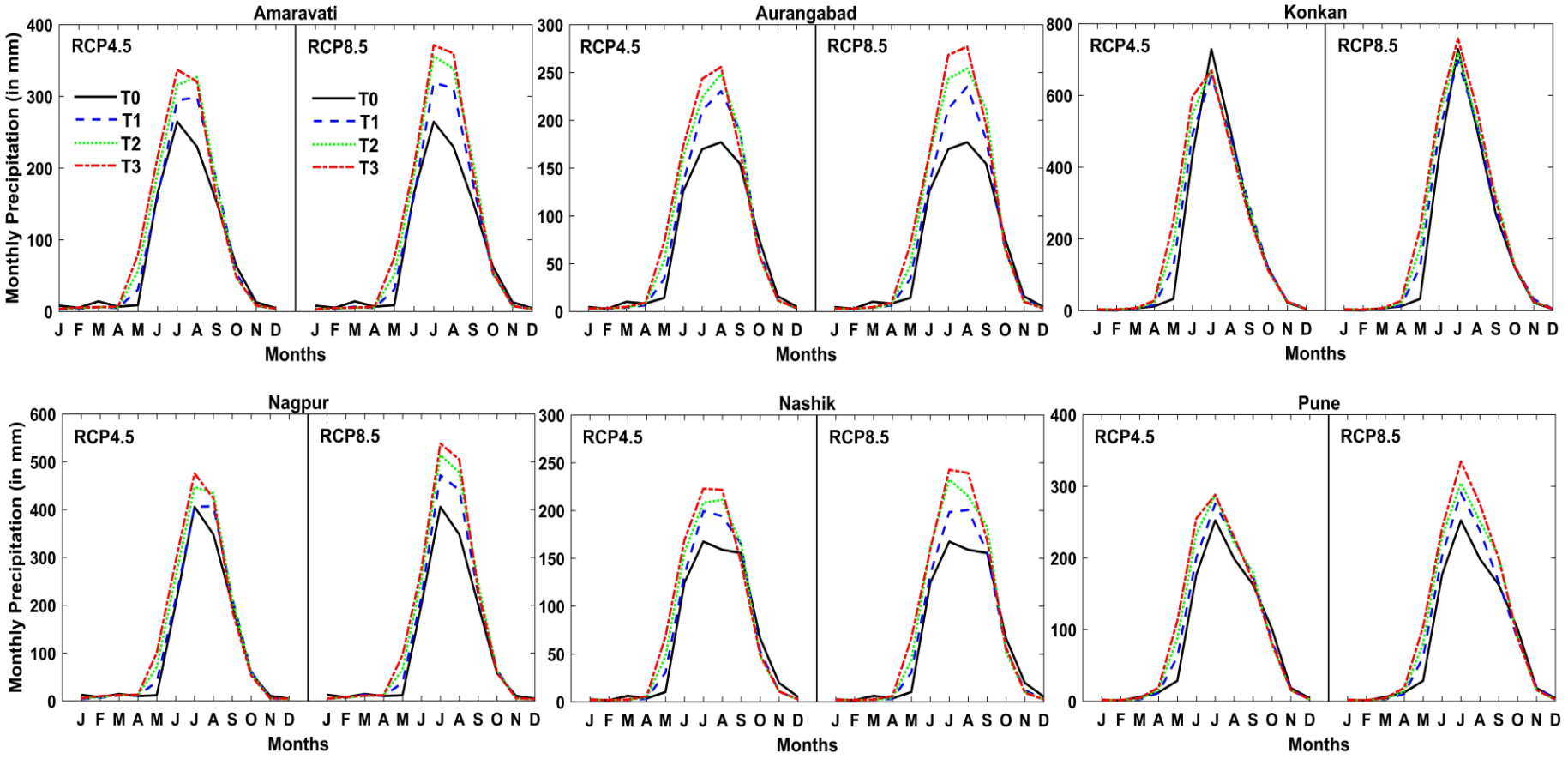

Figure 7.3: Monthly precipitation variability over different regions under RCP4.5 and 8.5 scenarios

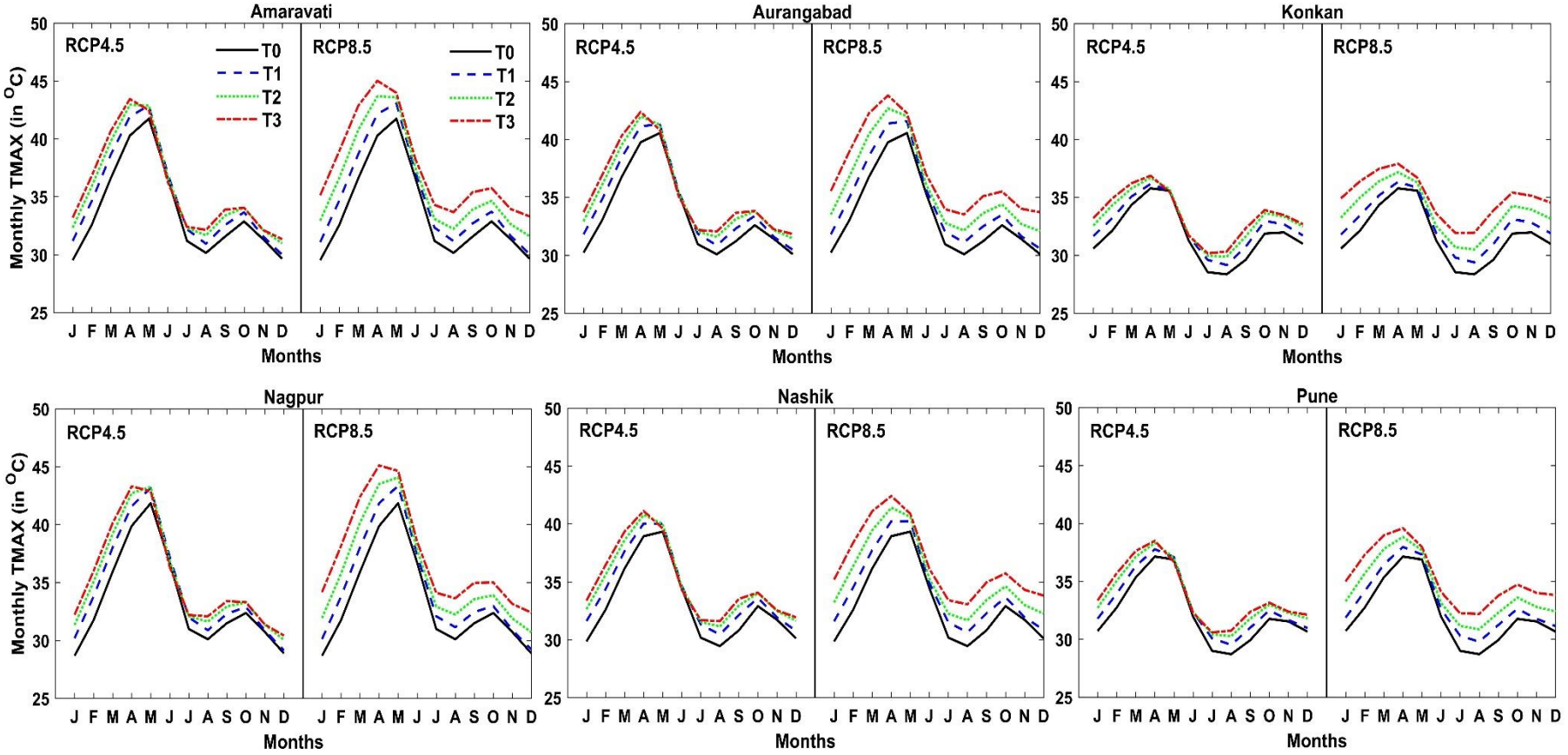

Figure 7.4: Monthly Tmax variability over different regions under RCP4.5 and 8.5 scenarios

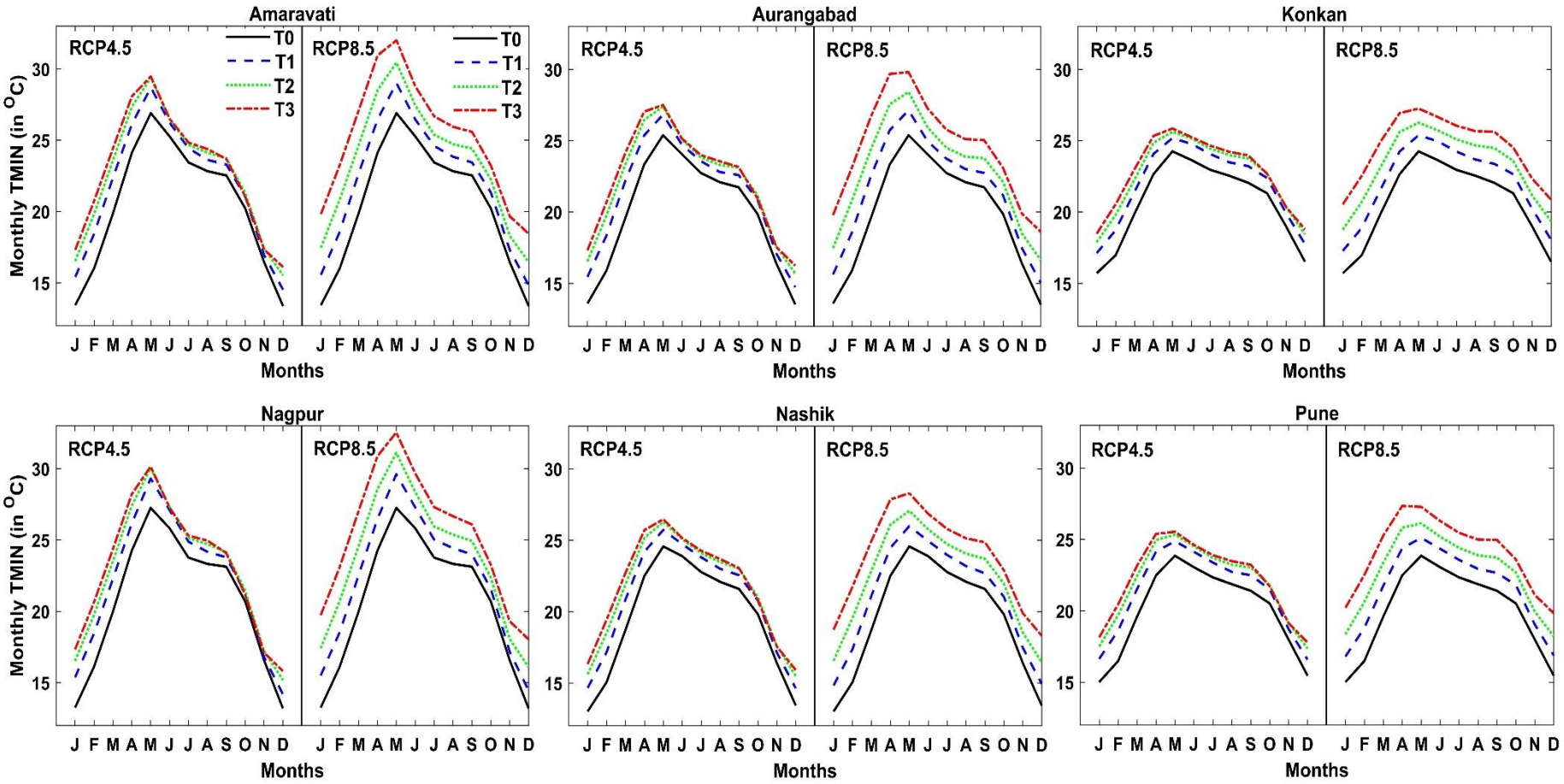

Figure 7.5: Monthly Tmin variability over different regions under RCP4.5 and 8.5 scenario

The general agreement among the climate simulations projects towards a warmer world during the 21st century (IPCC, 2014b; Meehl et al., 2007) and hence, an increase in the PET can be expected as it is driven by the temperature. The projected PET over the study area is presented in Figure 7.6. It can be noted from the figure that there is no significant variation in MMM of monthly PET between the two scenarios over all the regions. However, an increase in the PET is projected during the months from January to April over Amaravati, Aurangabad, Nagpur, and Nashik with T1<T2<T3. The projected increase in the evaporative demand does not necessarily intensify the drought properties over the region (Spinoni et al., 2019). However, the collective influence of both precipitation and PET will control the characteristics and properties of drought.

7.4.3 Drought properties & its projection during the 21st century

7.4.3.1 SPEI drought frequency

In the present study, the drought frequency is computed for severe and extreme drought conditions. Figure 7.7 represents the SPEI drought frequency over different regions under RCP4.5 and 8.5 scenarios for short-term scale. The grouped box plot is developed to make the comparison of drought frequency between severe and extreme drought classes. The boxplot represents the MMM of all the nineteen GCMs over the grid points for a particular region. It should be noted that the number of grid points are different for each region. In particular, Amaravati, Aurangabad, Konkan, Nagpur, Nashik, and Pune include 25, 35, 17, 18, 30, and 29 grid points, respectively. The summation of all the individual grid points is greater than the total number of grid points inside the Maharashtra as the inside regions share the common boundary with other regions.

To analyse the temporal variability, three segments (T1, T2, and T3) of the future period are compared with the historical (T0). The change in the drought frequency is computed based on percentage change in the mean. It is projected that for all the future segments and all the regions, the drought frequency for extreme drought condition is likely to increase under RCP4.5 and 8.5. For instance, the percentage increase over Amaravati varies from 46 to 92% in RCP4.5 and 38 to 115% in RCP8.5, over Aurangabad 20 to 53% in RCP4.5 and 13 to 80% in RCP8.5, over Konkan 42 to 50% in RCP4.5 and 7 to 71% in RCP8.5, over Nagpur 50 to 100 % in RCP4.5 and 42 to 133% in RCP8.5, over Nashik 53 to 92% in RCP4.5 and 46 to 115% in RCP8.5, and over Pune 25 to 38% in RCP4.5 and 38 to 63% in RCP8.5 for short-term drought condition.

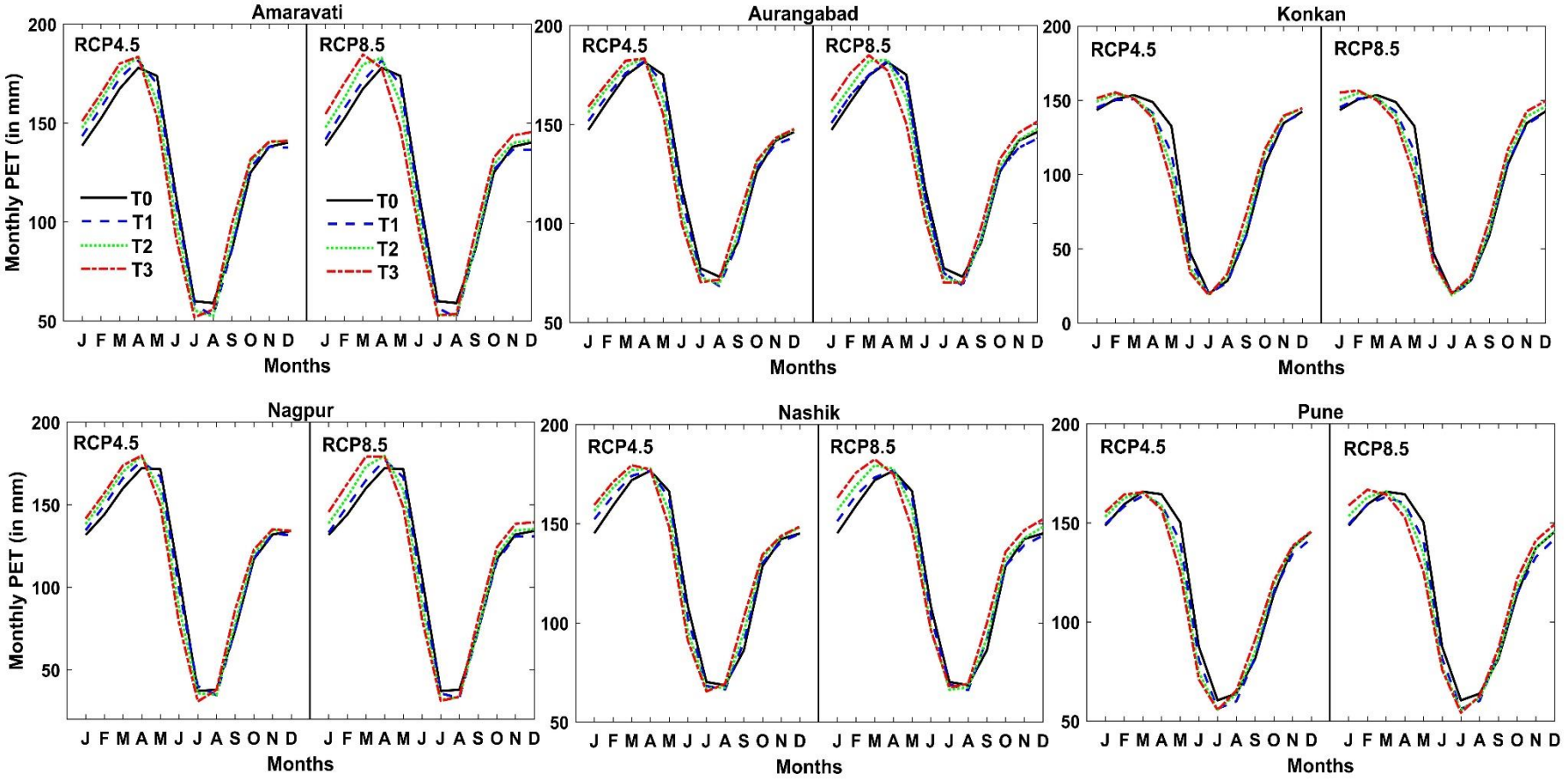

Figure 7.6: Monthly PET variability over different regions under RCP4.5 and 8.5 scenarios

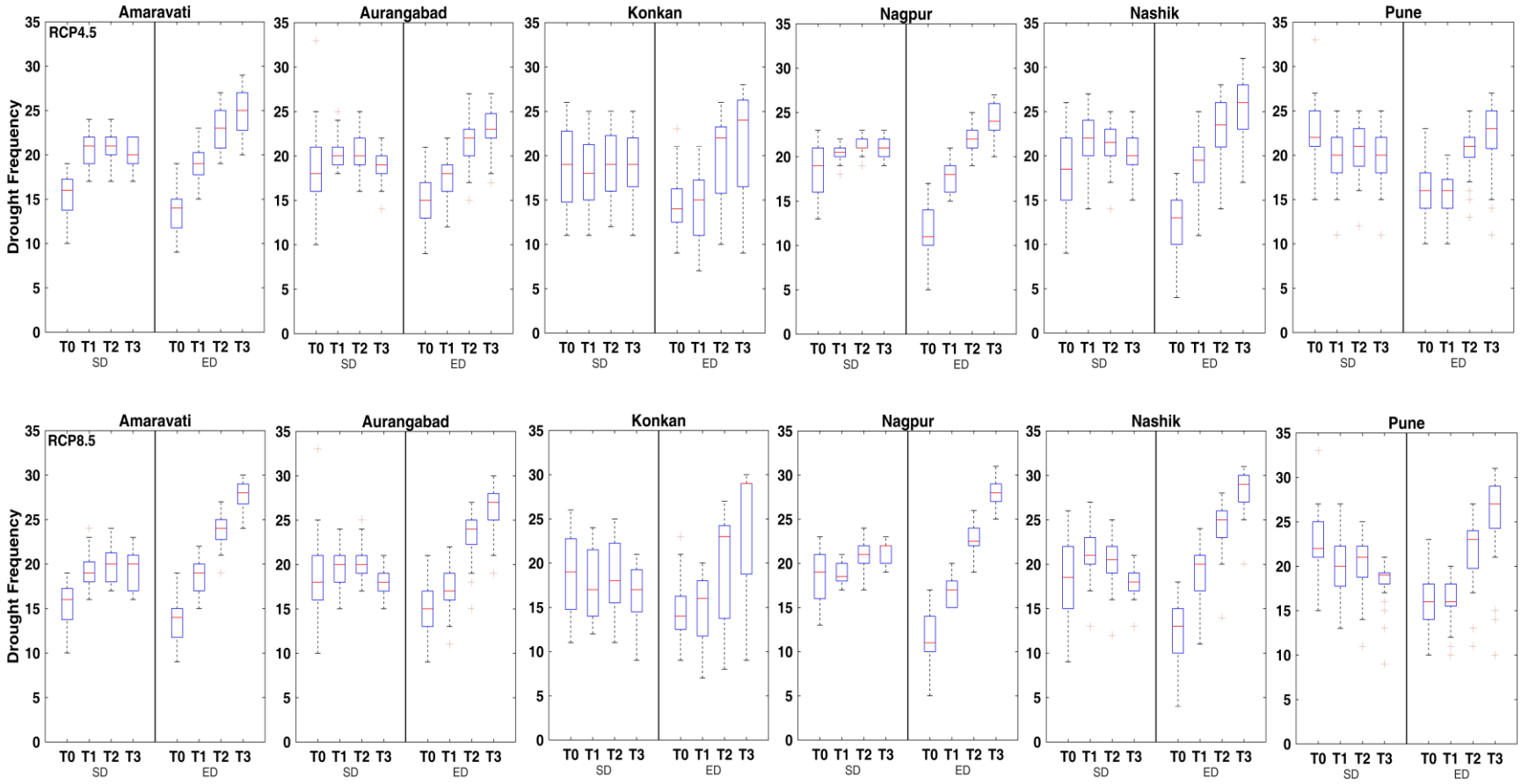

Figure 7.7: Grouped boxplot of historical and future drought frequency over different regions for short-term drought based on SPEI. SD and ED refers to Severe Drought and Extreme Drought, respectively

Likewise, the percentage change in frequency of severe drought is likely to increase under both the scenarios over most of the regions except Pune and Konkan region. For instance, over Amaravati 33 to 40% in RCP4.5 and 26 to 33% in RCP8.5 and over Nashik, the percentage increase varies from 5 to 15% in RCP4.5 and 5 to 11% in RCP 8.5, among others.

Similarly, the spatio-temporal variability of drought frequency over different regions under RCP4.5 and 8.5 scenarios for long-term scale is presented in Figure 7.8. It is noticed that the percentage change of severe drought frequency is likely to either decrease or remain insignificant with respect to T0 under both the scenarios over all the regions. Similarly, the percentage change of extreme drought is projected to increase or remain unchanged no change as compared to T0 under both the scenarios except over Aurangabad (during T1 in RCP8.5). The highest positive change is noticed over Konkan, i.e., 100 to 150% in RCP4.5 and 50 to 150% in RCP8.5.

7.4.3.2 SPI drought frequency

Figure 7.9 represents the SPI drought frequency over different regions under RCP4.5 and 8.5 scenarios for short-term scale. It is projected that for all the future segments (except T3 in RCP4.5 over Aurangabad) and all the regions the drought frequency for severe drought condition is likely to increase under RCP4.5 and 8.5. For instance, the percentage increase over Amaravati varies from 11 to 33% in RCP4.5 and 22 to 33% in RCP8.5, over Konkan 25% in RCP4.5 and 25 to 37% in RCP8.5, over Nagpur 9 to 18 % in both RCP4.5 and 8.5, over Nashik 12.5% in RCP4.5 and 12.5 to 25% in RCP8.5, and over Pune 10 to 20% in RCP4.5 and 20 to 30% in RCP8.5 for short-term drought condition. Likewise, the percentage change in frequency of extreme drought is likely to increase under both the scenarios over all the regions with a significantly larger magnitude than severe drought in short-term drought condition. For instance, over Nagpur and Nashik the percentage increase in RCP4.5 and 8.5 varies between 100 to 120%, and 100 to 140%, respectively, among others. Similarly, the spatio-temporal variability of drought frequency over different regions under RCP4.5 and 8.5 scenarios for long-term scale is presented in Figure 7.10. It is noticed that except over Amaravati (during T1 in RCP4.5) and Konkan (during T1 and T2 in RCP4.5 and T1 in RCP8.5), the percentage change of severe drought frequency is likely to decrease or no significant change with respect to T0 under both the scenarios. Likewise, the percentage change of extreme drought is projected to increase or no change as compared to T0 under

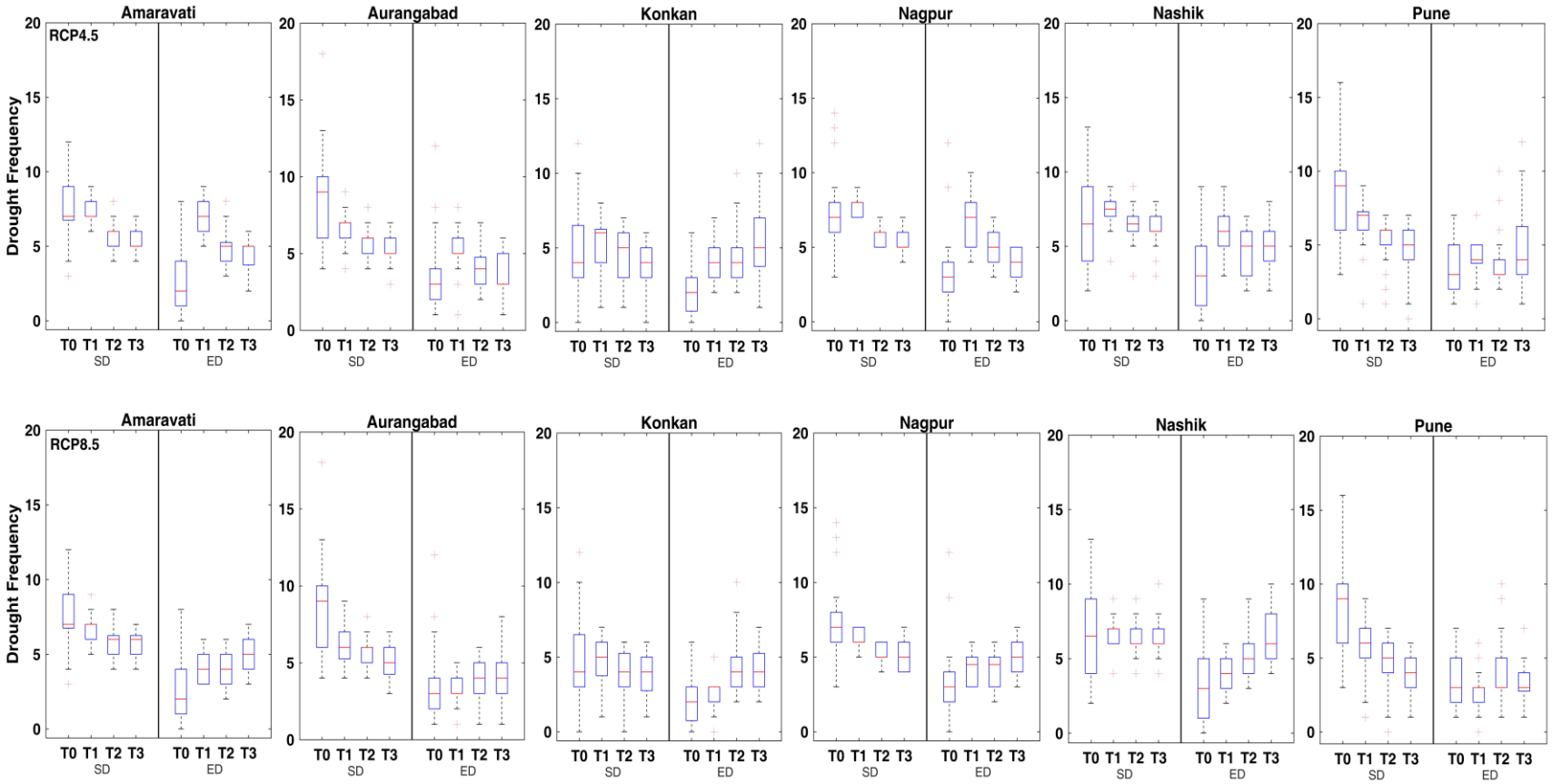

Figure 7.8: Grouped boxplot of historical and future drought frequency over different regions for long-term drought based on SPEI.

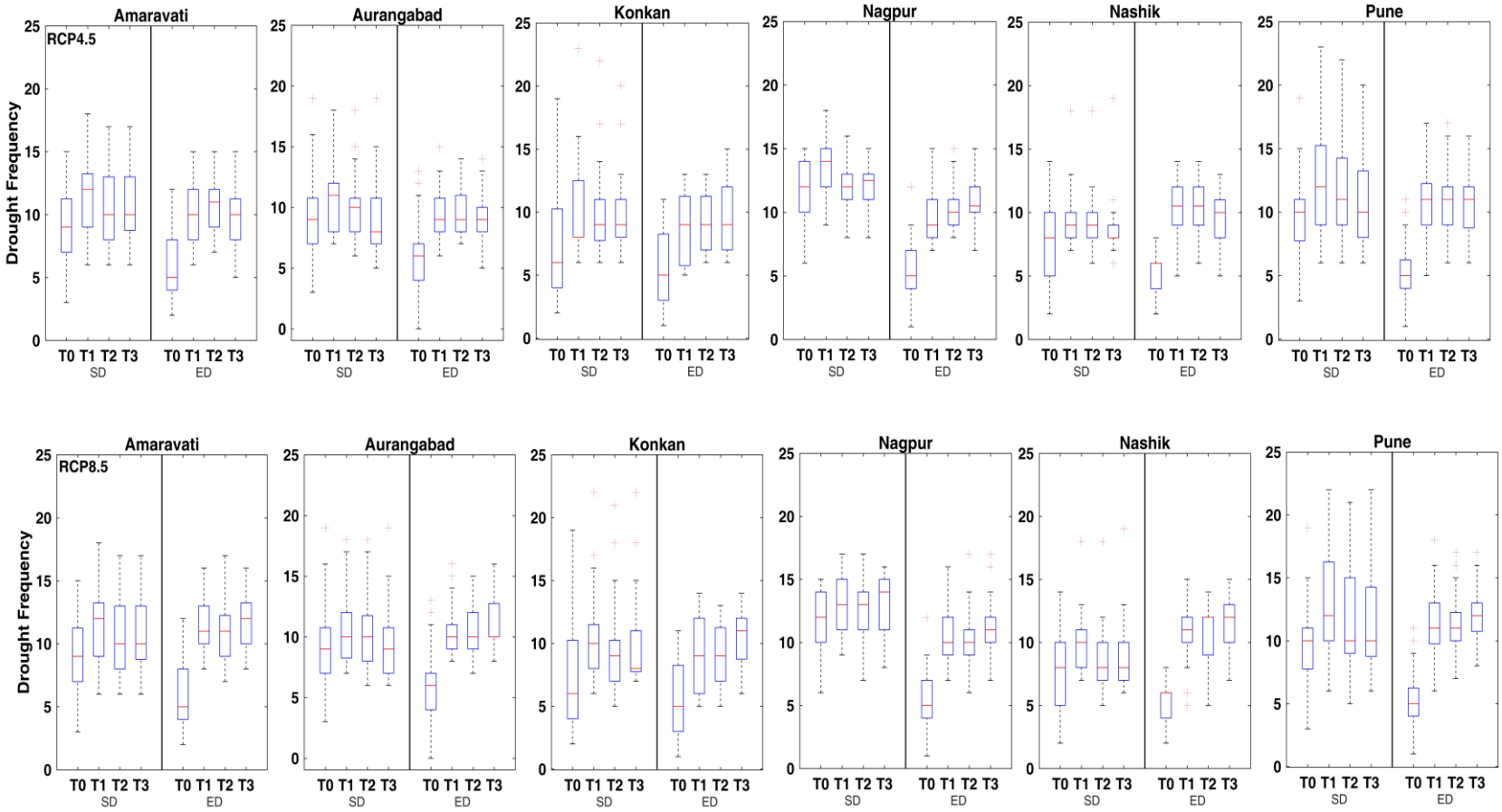

Figure 7.9: Grouped boxplot of historical and future drought frequency over different regions for short-term drought based on SPI

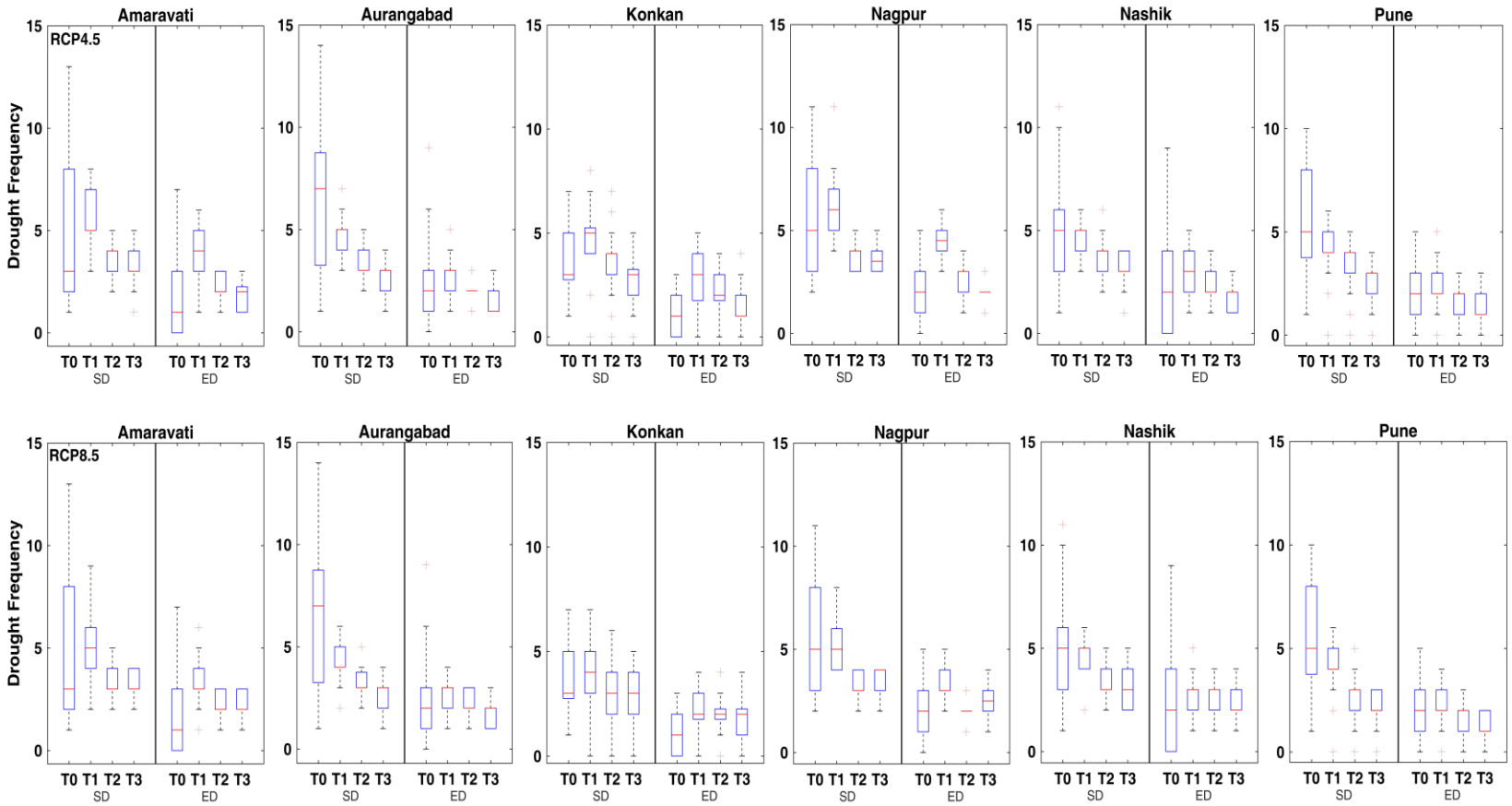

Figure 7.10: Grouped boxplot of historical and future drought frequency over different regions for long-term drought based on SPI

both the scenarios except over Aurangabad (during T3 in RCP4.5), over Pune (during T3 in RCP4.5), and over Pune (during T3 in RCP8.5). The highest positive change is noticed over Konkan, i.e., 100 to 200% in RCP4.5 and 8.5.

7.4.3.3 SPEI drought severity

The MMM of all the climate models over the grid points is plotted in the form of boxplot and depicted under Figure 7.11. It is observed from the figure that during short-term scale drought the severity over Amaravati (42 to127% in RCP4.5 and 39 to 218% in RCP8.5), Aurangabad (19 to 100% in RCP4.5 and 20 to 172% in RCP8.5), Konkan (44 to 61% in RCP4.5 and 4 to 112% in RCP8.5), Nagpur (35 to 95% in RCP4.5 and 32 to 180% in RCP8.5), Nashik (46 to 155% in RCP4.5 and 53 to 257% in RCP8.5), and Pune (32 to 51% in RCP4.5 and 28 to 93% in RCP8.5) is likely to increase during 21st century over both the scenarios. The percentage change is computed for the change in mean (from the boxplot) between historical and future segments. Similarly, percentage change of severity as compared to T0 is observed for long-term scale drought over Amaravati (up to 53% in RCP4.5 and up to 60% in RCP8.5), Aurangabad (up to 20% in RCP4.5 and 46% in RCP8.5), Konkan (2% in RCP4.5 and up to 78% in RCP8.5), Nagpur (up to 33% in RCP4.5 and 24% in RCP8.5), Nashik (up to 33% in RCP4.5 and up to 90% in RCP8.5). However, during long-term scale, the projected change with respect to T0 is likely to decrease during T1 and T2 in RCP8.5 over Pune (-9 to -26%), during T2 in RCP8.5 over Konkan (-5%) and Nagpur (-3%).

7.4.3.4 SPI drought severity

The MMM of all the climate models over the grid points is plotted in the form of boxplot and depicted under Figure 7.12. The grouped boxplot for each region is plotted to present the average severity between RCP4.5 and 8.5. It is observed from the figure that during short-term scale drought the severity over Amaravati (8 to16% in RCP4.5 and 12 to 28% in RCP8.5), Konkan (32 to 44% in RCP4.5 and 29 to 64% in RCP8.5), Nagpur (17 to 24% in RCP4.5 and 19 to 40% in RCP8.5), Nashik (16 to 18% in RCP4.5 and 16 to 38% in RCP8.5), and Pune (10 to 15% in RCP4.5 and 8 to 28% in RCP8.5) is likely to increase during 21st century over both the scenarios. The percentage change is computed for the change in mean (from the boxplot) between historical and future segments. However, over Aurangabad, the severity is projected to increase (7 to 25%) only in RCP8.5 scenario. Similarly, decreasing or not significant change of severity as compared to T0 is observed for long-term scale drought

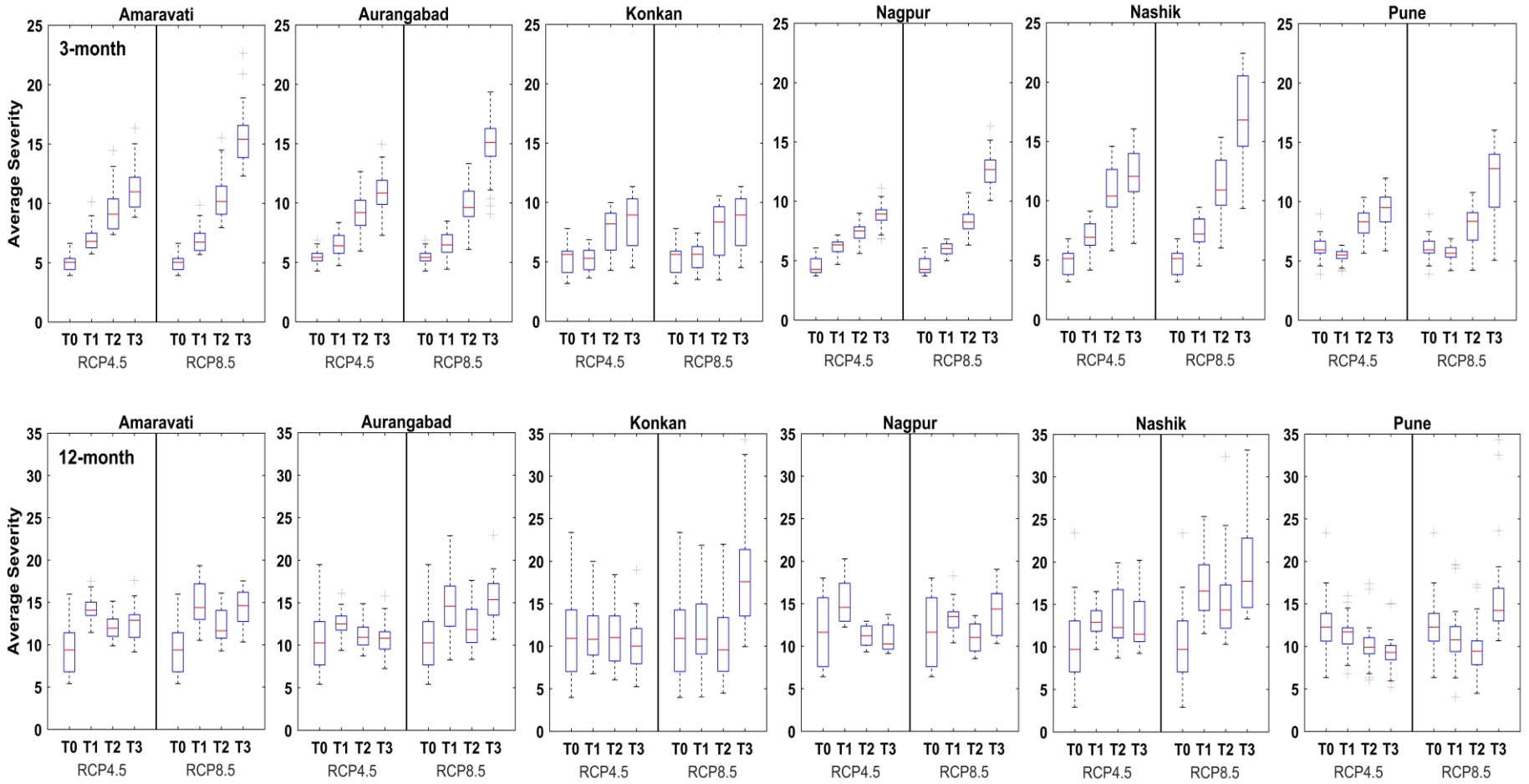

Figure 7.11: Grouped boxplot of historical and future drought severity over different regions under RCP4.5 and 8.5 scenarios. The upper panel presents short-term drought and the lower one presents long-term drought based on SPEI

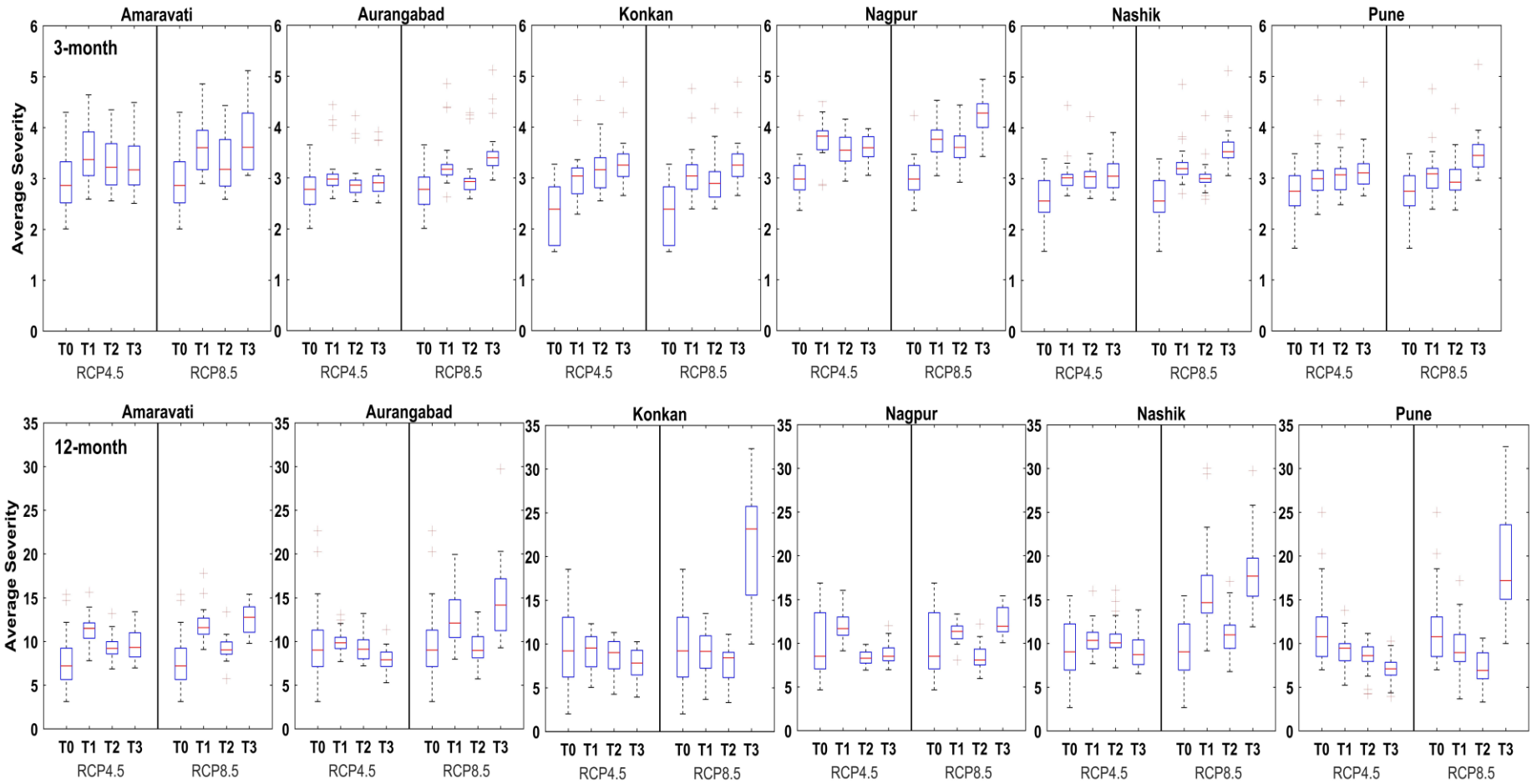

Figure 7.12: Grouped boxplot of historical and future drought severity over different regions under RCP4.5 and 8.5 scenarios. The upper panel presents short-term drought and the lower one presents long-term drought based on SPI

over Aurangabad (up to -17% in RCP4.5), Konkan (-8 to -22% in RCP4.5 and T1 (-9%), T2 (-20%) in RCP8.5), Nagpur (T2 (-14%) and T3 (-9%) in RCP4.5 and T2 (-13%) in RCP8.5), and Pune (-21 to -38% in RCP4.5 and T1 (-18%) and T2 (-37%) for RCP8.5). However, during long-term scale, the projected change with respect to T0 is likely to increase during T3 in RCP8.5 over Aurangabad (53%), Konkan (127%), Nashik (97%), Pune (67%) and under both the scenarios over Amaravati (20 to 45% in RCP4.5 and 19 to 63% in RCP8.5). In most of the cases, the increase in the severity under RCP8.5 is more than RCP4.5 for both the drought scales. In addition, the lower level or minimum value of severity has increased significantly over all the regions in short-term scale and over all the regions except for Pune in long-term scale under RCP4.5 and RCP8.5 (except for T3).

7.4.3.5 SPEI drought duration

Figure 7.13 presents the average drought duration of MMM over different regions for short- and long-term drought conditions and different scenarios in the form of a grouped boxplot. It is observed from the figure that the variability of drought duration is projected to increase significantly in future for short-term drought. Precisely, the minimum value of duration is likely to increase significantly as compared to the historical period. The percentage change is computed over all the region with respect to the mean value. The highest percentage increase in the drought duration (i.e., 63%) is observed over Nashik in RCP8.5 followed by 52% over Amaravati in RCP8.5. No significant change is observed during T1 over Konkan in RCP4.5 and over Konkan and Pune in RCP8.5. While considering the long-term scale drought condition, the projected change in the drought duration for different regions and two scenarios are as follows. Amaravati and Nashik have shown an increase in the percentage of drought duration for all the time periods in RCP4.5 and RCP8.5. However, the percentage decrease in the drought duration is noticed over Pune under both the scenarios, over Konkan in RCP4.5, and over Nashik in RCP8.5. No significant change is noticed over Aurangabad under RCP4.5 scenario.

7.4.3.6 SPI drought duration

Figure 7.14 presents the average drought duration of MMM over different regions for short- and long-term drought conditions and different scenarios in the form of grouped boxplot. It is observed from the figure that the variability of drought duration is projected to decrease significantly in future. Precisely, the minimum value of duration is likely to increase significantly as compared to the historical period. The percentage change is computed over

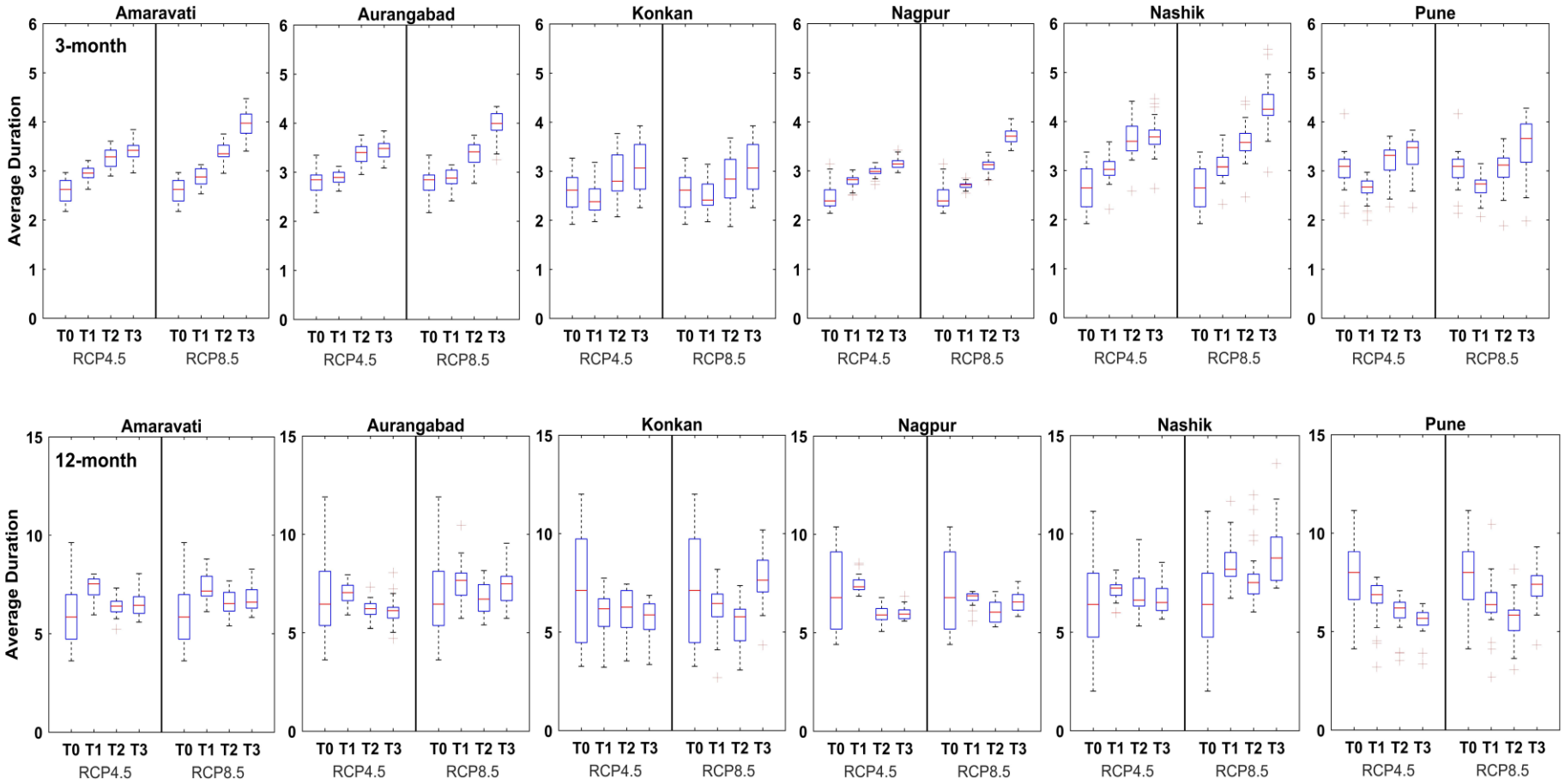

Figure 7.13: Grouped boxplot of historical and future drought duration over different regions under RCP4.5 and 8.5 scenarios. The upper panel presents short-term drought and the lower one presents long-term drought based on SPEI

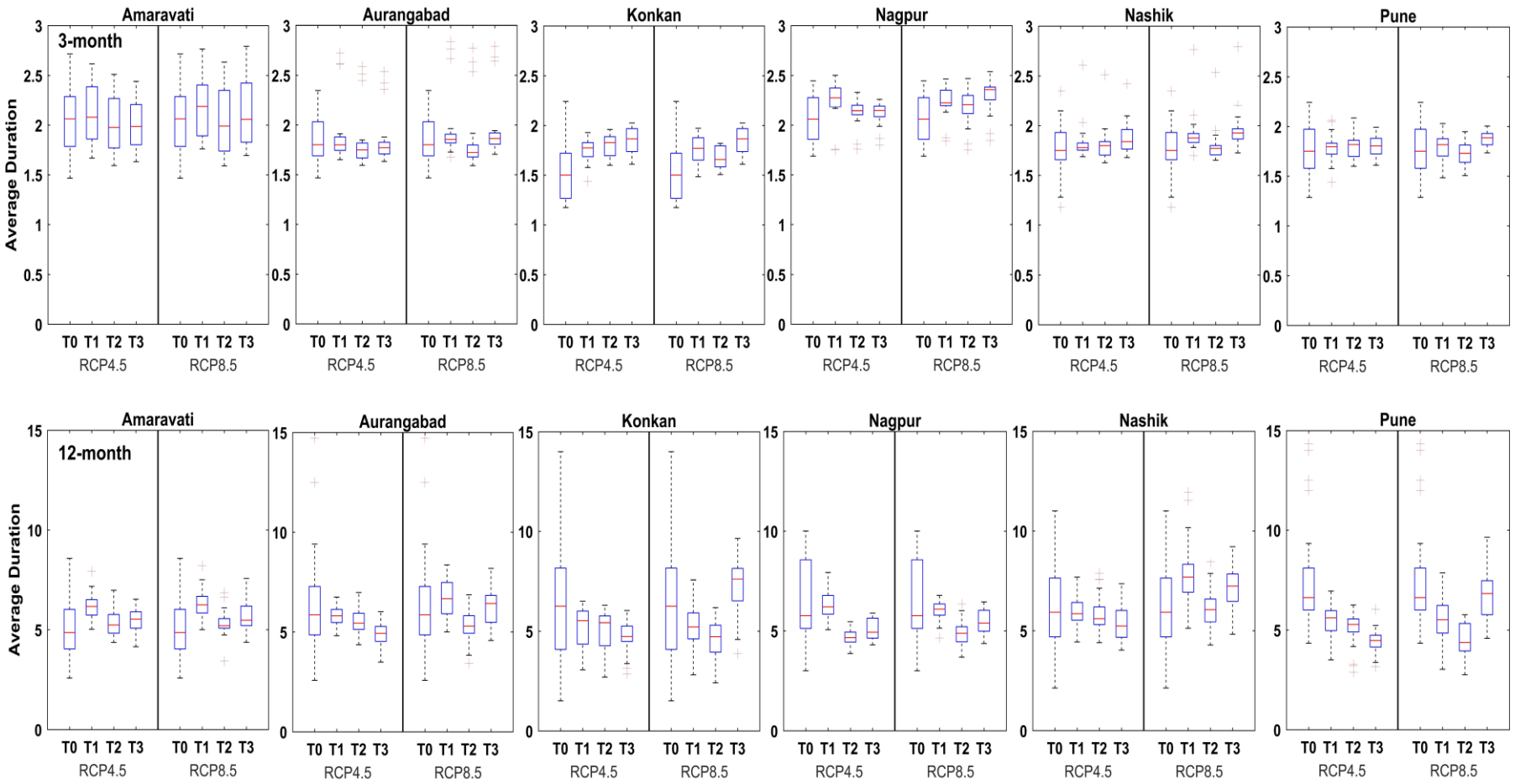

Figure 7.14: Grouped boxplot of historical and future drought duration over different regions under RCP4.5 and 8.5 scenarios. The upper panel presents short-term drought and the lower one presents long-term drought based on SPI

all the region with respect to the mean value. Over Amaravati, Aurangabad, Nagpur, Nashik, and Pune the change in the drought duration with respect to historical is not significant for the short-term drought condition in RCP4.5 and in RCP8.5. In addition, there is an increase in the drought duration of 12% and 10% during T3 in RCP8.5 over Nagpur and Nashik, respectively. However, in Konkan, the drought duration for short-term drought condition is likely to increase 15 to 21% in RCP4.5 and 10 to 24% in RCP8.5. While considering the long-term scale drought condition, the projected change in the drought duration for different regions and two scenarios are as follows. T2 and T3 over Amaravati have no significant change in both the scenarios; however, 18% and 22% increase is projected during T1 in RCP4.5 and RCP 8.5, respectively. Except Amaravati, the change in the drought duration is likely to decrease or exhibits no significant change over all other regions for both the RCP scenarios. For example, the percentage decrease over Konkan and Pune is expected in the range of -25 to -30% and -28 to 41%, respectively under RCP4.5 and -7 to -31% and -10 to -41%, respectively under RCP8.5.

7.4.3.7 SPEI drought peak

The MMM of average drought peak over most of the regions is projected to increase under both the scenarios (Figure 7.15) during short and long-term drought conditions. It should be noted that the absolute value of peak is presented in the grouped boxplot. Precisely, for short-term drought condition, the peak over Amaravati (30 to 95% in RCP4.5 and 30 to 141% in RCP8.5), Aurangabad (14 to 75% in RCP4.5 and 16 to 119% in RCP8.5), Konkan (3 to 52% in RCP4.5 and 9 to 90% in RCP8.5), Nagpur (33 to 88% in RCP4.5 and 33 to 136% in RCP8.5), Nashik (29 to 105% in RCP4.5 and 33 to 156% in RCP8.5), and Pune (up to 52% in RCP4.5 and 2 to 92% in RCP8.5) is projected to increase during the 21st century. Similarly, for long-term drought condition, the peak over Amaravati (26 to 33 % in RCP4.5 and 28 to 34% in RCP8.5), Aurangabad (15 to 17% in RCP4.5 and 17 to 22% in RCP8.5), Konkan (19 to 21% in RCP4.5 and 18 to 38% in RCP8.5), Nagpur (19 to 33% in RCP4.5 and 20 to 37% in RCP8.5), Nashik (18 to 23% in RCP4.5 and 23 to 35% in RCP8.5), and Pune (4 to 7% in RCP4.5 and 1 to 13% in RCP8.5) is likely to increase. In addition, the increase in case of RCP8.5 is larger than RCP4.5 for both the drought conditions.

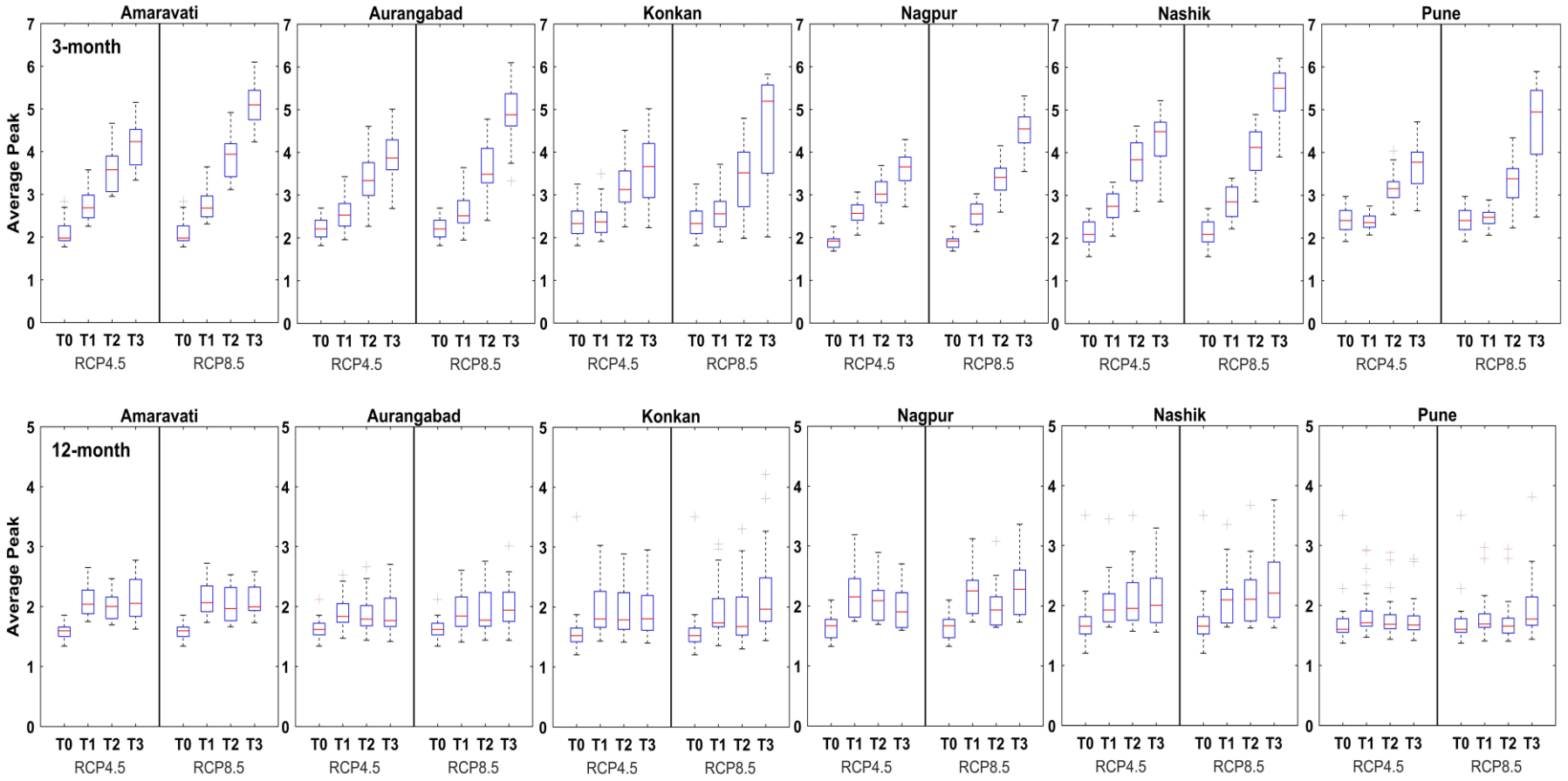

Figure 7.15: Grouped boxplot of historical and future drought peak over different regions under RCP4.5 and 8.5 scenarios. The upper panel presents short-term drought and the lower one presents long-term drought based on SPEI

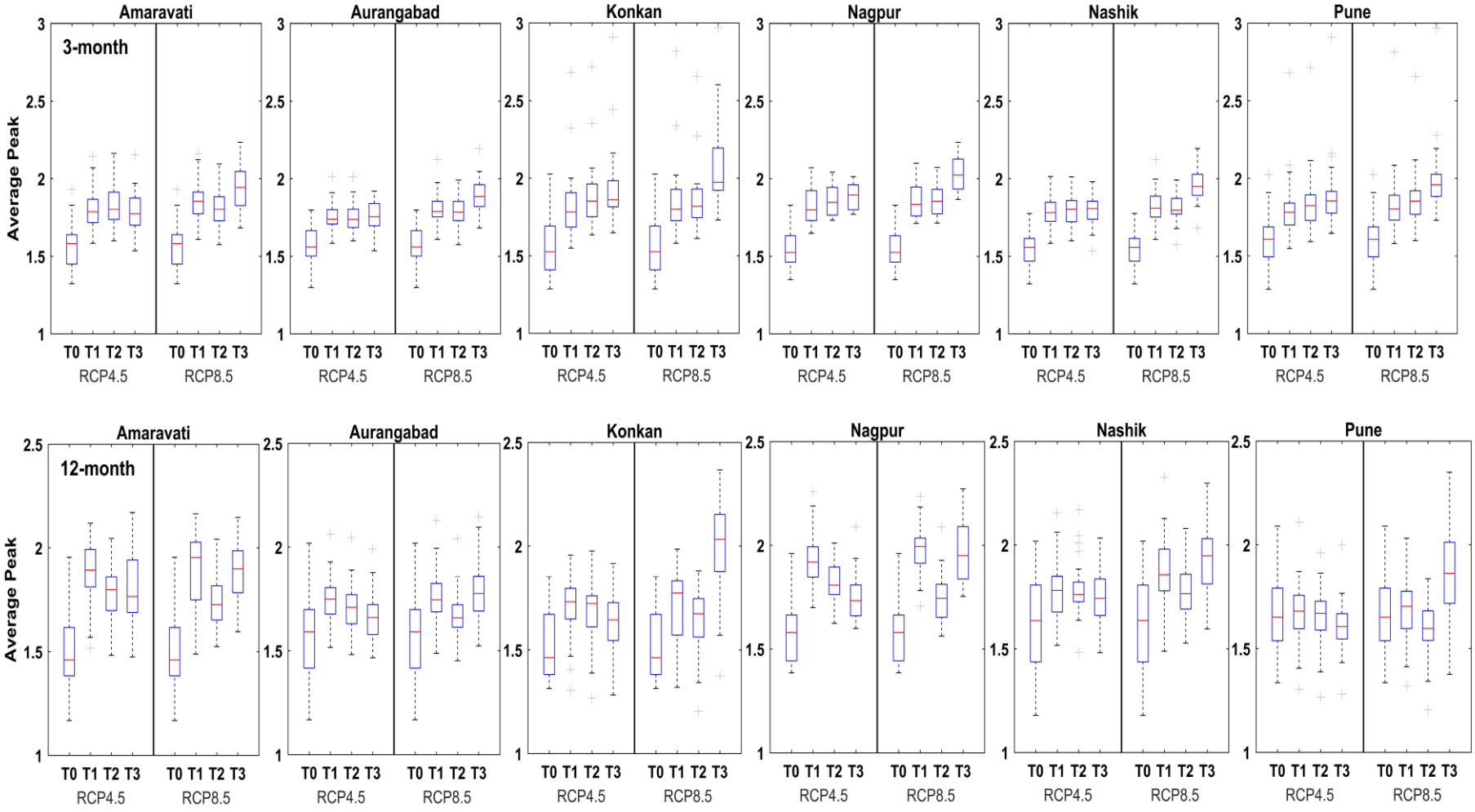

Figure 7.16: Grouped boxplot of historical and future drought peak over different regions under RCP4.5 and 8.5 scenarios. The upper panel presents short-term drought and the lower one presents long-term drought based on SPI

7.4.3.8 SPI drought peak

The MMM of average drought peak over most of the regions is projected to increase under both the scenarios (Figure 7.16) during short and long-term drought conditions. It should be noted that the absolute value of peak is presented in the grouped boxplot. Precisely, for short-term drought condition, the peak over Amaravati (14 to 16% in RCP4.5 and 16 to 24% in RCP8.5), Aurangabad (11% in RCP4.5 and 14 to 21% in RCP8.5), Konkan (18 to 25% in RCP4.5 and 19 to 33% in RCP8.5), Nagpur (18 to 22% in RCP4.5 and 20 to 31% in RCP8.5), Nashik (15 to 17% in RCP4.5 and 17 to 27% in RCP8.5), and Pune (13 to 18% in RCP4.5 and 15 to 24% in RCP8.5) is projected to increase during 21st century. Similarly for long-term drought condition, the peak over Amaravati (19 to 26 % in RCP4.5 and 16 to 27% in RCP8.5), Aurangabad (4 to 10% in RCP4.5 and 6 to 14% in RCP8.5), Konkan (7 to 11% in RCP4.5 and 6 to 30% in RCP8.5), Nagpur (10 to 21% in RCP4.5 and 10 to 25% in RCP8.5), Nashik (7 to 10% in RCP4.5 and 10 to 20% in RCP8.5), and Pune (12% during T3 in RCP8.5) is likely to increase. In addition, the increase in case of RCP8.5 is larger than RCP4.5 for both the drought conditions.

7.4.3.9 SPEI drought areal spread

The areal spread is calculated for each month considering the number of grid points under the classification of extreme drought and their summation in terms of area. Subsequently, the computed area is divided by the total area to find out the fraction of area affected. An empirical cumulative distribution function (ECDF) is computed for each GCM, and the mean ECDF of all the GCMs is plotted against the historical period to examine the change in the monthly areal spread. Figure 7.17 presents the monthly spatial extent of extreme drought for short-term drought under both scenarios.

It is evident from the figure that the monthly spatial extent of extreme drought is projected to increase with respect to historical over all the regions. Similarly, the monthly spatial extent of extreme drought is likely to increase for long-term drought (except for Pune) as well (Figure 7.18). In particular, under short-term drought, the areal spread over Amaravati (61 to 150% in RCP4.5 and 54 to 223% in RCP8.5), Aurangabad (17 to 94% in RCP4.5 and 17 to 152% in RCP8.5), Konkan (3 to 98% in RCP4.5 and 11 to 158% in RCP8.5), Nagpur (60 to 143% in RCP4.5 and 45 to 243% in RCP8.5), Nashik (137 to 300% in RCP4.5 and 144 to 419% in RCP8.5), and Pune (5 to 69% in RCP4.5 and 49 to 111% in RCP8.5) is projected to

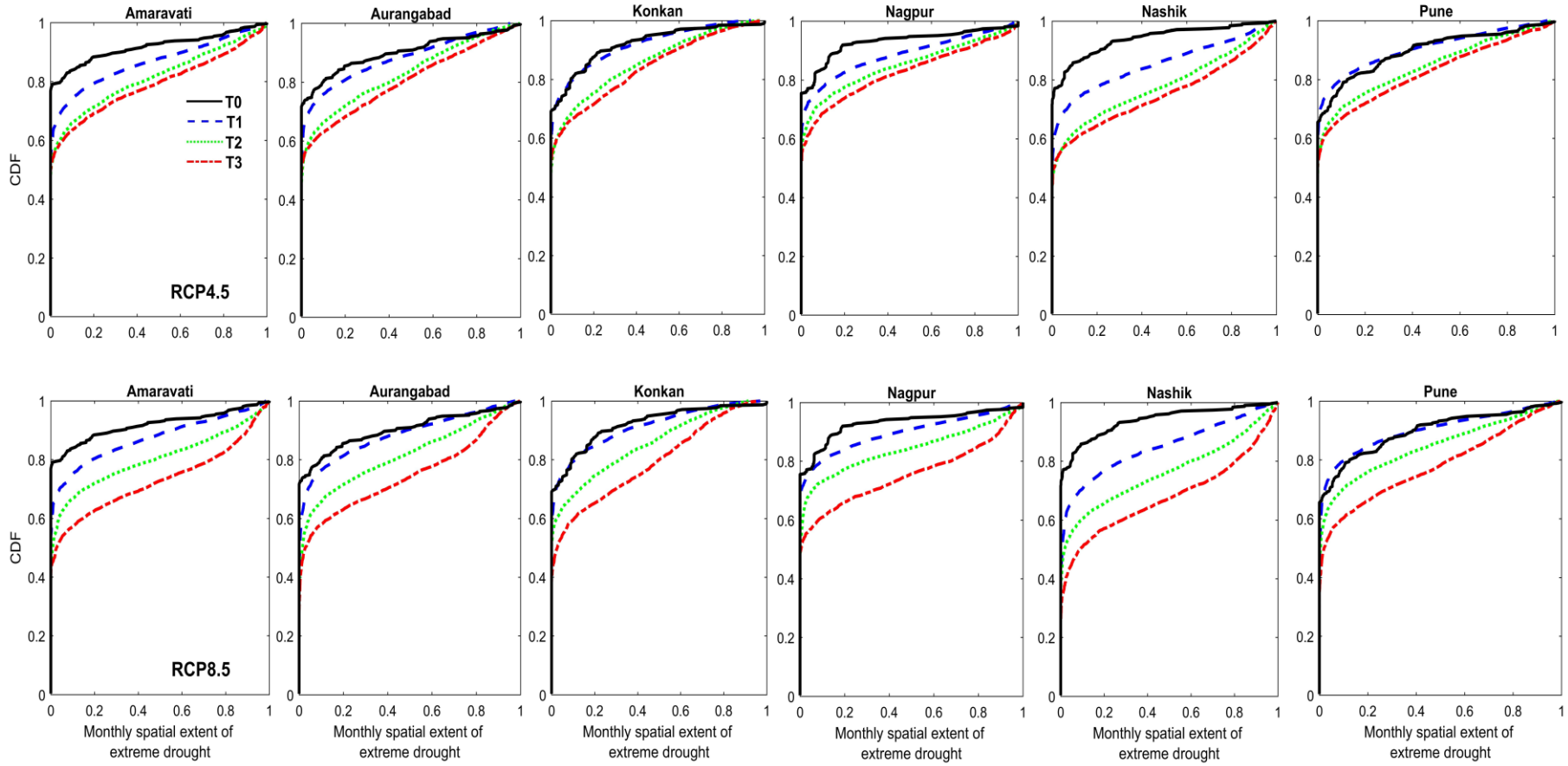

Figure 7.17: The mean ECDF of monthly spatial extent of extreme drought during T1, T2, and T3 over different regions for short-term drought based on SPEI

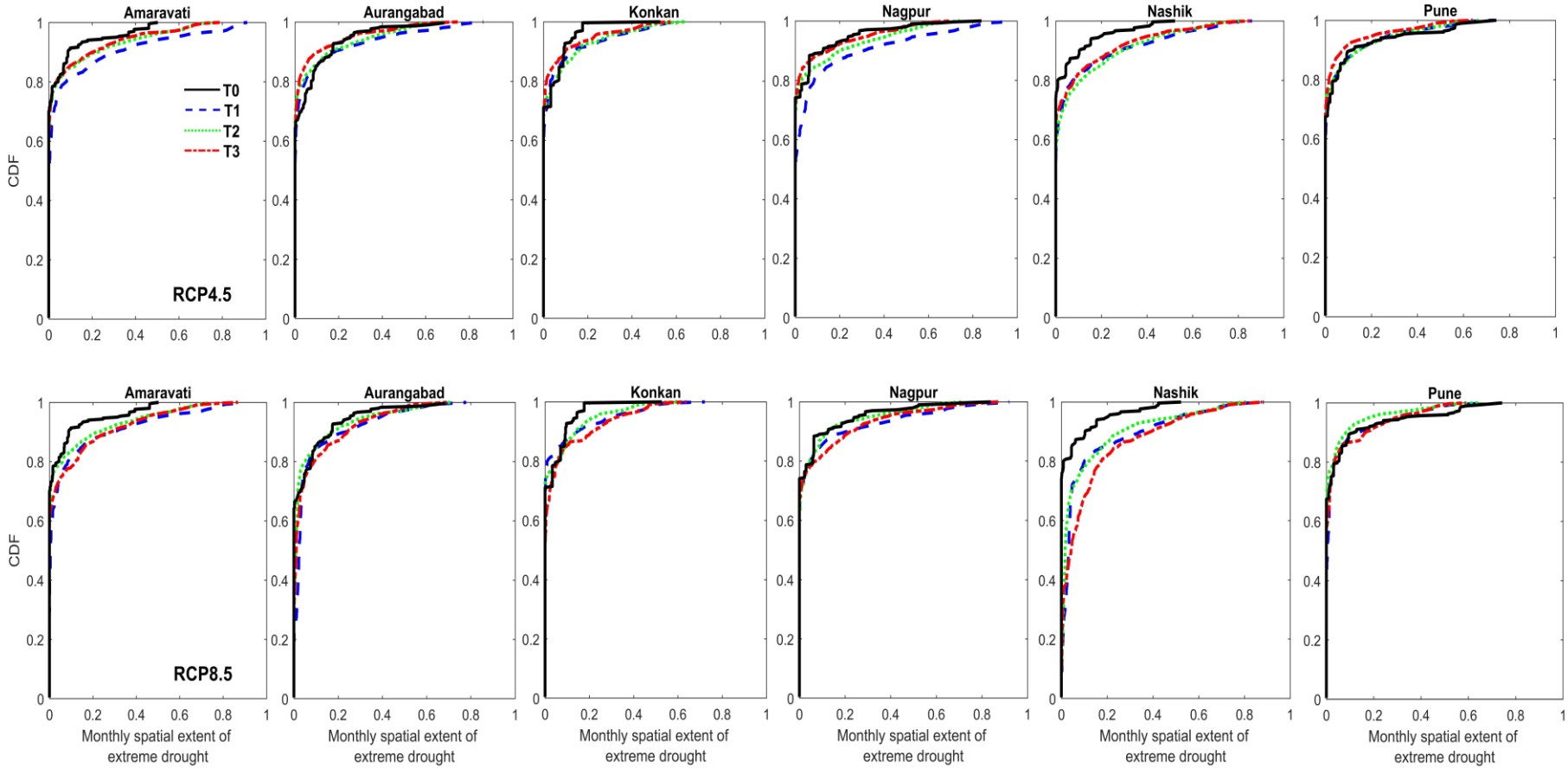

Figure 7.18: The mean ECDF of monthly spatial extent of extreme drought during T1, T2, and T3 over different regions for long-term drought based on SPEI

increase during the 21st century. Similarly, for long-term drought, over Amaravati (50 to 131% in RCP4.5 and 64 to 118% in RCP8.5), Aurangabad (1 to 24% during T1 & T2 in RCP4.5 and 12 to 46% in RCP8.5), Konkan (27 to 70% in RCP4.5 and 46 to 103% in RCP8.5), Nagpur (1 to 110% in RCP4.5 and 11 to 54% in RCP8.5), and Nashik (113 to 146% in RCP4.5 and 174 to 275% in RCP8.5) the areal spread of extreme drought is likely to increase.

7.4.3.10 SPI drought areal spread

Figure 7.19 presents the monthly spatial extent of extreme drought for short-term drought under both the scenarios. It is evident from the figure that the monthly spatial extent of extreme drought is projected to increase with respect to historical over all the regions. There is no significant difference among the three future segments and between the two scenarios. Similarly, the monthly spatial extent of extreme drought is likely to increase for long-term drought as well (Figure 7.20). In particular, under short-term drought, the areal spread over Amaravati (73 to 95% in RCP4.5 and 93 to 121% in RCP8.5), Aurangabad (37 to 49% in RCP4.5 and 62 to 84% in RCP8.5), Konkan (60 to 90% in RCP4.5 and 59 to 112% in RCP8.5), Nagpur (126 to 141% in RCP4.5 and 120 to 165% in RCP8.5), Nashik (100 to 111% in RCP4.5 and 128 to 151% in RCP8.5), and Pune (95 to 104% in RCP4.5 and 98 to 131% in RCP8.5) is projected to increase during 21st century. Similarly, for long-term drought, over Amaravati (43 to 204% in RCP4.5 and 96 to 214% in RCP8.5), Aurangabad (9 to 49% during T1 & T2 in RCP4.5 and 29 to 107% in RCP8.5), Konkan (44 to 167% in RCP4.5 and 110 to 177% in RCP8.5), Nagpur (7 to 169% in RCP4.5 and 28 to 109% in RCP8.5), Nashik (23 to 97% in RCP4.5 and 112 to 199% in RCP8.5), and Pune (8% during T1 in RCP4.5 and 7% during T1 in RCP8.5) the areal spread of extreme drought is likely to increase. Conversely, during T2 and T3, the areal spread of drought is projected to decrease over Pune under both the scenarios and over Aurangabad during T3 under RCP4.5 scenario only.

7.4.4 Temperature and its implications on meteorological drought

In the present study, the influence of temperature on meteorological drought is examined through the SPEI drought index. Although the comparison between SPI and SPEI is available in the literature based on GCM and Regional Climate Model (RCM) outputs (Spinoni et al., 2019; Touma et al., 2015); however, no corresponding detailed study is available that

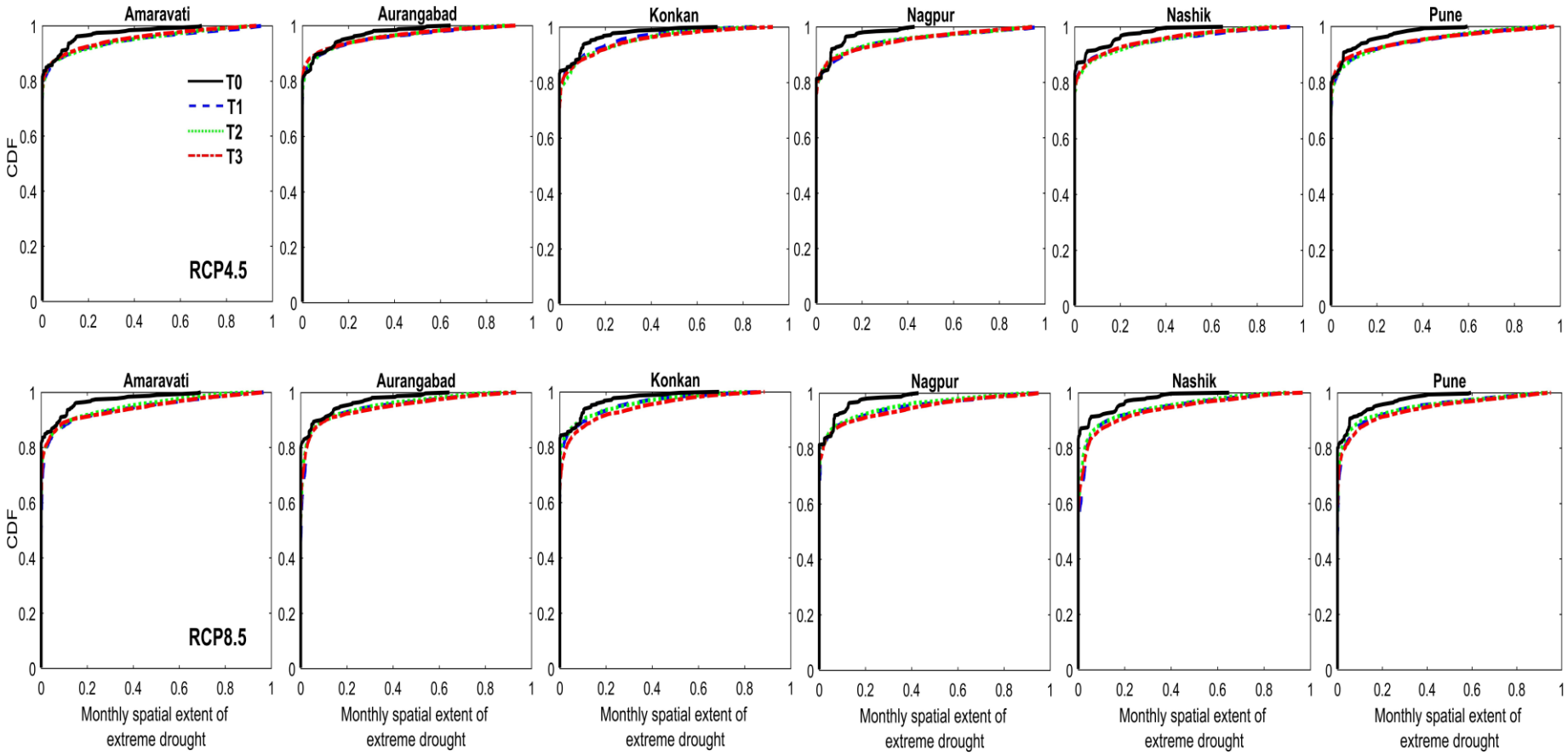

Figure 7.19: The mean ECDF of monthly spatial extent of extreme drought during T1, T2, and T3 over different regions for short-term drought based on SPI

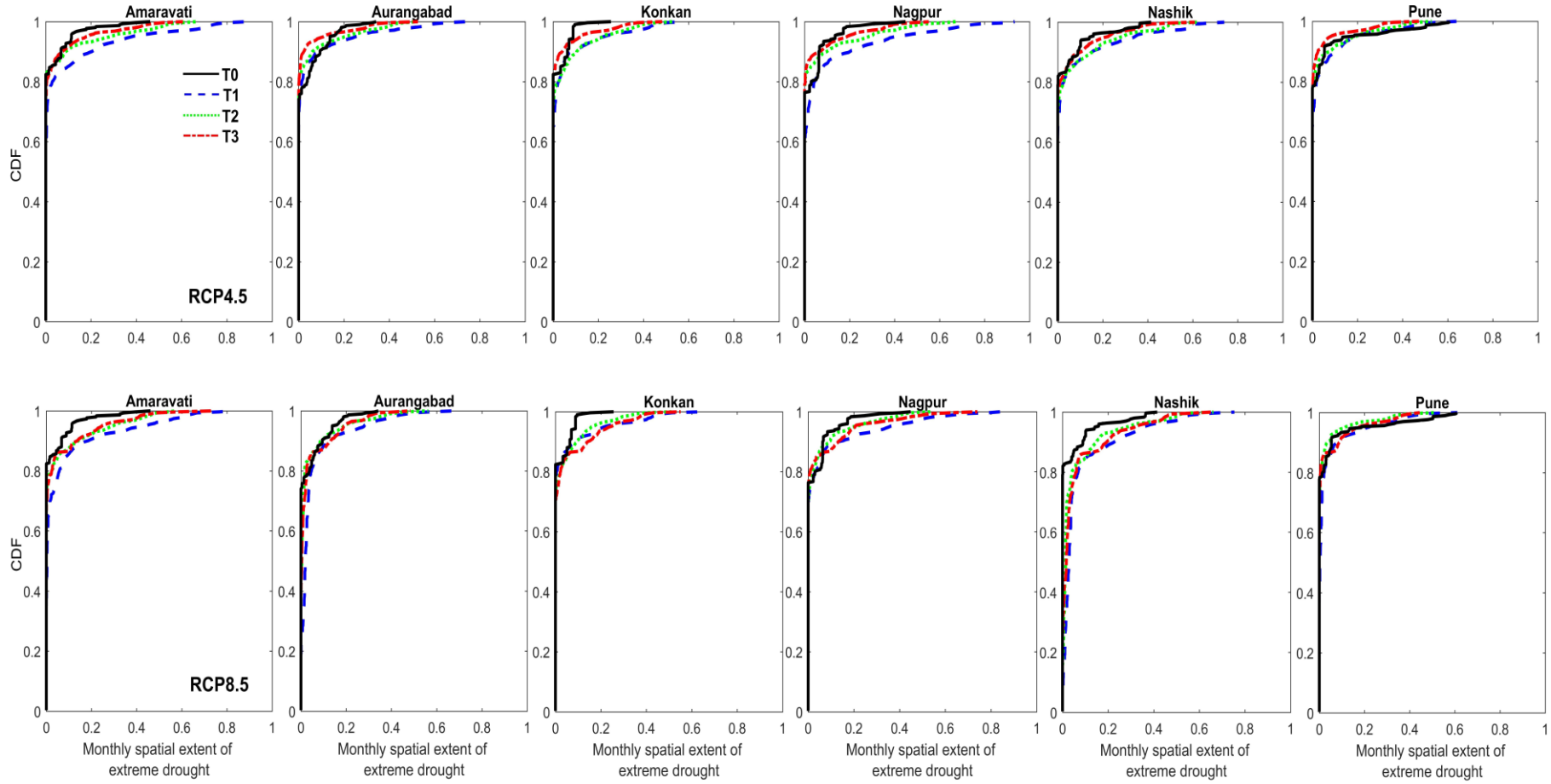

Figure 7.20: The mean ECDF of monthly spatial extent of extreme drought during T1, T2, and T3 over different regions for long-term drought based on SPI

incorporates the projections from the NEX-GDDP experiments. Past analysis reveals that the increase in the drying tendency (i.e., increase in evapotranspiration) outweighs the increase in wetting tendency (i.e., increase in the rainfall). Therefore, the future projections of drought are likely to vary between the index that considers only precipitation and the index which involves both precipitation and evapotranspiration (and hence temperature).

In order to examine the influence of temperature on meteorological drought, the difference in percentage (in fraction) of different drought properties between SPEI and SPI is carried out. Initially, the percentage of each drought properties with respect to the historical period is computed for both SPI and SPEI over all the divisions and time scale. Then, the percentage change in the case of SPEI is subtracted from the percentage change in the case of SPI. Here, the assumption is that subtracting the influence of precipitation from the combine influence of precipitation and temperature may provide an implication of temperature influence on meteorological drought. Figure 7.21 presents the percentage difference (in fraction) of different drought properties between SPEI and SPI. In other words, it represents the change in the percentage of different drought properties as the inclusion of temperature.

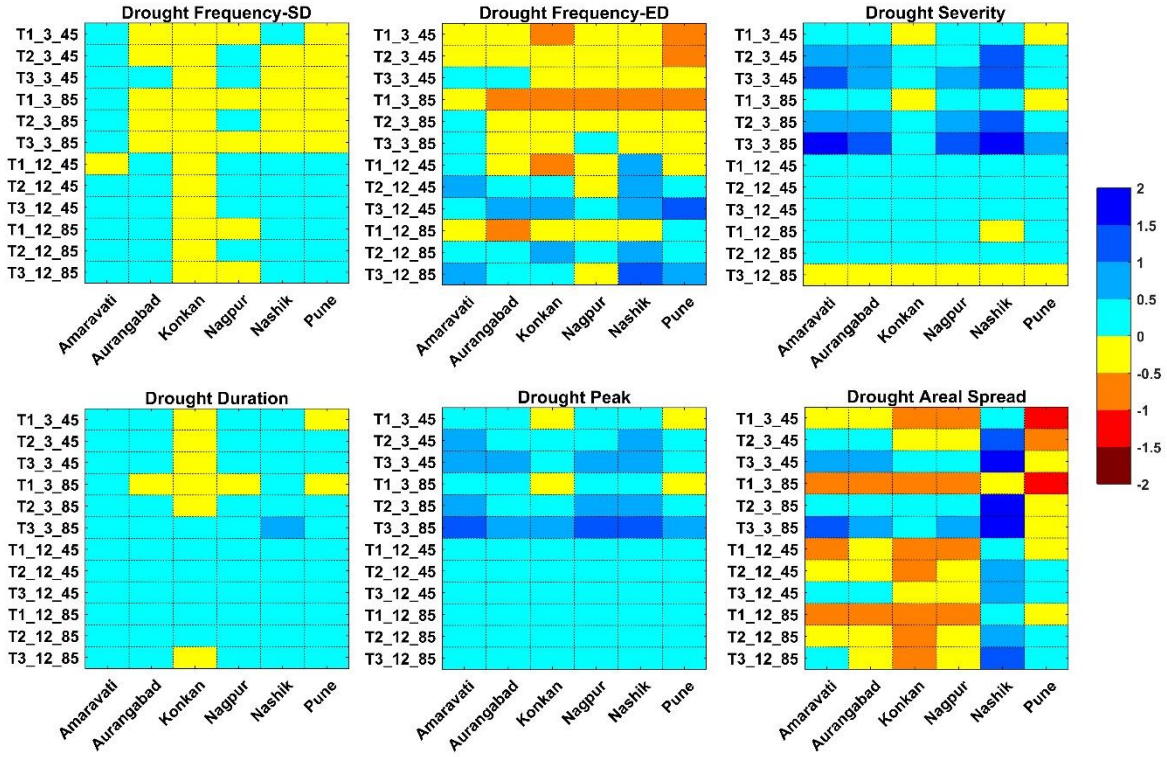

Figure 7.21: Percentage difference (in fraction) of different drought properties between SPEI and SPI. It represents the increase or decrease in the drought properties in SPEI with respect to SPI

In the figure, for instance, T1_3_45 defines the 3-month drought condition during T1 under RCP4.5 scenarios. It can be noted from the figure that over most of the regions and future time segments under both the scenarios, the percentage increase in drought properties like severity, duration and peak is more in case of SPEI than SPI for short and long-term drought conditions. In case of extreme drought frequency, the percentage change in the short-term drought condition decreases in SPEI than SPI in most of the cases. However, in long-term drought condition, the percentage change in extreme drought frequency increases in SPEI in most of the cases. A similar kind of pattern is noticed in case of severe drought frequency. In addition, over the Konkan, the decrease in percentage in case of SPEI as compared to SPI is observed over all the future time segments, under both the scenarios and in both drought conditions. In the case of areal spread of extreme drought condition based on SPEI, the decrease in the percentage is noticed over Amaravati, Aurangabad, Konkan, and Nagpur in long-term drought condition. The highest decrease is observed in the case of Pune during short-term drought condition.

7.4.5 Identification of hotspot regions

The identification of meteorological hotspots during the 21st century based on SPI and SPEI enables the agricultural and water resources planners to devise proper adaptation strategies during different climate change scenarios. To demarcate the hotspot regions, ±5% change in the drought properties with respect mean is considered as significant. It should be noted that there is no specific thumb rule to select the threshold to determine the significance. Here, ±5% is chosen to remain at a safe side in the rapidly changing climate scenarios. Four different drought properties such as extreme drought frequency, severity, peak, and extreme drought areal spread are considered to identify the hotspot zones.

The conditions based on which the hotspot is classified as follows, symbol "++++" defines a significant increase in all the four drought properties. The sign "+" ("-") denotes significant increase (decrease) in three drought properties out of four in SPEI and SPI. The "=" sign refers there is no significant change in the drought properties. The worst condition, which is used to identify the hotspot, is coloured with dark red and suggests "++++" conditions in both SPEI and SPI. The red colour represents "+" condition in both SPEI and SPI. The combination of conditions such as "+" in SPEI and "=" in SPI, "=" in both SPEI and SPI, and "=" in SPEI and "-" in SPI are denoted by pink, white, and blue, respectively. Though there may exist a larger number of alternatives based on different combination of conditions, the

present analysis considers the combinations that are observed over the study area. It should be noted that if at one drought index the condition is "++++" and for the other the condition is "=" or "-" then that particular region is demarcated as dashed line. The combination like "++++" and "+" is not observed over any region. Figure 7.22 presents the different combinations, as discussed above.

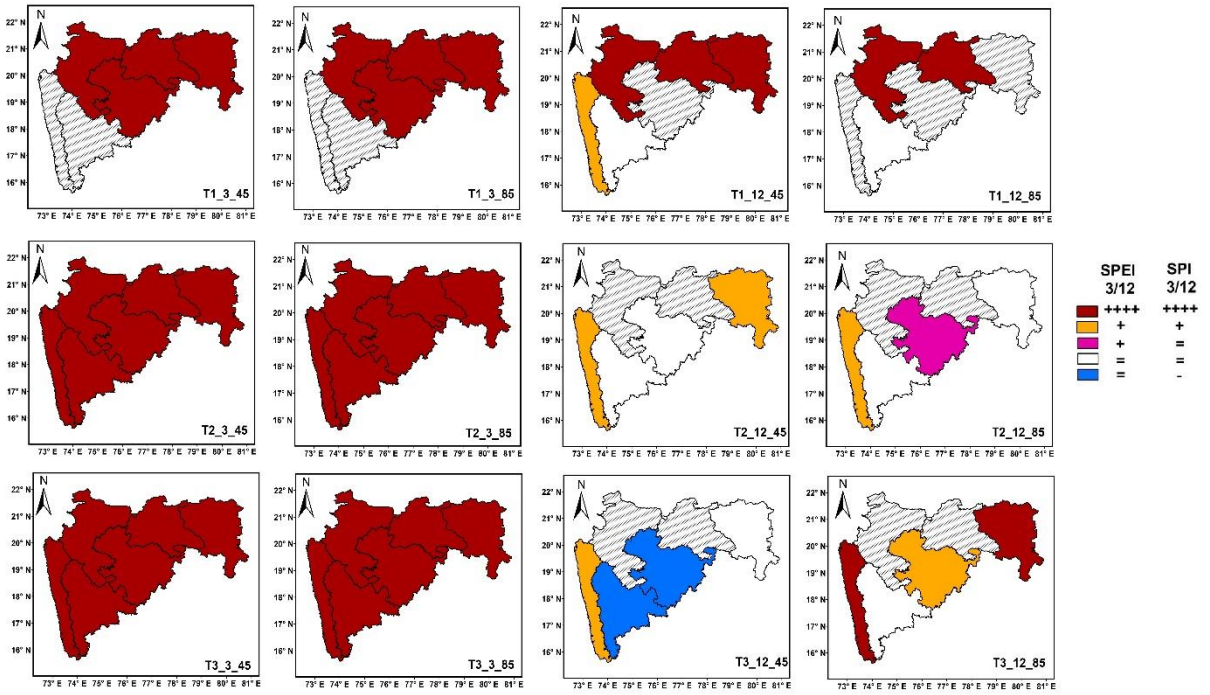

Figure 7.22: Identification of drought hotspots over Maharashtra for short- (two columns from left) and long- (two columns from right) term drought conditions

It is evident from the figure that for short-term drought (four columns from left) condition, during T2 and T3, all the regions are expected to fall in the hotspot category under both the RCP scenarios. However, during T1, except Konkan and Pune, all other regions come under hotspot category. The picture for long-term drought (four columns from right) condition is quite different from the short-term. During T1 and RCP4.5 (RCP8.5), Amaravati, Nagpur, and Nashik (Amaravati, and Nashik) are likely to come under hotspot. No hotspot region is identified during T2 for both the scenarios and T3 in RCP4.5. However, Konkan and Nagpur are identified under hotspot classification during T3 under RCP8.5. The less frequent and severe drought event regions are noticed in long-term drought condition. For instance, Pune during T1 for both the scenarios, Pune and Aurangabad (during T2 in RCP4.5), Pune and Nagpur (during T2 in RCP8.5), Pune, Amaravati, and Nagpur (during T3 in RCP4.5), and Pune (during T3 in RCP8.5). Moreover, for SPEI, the unrecorded past extreme events are

likely to be noticed in future and not in case of SPI. In this sense, excluding temperature from the computation of meteorological drought could mislead the outcomes.

7.5 Discussion and summary

Concurrent increase or decrease of future hydro-meteorological variables makes it cumbersome to understand the regional future meteorological droughts characteristics. Hence, the role of climate variables in modulating drought attributes at regional scale impose needs to be examined. The present study makes an attempt to answer the three important questions in terms of future meteorological drought characteristics and drought hotspot identification using different drought indices and outputs from the nineteen NEX-GDDP simulations.

The monthly precipitation and temperature are expected to increase in the future climate change scenarios with more increase evident in case of RCP8.5 than RCP4.5. Therefore, in a broader sense, the projected climatology over Maharashtra is likely to be wetting and warming during the 21st century. The present findings are similar to those obtained by TERI (2014). The increase in temperature and precipitation over the study area can be attributed to the increasing rate of global warming (Yaduvanshi et al., 2019). In addition, the compounding changes in the season precipitation and temperature will affect the water availability (Konapala et al., 2020). In particular, the spatio-temporal variability of precipitation and temperature may alter the surface hydraulic conditions and can cause a shift in water balance over and under the ground (Sapriza-Azuri et al., 2015).

The future projections of different drought properties are likely to increase mostly for the short-term drought condition. However, the drought properties like peak and areal spread are expected to increase for both short and long-term drought conditions. In addition, the frequency of severe and extreme drought is projected to increase under short-term drought condition. The present findings are in line with those obtained by Gupta and Jain (2018), Bisht et al. (2019) using various sets of global climate model datasets. The increase in the temperature leads to enhance the atmospheric water demand in the regions and subsequently, is likely to increase the drought frequency (Aadhar and Mishra, 2018; Greve et al., 2014). Therefore, in order to formulate the resilient adaptation strategies and policies to combat the future drought events, special attention should be given to the overall development of the farming community (P. Udmale et al., 2014).

The comparative analysis between the SPI and SPEI demonstrates the significant importance of temperature in modulating the future drought events (Ahmadalipour et al., 2017; Spinoni et al., 2020). In the present study, the drought properties like severity, duration, and peak are expected to increase more in case of SPEI as compared to SPI over most of the regions. Though the precipitation amount is likely to increase in the future, it does not confirm the decrease in the drought properties as atmospheric water demand is expected to increase in future warming climate (Roderick et al., 2015; Scheff and Frierson, 2015; W. Y. Wu et al., 2020). Moreover, the present findings suggest that agriculture over the regions can be affected due to the crop sensitivity to evapotranspiration (Jensen and Allen, 2016; Tabari and Hosseinzadeh Talaee, 2014). However, the long-scale water availability can be less impacted as it primarily depends on precipitation.

From the present analysis. It is found that for short-term drought condition all the regions are identified as meteorological drought hotspots during 2022-2047 (except Konkan and Pune), 2048-2073, and 2074-2099. However, the number of hotspot regions decreases in long-term drought condition as compared to short-term drought condition. For instance, during 2022-2047 and RCP4.5 (RCP8.5), Amaravati, Nagpur, and Nashik (Amaravati, and Nashik) are likely to come under hotspot category. Konkan and Nagpur are identified under hotspot classification during 2074-2099 under RCP8.5. In this sense, effective and sustainable preparedness is needed to alleviate the drought risk in the future climate change scenario. In addition, policy makers should consider the regional drought vulnerabilities while formulating policies (Gupta and Jain, 2018). In this regard, key recommendation could be the conservation and enhancement of water storage, groundwater recharge to improve the water use efficiency.

In summary, the significant findings from the present analysis point to the fact that with the increase in the monthly mean temperature and precipitation (more in case of RCP8.5 than RCP4.5), Maharashtra is likely to be wetting and warming during the 21st century except for Konkan region as compared to historical. In Konkan region, the warmer climatology is likely to prevail with no significant change in the monthly precipitation variability. The drought properties like peak and areal spread are expected to increase for both short and long-term drought conditions in most of the regions. The frequency of severe and extreme droughts is likely to increase in the short-term drought condition with no sign of decrease at any time segments and regions. Temperature plays an important role in modulating the meteorological droughts and the present study notices the same in most of the cases in all the drought properties especially in drought severity, duration, and peak. The number of hotspot regions

decreases in long-term drought condition as compared to short-term drought condition. With increasing drought variability in future, the next chapter deals in developing the seasonal Severity-Area-Frequency (SAF) relationship using the future projections from GCMs under different scenarios.

Chapter 8

Investigating Future Seasonal Drought Severity-Area-Frequency (SAF) Curve

8.1 Introduction

The demand of water has increased profoundly due to population growth and expansion of agricultural and industrial sectors. On the other hand, the dual pressure of climate change and its spatio-temporal variability has contributed to water scarcity. The recurrent water scarcity is likely to influence the economic and human development, and natural hazards with increased severity can aggravate the situation (Amarasinghe et al., 2020). The modulation in the various extreme weather events, as a result of changing climatic conditions, influences the frequency and severity of different natural hazards (e.g., drought, flood, among others).

At least once every three years, India is negatively impacted by drought conditions and considered amongst the most vulnerable and drought-prone countries in the world (A.K. Mishra and Singh, 2010; Mishra et al., 2019). In recent times, prolonged and widespread drought condition with increased frequency has been observed over India (A.K. Mishra and Singh, 2010; Sharma and Goyal, 2020). Hence, it is well understood that drought is likely to affect the overall economy of the country under the climate sensitive economic sectors in India (Shah and Mishra, 2020; P. Udmale et al., 2014). With this understanding, projection of future drought at short- and long-term scales enable to formulate improved management practices i.e., water harvesting schemes, land management practices, drought resistant technologies, groundwater management practices, crop and livestock insurance etc. in order to tackle with the adverse consequences of future drought events. General Circulation Models (GCMs) are considered as credible tools in simulating long-term climate projections under different climate change scenarios (Her et al., 2019; Mishra and Singh, 2009; Shivam et al., 2017). In general, GCMs are modelled mathematically by considering the physical processes across ocean, land and atmosphere (Sachindra et al., 2013).

However, initial parametrisation, formulation, model structure, and input data used for development of GCMs can impose uncertainty in the final climate projections (Khan et al., 2020; Mishra et al., 2014b). Likewise, the uncertainty associated with the future climatic scenarios can be attributed to incomplete understanding and unpredictability about the foreseen climate (New and Hulme, 2000). Thus, in order to devise sustainable planning and decision- making, the practitioners should consider the uncertainty for future climate scenarios (Höllermann and Evers, 2017). With this understanding, previous studies used different techniques but are not limited to sensitivity analysis (Mearns et al., 1996), Monte Carlo simulation (Shackley et al., 1998), reliability ensemble averaging (Giorgi and Mearns, 2003), imprecise probability (Ghosh and Mujumdar, 2009), Fuzzy uncertainty analysis (Najafi and Hessami Kermani, 2017), Bayesian analysis (Das and Umamahesh, 2018). In the present study, in order to quantify the GCM and scenario uncertainty, possibility theory is used. The possibility theory assigns the possibility distribution based on the ability of GCMs and emission scenarios to model the recent past under climate forcing. The possibility approach is computationally inexpensive, straightforward, and useful in addressing partially inconsistent knowledge and linguistic information based on intuitions (Mujumdar and Ghosh, 2008).

The past records of different drought indices show increased aridity over many land areas since 1950 (Dai, 2011b). Moreover, the drought risk is likely to increase in the twenty-first century as suggested by different studies (Burke and Brown, 2008; Rind et al., 1990; Spinoni et al., 2019). Thus, it is necessary to incorporate different drought characteristics in order to evaluate the changes in drought events properly. For example, Severity-Area-Frequency (SAF) relationship curve can be used for providing quantitative information about drought through characterising various attributes of drought like return period, areal extent and severity (Henriques and Santos, 1999). Therefore, SAF relationship has been used to understand the nature of spatio-temporal characteristics of drought at regional scale. For example, Reddy and Ganguli (2013) used SAF analysis to understand the drought characteristics over western Rajasthan (India); recurrence pattern of meteorological drought severity was carried out using SAF curve in the upper Blue Nile river region (Khadr, 2017); SAF was used to perform the regional analysis of drought in Lake Urmia basin, Iran (Amirataee et al., 2018) and Heihe River basin (China) (Z. Li et al., 2020). However, most of the SAF analysis studies are executed for the historical time period. Thus, the present study focuses on the possible future variability in the seasonal SAF curve ascertaining the uncertainties associated with GCMs and scenarios.

The purpose of this study is to develop seasonal (pre-monsoon, monsoon, post-monsoon, Rabi, and Kharif) SAF curve under meteorological drought condition over the study area. In addition, the study aims to make the future projection of the seasonal SAF curve ascertaining the uncertainty associated with GCMs and scenarios. The SPEI drought index is used as an indicator of meteorological drought. In order to project for the future time period, nineteen different GCMs under two different Representative Concentration Pathways (RCPs) 4.5 and 8.5 are chosen. Maharashtra, as a drought-prone state is selected to perform the analysis. To the best of the authors' knowledge, no such multifaceted investigation of drought has been carried out over Maharashtra. It is expected that the outcomes from the present study can be helpful in drought risk mitigation planning over the study area.

8.2 Methodology

8.2.1 Possibility theory for uncertainty analysis

In order to facilitate the risk-based studies on future hydrologic extremes, modelling of GCM and scenario uncertainty plays an important role. In the present climate change scenario, it is relevant to evaluate the usefulness of GCMs in modelling climate change impact and to analyse the ability of scenario to represent the present situation. In this sense, possibility distribution is used to analyse the GCM and scenario uncertainties based on the performance in capturing the climate change signals during the recent past. Zadeh (1999) proposed the possibility theory to address inconsistent knowledge and incomplete information (Dubois, 2006). In the present study, the possibility theory is based on the ability of GCM and scenario to simulate the SPEI value at 3-, 4-, and 6-month scales during recent past i.e., T0. Being a measure of how well a GCM with a particular scenario predicts the SPEI values during T0, the Nash-Sutcliffe Efficiency (NSE) is used which provides a measure of possibility value. Unlike the probability, possibility is primarily ordinal and is not associated with frequency of experiments (Mujumdar and Ghosh 2008). The possibility theory postulates that if a variable X in the universe Ω is not possible to estimate precisely, then the possibility that X can take the value x can be expressed mathematically as (Spott, 1999)

$$\Pi_X(x):\Omega \rightarrow [0,1] \tag{8.1}$$

where, $\Pi_X(x) = 1$ ($\Pi_X(x) = 0$) suggests that X = x is possible (impossible) without any restriction. The property of possibility distribution defines that there must be at least one $\tilde{x}$ such that $\Pi_X(x) = 1$ and this property is known as normalization (Spott 1999). The uncertainty analysis is carried out at each grid point under 3-, 4-, 6-month scales to access the GCM and scenario uncertainties. In order to satisfy the normalization property, the results obtained from NSE for nineteen GCMs and two scenarios are divided by the maximum NSE value and the normalized value is considered as the possibility value for a corresponding GCM and scenario.

8.2.2 Formulation of SAF curves for Seasonal Droughts

The SAF relationship is commonly used to visualize and interpret the drought at regional scale. The SAF curve defines the cumulative drought affected areas for the chosen severity level under different return periods. Therefore, it enables to provide quick and effective interpretation of drought condition in order to take sustainable mitigation measures (Bonaccorso et al., 2015). In this study, the seasons: pre-monsoon, monsoon, post-monsoon, Rabi and Kharif are considered for seasonal drought analysis.

It should be noted that the calculation is carried out after performing the GCM and scenario uncertainty. The following steps are employed to derive the SAF curve over the study area: (i) SPEI drought indicator is computed for 3-, 4- and 6-month time scales, where 3-month time scale for pre-monsoon, post-monsoon season, 4-month time scale for monsoon and kharif season, and 6-month time scale for rabi season, (ii) the drought indicator value less than zero is taken into consideration for the further analysis, (iii) the frequency analysis is carried out by considering the non-zero values using extreme value, normal, exponential, gamma, lognormal, and Weibull distributions at each grid point for different drought time scale, (iv) the severity as return levels for different return periods such as 5, 10, 25, 50, and 100 are computed using the statistical parameter estimated for the corresponding grid point and suitable distribution, (v) the spatial extent of drought occurrence is computed in terms of percentage of area for different threshold values of drought severity, (vi) finally, the values of severity, areal extent, and frequency are linked to construct the SAF curve.

It is worth mentioning that the analysis is carried out over each division. Initially, the weight of each grid point corresponding to any division shapefile is computed. The weight defines the percentage of grid area fall within the division shapefile. For example, if the weight value of a grid is 0.7 (1), then 70% of the grid area (complete grid) comes inside the shapefile. The computation for all the divisions is performed using “raster” package in R developed by Hijmans et al. (2019). The present study considers five different severity values i.e., -1, -1.5, -2, -2.5, -3 as threshold to calculate the drought-affected area below the threshold severity level. Moreover, the threshold severity values are interpolated for the drought-affected area using cubic interpolation technique.

In the present study, drought at 3-, 4-, and 6-month time scales are examined which represent short-term to seasonal drought condition. The analysis would be help in identifying the

operational definition of drought i.e., from meteorological to hydrological drought. In particular, 3- to 4-month scale drought conditions highlight the soil moisture condition that would help in guiding the agricultural operation. Similarly, 6-month scale drought condition reflects the hydrological condition depending on the region and time of year.

8.3 Results

8.3.1 Uncertainty analysis and future projection of meteorological variables

The performance measure NSE is computed for nineteen GCMs under RCP4.5 and 8.5 scenarios based on their prediction of SPEI at 3-, 4-, and 6-month time scales in the recent past (from 1993 to 2018). The possibility value is computed by dividing the maximum NSE value with the NSE value of each model. This operation is carried out for each grid point separately. Figure 8.1 presents the distribution of different GCMs and scenarios across the study area for 3-month time scale. Figure 8.2 and Figure 8.3 depict the suitable GCM and scenario for 4- and 6- month scales, respectively. It can be noted that for 3- month scale, RCP4.5 (RCP8.5) scenario is considered as most possible scenario over 54% (46%) of total grid points. Similarly, most possible scenario for 4-month time scale (6-month scale) is found to be 53% (38%) of total grids for RCP4.5 and 47% (62%) of total grids for RCP8.5.

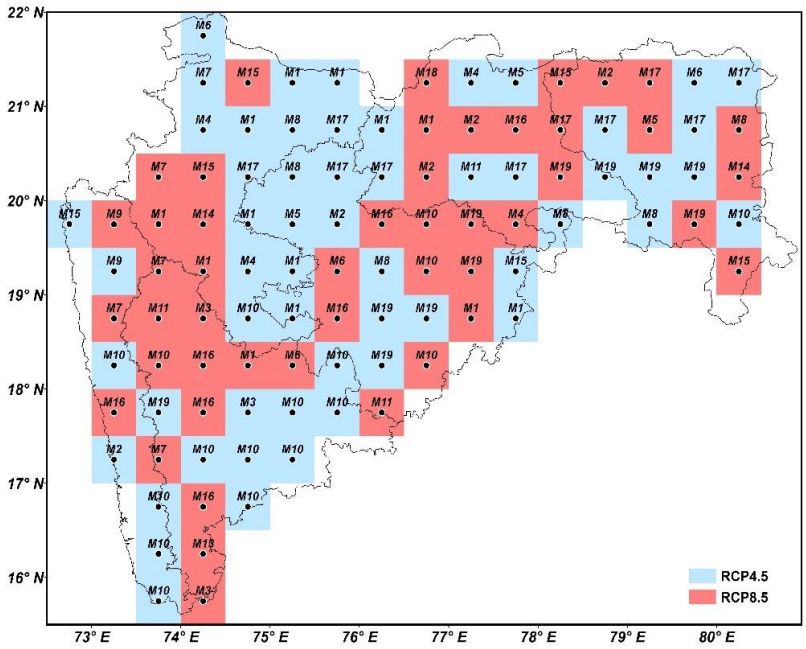

Figure 8.1: Most suitable GCM/scenario at each grid point for 3-month time scale SPEI after uncertainty analysis

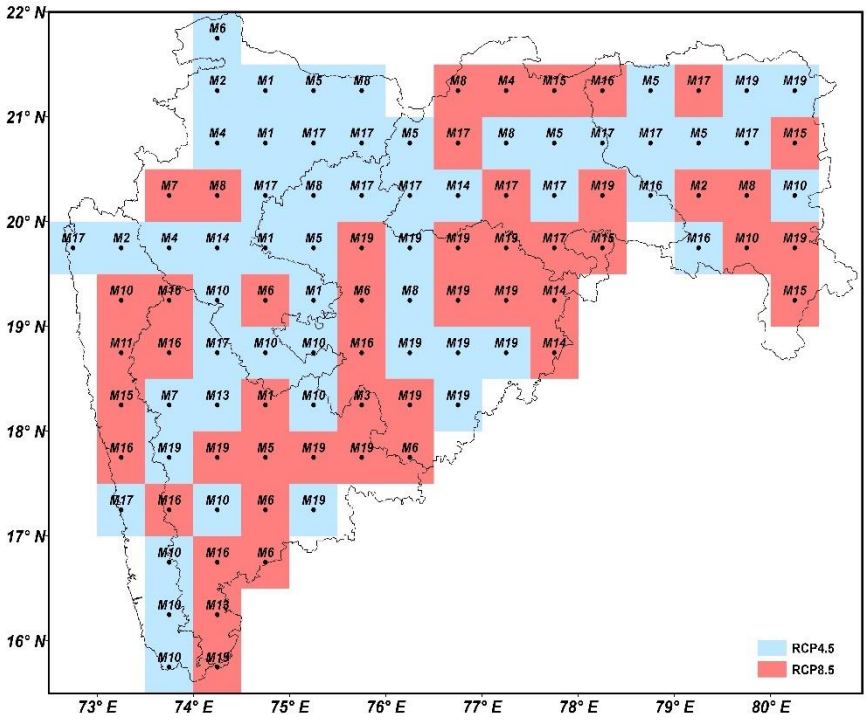

Figure 8.2: Most suitable GCM/scenario at each grid point for 4-month time scale SPEI after uncertainty analysis

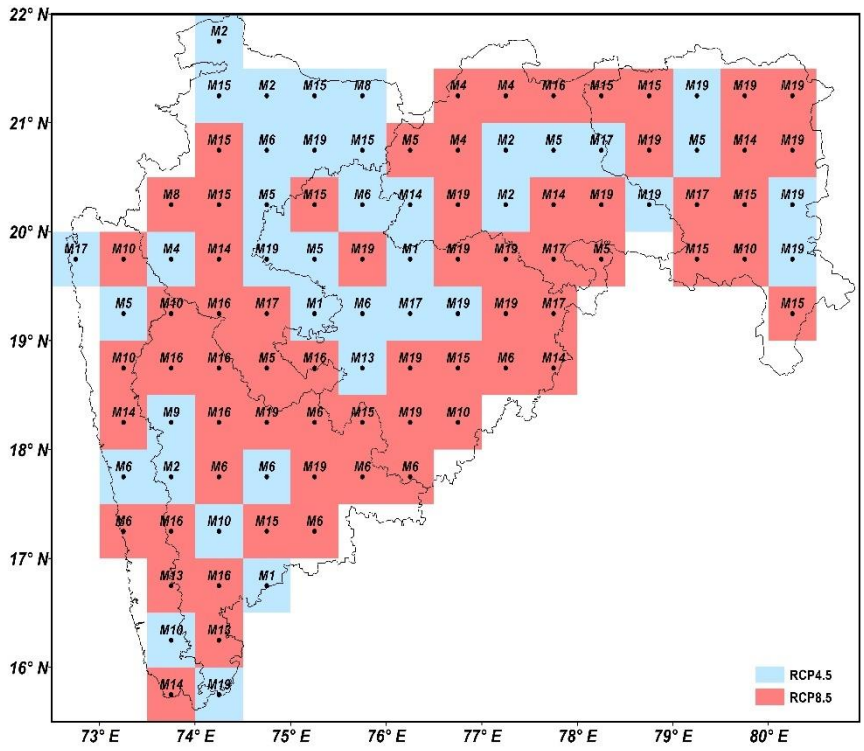

Figure 8.3: Most suitable GCM/scenario at each grid point for 6-month time scale SPEI after uncertainty analysis

Considering the most possible GCM and scenario at each grid point, the spatio-temporal variabilities with respect to T0 for different variables such as precipitation, potential evapotranspiration, maximum and minimum temperature are computed and plotted. Figure 8.4 presents the spatio-temporal variability (% change) of precipitation for different seasons during T1, T2, and T3 time periods. Similarly, Figure 8.5, Figure 8.6, and Figure 8.7 shows the spatio-temporal variability of potential evapotranspiration, maximum and minimum temperature, respectively. From Figure 8.4, it can be noted that the precipitation magnitude is projected to increase (decrease) in pre-monsoon by 65-79% (21-35%), in monsoon by 83-90% (10-17%), in post-monsoon by 18-27% (73-82%), in Kharif by 79-86% (14-21%), in Rabi by 18-29% (71-82%) of total grid area between T1 and T3. In case of potential evapotranspiration, it is projected to increases (decrease) in pre-monsoon by 49-57% (43-51%), in monsoon by 24-44% (56-76%), in post-monsoon by 50-84% (16-50%), in Kharif by 50-69% (31-50%), in Rabi by 69-88% (12-31%) of total area during T1 and T3. However, the future variability in maximum and minimum temperature is expected to increase over most of the gridded area for all the seasons with maximum variability in case of minimum temperature. In addition, it is noticed that the magnitude maximum and minimum temperature is likely to increase from T1 to T3 as compared to T0.

8.3.2 Seasonal variability of SPEI under climate change

Based on the classification of SPEI, moderate, severe, and extreme drought conditions are analysed for future periods and compared with T0. Figure 8.8 presents the season-wise frequency of different drought conditions across the study area. The red circle in the boxplot represents the mean frequency value. It is noted that the frequency of moderate drought condition (Top panel of Figure 8.8) is expected to decrease during Kharif, monsoon, and pre-monsoon seasons as compared to historical period. In case of Rabi season, the mean frequency of moderate drought condition is likely to increase during T1 and decrease gradually in T2 and T3. The mean frequency of severe drought condition is projected to have no significant change in future as compared to T0 during Kharif, monsoon, and pre-monsoon seasons. However, it is likely to increase during post-monsoon and Rabi seasons. The future projection of extreme drought condition shows an increasing frequency in post-monsoon, pre-monsoon, and Rabi seasons, while no change is observed during Kharif and monsoon seasons as compared to T0.

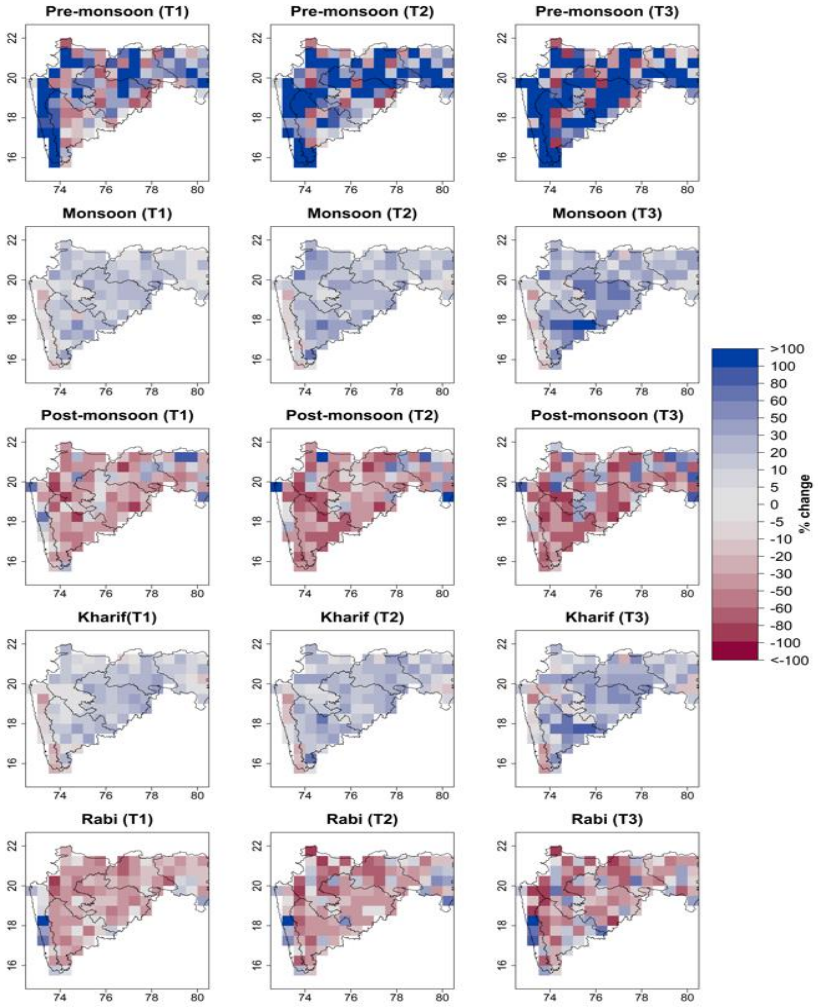

Figure 8.4: Spatio-temporal variability of precipitation (in percentage) for different seasons

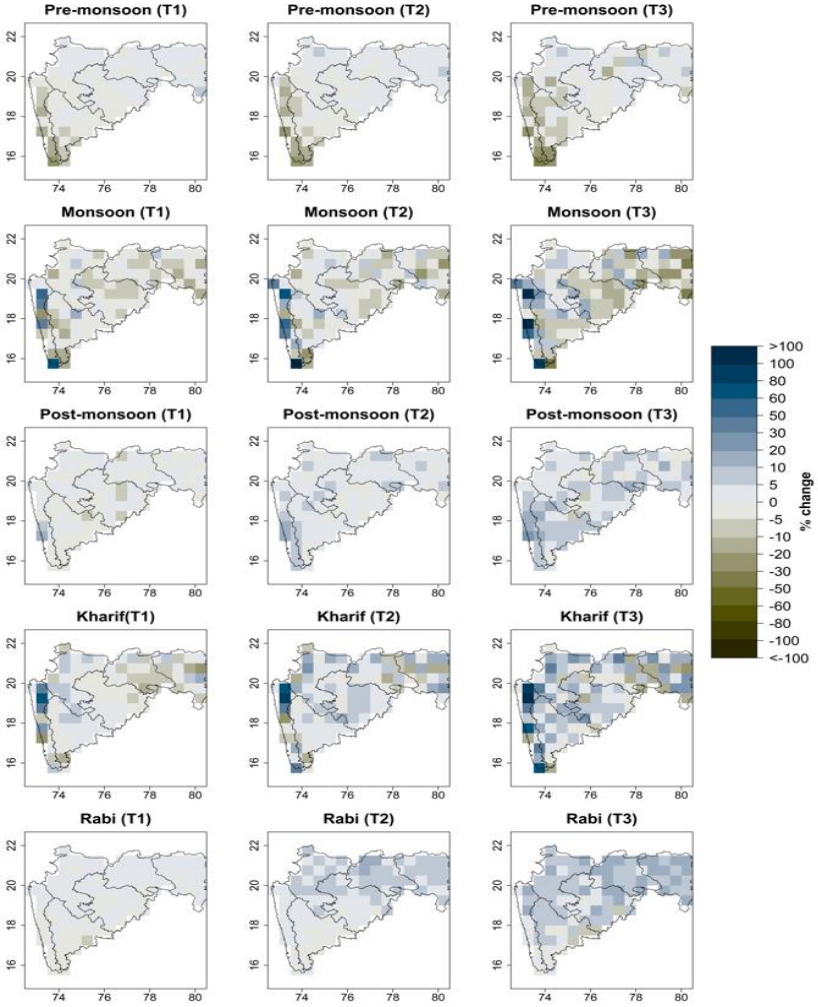

Figure 8.5: Spatio-temporal variability of potential evapotranspiration (in percentage) for different seasons

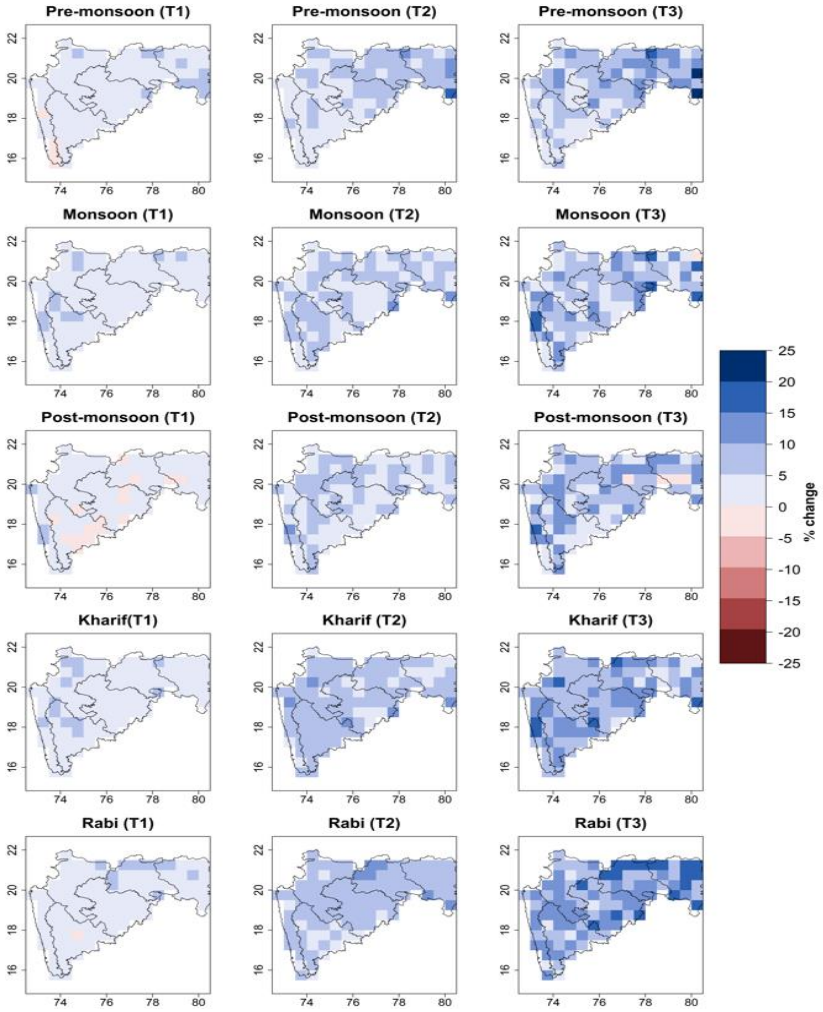

Figure 8.6: Spatio-temporal variability of maximum temperature (in percentage) for different seasons

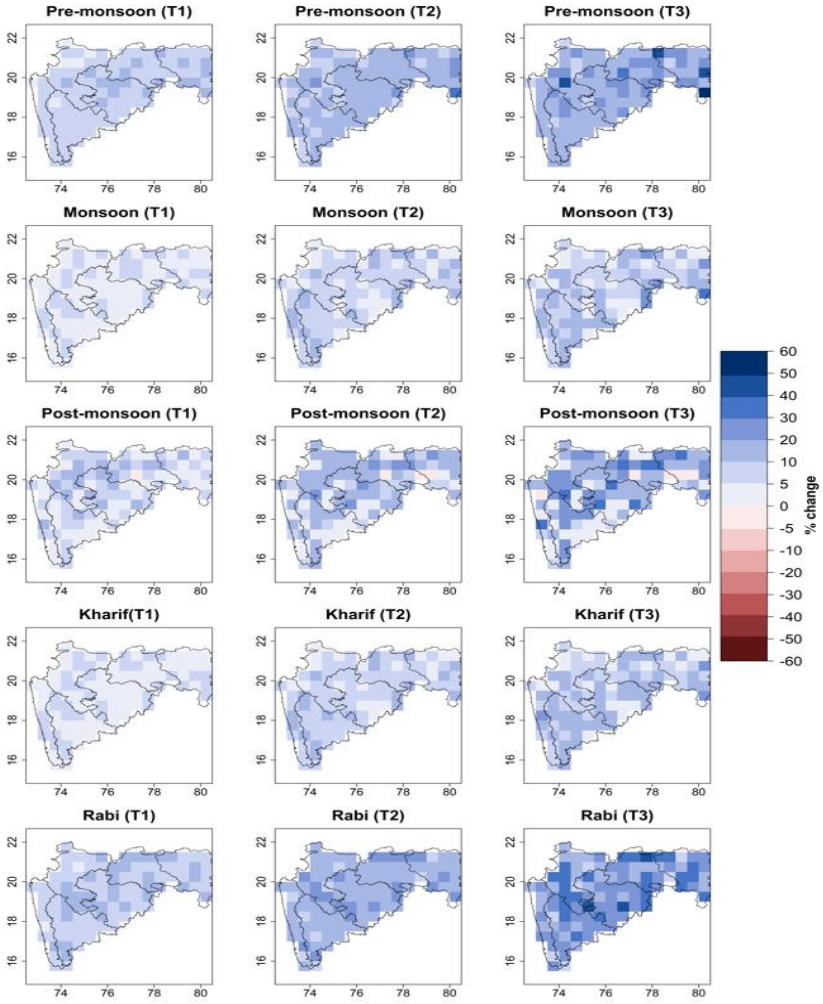

Figure 8.7: Spatio-temporal variability of minimum temperature (in percentage) for different seasons

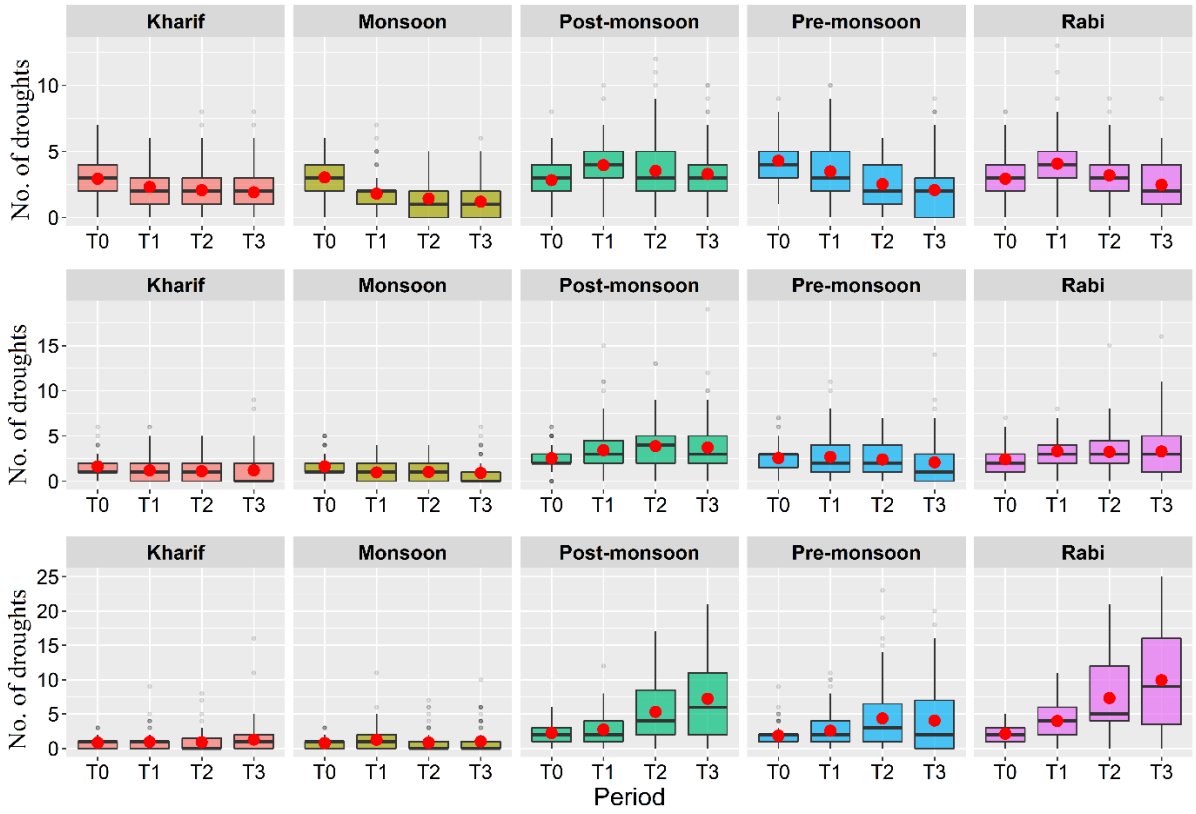

Figure 8.8: Number of events of different drought conditions such as moderate (upper), severe (middle), and extreme (lower) for all the seasons

8.3.3 Analysis of SAF curve over different regions

In this section, SAF curves are analysed over Amaravati, Aurangabad, Konkan, Nagpur, Nashik, and Pune regions for 5-, 10-, 25-, 50-, and 100-yr return periods in different seasons and compared with T0 period. It should be noted that the severity return levels are computed using the selected distribution for different return periods. As discussed, five different severity values i.e., -1, -1.5, -2, -2.5, -3 are chosen to develop the SAF curve. Here, the results are presented separately for different regions.

8.3.3.1 SAF curve for Amaravati

Figure 8.9 shows the area affected by different severity levels under different return periods during pre-monsoon season over Amaravati region. The top, middle, and bottom panels present for T1, T2, and T3 periods, respectively. The black line corresponds to T0 period, red line defines future simulation, and dashed red line represents the 95% confidence interval of future simulation. During pre-monsoon season, in the case of the 5-year return period, the area affected by different severity of drought is likely to increase for all the future time periods as

compared to T0. The area affected by the SPEI severity level less than -1.7 (for 10-year), -2.3 (for 25-year), -2.4 (for 50-year), and -2.9 (for 100-year) is projected to increase during T1, T2, and T3 periods over Amaravati region. In case of monsoon season (refer to Figure 8.10 (a)), the percentage of area is likely to increase below the SPEI severity level of -1.2 (for 5-year during all time periods), -1.3 (for 10-year during T1), -1.4 (for 10-year during T2), -1.5 (for 10-year during T3), -1.7 (for 25-year during T1), -2.0 (for 25-year during T2), -2.1(for 25-year during T3), -1.8 (for 50-year during T1), -2.2 (for 50-year during T2 and T3), -1.7 (for 100-year during T1), -2.3 (for 100-year during T2), and -1.9 (for 100-year during T3). During post-monsoon season (refer to Figure 8.10 (b)), the drought affected area is likely to decrease during T1 for all the return periods. Similarly, for T2 and T3 periods, the drought area is projected to decrease for high return period severity values as compared to T0. In the case of Kharif season (refer to Figure 8.10 (c)), the projected drought area is likely to increase over more severe drought conditions for all the return periods and future time steps. Most of the cases in Rabi season (refer to Figure 8.10 (d)), the projected drought-prone area is likely to increase for different severity levels during the 21st century.

8.3.3.2 SAF curve for Aurangabad

The SAF curve related to the Aurangabad division is presented in Figure 8.11. Figure 8.11 (a) describes the SAF curve for pre-monsoon season. It can be noted that for more severe drought condition, the percentage of affected area is likely to increase for all return periods and future time steps as compared to T0. For 50- and 100- year return periods, the entire area is projected to affect by the drought severity between -1.5 and -1. The SAF curve for monsoon season is presented in Figure 8.11 (b). For the future time period T2, for most of the return periods, it is observed that the projected drought-affected area for different severity levels is likely to decrease. In the case of T1 period, for more severe condition the percentage of area is expected to increase. For 50- and 100-year return periods, the drought-affected area is reduced significantly during T3 as compared to T0. Figure 8.11 (c) and Figure 8.11 (e) present the SAF curves for post-monsoon and Rabi seasons. It can be observed that for both the seasons that the projected drought areas under different severity levels are expected to increase for all return periods and future time steps. However, in the Kharif season (Figure 8.11 (d)), the future projected SAF curves under most of the return periods and time steps are likely to be less severe than T0.

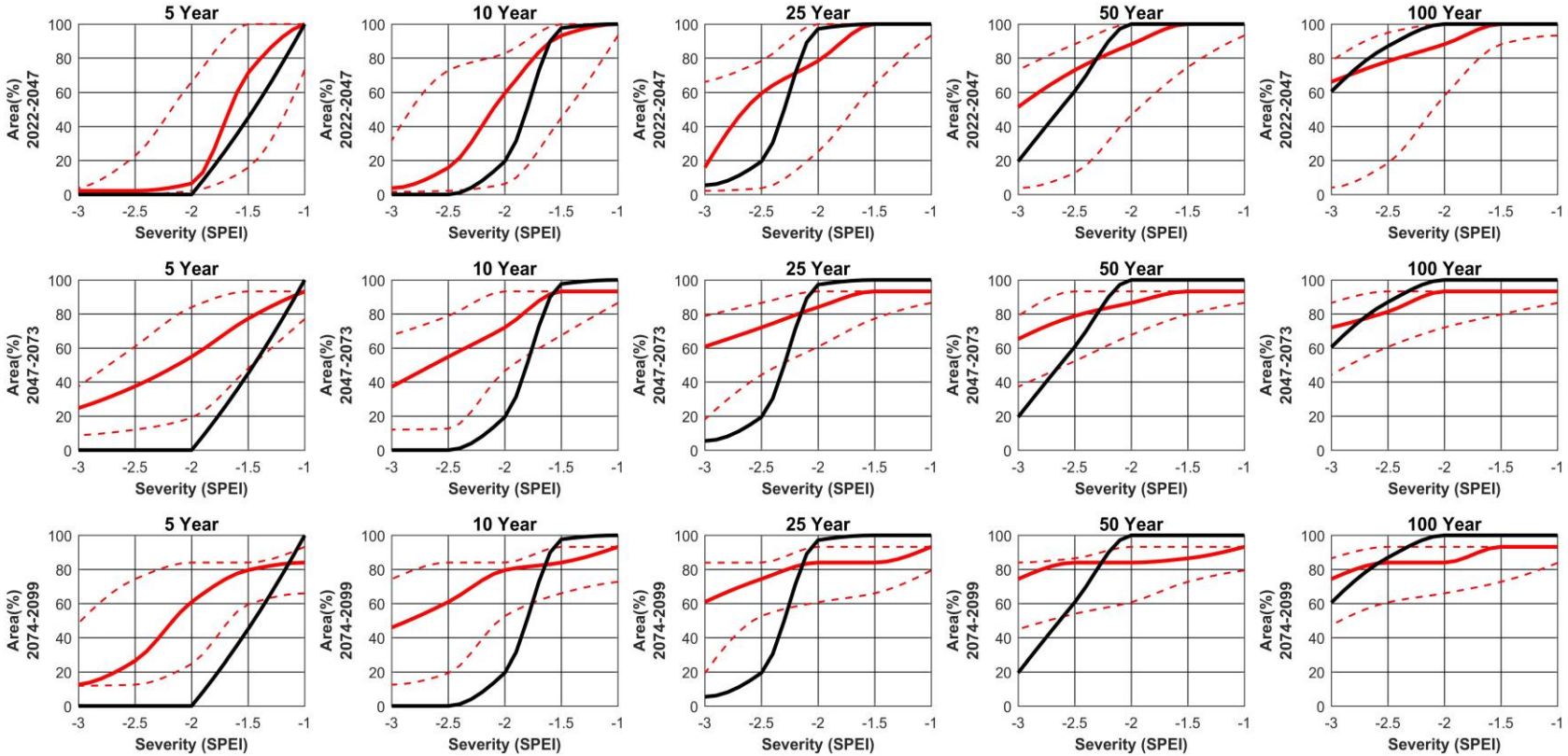

Figure 8.9: SAF curve for pre-monsoon season over Amaravati region. The top, middle, and bottom panels present for T1, T2, and T3 periods, respectively. The black line corresponds to T0 period, red line defines future simulation, and dashed red line represents the 95% confidence interval

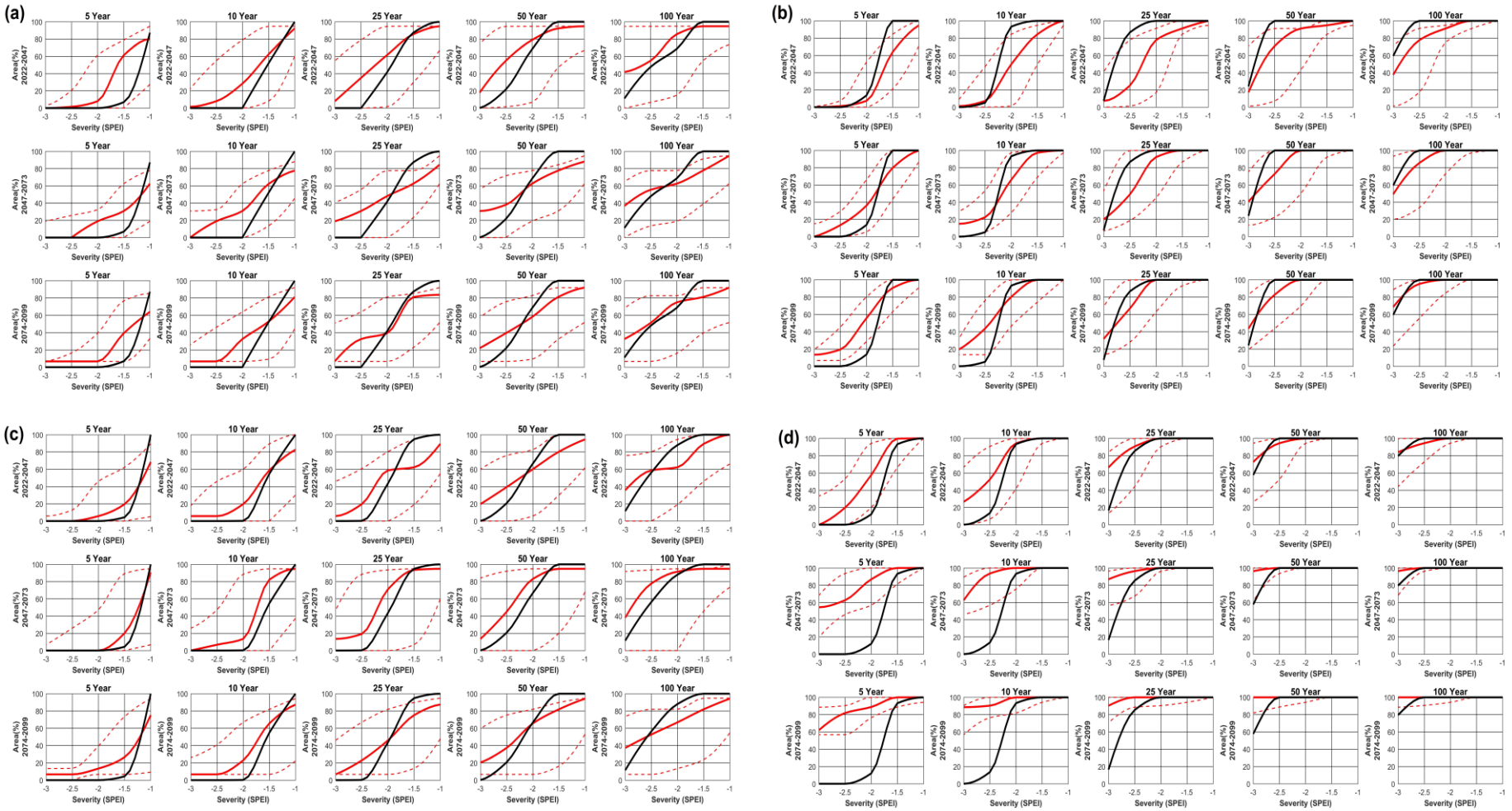

Figure 8.10: SAF curve for Amaravati region. (a) for monsoon, (b) for post-monsoon, (c) for Kharif, (d) for Rabi

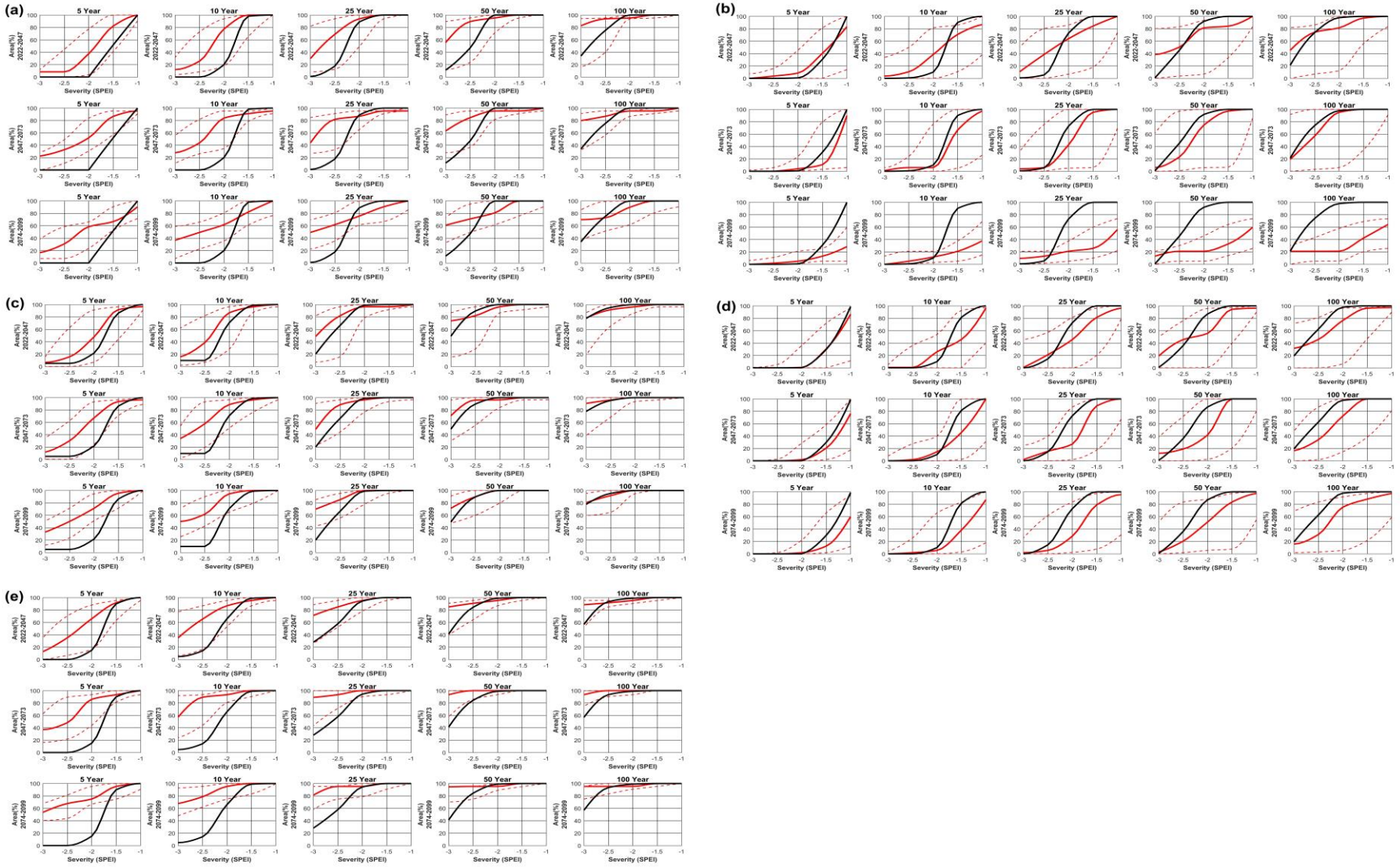

Figure 8.11: SAF curve for Aurangabad region. (a) for pre-monsoon, (b) for monsoon, (c) for post-monsoon, (d) for Kharif, (e) for Rabi

8.3.3.3 SAF curve for Konkan

The seasonal SAF curve for the Konkan region is presented in Figure 8.12. Figure 8.12 (a), Figure 8.12 (b), Figure 8.12 (c), Figure 8.12 (d), and Figure 8.12 (e) denote pre-monsoon, monsoon, post-monsoon, Kharif, and Rabi seasons, respectively. The future projected SAF curves are likely to decrease as compared to T0 for most of the return periods in pre-monsoon season. During monsoon season, the future drought-prone area may increase for more severe drought conditions under high return periods. For the severity level less than -1.8, the drought-affected area is likely to increase as compared to T0. In most of the cases, an increase in drought-affected area is observed during post-monsoon season. With increase in the return period, the area under the drought is likely to decrease in Kharif season. For higher return period, the area under the severe drought condition is expected to increase. During Rabi season, the SAF curves for 50- and 100- year return periods and all future time steps are projected to decrease as compared to T0. In case of T1 time step, the drought-affected area for most of the severity levels is likely to reduce. However, the percentage of area under drought may increase for the severity level less than -2.0 during T2, and T3 periods under 5- and 10-year return periods.

8.3.3.4 SAF curve for Nagpur

The SAF curve for the Nagpur region is shown in Figure 8.13. The pre-monsoon SAF curve (Figure 8.13 (a)) shows an increase in the percentage drought area in T2 future period. The difference between future simulated and observed SAF curve is larger during T3 than T1. During Monsoon season (Figure 8.13 (b)), it is observed that 0% area is affected by drought for severity level less than -2.5 for 5- and 10- year return periods in future. The future SAF curve under 100-year return period during T2 and T3 time steps is likely to decrease as compared to T0. In most of the cases the future simulated area under drought is expected to decrease in post-monsoon season (Figure 8.13 (c)). In Kharif season (Figure 8.13 (d)), for most of the return periods, the percentage area increases (decreases) for high (low) severity level as compared to T0. During T1 and T2, the area under drought is projected to decrease under 100-year return period. However, the areal drought condition may increase during Rabi season under all the return periods in future.

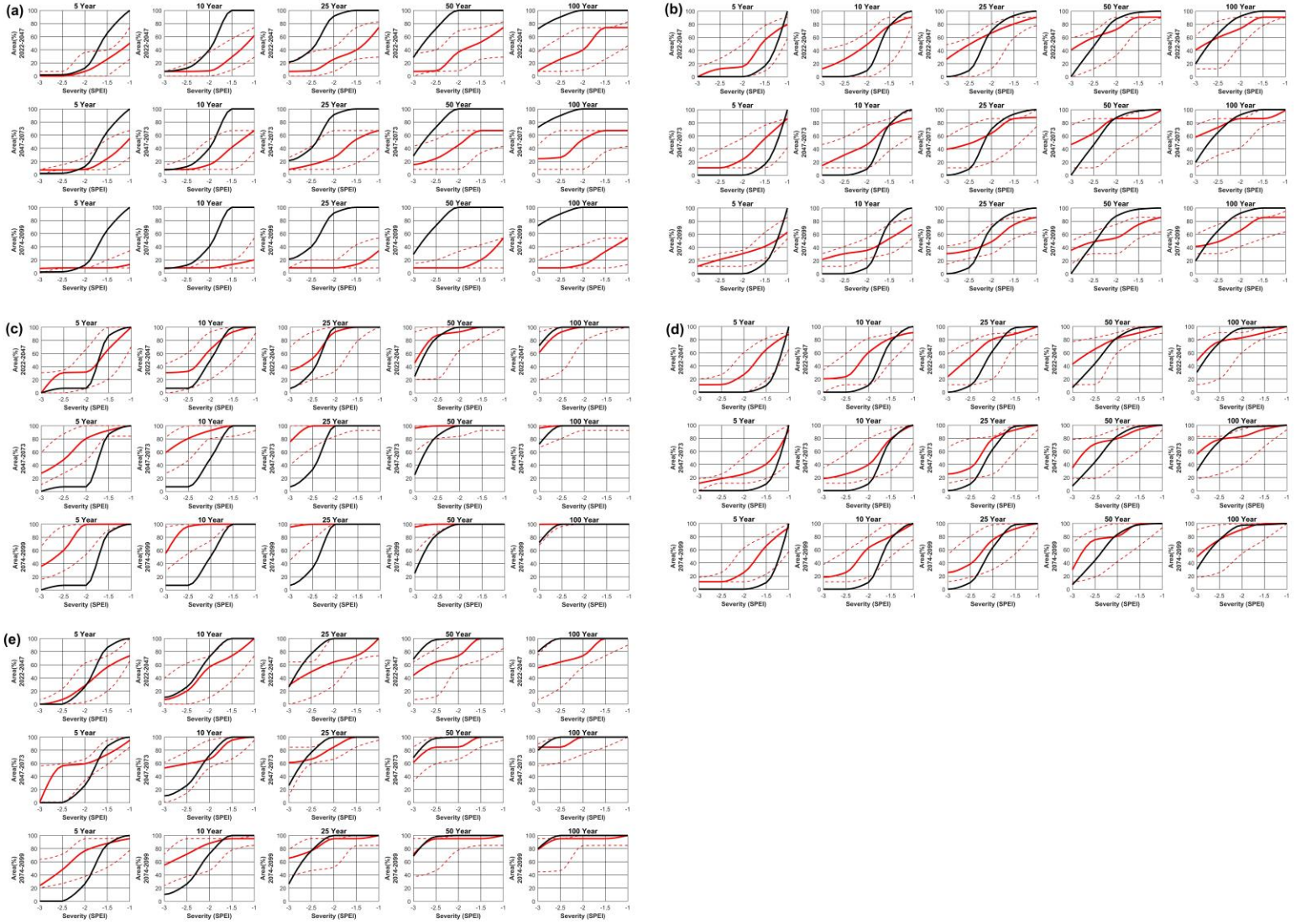

Figure 8.12: SAF curve for Konkan region. (a) for pre-monsoon, (b) for monsoon, (c) for post-monsoon, (d) for Kharif, (e) for Rabi

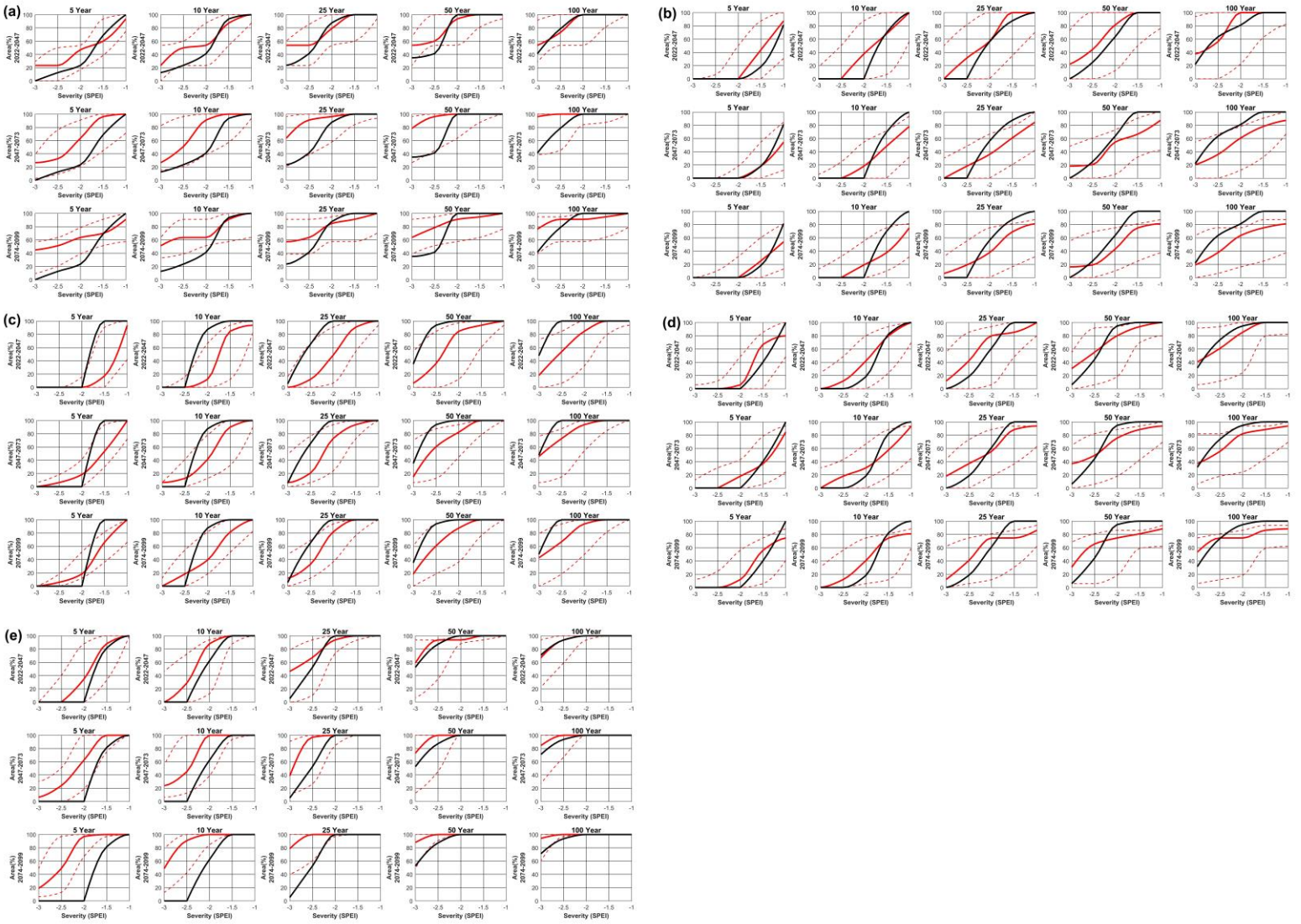

Figure 8.13: SAF curve for Nagpur region. (a) for pre-monsoon, (b) for monsoon, (c) for post-monsoon, (d) for Kharif, (e) for Rabi

8.3.3.5 SAF curve for Nashik

Figure S11 depicts the SAF curve for Nashik region. In pre-monsoon season (Figure 8.14 (a)), the increment in future projected drought-prone area is observed under all the return periods for T1 time step. During T2 period, with increase in return period, the area under drought is shifted towards the more severe drought condition. A similar kind of observation is also noticed in case of T3 period. During monsoon season, in most of the cases the percentage of areal drought has increased as compared to T0 in different return periods (Figure 8.14 (b)). The post-monsoon season (Figure 8.14 (c)) shows less variability in case of 25-, 50-, and 100-year return periods. In general, the projected drought area is expected to increase during the season. In Kharif season (Figure 8.14 (d)), a significant increment in the areal coverage of drought is observed for all the return periods during T3 as compared to T1 and T2. Similar to Nagpur region, the areal drought condition may increase during Rabi season under all the return periods in future (Figure 8.14 (e)).

8.3.3.6 SAF curve for Pune

For Pune region, the SAF curve is presented in Figure 8.15. It is noticed that the area under the drought is likely to decrease during pre-monsoon season (Figure 8.15 (a)) under high return period. However, during T2 period, the drought-affected area for more severe drought condition may increase under 5- and 10- year return periods. A gradual decrease in the drought area is expected in future with increase in the return period during monsoon season (Figure 8.15 (b)). However, it is observed that the SAF curves for all the return periods are likely to increase in all future periods as compared to T0 during post-monsoon season (Figure 8.15 (c)). In Kharif season (Figure 8.15 (d)), at high return levels the drought-affected areas are likely to decrease for all the future time steps. However, for 5-, 10-, and 25- year return periods, the SAF curve is likely to increase for severe drought conditions in future. Similar to post-monsoon season, the areal drought condition may increase during Rabi season under all the return periods in future (Figure 8.15 (e)).

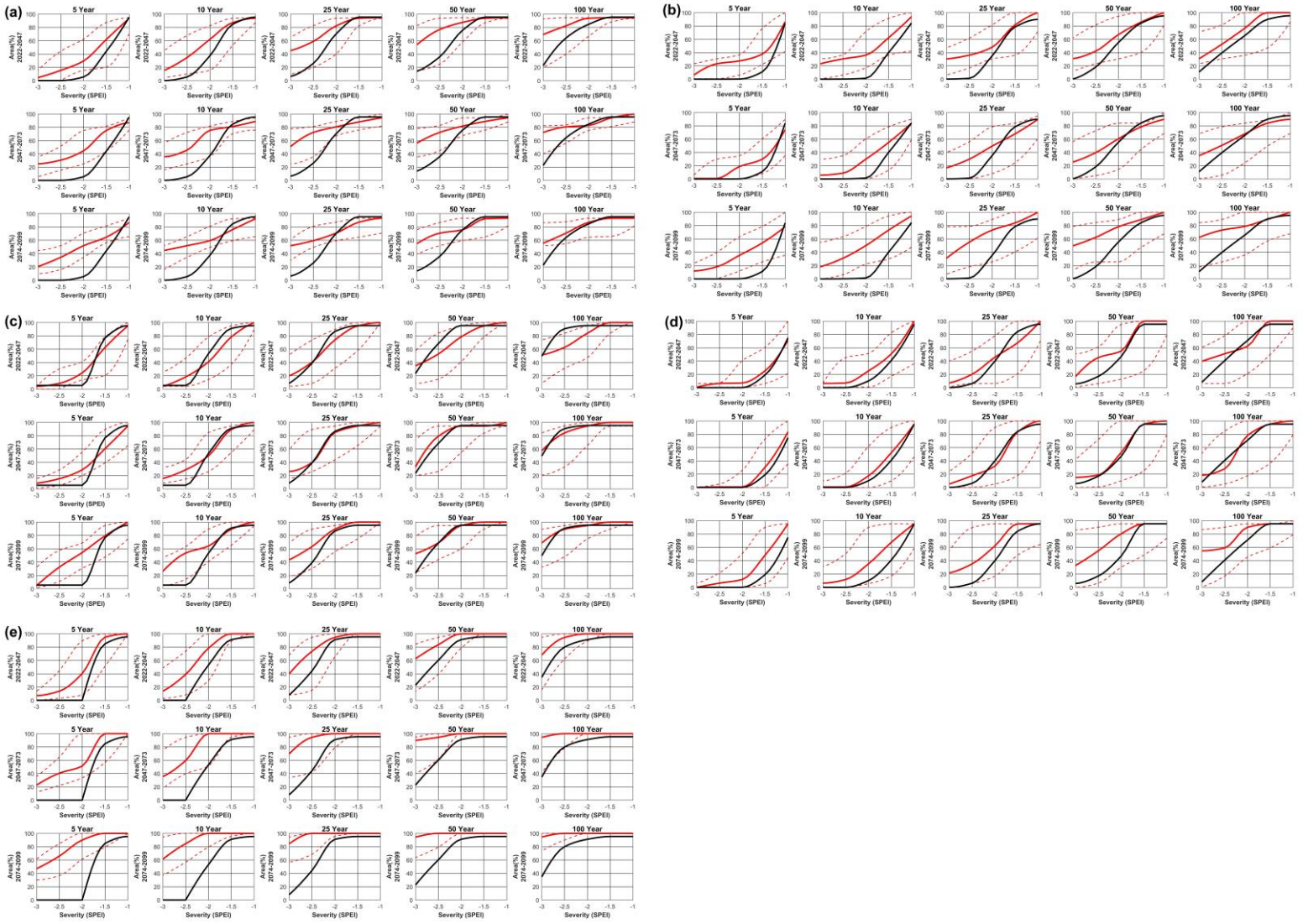

Figure 8.14: SAF curve for Nashik region. (a) for pre-monsoon, (b) for monsoon, (c) for post-monsoon, (d) for Kharif, (e) for Rabi

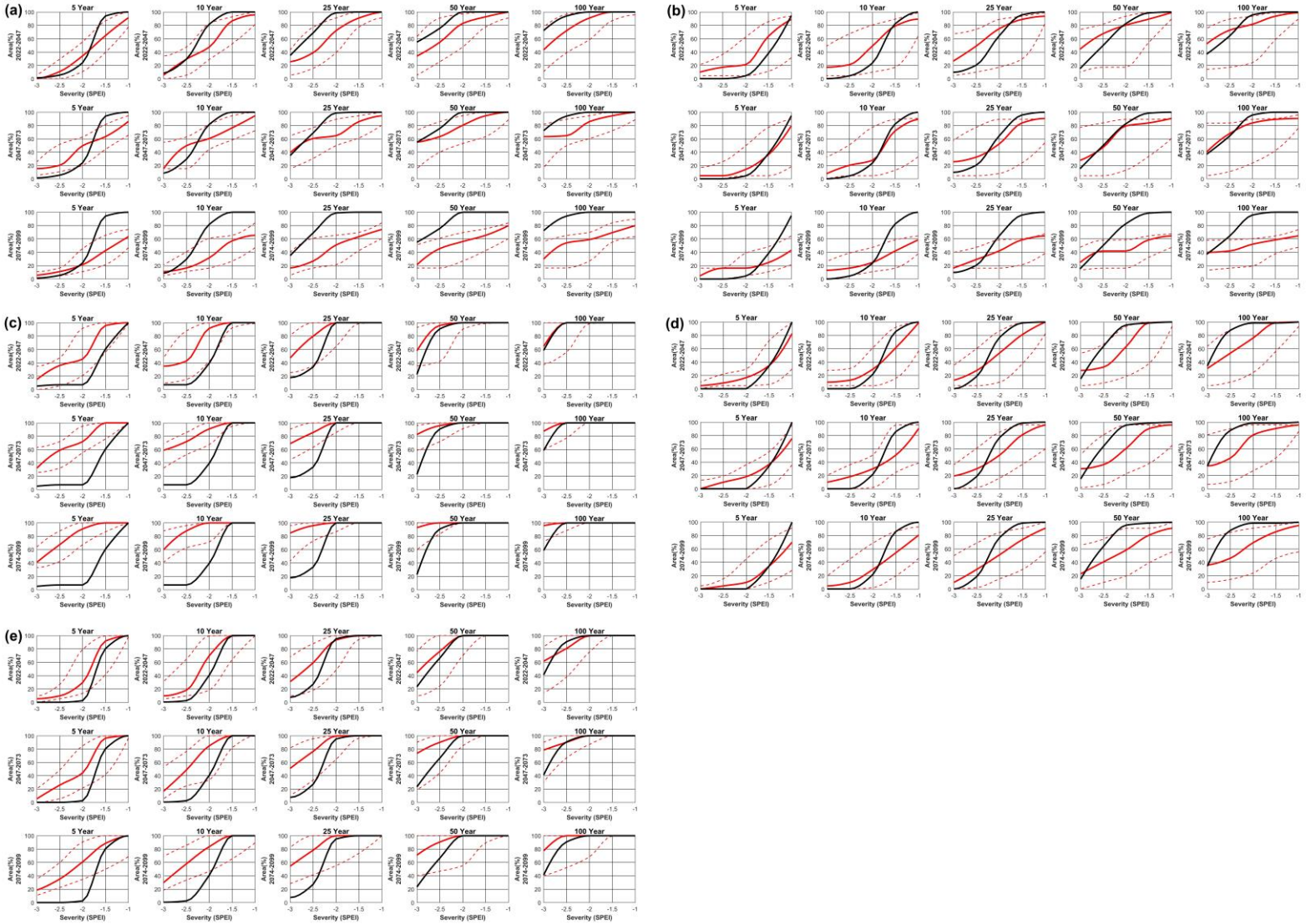

Figure 8.15: SAF curve for Pune region. (a) for pre-monsoon, (b) for monsoon, (c) for post-monsoon, (d) for Kharif, (e) for Rabi

8.3.4 Changes in future drought-affected area

The changes in drought-affected areas are plotted using heatmaps. Figure 8.16 presents the percentage in the drought-affected area in different seasons with respect to T0 period. The upper panel defines Amaravati region and lower panel refers to Aurangabad region. Similarly, Figures 8.17 and Figures 8.18 present the percentage area change for Konkan (upper panel), Nagpur (lower panel), and Nashik (upper panel), Pune (lower panel), respectively. It can be noted that for higher magnitude of drought severity the percentage area under different return periods is likely to increase for Amaravati. The increment in the drought prone area is observed in case of pre-monsoon and Rabi seasons for Amaravati and Aurangabad divisions. However, there will be significant decrement or no significant change in drought-affected area for lower magnitude of drought severity. In a similar way, in Konkan division, there is no sign of increment in drought-affected area during pre-monsoon season. However, during other seasons, there is a significant increase in drought-affected area for extreme drought condition except for T1 future period during Rabi season. Likewise, in Nagpur, pre-monsoon and Rabi seasons and in Pune, post-monsoon and Rabi seasons are comparatively more affected by drought in future time periods. However, as compared to other divisions, Nashik is likely to deal with the increment in drought-affected area during most of the seasons in future as compared to T0 period.

8.4 Discussion and summary

The concurrent variability in hydro-meteorological variables makes it difficult to understand the regional drought severity during different seasons. Hence, analysing the seasonal drought characteristics under the influence of climate change needs to be examined. The present study makes an attempt to understand the drought attributes during different seasons by developing and comparing the SAF relationship for historical and future periods. The future meteorological outputs from nineteen NEX-GDDP simulations under two emission scenarios are used. Prior to the analysis, uncertainty associated with GCM and scenario is analysed using the possibility theory. Based on the analysis, the most possible GCM and scenario at each grid point for 3-, 4-, and 6-month time scale are selected. It should be noted that the GCM/scenario with a possibility value of 1 does not mean that the selected GCM/scenario perfectly projects the climate change at that particular grid. However, it denotes the

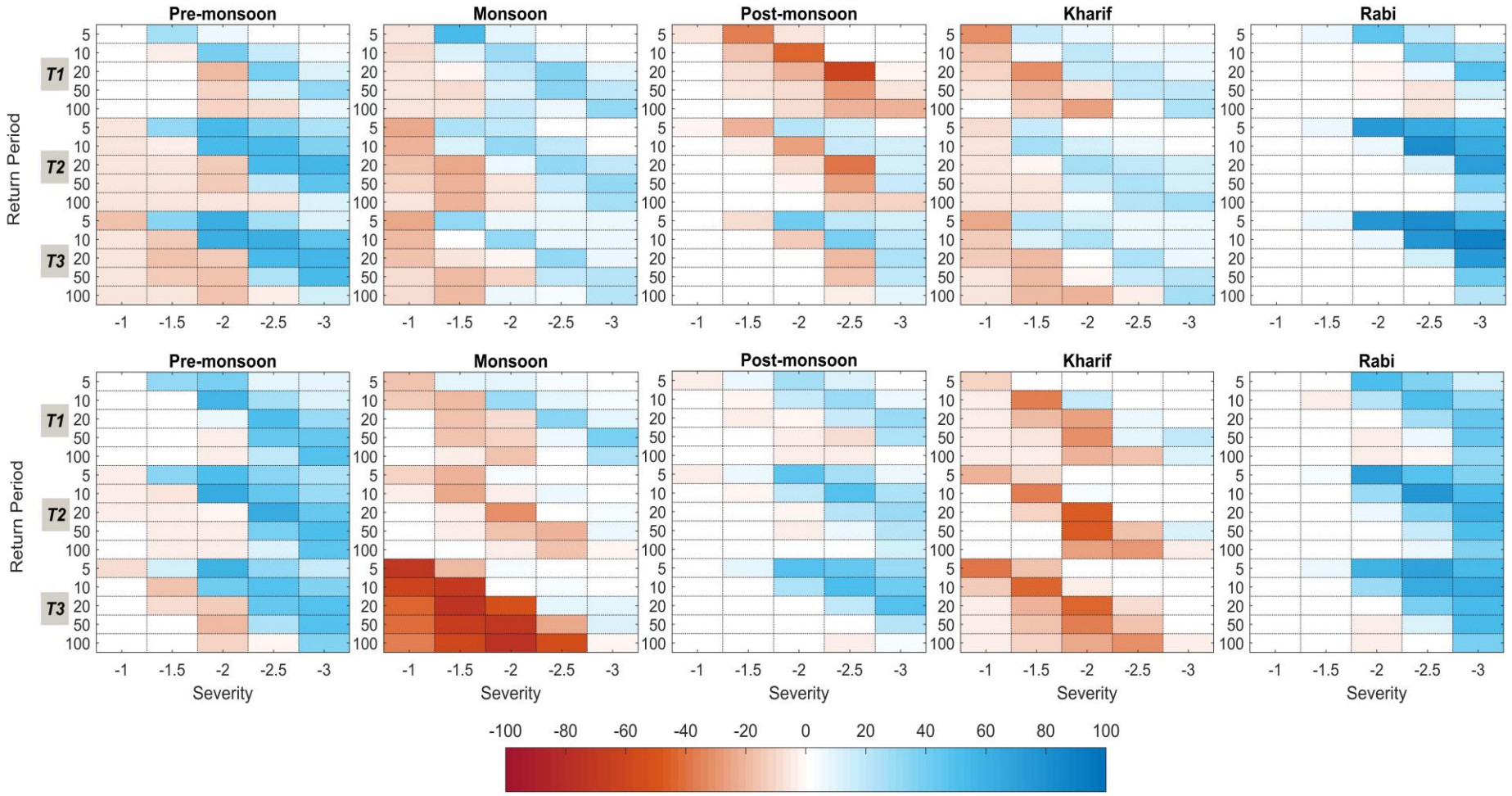

Figure 8.16: Heatmaps showing percentage change in drought areal extent for Amaravati (upper) and Aurangabad (lower) divisions under different seasons

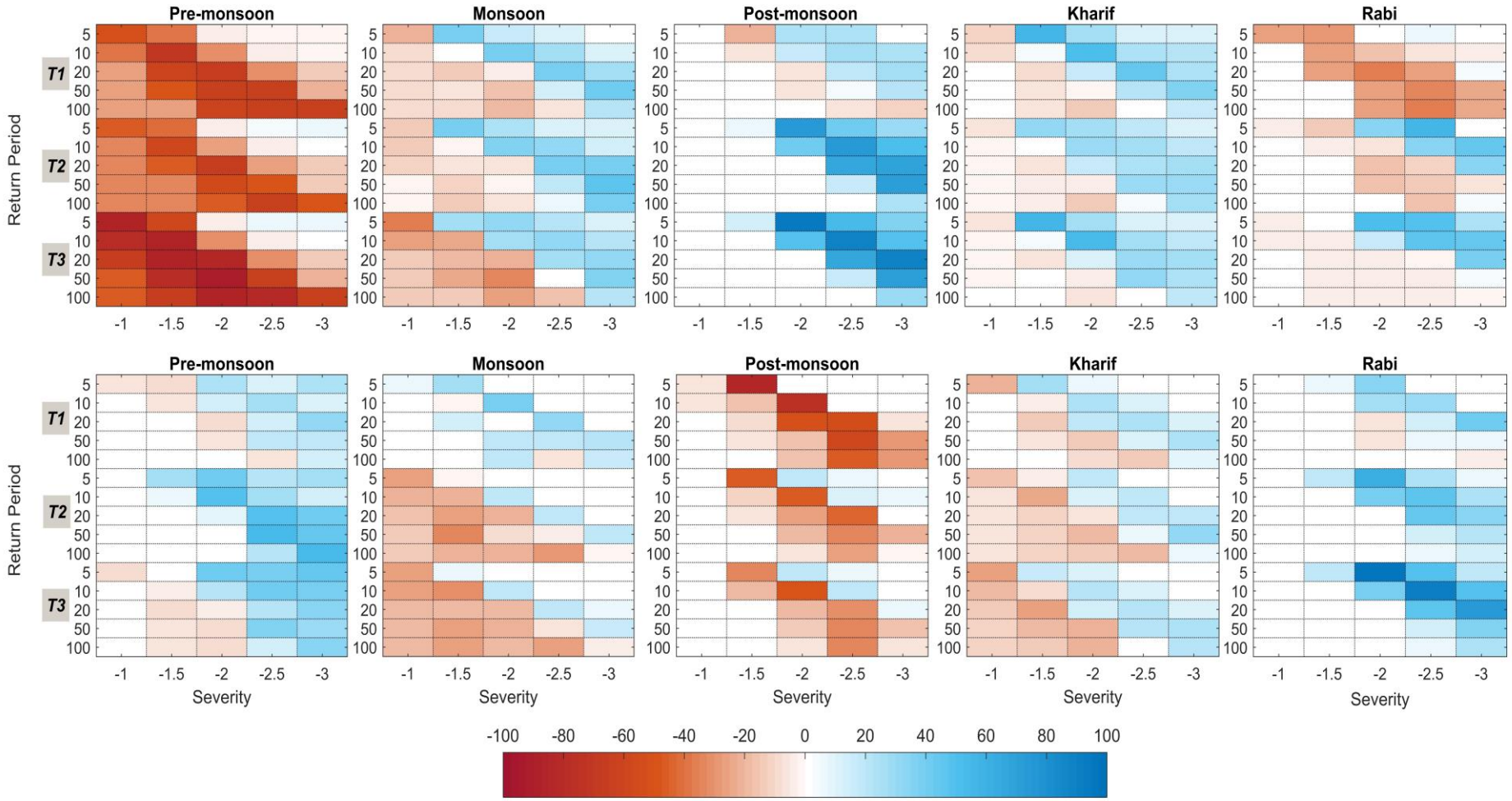

Figure 8.17: Heatmaps showing percentage change in drought areal extent for Konkan (upper) and Nagpur (lower) divisions under different seasons

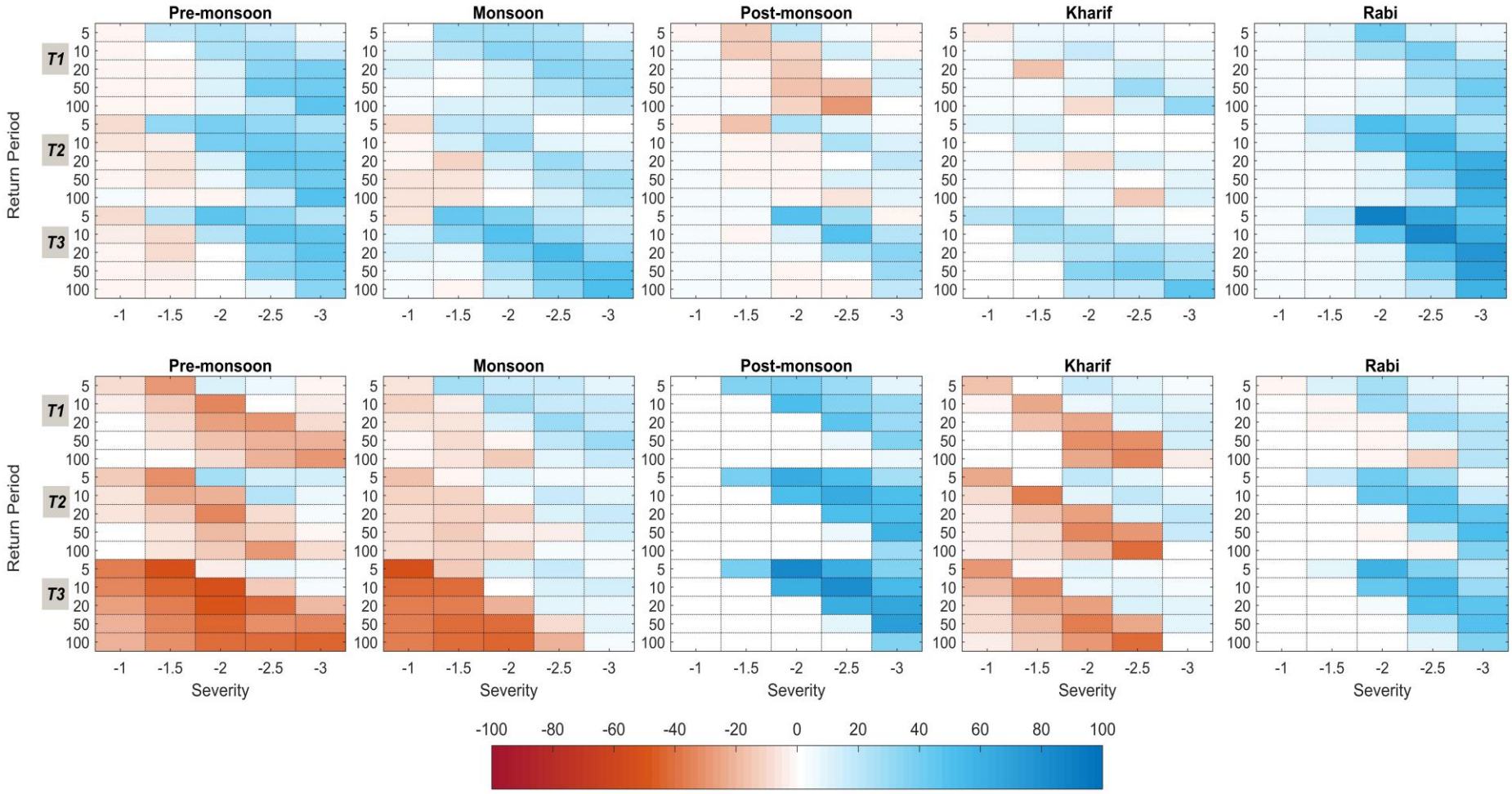

Figure 8.18: Heatmaps showing percentage change in drought areal extent for Konkan (upper) and Nagpur (lower) divisions under different seasons

nonexistence of any better GCM/scenario to capture the climate change variability at that grid point. The future temperature for all the seasons and precipitation for pre-monsoon, monsoon, and Kharif seasons are expected to increase.

The evaluation of drought SAF relationship curves for analysing drought characteristics enable to compare the drought attributes during each season across the study area during T0 period. It can be clearly distinguished from the SAF curve that mild drought conditions with less severity i.e., SPEI value between -1.5 and -1.0 cover more area for each return period. However, in most of the cases in future period, the SAF curves for different seasons indicate increase in area with severity magnitude less than equal to -2.0. The outcomes manifest that the study area is sensitive towards extreme drought occurrences. Additionally, area corresponding to high return period increases as compared to the lower return period.

The outcomes obtained from this study confirm similar types of findings resulted from previous studies based on seasonal drought analysis associated with different range of drought severity and return periods for evaluating drought-affected areas. Ahmed et al., (2019) reported that large areas were drought-affected in Pakistan for higher return period by assessing the drought characteristics with the use of SAF curves. Drought characteristics vary regionally depending on its geographic and climatic condition. In addition, the uncertainties in drought-affected areas may arise due to the differences in methodologies, variation in data obtained from different sources including GCMs. Therefore, drought characteristics have been calculated here per division wise for better understanding which appears to be more useful to improve the socio-economic condition in Maharashtra.

From the analysis of drought characteristics among all seasons across each division of Maharashtra, it is observed that there is an increment in percentage of the drought-affected area especially for the higher magnitude of severity in future period. Previous studies have already reported about the increment in drought-affected area with long term and severe droughts in different parts of the world (Amirataee et al., 2018; Himayoun and Roshni, 2019). In addition, it has also been suggested in recent studies that the drought events with rise in severity and frequency will continuously increase in many regions across the world in coming decades due to projected climate change factors (Bisht et al., 2019; Sharma and Mujumdar, 2017). Specifically, the regions with frequent drought events will be highly prone to future drought occurrences due to climate change scenarios (Kundzewicz et al., 2008). In future, the

severe and extreme drought occurrences are expected to increase with large spatial extent over each division.

In summary, the significant findings from the present analysis point to the fact that the precipitation magnitude is expected to increase in pre-monsoon, monsoon, and Kharif seasons over most of the areas in Maharashtra. Except for monsoon season, the potential evapotranspiration is projected to increase over 50% of the total area. Increase in the temperature profile is noticed over all the regions in Maharashtra during the 21st century. The extreme drought condition during post-monsoon, pre-monsoon and Rabi seasons shows an increase in the frequency as compared to historical period. The SAF curve reveals that, in most of the cases, the percentage of drought-affected area is expected to increase for high magnitude of severity. In addition, the highest increment in the drought-affected area is observed during the Rabi season in future.

Chapter 9

Summary and conclusions

9.1 Introduction

The research reported in this thesis contributes towards understanding the drought characterization, propagation, and risk over Indian region. The drought characterization is performed using the influence on the large-scale climatic oscillations and regional hydro-meteorological variabilities using the gridded data. The non-stationary analysis is carried out for meteorological, hydrological and agricultural drought events. In addition, the socio-economic drought is evaluated using the demand from different sectors under stationary assumption. Further, the duration of drought propagation from meteorological to hydrological and meteorological to agricultural drought conditions is examined using the non-stationary drought indices. Next, the agricultural drought risk is computed using the multivariate

analysis for different crops. Here, copula is used for multivariate analysis. Future projection of meteorological drought is evaluated using the outputs from several GCMs under different climate change scenarios. In addition, identification of future drought hotspot regions is carried out under different scenarios. Lastly, seasonal Severity-Area-Frequency (SAF) relationship curve is developed after analysing the uncertainty associated with GCMs and scenarios. The following paragraphs give a summary and conclusions of the study presented in the thesis.

- In order to understand the influence of external drivers on the drought events, non-stationary drought analysis is carried out over one of the most drought affected states i.e., Maharashtra. Two different drought indices, namely precipitation-based Standardized Precipitation Index (SPI) and precipitation and potential evapotranspiration (PET) based Reconnaissance Drought Index (RDI), are considered for the analysis. The large-scale climatic oscillations like Indian Summer Monsoon Index (ISMI), Southern Oscillation Index (SOI), Sea Surface Temperature (SST), and Indian Ocean Dipole (IOD) are used as covariates. The Generalized Additive Model in Location, Scale and Shape (GAMLSS) package in R environment is used to perform the analysis over 103 grid points (0.5^{o} Lat x 0.5^{o} Lon) covering the Maharashtra. The study is conducted for different time scales of drought events such as 3-, 6-, 9-, 12-, 24- month time scales. The non-stationary analysis is performed by varying the location parameter of the gamma and lognormal distributions of SPI and RDI drought indices, respectively. Finally, different drought properties such as severity, duration, frequency, peak are calculated for moderate, severe and extreme drought conditions. It is found that the non-stationary model outperforms the stationary approach over all time scales. The ISMI is likely to influence droughts on smaller scales. However, the IOD, SST, and SOI are expected to modulate larger-scale drought events. Comparative study of the probability plots of drought properties reveals that, though there are noticeable variabilities between the stationary and non-stationary conditions on all time scales, a significant difference is noticed on the 3-, 6, and 9-month time scales. A comparative study with respect to historical drought assessments reveals that the presence of non-stationarity cannot be ignored for developing sustainable mitigation and adaptation strategy.

- From Chapter 3 and Chapter 4, it is found that non-stationary analysis of drought events has significant importance in the scenario of climate change. Thus, drought properties of meteorological, hydrological and agricultural drought events are evaluated across India under non-stationary approach. Here, Standardized Precipitation Evapotranspiration Index (SPEI), Standardized Runoff Index (SRI), and Standardized Soil moisture Index (SSI) are used to characterize the meteorological, hydrological, and agricultural drought, respectively. The study is performed over 1170 grid points at a grid resolution of 0.5^{o} Lat x 0.5^{o} Lon over India. In case of SRI index, only the meteorological variables (precipitation, PET, relative humidity, and wind speed) are considered as covariates for non-stationary modelling. However, for SSI, the meteorological variables such as precipitation, air temperature, and soil temperature are considered as covariates. The runoff datasets are obtained from five different sources (ECMWF Reanalysis 5th Generation (ERA5), Famine Early Warning Systems Network Land Data Assimilation System (FLDAS), Global Land Data Assimilation System (GLDAS), Modern-Era Retrospective analysis for Research and Applications version 2 (MERRA-2), and National Centers for Environmental Prediction (NCEP)). Similarly, the soil moisture datasets are obtained from six diverse sources (Climate Prediction Center (CPC), ERA5, FLDAS, GLDAS, MERRA-2, and NCEP). In addition to meteorological, hydrological and agricultural droughts, socio-economic drought events are also computed. However, the socio-economic drought is evaluated based on the stationary approach. It is found from the analysis that the non-stationary model outperforms the stationary analysis for meteorological, hydrological and agricultural drought indices. The meteorological drought properties (drought events and duration) are more severe as compared to the hydrological drought. The large duration and more severe hydrological droughts are observed mostly over southern and northern parts of India. The high agricultural drought duration and severity are observed over the northern parts and some patches of northeast and northwest regions of India. The high value of socio-economic drought severity is noticed over Punjab and Haryana.

- In addition to the drought properties, the drought propagation from meteorological to hydrological and meteorological to agricultural is investigated incorporating the non-stationary drought indices developed in Chapter 4. The drought propagation time is

computed for 1170 grids blanketing the entire India based on differences between the initiation to initiation (Δs), peak to peak (Δp) and termination to termination (Δe). In addition, the internal propagation of drought is estimated with the help of variable motion relationship of speed-time process. In addition, the drought development period (DDP) and drought recovery period (DRP) are analysed. The rate of change of cumulative drought deficit for development and recovery phases are computed to evaluate the Instantaneous Development Speed (IDS) and Instantaneous Recovery Speed (IRS), respectively. It is found that locations with the high value of DDP are also having high value of DRP in both the cases (hydrological and agricultural). In case of hydrological drought, most of the area in India has the IDS and IRS values between 0.40 and 0.60 per month. However, the same varies between 0.20 and 0.60 per month in the case of agricultural drought. The meteorological to hydrological propagation time in case of Δs varies between 4 and 9 months with 62% of total area falling under 6 to 7 months followed by 20% of total area under 7 to 8 months. In the case of Δp, the time of propagation varies from 9 to 12 months over 74% of the total area. About 70% of total area, the time of propagation in Δe ranges from 15 to 20 months. In case of Δs, the propagation from meteorological to agricultural is found to be 5 to 6 months and 6 to 7 months over 39% and 53% of the total area, respectively. Similarly, the drought propagation over about 95% of total area ranges from 9 to 15 months under Δp condition. The time to propagation varies between 10 to 15 months over 32% and 15 to 20 months over 65% of total area in case of Δe. It is found that the drought propagation and its characteristics are underestimated over most of the regions in India when computed with stationary analysis.

- As an agrarian country, India's economy largely depends on agricultural productivity. Therefore, it is of utmost importance to examine the agricultural drought risk for different crops. The agricultural drought risk in terms of conditional probability of crop loss with respect to different drought severities is analysed. Different drought indices namely SPEI, SSI, Vegetation Condition Index (VCI) and Temperature Condition Index (TCI) are used to evaluate the conditional probability. The bivariate analysis using the copula theory is performed to understand the dependence structure between drought conditions and crop yield anomalies (cotton, groundnut, rice, and wheat) over the Maharashtra province in India during 1998-2015. Total of five

different copulas namely, Gaussian, Student's t-copula, Clayton, Gumbel, and Frank are used to analyse the bivariate joint dependence structure between yield anomalies and dominant drought indicator. The significant findings from the present analysis point to the fact that the drought hazard is primarily characterized by SPEI drought indicator in all the crops. The higher probability of drought risk under moderate and extreme drought conditions are modelled by Clayton copula suggesting greater probabilities of joint extreme low values. With increase in the drought severity the conditional probability of agricultural drought risk is likely to increase. In addition, it is observed that the exclusion of non-stationarity will underestimate the agricultural risk, which will significantly affect the planning and management of agricultural sustainability over the study area.

- Understanding the adverse consequences of drought events on various sectors, it is necessary to examine the future variability of drought under different climate change scenarios. Chapter 7 includes the outputs from nineteen different GCMs from NEX-GDDP under Representative Concentration Pathway (RCP) 4.5 and 8.5 scenarios to characterize the future short (3-month scale) and long (12-month scale) term meteorological drought over Maharashtra province. In addition, future meteorological drought hotspot regions are evaluated over the study area based on different drought properties. In order to identify the implications of temperature on drought, SPEI drought index is chosen along with SPI index. The significant findings from the analysis point to the fact that with the increase in the monthly mean temperature and precipitation (more in case of RCP8.5 than RCP4.5), Maharashtra is likely to be wetting and warming during the 21st century except for Konkan region as compared to historical. In Konkan region, the warmer climatology is likely to prevail with no significant change in the monthly precipitation variability. The drought properties like peak and areal spread are expected to increase for both short and long-term drought conditions in most of the regions. The frequency of severe and extreme droughts is likely to increase in the short-term drought condition with no sign of decrease at any time segments and regions. Temperature plays an important role in modulating the meteorological droughts and the present study notices the same in most of the cases in all the drought properties especially in drought severity, duration, and peak. The

number of hotspot regions decreases in long-term drought condition as compared to short-term drought condition.

- In the Chapter 8, the seasonal SAF relationship curve for meteorological droughts is projected for various divisions in Maharashtra corresponding to five different seasons namely pre-monsoon, monsoon, post-monsoon, Kharif and Rabi. The uncertainty associated with GCMs, and scenarios is assessed using possibility theory. The SPEI drought index is used as an indicator of meteorological drought. In order to project for the future time period, nineteen different GCMs under two different Representative Concentration Pathways (RCPs) 4.5 and 8.5 are chosen. The significant findings from the present analysis point to the fact that the precipitation magnitude is expected to increase in pre-monsoon, monsoon, and Kharif seasons over most of the areas in Maharashtra. Except for monsoon season, the potential evapotranspiration is projected to increase over 50% of the total area. Increase in the temperature profile is noticed over all the regions in Maharashtra during the 21st century. The extreme drought condition during post-monsoon, pre-monsoon and Rabi seasons shows an increase in the frequency as compared to historical period. The SAF curve reveals that, in most of the cases, the percentage of drought-affected area is expected to increase for high magnitude of severity. In addition, the highest increment in the drought-affected area is observed during the Rabi season in future.

In the continually climate change scenario, it is of great concern to revisit, rethink, and improve the existing computational aspects of drought indexes. In general, the commonly used drought indexes do not encompass environmental changes. Therefore, the nonstationary estimation of drought indexes can incorporate the development of meteorological variables in a changing environment. More precisely, the time-varying nature of meteorological variables are updated with time, providing a robust and suitable drought assessment. Not only the meteorological drought, the non-stationary analysis of hydrological, and agricultural drought indices will help the water and agricultural managers to devise sustainable management practices. To devise sustainable drought management practices, it is inevitable to understand the propagation of drought from one form to another. In addition, the inclusion of large-scale climate indices and regional hydro-meteorological variability in understanding the propagation of drought enable to cope with the changing climate scenario. The grid wise examination of drought propagation will provide important drought characteristics at local

scale which can assist water managers and policy makers to devise sustainable management practices. The implications from the agricultural drought risk suggest making agricultural practices climate resistant and water effective. The outcomes obtained during the investigation of the future drought analysis should be considered as indicative about the response of the study area to the climate change rather than conclusive.

With respect to the different "Sustainable Development" goals proposed by United Nations (https://sdgs.un.org/goals), the outcomes from the present study can be linked to the following goals, (i) Climate Action, (ii) Clean Water and Sanitation, (iii) Life on Land. The goal "Climate Action" enables to take prompt action to combat climate change and its impact. In the present analysis, the changeability in the large-scale climatic indices is incorporated in modeling the drought index. The variability in the large-scale climatic indices is modulated due to the change in the climate and their interaction with the ocean. In this sense, the newly developed drought index would help in devising the effective drought management strategies to combat climate change. Similarly, the goal "Clean Water and Sanitation" aims to ensure the availability and sustainable management of water. In the present study, the variability of available water at regional scale is characterised using the hydrological drought index. In addition, the variability in water availability due to the meteorological drought condition is assessed through its propagation phenomena which would help in formulating the sustainable management plans to ensure the water availability. Lastly, the goal "Life on Land" ensures to protect, restore, and promote sustainable use of terrestrial ecosystems. Under this goal, desertification, land degradation, and drought is considered as one of the topics to fulfil the motive. The present study deals with the propagation of one drought to another under the influence of climate change and future projection of drought that help in developing the strategies to promote resilience and disaster risk management.

9.2 Scope for future studies

The present research is devoted to characterize drought events under non-stationary condition, to understand the propagation from one drought to another drought, to evaluate the agricultural risk associated with droughts and future projection of drought characteristics under different climate change scenarios. However, many challenges still exist in the field of hydrological extremes. Hence, following would be possible future works.

- Investigation of drought propagation can be improved by incorporating the catchment characteristics, types of soil and groundwater component.
- Identification of hotspots based on the internal propagation of drought and propagation from one form to another form facilitates sustainable development strategies.
- The socio-economic drought can be examined with the combined effect of meteorological, hydrological and agricultural drought to examine the impact of any individual drought type on socio-economic condition.
- Future drought propagation study can be carried out based on the outputs from different GCMs under recently developed CMIP6 experiment.
- Future hydrological and agricultural drought hotspots can be identified by forcing the GCMs simulated meteorological data into hydrological model.

References

1. Aadhar, S., Mishra, V., 2020. Increased drought risk in South Asia under warming climate: Implications of uncertainty in potential evapotranspiration estimates. J. Hydrometeorol. JHM-D-19-0224.1. https://doi.org/10.1175/JHM-D-19-0224.1
2. Aadhar, S., Mishra, V., 2018. Impact of Climate Change on Drought Frequency over India. Clim. Chang. Water Resour. India 117–129.
3. Aadhar, S., Mishra, V., 2017. High-resolution near real-time drought monitoring in South Asia. Sci. Data 4, 170145. https://doi.org/10.1038/sdata.2017.145
4. Abramowitz, M., Stegun, I.A., 1965. Handbook of mathematical functions.
5. Adhyani, N.L., June, T., Sopaheluwakan, A., 2017. Exposure to Drought: Duration, Severity and Intensity (Java, Bali and Nusa Tenggara). IOP Conf. Ser. Earth Environ. Sci. 58. https://doi.org/10.1088/1755-1315/58/1/012040
6. AghaKouchak, A., Feldman, D., Hoerling, M., Huxman, T., Lund, J., 2015. Water and climate: Recognize anthropogenic drought. Nature 524, 409–411. https://doi.org/10.1038/524409a
7. Agilan, V., Umamahesh, N. V., 2018. El Niño Southern Oscillation cycle indicator for modeling extreme rainfall intensity over India. Ecol. Indic. 84, 450–458. https://doi.org/10.1016/j.ecolind.2017.09.012
8. Agutu, N.O., Awange, J.L., Ndehedehe, C., Mwaniki, M., 2020. Consistency of agricultural drought characterization over Upper Greater Horn of Africa (1982–2013): Topographical, gauge density, and model forcing influence. Sci. Total Environ. 709. https://doi.org/10.1016/j.scitotenv.2019.135149
9. Ahmadalipour, A., Moradkhani, H., 2018. Multi-dimensional assessment of drought vulnerability in Africa: 1960–2100. Sci. Total Environ. 644, 520–535. https://doi.org/10.1016/j.scitotenv.2018.07.023
10. Ahmadalipour, A., Moradkhani, H., Svoboda, M., 2017. Centennial drought outlook over the CONUS using NASA-NEX downscaled climate ensemble. Int. J. Climatol. 37, 2477–2491. https://doi.org/10.1002/joc.4859
11. Ahmed, K., Shahid, S., Chung, E.S., Wang, X. jun, Harun, S. Bin, 2019. Climate change uncertainties in seasonal drought severity-area-frequency curves: Case of arid region of Pakistan. J. Hydrol. https://doi.org/10.1016/j.jhydrol.2019.01.019

12. Ajaz, A., Taghvaeian, S., Khand, K., Gowda, P.H., Moorhead, J.E., 2019. Development and evaluation of an agricultural drought index by harnessing soil moisture and weather data. Water (Switzerland) 11. https://doi.org/10.3390/w11071375
13. Akaike, H., 1974. A New Look at the Statistical Model Identification. IEEE Trans. Automat. Contr. 19, 716–723. https://doi.org/10.1109/TAC.1974.1100705
14. Alexander, L. V., Uotila, P., Nicholls, N., 2009. Influence of sea surface temperature variability on global temperature and precipitation extremes. J. Geophys. Res. 114, D18116. https://doi.org/10.1029/2009JD012301
15. Ali, Z., Hussain, I., Faisal, M., Shoukry, A.M., Gani, S., Ahmad, I., 2019. A framework to identify homogeneous drought characterization regions. Theor. Appl. Climatol. 137, 3161–3172. https://doi.org/10.1007/s00704-019-02797-w
16. Allan, R.P., Barlow, M., Byrne, M.P., Cherchi, A., Douville, H., Fowler, H.J., Gan, T.Y., Pendergrass, A.G., Rosenfeld, D., Swann, A.L.S., Wilcox, L.J., Zolina, O., 2020. Advances in understanding large-scale responses of the water cycle to climate change. Ann. N. Y. Acad. Sci. 1472, 49–75. https://doi.org/10.1111/nyas.14337
17. Allan, R.P., Liu, C., Zahn, M., Lavers, D.A., Koukouvagias, E., Bodas-Salcedo, A., 2014. Physically Consistent Responses of the Global Atmospheric Hydrological Cycle in Models and Observations. Surv. Geophys. 35, 533–552. https://doi.org/10.1007/s10712-012-9213-z
18. Amarasinghe, U., Amarnath, G., Alahacoon, N., Ghosh, S., 2020. How Do Floods and Drought Impact Economic Growth and Human Development at the Sub-National Level in India? Climate 8, 123. https://doi.org/10.3390/cli8110123
19. Amirataee, B., Montaseri, M., Rezaie, H., 2018. Regional analysis and derivation of copula-based drought Severity-Area-Frequency curve in Lake Urmia basin, Iran. J. Environ. Manage. https://doi.org/10.1016/j.jenvman.2017.10.027
20. Anderson, M.C., Norman, J.M., Mecikalski, J.R., Otkin, J.A., Kustas, W.P., 2007. A climatological study of evapotranspiration and moisture stress across the continental United States based on thermal remote sensing: 1. Model formulation. J. Geophys. Res. Atmos. 112. https://doi.org/10.1029/2006JD007506
21. Apurv, T., Cai, X., 2020. Drought Propagation in Contiguous U.S. Watersheds: A Process-Based Understanding of the Role of Climate and Watershed Properties. Water Resour. Res. 56. https://doi.org/10.1029/2020WR027755

22. Apurv, T., Sivapalan, M., Cai, X., 2017. Understanding the Role of Climate Characteristics in Drought Propagation. Water Resour. Res. 53, 9304–9329. https://doi.org/10.1002/2017WR021445
23. Ashok, K., Saji, N.H., 2007. On the impacts of ENSO and Indian Ocean dipole events on sub-regional Indian summer monsoon rainfall. Nat. Hazards 42, 273–285. https://doi.org/10.1007/s11069-006-9091-0
24. Bai, P., Liu, X., Yang, T., Liang, K., Liu, C., 2016. Evaluation of streamflow simulation results of land surface models in GLDAS on the tibetan plateau. J. Geophys. Res. 121, 12,180-12,197. https://doi.org/10.1002/2016JD025501
25. Ballarin, A.S., Barros, G.L., Cabrera, M.C.M., Wendland, E.C., 2021. A copula-based drought assessment framework considering global simulation models. J. Hydrol. Reg. Stud. 38. https://doi.org/10.1016/j.ejrh.2021.100970
26. Bandyopadhyay, A., Bhadra, A., Swarnakar, R.K., Raghuwanshi, N.S., Singh, R., 2012. Estimation of reference evapotranspiration using a user-friendly decision support system: DSS_ET. Agric. For. Meteorol. 154–155, 19–29. https://doi.org/10.1016/j.agrformet.2011.10.013
27. Bandyopadhyay, N., Bhuiyan, C., Saha, A.K., 2020. Drought mitigation: Critical analysis and proposal for a new drought policy with special reference to Gujarat (India). Prog. Disaster Sci. 5, 100049. https://doi.org/10.1016/j.pdisas.2019.100049
28. Barella-Ortiz, A., Quintana-Seguí, P., 2019. Evaluation of drought representation and propagation in regional climate model simulations across Spain. Hydrol. Earth Syst. Sci. 23, 5111–5131. https://doi.org/10.5194/hess-23-5111-2019
29. Barker, L.J., Hannaford, J., Chiverton, A., Svensson, C., 2016. From meteorological to hydrological drought using standardised indicators. Hydrol. Earth Syst. Sci. 20, 2483–2505. https://doi.org/10.5194/hess-20-2483-2016
30. Bateni, M.M., Behmanesh, J., De Michele, C., Bazrafshan, J., Rezaie, H., 2018. Composite Agrometeorological Drought Index Accounting for Seasonality and Autocorrelation. J. Hydrol. Eng. 23, 04018020. https://doi.org/10.1061/(asce)he.1943-5584.0001654
31. Bazrafshan, J., 2017. Effect of Air Temperature on Historical Trend of Long-Term Droughts in Different Climates of Iran. Water Resour. Manag. 31, 4683–4698. https://doi.org/10.1007/s11269-017-1773-8
32. Bazrafshan, J., Cheraghalizadeh, M., Shahgholian, K., 2022. Development of a Non-

stationary Standardized Precipitation Evapotranspiration Index (NSPEI) for Drought Monitoring in a Changing Climate. Water Resour. Manag. https://doi.org/10.1007/s11269-022-03209-x

33. Bazrafshan, J., Hejabi, S., 2018. A Non-Stationary Reconnaissance Drought Index (NRDI) for Drought Monitoring in a Changing Climate. Water Resour. Manag. 32, 2611–2624. https://doi.org/10.1007/s11269-018-1947-z
34. Beguería, S., Angulo-Martínez, M., Vicente-Serrano, S.M., López-Moreno, J.I., El-Kenawy, A., 2011. Assessing trends in extreme precipitation events intensity and magnitude using non-stationary peaks-over-threshold analysis: a case study in northeast Spain from 1930 to 2006. Int. J. Climatol. 31, 2102–2114. https://doi.org/10.1002/joc.2218
35. Bevacqua, A.G., Chaffe, P.L.B., Chagas, V.B.P., AghaKouchak, A., 2021. Spatial and temporal patterns of propagation from meteorological to hydrological droughts in Brazil. J. Hydrol. 603. https://doi.org/10.1016/j.jhydrol.2021.126902
36. Bhardwaj, K., Shah, D., Aadhar, S., Mishra, V., 2020. Propagation of Meteorological to Hydrological Droughts in India. J. Geophys. Res. Atmos. 125. https://doi.org/10.1029/2020JD033455
37. Bisht, D.S., Sridhar, V., Mishra, A., Chatterjee, C., Raghuwanshi, N.S., 2019. Drought characterization over India under projected climate scenario. Int. J. Climatol. 39, 1889–1911. https://doi.org/10.1002/joc.5922
38. Blauhut, V., Gudmundsson, L., Stahl, K., 2015. Towards pan-European drought risk maps: Quantifying the link between drought indices and reported drought impacts. Environ. Res. Lett. 10. https://doi.org/10.1088/1748-9326/10/1/014008
39. Bokusheva, R., Kogan, F., Vitkovskaya, I., Conradt, S., Batyrbayeva, M., 2016. Satellite-based vegetation health indices as a criteria for insuring against drought-related yield losses. Agric. For. Meteorol. 220, 200–206. https://doi.org/10.1016/j.agrformet.2015.12.066
40. Bonaccorso, B., Peres, D.J., Castano, A., Cancelliere, A., 2015. SPI-Based Probabilistic Analysis of Drought Areal Extent in Sicily. Water Resour. Manag. 29, 459–470. https://doi.org/10.1007/s11269-014-0673-4
41. Bonsal, B.R., Wheaton, E.E., Chipanshi, A.C., Lin, C., Sauchyn, D.J., Wen, L., 2011. Drought Research in Canada: A Review. Atmosphere-Ocean 49, 303–319. https://doi.org/10.1080/07055900.2011.555103

42. Borgomeo, E., Pflug, G., Hall, J.W., Hochrainer-Stigler, S., 2015. Assessing water resource system vulnerability to unprecedented hydrological drought using copulas to characterize drought duration and deficit. Water Resour. Res. 51, 8927–8948. https://doi.org/10.1002/2015WR017324
43. Bosmans, J.H.C., Van Beek, L.P.H., Sutanudjaja, E.H., Bierkens, M.F.P., 2017. Hydrological impacts of global land cover change and human water use. Hydrol. Earth Syst. Sci. 21, 5603–5626. https://doi.org/10.5194/hess-21-5603-2017
44. Botai, J.O., Botai, C.M., de Wit, J.P., Muthoni, M., Adeola, A.M., 2019. Analysis of drought progression physiognomies in South Africa. Water (Switzerland) 11. https://doi.org/10.3390/w11020299
45. Brown, J.F., Wardlow, B.D., Tadesse, T., Hayes, M.J., Reed, B.C., 2008. The Vegetation Drought Response Index (VegDRI): A New Integrated Approach for Monitoring Drought Stress in Vegetation. GIScience Remote Sens. 45, 16–46. https://doi.org/10.2747/1548-1603.45.1.16
46. Burke, E.J., Brown, S.J., 2008. Evaluating uncertainties in the projection of future drought. J. Hydrometeorol. 9, 292–299. https://doi.org/10.1175/2007JHM929.1
47. Burke, E.J., Perry, R.H.J., Brown, S.J., 2010. An extreme value analysis of UK drought and projections of change in the future. J. Hydrol. 388, 131–143. https://doi.org/10.1016/j.jhydrol.2010.04.035
48. Cai, W., Santoso, A., Wang, G., Weller, E., Wu, L., Ashok, K., Masumoto, Y., Yamagata, T., 2014. Increased frequency of extreme Indian Ocean Dipole events due to greenhouse warming. Nature 510, 254–258. https://doi.org/10.1038/nature13327
49. Cancelliere, A., 2017. Non Stationary Analysis of Extreme Events. Water Resour. Manag. 31, 3097–3110. https://doi.org/10.1007/s11269-017-1724-4
50. Cao, F., Gao, T., 2019. Effect of climate change on the centennial drought over China using high-resolution NASA-NEX downscaled climate ensemble data. Theor. Appl. Climatol. 138, 1189–1202. https://doi.org/10.1007/s00704-019-02895-9
51. Cavazos, T., Rivas, D., 2004. Variability of extreme precipitation events in Tijuana, Mexico. Clim. Res. 25, 229–243. https://doi.org/10.3354/cr025229
52. Cavus, Y., Aksoy, H., 2020. Critical drought severity/intensity-duration-frequency curves based on precipitation deficit. J. Hydrol. 584. https://doi.org/10.1016/j.jhydrol.2019.124312
53. Chang, J., Li, Y., Wang, Y., Yuan, M., 2016. Copula-based drought risk assessment

combined with an integrated index in the Wei River Basin, China. J. Hydrol. 540, 824–834. https://doi.org/10.1016/j.jhydrol.2016.06.064

54. Chang, X., Wang, B., Yan, Y., Hao, Y., Zhang, M., 2019. Characterizing effects of monsoons and climate teleconnections on precipitation in China using wavelet coherence and global coherence. Clim. Dyn. 52, 5213–5228. https://doi.org/10.1007/s00382-018-4439-1
55. Chattopadhyay, R., Phani, R., Sabeerali, C.T., Dhakate, A.R., Salunke, K.D., Mahapatra, S., Rao, A.S., Goswami, B.N., 2015. Influence of extratropical sea-surface temperature on the Indian summer monsoon: an unexplored source of seasonal predictability. Q. J. R. Meteorol. Soc. 141, 2760–2775. https://doi.org/10.1002/qj.2562
56. Chen, N., Li, R., Zhang, X., Yang, C., Wang, X., Zeng, L., Tang, S., Wang, W., Li, D., Niyogi, D., 2020. Drought propagation in Northern China Plain: A comparative analysis of GLDAS and MERRA-2 datasets. J. Hydrol. 588. https://doi.org/10.1016/j.jhydrol.2020.125026
57. Chen, S., Liu, W., Ye, T., 2020. Dataset of trend-preserving bias-corrected daily temperature, precipitation and wind from NEX-GDDP and CMIP5 over the Qinghai-Tibet Plateau. Data Br. 31, 105733. https://doi.org/10.1016/j.dib.2020.105733
58. Cheng, L., Aghakouchak, A., 2014. Nonstationary precipitation intensity-duration-frequency curves for infrastructure design in a changing climate. Sci. Rep. 4, 1–6. https://doi.org/10.1038/srep07093
59. Clayton, D.G., 1978. A model for association in bivariate life tables and its application in epidemiological studies of familial tendency in chronic disease incidence. Biometrika 65, 141–151. https://doi.org/10.1093/biomet/65.1.141
60. Cole, T.J., Green, P.J., 1992. Smoothing reference centile curves: The lms method and penalized likelihood. Stat. Med. 11, 1305–1319. https://doi.org/10.1002/sim.4780111005
61. Coles, S., 2001. An introduction to statistical modeling of extreme values. Springer, London.
62. Cook, B.I., Mankin, J.S., Marvel, K., Williams, A.P., Smerdon, J.E., Anchukaitis, K.J., 2020. Twenty-First Century Drought Projections in the CMIP6 Forcing Scenarios. Earth's Futur. 8. https://doi.org/10.1029/2019EF001461
63. Dai, A., 2013. Increasing drought under global warming in observations and models.

Nat. Clim. Chang. 3, 52–58. https://doi.org/10.1038/nclimate1633

64. Dai, A., 2011a. Drought under global warming: A review. Wiley Interdiscip. Rev. Clim. Chang. 2, 45–65. https://doi.org/10.1002/wcc.81
65. Dai, A., 2011b. Characteristics and trends in various forms of the Palmer Drought Severity Index during 1900-2008. J. Geophys. Res. Atmos. 116. https://doi.org/10.1029/2010JD015541
66. Dai, A.G., 2013. Increasing drought under global warming in observations and models. Nat. Clim. Chang. 3, 52–58. https://doi.org/10.1038/nclimate1633
67. Dai, M., Huang, S., Huang, Q., Leng, G., Guo, Y., Wang, L., Fang, W., Li, P., Zheng, X., 2020. Assessing agricultural drought risk and its dynamic evolution characteristics. Agric. Water Manag. 231. https://doi.org/10.1016/j.agwat.2020.106003
68. Dalezios, N.R., Blanta, A., Spyropoulos, N. V., Tarquis, A.M., 2014. Risk identification of agricultural drought for sustainable Agroecosystems. Nat. Hazards Earth Syst. Sci. 14, 2435–2448. https://doi.org/10.5194/nhess-14-2435-2014
69. Dandekar, P., 2013. Drought in Maharashtra: The real story. India Together.
70. Das, J., Jha, S., Goyal, M.K., 2020a. Non-stationary and copula-based approach to assess the drought characteristics encompassing climate indices over the Himalayan states in India. J. Hydrol. 580. https://doi.org/10.1016/j.jhydrol.2019.124356
71. Das, J., Jha, S., Goyal, M.K., 2020b. On the relationship of climatic and monsoon teleconnections with monthly precipitation over meteorologically homogenous regions in India: Wavelet & global coherence approaches, Atmospheric Research. https://doi.org/10.1016/j.atmosres.2020.104889
72. Das, J., Jha, S., Goyal, M.K., Surampalli, R.Y., 2020c. Challenges of Sustainability in Agricultural Management, in: Sustainability. Wiley, pp. 339–356. https://doi.org/10.1002/9781119434016.ch16
73. Das, J., Umamahesh, N. V., 2021. Investigating risk, reliability and return period under the influence of large scale modes, and regional hydrological variability in hydrologic extremes. Hydrol. Sci. J. 1–17. https://doi.org/10.1080/02626667.2021.1998512
74. Das, J., Umamahesh, N. V., 2018. Assessment of uncertainty in estimating future flood return levels under climate change. Nat. Hazards 1–16. https://doi.org/10.1007/s11069-018-3291-2

75. Das, P.K., Das, R., Das, D.K., Midya, S.K., Bandyopadhyay, S., Raj, U., 2020. Quantification of agricultural drought over Indian region: a multivariate phenology-based approach. Nat. Hazards 101, 255–274. https://doi.org/10.1007/s11069-020-03872-6
76. Debele, S.E., Strupczewski, W.G., Bogdanowicz, E., 2017. A comparison of three approaches to non-stationary flood frequency analysis. Acta Geophys. 65, 863–883. https://doi.org/10.1007/s11600-017-0071-4
77. Diaz, V., Corzo Perez, G.A., Van Lanen, H.A.J., Solomatine, D., Varouchakis, E.A., 2020. Characterisation of the dynamics of past droughts. Sci. Total Environ. 718. https://doi.org/10.1016/j.scitotenv.2019.134588
78. Ding, Y., Gong, X., Xing, Z., Cai, H., Zhou, Z., Zhang, D., Sun, P., Shi, H., 2021a. Attribution of meteorological, hydrological and agricultural drought propagation in different climatic regions of China. Agric. Water Manag. 255. https://doi.org/10.1016/j.agwat.2021.106996
79. Ding, Y., Xu, J., Wang, X., Cai, H., Zhou, Z., Sun, Y., Shi, H., 2021b. Propagation of meteorological to hydrological drought for different climate regions in China. J. Environ. Manage. 283. https://doi.org/10.1016/j.jenvman.2021.111980
80. Douville, H., Raghavan, K., Renwick, J., Allan, R.P., Arias, P.A., Barlow, M., Cerezo-Mota, R., Cherchi, A., Gan, T.Y., Gergis, J., 2021. Water cycle changes. Clim. Chang.
81. Du, C., Chen, J., Nie, T., Dai, C., 2021. Spatial–temporal changes in meteorological and agricultural droughts in Northeast China: change patterns, response relationships and causes. Nat. Hazards. https://doi.org/10.1007/s11069-021-04940-1
82. Dubois, D., 2006. Possibility theory and statistical reasoning. Comput. Stat. Data Anal. 51, 47–69. https://doi.org/10.1016/j.csda.2006.04.015
83. Dutta, D., Kundu, A., Patel, N.R., 2013. Predicting agricultural drought in eastern Rajasthan of India using NDVI and standardized precipitation index. Geocarto Int. 28, 192–209. https://doi.org/10.1080/10106049.2012.679975
84. Fan, Y., van den Dool, H., 2004. Climate Prediction Center global monthly soil moisture data set at 0.5° resolution for 1948 to present. J. Geophys. Res. D Atmos. 109, D10102. https://doi.org/10.1029/2003JD004345
85. Fang, B., Kansara, P., Dandridge, C., Lakshmi, V., 2021. Drought monitoring using high spatial resolution soil moisture data over Australia in 2015–2019. J. Hydrol.

594. https://doi.org/10.1016/j.jhydrol.2021.125960

86. Favre, A.-C., El Adlouni, S., Perreault, L., Thiémonge, N., Bobée, B., 2004. Multivariate hydrological frequency analysis using copulas. Water Resour. Res. 40. https://doi.org/10.1029/2003WR002456
87. Feng, K., Su, X., Singh, V.P., Ayantobo, O.O., Zhang, G., Wu, H., Zhang, Z., 2021. Dynamic evolution and frequency analysis of hydrological drought from a three-dimensional perspective. J. Hydrol. 600. https://doi.org/10.1016/j.jhydrol.2021.126675
88. Feng, X., Merow, C., Liu, Z., Park, D.S., Roehrdanz, P.R., Maitner, B., Newman, E.A., Boyle, B.L., Lien, A., Burger, J.R., Pires, M.M., Brando, P.M., Bush, M.B., McMichael, C.N.H., Neves, D.M., Nikolopoulos, E.I., Saleska, S.R., Hannah, L., Breshears, D.D., Evans, T.P., Soto, J.R., Ernst, K.C., Enquist, B.J., 2021. How deregulation, drought and increasing fire impact Amazonian biodiversity. Nature 597, 516–521. https://doi.org/10.1038/s41586-021-03876-7
89. Ferreira, V.G., Montecino, H.C., Ndehedehe, C.E., Heck, B., Gong, Z., de Freitas, S.R.C., Westerhaus, M., 2018. Space-based observations of crustal deflections for drought characterization in Brazil. Sci. Total Environ. 644, 256–273. https://doi.org/10.1016/j.scitotenv.2018.06.277
90. Forootan, E., Khaki, M., Schumacher, M., Wulfmeyer, V., Mehrnegar, N., van Dijk, A.I.J.M., Brocca, L., Farzaneh, S., Akinluyi, F., Ramillien, G., Shum, C.K., Awange, J., Mostafaie, A., 2019. Understanding the global hydrological droughts of 2003–2016 and their relationships with teleconnections. Sci. Total Environ. 650, 2587–2604. https://doi.org/10.1016/j.scitotenv.2018.09.231
91. Frame, D.J., Rosier, S.M., Noy, I., Harrington, L.J., Carey-Smith, T., Sparrow, S.N., Stone, D.A., Dean, S.M., 2020. Climate change attribution and the economic costs of extreme weather events: a study on damages from extreme rainfall and drought. Clim. Change 162, 781–797. https://doi.org/10.1007/s10584-020-02729-y
92. Frischen, J., Meza, I., Rupp, D., Wietler, K., Hagenlocher, M., 2020. Drought risk to agricultural systems in Zimbabwe: A spatial analysis of hazard, exposure, and vulnerability. Sustain. 12. https://doi.org/10.3390/su12030752
93. Fu, A., Li, W., Chen, Y., Wang, Y., Hao, H., Li, Y., Sun, F., Zhou, H., Zhu, C., Hao, X., 2021. The effects of ecological rehabilitation projects on the resilience of an extremely drought-prone desert riparian forest ecosystem in the Tarim River Basin,

Xinjiang, China. Sci. Rep. 11. https://doi.org/10.1038/s41598-021-96742-5

94. Ganguli, P., Reddy, M.J., 2014. Evaluation of trends and multivariate frequency analysis of droughts in three meteorological subdivisions of western India. Int. J. Climatol. 34, 911–928. https://doi.org/10.1002/joc.3742
95. Ganguly, D., Rasch, P.J., Wang, H., Yoon, J., 2012. Fast and slow responses of the South Asian monsoon system to anthropogenic aerosols. Geophys. Res. Lett. 39. https://doi.org/10.1029/2012GL053043
96. Gao, M., Mo, D., Wu, X., 2016. Nonstationary modeling of extreme precipitation in China. Atmos. Res. 182, 1–9. https://doi.org/10.1016/j.atmosres.2016.07.014
97. Ge, Y., Apurv, T., Cai, X., 2016. Spatial and temporal patterns of drought in the Continental U.S. during the past century. Geophys. Res. Lett. 43, 6294–6303. https://doi.org/10.1002/2016GL069660
98. Geethalakshmi, V., Yatagai, A., Palanisamy, K., Umetsu, C., 2009. Impact of ENSO and the Indian Ocean Dipole on the north-east monsoon rainfall of Tamil Nadu State in India. Hydrol. Process. 23, 633–647. https://doi.org/10.1002/hyp.7191
99. Gelaro, R., McCarty, W., Suárez, M.J., Todling, R., Molod, A., Takacs, L., Randles, C.A., Darmenov, A., Bosilovich, M.G., Reichle, R., Wargan, K., Coy, L., Cullather, R., Draper, C., Akella, S., Buchard, V., Conaty, A., da Silva, A.M., Gu, W., Kim, G.-K., Koster, R., Lucchesi, R., Merkova, D., Nielsen, J.E., Partyka, G., Pawson, S., Putman, W., Rienecker, M., Schubert, S.D., Sienkiewicz, M., Zhao, B., 2017. The Modern-Era Retrospective Analysis for Research and Applications, Version 2 (MERRA-2). J. Clim. 30, 5419–5454. https://doi.org/10.1175/JCLI-D-16-0758.1
100. Gevaert, A.I., Veldkamp, T.I.E., Ward, P.J., 2018. The effect of climate type on timescales of drought propagation in an ensemble of global hydrological models. Hydrol. Earth Syst. Sci. 22, 4649–4665. https://doi.org/10.5194/hess-22-4649-2018
101. Ghosh, S., Mujumdar, P.P., 2009. Climate change impact assessment: Uncertainty modeling with imprecise probability. J. Geophys. Res. 114, D18113. https://doi.org/10.1029/2008JD011648
102. Gidey, E., Dikinya, O., Sebego, R., Segosebe, E., Zenebe, A., 2018. Analysis of the long-term agricultural drought onset, cessation, duration, frequency, severity and spatial extent using Vegetation Health Index (VHI) in Raya and its environs, Northern Ethiopia. Environ. Syst. Res. 7, 13. https://doi.org/10.1186/s40068-018-0115-z

103. Gilroy, K.L., McCuen, R.H., 2012. A nonstationary flood frequency analysis method to adjust for future climate change and urbanization. J. Hydrol. 414–415, 40–48. https://doi.org/10.1016/j.jhydrol.2011.10.009
104. Giorgi, F., Mearns, L.O., 2003. Probability of regional climate change based on the Reliability Ensemble Averaging (REA) method. Geophys. Res. Lett. 30, 2–5. https://doi.org/10.1029/2003GL017130
105. Giorgi, F., Raffaele, F., Coppola, E., 2019. The response of precipitation characteristics to global warming from climate projections. Earth Syst. Dyn. 10, 73–89. https://doi.org/10.5194/esd-10-73-2019
106. González, J., Valdés, J.B., 2006. New drought frequency index: Definition and comparative performance analysis. Water Resour. Res. 42. https://doi.org/10.1029/2005WR004308
107. González, J., Valdés, J.B., 2003. Bivariate Drought Recurrence Analysis Using Tree Ring Reconstructions. J. Hydrol. Eng. 8, 247–258. https://doi.org/10.1061/(asce)1084-0699(2003)8:5(247)
108. Gore, P.G., Ray, K.C.., 2002. VARIABILITY IN DROUGHT INCIDENCE OVER DISTRICTS OF MAHARASHTRA. Mausam,53 4, 533–538.
109. Greve, P., Orlowsky, B., Mueller, B., Sheffield, J., Reichstein, M., Seneviratne, S.I., 2014. Global assessment of trends in wetting and drying over land. Nat. Geosci. 7, 716–721. https://doi.org/10.1038/ngeo2247
110. Grimaldi, S., Serinaldi, F., 2006. Asymmetric copula in multivariate flood frequency analysis. Adv. Water Resour. 29, 1155–1167. https://doi.org/10.1016/j.advwatres.2005.09.005
111. Gu, G., Adler, R.F., Huffman, G.J., Curtis, S., 2007. Tropical rainfall variability on interannual-to-interdecadal and longer time scales derived from the GPCP monthly product. J. Clim. 20, 4033–4046. https://doi.org/10.1175/JCLI4227.1
112. Gudmundsson, L., Bremnes, J.B., Haugen, J.E., Engen-Skaugen, T., 2012. Technical Note: Downscaling RCM precipitation to the station scale using statistical transformations – A comparison of methods. Hydrol. Earth Syst. Sci. https://doi.org/10.5194/hess-16-3383-2012
113. Gudmundsson, L., Stagge, J.H., 2015. Package SCI: Standardized Climate Indices such as SPI, SRI or SPEI, R package version 1.0. 1.
114. Guo, D., Westra, S., Maier, H.R., 2017. Sensitivity of potential evapotranspiration to

changes in climate variables for different Australian climatic zones. Hydrol. Earth Syst. Sci. 21, 2107–2126. https://doi.org/10.5194/hess-21-2107-2017

115. Guo, H., Li, M., Nzabarinda, V., Bao, A., Meng, X., Zhu, L., Maeyer, P. De, 2022. Assessment of Three Long-Term Satellite-Based Precipitation Estimates against Ground Observations for Drought Characterization in Northwestern China. Remote Sens. 14. https://doi.org/10.3390/rs14040828
116. Guo, H., Wang, R., Garfin, G.M., Zhang, A., Lin, D., Liang, Q., Wang, J., 2021. Rice drought risk assessment under climate change: Based on physical vulnerability a quantitative assessment method. Sci. Total Environ. 751. https://doi.org/10.1016/j.scitotenv.2020.141481
117. Gupta, A., Rico-Medina, A., Caño-Delgado, A.I., 2020. The physiology of plant responses to drought. Science (80-.). 368, 266–269. https://doi.org/10.1126/science.aaz7614
118. Gupta, R., Somanathan, E., Dey, S., 2017. Global warming and local air pollution have reduced wheat yields in India. Clim. Change 140, 593–604. https://doi.org/10.1007/s10584-016-1878-8
119. Gupta, V., Jain, M.K., 2018. Investigation of multi-model spatiotemporal mesoscale drought projections over India under climate change scenario. J. Hydrol. 567, 489–509. https://doi.org/10.1016/j.jhydrol.2018.10.012
120. Hagman, G., Wijkman, A., Bendz, M., Beer, H., 1984. Prevention Better Than Cure: Report on Human and Environmental Disasters in the Third World. Swedish Red Cross.
121. Han, Z., Huang, S., Huang, Q., Leng, G., Wang, H., Bai, Q., Zhao, J., Ma, L., Wang, L., Du, M., 2019. Propagation dynamics from meteorological to groundwater drought and their possible influence factors. J. Hydrol. 578. https://doi.org/10.1016/j.jhydrol.2019.124102
122. Hanson, P.J., Weltzin, J.F., 2000. Drought disturbance from climate change: Response of United States forests. Sci. Total Environ. 262, 205–220. https://doi.org/10.1016/S0048-9697(00)00523-4
123. Hao, Z., AghaKouchak, A., 2014. A Nonparametric Multivariate Multi-Index Drought Monitoring Framework. J. Hydrometeorol. 15, 89–101. https://doi.org/10.1175/JHM-D-12-0160.1
124. Hao, Z., AghaKouchak, A., 2013. Multivariate Standardized Drought Index: A

parametric multi-index model. Adv. Water Resour. 57, 12–18. https://doi.org/10.1016/j.advwatres.2013.03.009

125. Hao, Z., Singh, V.P., 2015. Drought characterization from a multivariate perspective: A review. J. Hydrol. 527, 668–678. https://doi.org/10.1016/j.jhydrol.2015.05.031
126. Haslinger, K., Koffler, D., Schöner, W., Laaha, G., 2014. Exploring the link between meteorological drought and streamflow: Effects of climate-catchment interaction. Water Resour. Res. 50, 2468–2487. https://doi.org/10.1002/2013WR015051
127. He, B., Wu, J., Lü, A., Cui, X., Zhou, L., Liu, M., Zhao, L., 2013. Quantitative assessment and spatial characteristic analysis of agricultural drought risk in China. Nat. Hazards 66, 155–166. https://doi.org/10.1007/s11069-012-0398-8
128. He, X., Guan, H., 2013. Multiresolution analysis of precipitation teleconnections with large-scale climate signals: A case study in South Australia. Water Resour. Res. 49, 6995–7008. https://doi.org/10.1002/wrcr.20560
129. He, Y., Bárdossy, A., Brommundt, J., 2006. NON-STATIONARY FLOOD FREQUENCY ANALYSIS IN SOUThERN GERMANY, in: Proc. 7th International Conference on HydroScience and Engineering. p. 16.
130. Hellwig, J., Graaf, I.E.M., Weiler, M., Stahl, K., 2020. Large-Scale Assessment of Delayed Groundwater Responses to Drought. Water Resour. Res. 56. https://doi.org/10.1029/2019WR025441
131. Henriques, A.G., Santos, M.J.J., 1999. Regional drought distribution model. Phys. Chem. Earth, Part B Hydrol. Ocean. Atmos. https://doi.org/10.1016/S1464-1909(98)00005-7
132. Her, Y., Yoo, S.H., Cho, J., Hwang, S., Jeong, J., Seong, C., 2019. Uncertainty in hydrological analysis of climate change: multi-parameter vs. multi-GCM ensemble predictions. Sci. Rep. 9. https://doi.org/10.1038/s41598-019-41334-7
133. Hersbach, H., Bell, B., Berrisford, P., Hirahara, S., Horányi, A., Muñoz-Sabater, J., Nicolas, J., Peubey, C., Radu, R., Schepers, D., Simmons, A., Soci, C., Abdalla, S., Abellan, X., Balsamo, G., Bechtold, P., Biavati, G., Bidlot, J., Bonavita, M., Chiara, G., Dahlgren, P., Dee, D., Diamantakis, M., Dragani, R., Flemming, J., Forbes, R., Fuentes, M., Geer, A., Haimberger, L., Healy, S., Hogan, R.J., Hólm, E., Janisková, M., Keeley, S., Laloyaux, P., Lopez, P., Lupu, C., Radnoti, G., Rosnay, P., Rozum, I., Vamborg, F., Villaume, S., Thépaut, J., 2020. The ERA5 global reanalysis. Q. J. R. Meteorol. Soc. 146, 1999–2049. https://doi.org/10.1002/qj.3803

134. Hewitson, B.C., Daron, J., Crane, R.G., Zermoglio, M.F., Jack, C., 2014. Interrogating empirical-statistical downscaling. Clim. Change 122, 539–554. https://doi.org/10.1007/s10584-013-1021-z
135. Hijmans, R.J., van Etten, J., Sumner, M., Cheng, J., Bevan, A., Bivand, R., Busetto, L., Canty, M., Forrest, D., Ghosh, A., 2019. Package raster: Geographic Data Analysis and Modeling.
136. Himayoun, D., Roshni, T., 2019. Spatio-temporal variation of drought characteristics, water resource availability and the relation of drought with large scale climate indices: A case study of Jhelum basin, India. Quat. Int. https://doi.org/10.1016/j.quaint.2019.07.018
137. Ho, S., Tian, L., Disse, M., Tuo, Y., 2021. A new approach to quantify propagation time from meteorological to hydrological drought. J. Hydrol. 603. https://doi.org/10.1016/j.jhydrol.2021.127056
138. Hoerling, M., Eischeid, J., Perlwitz, J., 2010. Regional precipitation trends: Distinguishing natural variability from anthropogenic forcing. J. Clim. 23, 2131–2145. https://doi.org/10.1175/2009JCLI3420.1
139. Höllermann, B., Evers, M., 2017. Perception and handling of uncertainties in water management—A study of practitioners' and scientists' perspectives on uncertainty in their daily decision-making. Environ. Sci. Policy 71, 9–18. https://doi.org/10.1016/j.envsci.2017.02.003
140. Hu, J., Duan, A., 2015. Relative contributions of the Tibetan Plateau thermal forcing and the Indian Ocean Sea surface temperature basin mode to the interannual variability of the East Asian summer monsoon. Clim. Dyn. 45, 2697–2711. https://doi.org/10.1007/s00382-015-2503-7
141. Hu, Q., Feng, S., 2001. Variations of teleconnection of ENSO and interannual variation in summer rainfall in the Central United States. J. Clim. 14, 2469–2480. https://doi.org/10.1175/1520-0442(2001)014<2469:VOTOEA>2.0.CO;2
142. Huang, S., Huang, Q., Chang, J., Leng, G., 2016. Linkages between hydrological drought, climate indices and human activities: a case study in the Columbia River basin. Int. J. Climatol. 36, 280–290. https://doi.org/10.1002/joc.4344
143. Huang, S., Li, P., Huang, Q., Leng, G., Hou, B., Ma, L., 2017. The propagation from meteorological to hydrological drought and its potential influence factors. J. Hydrol. 547, 184–195. https://doi.org/10.1016/j.jhydrol.2017.01.041

144. Huang, S., Zhang, X., Chen, N., Li, B., Ma, H., Xu, L., Li, R., Niyogi, D., 2021. Drought propagation modification after the construction of the Three Gorges Dam in the Yangtze River Basin. J. Hydrol. 603. https://doi.org/10.1016/j.jhydrol.2021.127138
145. Ionita, M., Boroneanț, C., Chelcea, S., 2015. Seasonal modes of dryness and wetness variability over Europe and their connections with large scale atmospheric circulation and global sea surface temperature. Clim. Dyn. 45, 2803–2829. https://doi.org/10.1007/s00382-015-2508-2
146. Ionita, M., Lohmann, G., Rimbu, N., Chelcea, S., Dima, M., 2012. Interannual to decadal summer drought variability over Europe and its relationship to global sea surface temperature. Clim. Dyn. 38, 363–377. https://doi.org/10.1007/s00382-011-1028-y
147. IPCC, 2014a. Climate Change 2014: Synthesis Report. Contribution of Working Groups I, II and III to the Fifth Assessment Report of the Intergovernmental Panel on Climate Change. [Core Writing Team, R.K. Pachauri and L.A. Meyer (eds.)]. Geneva, Switzerland. https://doi.org/10.1017/CBO9781107415324
148. IPCC, 2014b. Climate Change 2014: Synthesis Report. Contribution of Working Groups I, II and III to the Fifth Assessment Report of the Intergovernmental Panel on Climate Change, Core Writing Team, R.K. Pachauri and L.A. Meyer. https://doi.org/10.1017/CBO9781107415324.004
149. Islam, A., Sikka, A.K., Saha, B., Singh, A., 2012. Streamflow Response to Climate Change in the Brahmani River Basin, India. Water Resour. Manag. 26, 1409–1424. https://doi.org/10.1007/s11269-011-9965-0
150. Jain, Shipra, Salunke, P., Mishra, S.K., Sahany, S., Choudhary, N., 2019. Advantage of NEX-GDDP over CMIP5 and CORDEX Data: Indian Summer Monsoon. Atmos. Res. 228, 152–160. https://doi.org/10.1016/j.atmosres.2019.05.026
151. Jain, Sahil, Saran, A., Mishra, V., 2019. On the causes and severity of the 2016-17 South India drought, in: AGU Fall Meeting 2019.
152. Javed, T., Zhang, J., Bhattarai, N., Sha, Z., Rashid, S., Yun, B., Ahmad, S., Henchiri, M., Kamran, M., 2021. Drought characterization across agricultural regions of China using standardized precipitation and vegetation water supply indices. J. Clean. Prod. 313. https://doi.org/10.1016/j.jclepro.2021.127866
153. Jehanzaib, M., Kim, T.-W., 2020. Exploring the influence of climate change-induced

drought propagation on wetlands. Ecol. Eng. 149, 105799. https://doi.org/10.1016/j.ecoleng.2020.105799

154. Jehanzaib, M., Sattar, M.N., Lee, J.-H., Kim, T.-W., 2020. Investigating effect of climate change on drought propagation from meteorological to hydrological drought using multi-model ensemble projections. Stoch. Environ. Res. Risk Assess. 34, 7–21. https://doi.org/10.1007/s00477-019-01760-5
155. Jehanzaib, M., Yoo, J., Kwon, H.H., Kim, T.W., 2021. Reassessing the frequency and severity of meteorological drought considering non-stationarity and copula-based bivariate probability. J. Hydrol. 603. https://doi.org/10.1016/j.jhydrol.2021.126948
156. Jensen, M.E., Allen, R.G., 2016. Evaporation, evapotranspiration, and irrigation water requirements, Evaporation, Evapotranspiration, and Irrigation Water Requirements. American Society of Civil Engineers, Reston, VA. https://doi.org/10.1061/9780784414057
157. Johnson, F., Sharma, A., 2015. What are the impacts of bias correction on future drought projections? J. Hydrol. 525, 472–485. https://doi.org/10.1016/j.jhydrol.2015.04.002
158. Jones, P.W., 1999. First- and second-order conservative remapping schemes for grids in spherical coordinates. Mon. Weather Rev. 127, 2204–2210. https://doi.org/10.1175/1520-0493(1999)127<2204:FASOCR>2.0.CO;2
159. Kanamitsu, M., Ebisuzaki, W., Woollen, J., Yang, S.-K., Hnilo, J.J., Fiorino, M., Potter, G.L., 2002. NCEP–DOE AMIP-II Reanalysis (R-2). Bull. Am. Meteorol. Soc. 83, 1631–1644. https://doi.org/10.1175/BAMS-83-11-1631
160. Kao, S.-C., Govindaraju, R.S., 2010. A copula-based joint deficit index for droughts. J. Hydrol. 380, 121–134. https://doi.org/10.1016/j.jhydrol.2009.10.029
161. Kao, S.C., Govindaraju, R.S., 2008. Trivariate statistical analysis of extreme rainfall events via the Plackett family of copulas. Water Resour. Res. 44. https://doi.org/10.1029/2007WR006261
162. Katz, R.W., Parlange, M.B., Naveau, P., 2002. Statistics of extremes in hydrology. Adv. Water Resour. 25, 1287–1304. https://doi.org/10.1016/S0309-1708(02)00056-8
163. Keellings, D., Engström, J., 2019. The future of drought in the Southeastern U.S.: Projections from downscaled CMIP5 models. Water (Switzerland) 11. https://doi.org/10.3390/w11020259

164. Kelkar, S.M., Kulkarni, A., Rao, K.K., 2020. Impact of climate variability and change on crop production in Maharashtra, India. Curr. Sci. 118, 1235–1245. https://doi.org/10.18520/cs/v118/i8/1235-1245
165. Kendall, M.G., 1955. Rank correlation methods. Hafner Publishing Co., Oxford, England.
166. Khadr, M., 2017. Temporal and spatial analysis of meteorological drought characteristics in the upper Blue Nile river region. Hydrol. Res. 48, 265–276. https://doi.org/10.2166/nh.2016.194
167. Khan, N., Shahid, S., Ahmed, K., Wang, X., Ali, R., Ismail, T., Nawaz, N., 2020. Selection of GCMs for the projection of spatial distribution of heat waves in Pakistan. Atmos. Res. https://doi.org/10.1016/j.atmosres.2019.104688
168. Kingston, D.G., Todd, M.C., Taylor, R.G., Thompson, J.R., Arnell, N.W., 2009. Uncertainty in the estimation of potential evapotranspiration under climate change. Geophys. Res. Lett. 36, L20403. https://doi.org/10.1029/2009GL040267
169. Kogan, F., 2002. World droughts in the new millennium from AVHRR-based vegetation health indices. Eos, Trans. Am. Geophys. Union 83, 557. https://doi.org/10.1029/2002EO000382
170. Kogan, F., Goldberg, M., Schott, T., Guo, W., 2015. Suomi NPP/VIIRS: improving drought watch, crop loss prediction, and food security. Int. J. Remote Sens. 36, 5373–5383. https://doi.org/10.1080/01431161.2015.1095370
171. Kogan, F.N., 1995. Application of vegetation index and brightness temperature for drought detection. Adv. Sp. Res. 15, 91–100. https://doi.org/10.1016/0273-1177(95)00079-T
172. Kogan, F.N., 1990. Remote sensing of weather impacts on vegetation in non-homogeneous areas. Int. J. Remote Sens. 11, 1405–1419. https://doi.org/10.1080/01431169008955102
173. Konapala, G., Mishra, A.K., Wada, Y., Mann, M.E., 2020. Climate change will affect global water availability through compounding changes in seasonal precipitation and evaporation. Nat. Commun. 11. https://doi.org/10.1038/s41467-020-16757-w
174. Kundzewicz, Z.W., Kaczmarek, Z., 2000. Coping with hydrological extremes. Water Int. 25, 66–75. https://doi.org/10.1080/02508060008686798
175. Kundzewicz, Z.W., Mata, L.J., Arnell, N.W., DÖLL, P., Jimenez, B., Miller, K., Oki,

T., ŞEN, Z., Shiklomanov, I., 2008. The implications of projected climate change for freshwater resources and their management. Hydrol. Sci. J. https://doi.org/10.1623/hysj.53.1.3

176. Lehner, F., Coats, S., Stocker, T.F., Pendergrass, A.G., Sanderson, B.M., Raible, C.C., Smerdon, J.E., 2017. Projected drought risk in 1.5°C and 2°C warmer climates. Geophys. Res. Lett. 44, 7419–7428. https://doi.org/10.1002/2017GL074117
177. Leng, G., Leung, L.R., Huang, M., 2016. Irrigation impacts on the water cycle and regional climate simulated by the ACME Model, in: American Geophysical Union, Fall Meeting 2016. pp. GC31B-1122.
178. Li, C., Singh, V.P., Mishra, A.K., 2013a. A bivariate mixed distribution with a heavy-tailed component and its application to single-site daily rainfall simulation. Water Resour. Res. 49, 767–789. https://doi.org/10.1002/wrcr.20063
179. Li, C., Singh, V.P., Mishra, A.K., 2013b. A bivariate mixed distribution with a heavy-tailed component and its application to single-site daily rainfall simulation. Water Resour. Res. 49, 767–789. https://doi.org/10.1002/wrcr.20063
180. Li, F., Zheng, Q., 2016. Probabilistic modelling of flood events using the entropy copula. Adv. Water Resour. 97, 233–240. https://doi.org/10.1016/j.advwatres.2016.09.016
181. Li, H., Wang, D., Singh, V.P., Wang, Y., Wu, Jianfeng, Wu, Jichun, Liu, J., Zou, Y., He, R., Zhang, J., 2019. Non-stationary frequency analysis of annual extreme rainfall volume and intensity using Archimedean copulas: A case study in eastern China. J. Hydrol. 571, 114–131. https://doi.org/10.1016/j.jhydrol.2019.01.054
182. Li, J.Z., Wang, Y.X., Li, S.F., Hu, R., 2015. A nonstationary standardized precipitation index incorporating climate indices as covariates. J. Geophys. Res. 120, 12,082-12,095. https://doi.org/10.1002/2015JD023920
183. Li, M., Wu, P., Ma, Z., 2020. A comprehensive evaluation of soil moisture and soil temperature from third-generation atmospheric and land reanalysis data sets. Int. J. Climatol. 40, 5744–5766. https://doi.org/10.1002/joc.6549
184. Li, Q., Chen, L., Xu, Y., 2022. Drought risk and water resources assessment in the Beijing-Tianjin-Hebei region, China. Sci. Total Environ. 832. https://doi.org/10.1016/j.scitotenv.2022.154915
185. Li, Z., Shao, Q., Tian, Q., Zhang, L., 2020. Copula-based drought severity-area-frequency curve and its uncertainty, a case study of Heihe River basin, China.

Hydrol. Res. 51, 867–881. https://doi.org/10.2166/nh.2020.173

186. Liu, L., Gudmundsson, L., Hauser, M., Qin, D., Li, S., Seneviratne, S.I., 2019. Revisiting assessments of ecosystem drought recovery. Environ. Res. Lett. 14. https://doi.org/10.1088/1748-9326/ab4c61
187. Liu, Q., Yang, Z., 2010. Quantitative estimation of the impact of climate change on actual evapotranspiration in the Yellow River Basin, China. J. Hydrol. 395, 226–234. https://doi.org/10.1016/j.jhydrol.2010.10.031
188. Liu, W.T., Kogan, F.N., 1996. Monitoring regional drought using the vegetation condition index. Int. J. Remote Sens. 17, 2761–2782. https://doi.org/10.1080/01431169608949106
189. Liu, X., Guo, P., Tan, Q., Xin, J., Li, Y., Tang, Y., 2019a. Drought risk evaluation model with interval number ranking and its application. Sci. Total Environ. 685, 1042–1057. https://doi.org/10.1016/j.scitotenv.2019.06.260
190. Liu, X., Guo, P., Tan, Q., Xin, J., Li, Y., Tang, Y., 2019b. Drought risk evaluation model with interval number ranking and its application. Sci. Total Environ. 685, 1042–1057. https://doi.org/10.1016/j.scitotenv.2019.06.260
191. Liu, X., Pan, Y., Zhu, X., Yang, T., Bai, J., Sun, Z., 2018. Drought evolution and its impact on the crop yield in the North China Plain. J. Hydrol. 564, 984–996. https://doi.org/10.1016/j.jhydrol.2018.07.077
192. Liu, X., Zhu, X., Zhang, Q., Yang, T., Pan, Y., Sun, P., 2020. A remote sensing and artificial neural network-based integrated agricultural drought index: Index development and applications. Catena 186. https://doi.org/10.1016/j.catena.2019.104394
193. Lloyd-Hughes, B., 2014. The impracticality of a universal drought definition. Theor. Appl. Climatol. 117, 607–611. https://doi.org/10.1007/s00704-013-1025-7
194. Lobell, D.B., Deines, J.M., Tommaso, S. Di, 2020. Changes in the drought sensitivity of US maize yields. Nat. Food 1, 729–735. https://doi.org/10.1038/s43016-020-00165-w
195. Lorenzo-Lacruz, J., Vicente-Serrano, S.M., González-Hidalgo, J.C., López-Moreno, J.I., Cortesi, N., 2013. Hydrological drought response to meteorological drought in the Iberian Peninsula. Clim. Res. 58, 117–131. https://doi.org/10.3354/cr01177
196. Lu, J., Carbone, G.J., Grego, J.M., 2019. Uncertainty and hotspots in 21st century projections of agricultural drought from CMIP5 models. Sci. Rep. 9, 4922.

https://doi.org/10.1038/s41598-019-41196-z

197. Ma, Y., Guga, S., Xu, J., Liu, X., Tong, Z., Zhang, J., 2022. Assessment of Maize Drought Risk in Midwestern Jilin Province: A Comparative Analysis of TOPSIS and VIKOR Models. Remote Sens. 14, 2399. https://doi.org/10.3390/rs14102399
198. Madadgar, S., AghaKouchak, A., Farahmand, A., Davis, S.J., 2017. Probabilistic estimates of drought impacts on agricultural production. Geophys. Res. Lett. 44, 7799–7807. https://doi.org/10.1002/2017GL073606
199. Maity, R., Kumar, D.N., 2007. Hydroclimatic teleconnection between global sea surface temperature and rainfall over India at subdivisional monthly scale. Hydrol. Process. 21, 1802–1813. https://doi.org/10.1002/hyp.6300
200. Mallya, G., Mishra, V., Niyogi, D., Tripathi, S., Govindaraju, R.S., 2015. Trends and variability of droughts over the Indian monsoon region. Weather Clim. Extrem. 12, 43–68. https://doi.org/10.1016/j.wace.2016.01.002
201. Mamalakis, A., Langousis, A., Deidda, R., Marrocu, M., 2017. A parametric approach for simultaneous bias correction and high-resolution downscaling of climate model rainfall. Water Resour. Res. 53, 2149–2170. https://doi.org/10.1002/2016WR019578
202. Manabe, S., Wetherald, R.T., 1967. Thermal Equilibrium of the Atmosphere with a Given Distribution of Relative Humidity. J. Atmos. Sci. 24, 241–259. https://doi.org/10.1175/1520-0469(1967)024<0241:teotaw>2.0.co;2
203. Manning, C., Widmann, M., Bevacqua, E., Van Loon, A.F., Maraun, D., Vrac, M., 2018. Soil Moisture Drought in Europe: A Compound Event of Precipitation and Potential Evapotranspiration on Multiple Time Scales. J. Hydrometeorol. 19, 1255–1271. https://doi.org/10.1175/JHM-D-18-0017.1
204. Maraun, D., Shepherd, T.G., Widmann, M., Zappa, G., Walton, D., Gutiérrez, J.M., Hagemann, S., Richter, I., Soares, P.M.M., Hall, A., Mearns, L.O., 2017. Towards process-informed bias correction of climate change simulations. Nat. Clim. Chang. 7, 764–773. https://doi.org/10.1038/nclimate3418
205. Martin, E.R., 2018. Future Projections of Global Pluvial and Drought Event Characteristics. Geophys. Res. Lett. 45, 11,913-11,920. https://doi.org/10.1029/2018GL079807
206. Masson-Delmotte, V., P.Z., Pörtner, H.-O., Roberts, D., Skea, J., Shukla, P.R., Pirani, A., Moufouma-Okia, W., Péan, C., Pidcock, R., Connors, S., Matthews,

J.B.R., Chen, Y., Zhou, X., Lonnoy, M.I.G.E., T., M., Tignor, M., Waterfield, T., 2018. Global warming of 1.5°C. An IPCC Special Report on the impacts of global warming of 1.5°C above pre-industrial levels and related global greenhouse gas emission pathways, in the context of strengthening the global response to the threat of climate change, Ipcc - Sr15.

207. Matiu, M., Ankerst, D.P., Menzel, A., 2017. Interactions between temperature and drought in global and regional crop yield variability during 1961-2014. PLoS One 12. https://doi.org/10.1371/journal.pone.0178339
208. Mazdiyasni, O., AghaKouchak, A., Davis, S.J., Madadgar, S., Mehran, A., Ragno, E., Sadegh, M., Sengupta, A., Ghosh, S., Dhanya, C.T., Niknejad, M., 2017. Increasing probability of mortality during Indian heat waves. Sci. Adv. 3. https://doi.org/10.1126/sciadv.1700066
209. Mazdiyasni, O., Sadegh, M., Chiang, F., AghaKouchak, A., 2019. Heat wave Intensity Duration Frequency Curve: A Multivariate Approach for Hazard and Attribution Analysis. Sci. Rep. 9. https://doi.org/10.1038/s41598-019-50643-w
210. McCabe, G.J., Betancourt, J.L., Gray, S.T., Palecki, M.A., Hidalgo, H.G., 2008. Associations of multi-decadal sea-surface temperature variability with US drought. Quat. Int. 188, 31–40. https://doi.org/10.1016/j.quaint.2007.07.001
211. McCabe, G.J., Wolock, D.M., 2011. Independent effects of temperature and precipitation on modeled runoff in the conterminous United States. Water Resour. Res. 47. https://doi.org/10.1029/2011WR010630
212. McCormick, B.C., Eshleman, K.N., Griffith, J.L., Townsend, P.A., 2009. Detection of flooding responses at the river basin scale enhanced by land use change. Water Resour. Res. 45. https://doi.org/10.1029/2008WR007594
213. Mckee, T.B., Doesken, N.J., Kleist, J., 1993. The relationship of drought frequency and duration to time scales. AMS 8th Conf. Appl. Climatol. 179–184. https://doi.org/citeulike-article-id:10490403
214. McNally, A., 2018. NASA/GSFC/HSL, 2018. FLDAS Noah Land Surface Model L4 Global Monthly 0.1 x 0.1 degree (MERRA-2 and CHIRPS), Greenbelt, MD, USA, Goddard Earth Sciences Data and Information Services Center (GES DISC) [WWW Document]. URL 10.5067/5NHC22T9375G
215. McNally, A., Arsenault, K., Kumar, S., Shukla, S., Peterson, P., Wang, S., Funk, C., Peters-Lidard, C.D., Verdin, J.P., 2017. A land data assimilation system for sub-

Saharan Africa food and water security applications. Sci. Data 4. https://doi.org/10.1038/sdata.2017.12

216. Mearns, L.O., Rosenzweig, C., Goldberg, R., 1996. The effect of changes in daily and interannual climatic variability on ceres-wheat: A sensitivity study. Clim. Change 32, 257–292. https://doi.org/10.1007/BF00142465
217. Meehl, G.A., Stocker, T.F., Collins, W.D., Friedlingstein, P., Gaye, T., Gregory, J.M., Kitoh, A., Knutti, R., Murphy, J.M., Noda, A., 2007. Global climate projections: Climate Change 2007: the physical science basis. Contribution of Working Group I to the Fourth Assessment Report of the Intergovernmental Panel on Climate Change. Cambridge, UK, Cambridge University Press.
218. Merabtene, T., Kawamura, A., Jinno, K., Olsson, J., 2002. Risk assessment for optimal drought management of an integrated water resources system using a genetic algorithm. Hydrol. Process. 16, 2189–2208. https://doi.org/10.1002/hyp.1150
219. Meza, F.J., 2013. Recent trends and ENSO influence on droughts in Northern Chile: An application of the Standardized Precipitation Evapotranspiration Index. Weather Clim. Extrem. 1, 51–58. https://doi.org/10.1016/j.wace.2013.07.002
220. Meza, I., Siebert, S., Döll, P., Kusche, J., Herbert, C., Rezaei, E.E., Nouri, H., Gerdener, H., Popat, E., Frischen, J., Naumann, G., Vogt, J. V., Walz, Y., Sebesvari, Z., Hagenlocher, M., 2020. Global-scale drought risk assessment for agricultural systems. Nat. Hazards Earth Syst. Sci. 20, 695–712. https://doi.org/10.5194/nhess-20-695-2020
221. Milly, P.C.D., Betancourt, J., Falkenmark, M., Hirsch, R.M., Kundzewicz, Z.W., Lettenmaier, D.P., Stouffer, R.J., 2008. Stationarity Is Dead: Whither Water Management? Science (80-.). 319, 573–574. https://doi.org/10.1126/science.1151915
222. Mishra, Ashok K., Singh, V.P., 2010. A review of drought concepts. J. Hydrol. 391, 202–216. https://doi.org/10.1016/j.jhydrol.2010.07.012
223. Mishra, A.K., Singh, V.P., 2010. A review of drought concepts. J. Hydrol. 391, 202–216. https://doi.org/10.1016/j.jhydrol.2010.07.012
224. Mishra, A.K., Singh, V.P., 2009. Analysis of drought severity-area-frequency curves using a general circulation model and scenario uncertainty. J. Geophys. Res. Atmos. https://doi.org/10.1029/2008JD010986
225. Mishra, A.K., Singh, V.P., Desai, V.R., 2009. Drought characterization: a

probabilistic approach. Stoch. Environ. Res. Risk Assess. 23, 41–55. https://doi.org/10.1007/s00477-007-0194-2

226. Mishra, V., Aadhar, S., Asoka, A., Pai, S., Kumar, R., 2016. On the frequency of the 2015 monsoon season drought in the Indo-Gangetic Plain. Geophys. Res. Lett. 43, 12,102-12,112. https://doi.org/10.1002/2016GL071407
227. Mishra, V., Lilhare, R., 2016. Hydrologic sensitivity of Indian sub-continental river basins to climate change. Glob. Planet. Change 139, 78–96. https://doi.org/10.1016/j.gloplacha.2016.01.003
228. Mishra, V., Shah, R., Azhar, S., Shah, H., Modi, P., Kumar, R., 2017. Reconstruction of droughts in India using multiple land surface models (1951–2015). Hydrol. Earth Syst. Sci. Discuss. 1–22. https://doi.org/10.5194/hess-2017-302
229. Mishra, V., Shah, R., Thrasher, B., 2014a. Soil Moisture Droughts under the Retrospective and Projected Climate in India *. J. Hydrometeorol. 2267–2292. https://doi.org/10.1175/JHM-D-13-0177.1
230. Mishra, V., Shah, R., Thrasher, B., 2014b. Soil Moisture Droughts under the Retrospective and Projected Climate in India. J. Hydrometeorol. 15, 2267–2292. https://doi.org/10.1175/JHM-D-13-0177.1
231. Mishra, V., Smoliak, B. V., Lettenmaier, D.P., Wallace, J.M., 2012. A prominent pattern of year-to-year variability in Indian Summer Monsoon Rainfall. Proc. Natl. Acad. Sci. 109, 7213–7217. https://doi.org/10.1073/pnas.1119150109
232. Mishra, V., Thirumalai, K., Jain, S., Aadhar, S., 2021. Unprecedented drought in South India and recent water scarcity. Environ. Res. Lett. 16. https://doi.org/10.1088/1748-9326/abf289
233. Mishra, V., Tiwari, A.D., Aadhar, S., Shah, R., Xiao, M., Pai, D.S., Lettenmaier, D., 2019. Drought and Famine in India, 1870–2016. Geophys. Res. Lett. 46, 2075–2083. https://doi.org/10.1029/2018GL081477
234. Mondal, A., Mujumdar, P.P., 2015. Return levels of hydrologic droughts under climate change. Adv. Water Resour. 75, 67–79. https://doi.org/10.1016/j.advwatres.2014.11.005
235. Mujumdar, P.P., Ghosh, S., 2008. Modeling GCM and scenario uncertainty using a possibilistic approach: Application to the Mahanadi River, India. Water Resour. Res. 44. https://doi.org/10.1029/2007WR006137
236. Mukherjee, S., Mishra, A., Trenberth, K.E., 2018. Climate Change and Drought: a

Perspective on Drought Indices, Current Climate Change Reports. https://doi.org/10.1007/s40641-018-0098-x

237. Najafi, R., Hessami Kermani, M.R., 2017. Uncertainty Modeling of Statistical Downscaling to Assess Climate Change Impacts on Temperature and Precipitation. Water Resour. Manag. 31, 1843–1858. https://doi.org/10.1007/s11269-017-1615-8
238. Naumann, G., Cammalleri, C., Mentaschi, L., Feyen, L., 2021. Increased economic drought impacts in Europe with anthropogenic warming. Nat. Clim. Chang. 11, 485–491. https://doi.org/10.1038/s41558-021-01044-3
239. New, M., Hulme, M., 2000. Representing uncertainty in climate change scenarios: a Monte-Carlo approach. Integr. Assess. 1, 203–213. https://doi.org/10.1023/A:1019144202120
240. New, M., Todd, M., Hulme, M., Jones, P., 2001. Precipitation measurements and trends in the twentieth century. Int. J. Climatol. 21, 1889–1922. https://doi.org/10.1002/joc.680
241. Niranjan Kumar, K., Rajeevan, M., Pai, D.S., Srivastava, A.K., Preethi, B., 2013. On the observed variability of monsoon droughts over India. Weather Clim. Extrem. 1, 42–50. https://doi.org/10.1016/j.wace.2013.07.006
242. Niu, J., Chen, J., Sivakumar, B., 2014. Teleconnection analysis of runoff and soil moisture over the Pearl River basin in southern China. Hydrol. Earth Syst. Sci. 18, 1475–1492. https://doi.org/10.5194/hess-18-1475-2014
243. Niyogi, D., Lei, M., Kishtawal, C., Schmid, P., Shepherd, M., 2017. Urbanization impacts on the summer heavy rainfall climatology over the eastern United States. Earth Interact. 21, 1–17. https://doi.org/10.1175/EI-D-15-0045.1
244. Núñez, J., Rivera, D., Oyarzún, R., Arumí, J.L., 2014. On the use of Standardized Drought Indices under decadal climate variability: Critical assessment and drought policy implications. J. Hydrol. 517, 458–470. https://doi.org/10.1016/j.jhydrol.2014.05.038
245. Ojha, R., Nagesh Kumar, D., Sharma, A., Mehrotra, R., 2013. Assessing severe drought and wet events over india in a future climate using a nested bias-correction approach. J. Hydrol. Eng. 18, 760–772. https://doi.org/10.1061/(ASCE)HE.1943-5584.0000585
246. Olsen, J., Kiang, J., Waskom, R., 2010. Workshop on Nonstationarity, Hydrologic Frequency Analysis, and Water Management. Color. Water Inst. Inf. Ser. 1–6.

247. Olsen, J.R., Lambert, J.H., Haimes, Y.Y., 1998. Risk of extreme events under nonstationary conditions. Risk Anal. 18, 497–510. https://doi.org/10.1111/j.1539-6924.1998.tb00364.x
248. Omer, A., Zhuguo, M., Yuan, X., Zheng, Z., Saleem, F., 2021. A hydrological perspective on drought risk-assessment in the Yellow River Basin under future anthropogenic activities. J. Environ. Manage. 289. https://doi.org/10.1016/j.jenvman.2021.112429
249. Pai, D.S., Sridhar, L., Rajeevan, M., Sreejith, O.P., Satbhai, N.S., Mukhopadyay, B., 2014. Development of a new high spatial resolution (0.25° × 0.25°) Long Period (1901-2010) daily gridded rainfall data set over India and its comparison with existing data sets over the region. Mausam 65, 1–18.
250. Palmer, W.C., 1965. Meteorological Drought. U.S. Weather Bur. Res. Pap. No. 45.
251. Panda, D.K., Kumar, A., Ghosh, S., Mohanty, R.K., 2013. Streamflow trends in the Mahanadi River basin (India): Linkages to tropical climate variability. J. Hydrol. 495, 135–149. https://doi.org/10.1016/j.jhydrol.2013.04.054
252. Pandey, R.P., Pandey, A., Galkate, R. V., Byun, H.-R., Mal, B.C., 2010. Integrating Hydro-Meteorological and Physiographic Factors for Assessment of Vulnerability to Drought. Water Resour. Manag. 24, 4199–4217. https://doi.org/10.1007/s11269-010-9653-5
253. Papaioannou, G., Kohnová, S., Bacigál, T., Szolgay, J., Hlavčová, K., Loukas, A., 2016. Joint modelling of flood peaks and volumes: A copula application for the Danube River. J. Hydrol. Hydromechanics 64, 382–392. https://doi.org/10.1515/johh-2016-0049
254. Park, J., Sung, J.H., Lim, Y.-J., Kang, H.-S., 2019. Introduction and application of non-stationary standardized precipitation index considering probability distribution function and return period. Theor. Appl. Climatol. 136, 529–542. https://doi.org/10.1007/s00704-018-2500-y
255. Parry, S., Prudhomme, C., Wilby, R.L., Wood, P.J., 2016a. Drought termination: Concept and characterisation. Prog. Phys. Geogr. 40, 743–767. https://doi.org/10.1177/0309133316652801
256. Parry, S., Wilby, R.L., Prudhomme, C., Wood, P.J., 2016b. A systematic assessment of drought termination in the United Kingdom. Hydrol. Earth Syst. Sci. 20, 4265–4281. https://doi.org/10.5194/hess-20-4265-2016

257. Parsons, D.J., Rey, D., Tanguy, M., Holman, I.P., 2019. Regional variations in the link between drought indices and reported agricultural impacts of drought. Agric. Syst. 173, 119–129. https://doi.org/10.1016/j.agsy.2019.02.015
258. Páscoa, P., Gouveia, C.M., Russo, A., Trigo, R.M., 2017. The role of drought on wheat yield interannual variability in the Iberian Peninsula from 1929 to 2012. Int. J. Biometeorol. 61, 439–451. https://doi.org/10.1007/s00484-016-1224-x
259. Pathak, H., Ladha, J.K., Aggarwal, P.K., Peng, S., Das, S., Singh, Y., Singh, B., Kamra, S.K., Mishra, B., Sastri, A.S.R.A.S., Aggarwal, H.P., Das, D.K., Gupta, R.K., 2003. Trends of climatic potential and on-farm yields of rice and wheat in the Indo-Gangetic Plains. F. Crop. Res. 80, 223–234. https://doi.org/10.1016/S0378-4290(02)00194-6
260. Paul, B.K., Rashid, H., 2017. Tropical Cyclones and Storm Surges, in: Climatic Hazards in Coastal Bangladesh. Elsevier, pp. 35–81. https://doi.org/10.1016/B978-0-12-805276-1.00002-8
261. Peña-Gallardo, M., Vicente-Serrano, S.M., Hannaford, J., Lorenzo-Lacruz, J., Svoboda, M., Domínguez-Castro, F., Maneta, M., Tomas-Burguera, M., Kenawy, A. El, 2019. Complex influences of meteorological drought time-scales on hydrological droughts in natural basins of the contiguous Unites States. J. Hydrol. 568, 611–625. https://doi.org/10.1016/j.jhydrol.2018.11.026
262. Peng, Z., Wang, Q.J., Bennett, J.C., Pokhrel, P., Wang, Z., 2014. Seasonal precipitation forecasts over China using monthly large-scale oceanic-atmospheric indices. J. Hydrol. 519, 792–802. https://doi.org/10.1016/j.jhydrol.2014.08.012
263. Penman, H.L., 1948. Natural evaporation from open water, hare soil and grass. Proc. R. Soc. Lond. A. Math. Phys. Sci. 193, 120–45. https://doi.org/10.1098/rspa.1948.0037
264. Peters, E., Torfs, P.J.J.F., van Lanen, H.A.J., Bier, G., 2003. Propagation of drought through groundwater - A new approach using linear reservoir theory. Hydrol. Process. 17, 3023–3040. https://doi.org/10.1002/hyp.1274
265. Pokhrel, Y., Felfelani, F., Satoh, Y., Boulange, J., Burek, P., Gädeke, A., Gerten, D., Gosling, S.N., Grillakis, M., Gudmundsson, L., Hanasaki, N., Kim, H., Koutroulis, A., Liu, J., Papadimitriou, L., Schewe, J., Müller Schmied, H., Stacke, T., Telteu, C.E., Thiery, W., Veldkamp, T., Zhao, F., Wada, Y., 2021. Global terrestrial water storage and drought severity under climate change. Nat. Clim. Chang. 11, 226–233.

https://doi.org/10.1038/s41558-020-00972-w

266. Ponce, V.M., Pandey, R.P., Ercan, S., 2000. Characterization of Drought across Climatic Spectrum. J. Hydrol. Eng. 5, 222–224. https://doi.org/10.1061/(asce)1084-0699(2000)5:2(222)
267. Poonia, V., Jha, S., Goyal, M.K., 2021. Copula based analysis of meteorological, hydrological and agricultural drought characteristics across Indian river basins. Int. J. Climatol. 41, 4637–4652. https://doi.org/10.1002/joc.7091
268. Prodhan, F.A., Zhang, J., Pangali Sharma, T.P., Nanzad, L., Zhang, D., Seka, A.M., Ahmed, N., Hasan, S.S., Hoque, M.Z., Mohana, H.P., 2022. Projection of future drought and its impact on simulated crop yield over South Asia using ensemble machine learning approach. Sci. Total Environ. 807. https://doi.org/10.1016/j.scitotenv.2021.151029
269. Pulwarty, R.S., Sivakumar, M.V.K., 2014. Information systems in a changing climate: Early warnings and drought risk management. Weather Clim. Extrem. 3, 14–21. https://doi.org/10.1016/j.wace.2014.03.005
270. Qiu, J., Shen, Z., Leng, G., Wei, G., 2021. Synergistic effect of drought and rainfall events of different patterns on watershed systems. Sci. Rep. 11. https://doi.org/10.1038/s41598-021-97574-z
271. Rajsekhar, D., Singh, V.P., Mishra, A.K., 2015. Integrated drought causality, hazard, and vulnerability assessment for future socioeconomic scenarios: An information theory perspective. J. Geophys. Res. 120, 6346–6378. https://doi.org/10.1002/2014JD022670
272. Rashid, M.M., Beecham, S., 2019. Development of a non-stationary Standardized Precipitation Index and its application to a South Australian climate. Sci. Total Environ. 657, 882–892. https://doi.org/10.1016/j.scitotenv.2018.12.052
273. Ray, D.K., Gerber, J.S., Macdonald, G.K., West, P.C., 2015. Climate variation explains a third of global crop yield variability. Nat. Commun. 6. https://doi.org/10.1038/ncomms6989
274. Reddy, M.J., Ganguli, P., 2013. Spatio-temporal analysis and derivation of copula-based intensity-area-frequency curves for droughts in western Rajasthan (India). Stoch. Environ. Res. Risk Assess. 27, 1975–1989. https://doi.org/10.1007/s00477-013-0732-z
275. Reddy, M.J., Ganguli, P., 2012. Risk Assessment of Hydroclimatic Variability on

Groundwater Levels in the Manjara Basin Aquifer in India Using Archimedean Copulas. J. Hydrol. Eng. 17, 1345–1357. https://doi.org/10.1061/(ASCE)HE.1943-5584.0000564

276. Ribeiro, A.F.S., Russo, A., Gouveia, C.M., Páscoa, P., 2019. Modelling drought-related yield losses in Iberia using remote sensing and multiscalar indices. Theor. Appl. Climatol. 136, 203–220. https://doi.org/10.1007/s00704-018-2478-5
277. Rigby, R.A., Stasinopoulos, D.M., 2005a. Generalized additive models for location, scale and shape (with discussion). J. R. Stat. Soc. Ser. C (Applied Stat. 54, 507–554. https://doi.org/10.1111/j.1467-9876.2005.00510.x
278. Rigby, R.A., Stasinopoulos, D.M., 2005b. Generalized additive models for location, scale and shape. J. R. Stat. Soc. Ser. C Appl. Stat. 54, 507–554. https://doi.org/10.1111/j.1467-9876.2005.00510.x
279. Rigby, R.A., Stasinopoulos, D.M., 1996. A semi-parametric additive model for variance heterogeneity. Stat. Comput. 6, 57–65. https://doi.org/10.1007/BF00161574
280. Rind, D., Goldberg, R., Hansen, J., Rosenzweig, C., Ruedy, R., 1990. Potential evapotranspiration and the likelihood of future drought. J. Geophys. Res. 95. https://doi.org/10.1029/jd095id07p09983
281. Rodell, M., Houser, P.R., Jambor, U., Gottschalck, J., Mitchell, K., Meng, C.-J., Arsenault, K., Cosgrove, B., Radakovich, J., Bosilovich, M., Entin, J.K., Walker, J.P., Lohmann, D., Toll, D., 2004. The Global Land Data Assimilation System. Bull. Am. Meteorol. Soc. 85, 381–394. https://doi.org/10.1175/BAMS-85-3-381
282. Roderick, M.L., Greve, P., Farquhar, G.D., 2015. On the assessment of aridity with changes in atmospheric CO2. Water Resour. Res. 51, 5450–5463. https://doi.org/10.1002/2015WR017031
283. Roxy, M.K., Ritika, K., Terray, P., Murtugudde, R., Ashok, K., Goswami, B.N., 2015. Drying of Indian subcontinent by rapid Indian Ocean warming and a weakening land-sea thermal gradient. Nat. Commun. 6, 7423. https://doi.org/10.1038/ncomms8423
284. Roy, I., 2017. Indian Summer Monsoon and El Niño Southern Oscillation in CMIP5 Models: A Few Areas of Agreement and Disagreement. Atmosphere (Basel). 8, 154. https://doi.org/10.3390/atmos8080154
285. Roy, I., Tedeschi, R.G., Collins, M., 2019. ENSO teleconnections to the Indian summer monsoon under changing climate. Int. J. Climatol. 39, 3031–3042.

https://doi.org/10.1002/joc.5999

286. Rupa Kumar, K., Krishna Kumar, K., Ashrit, R.G., Patwardhan, S.K., Pant, G.B., 2002. Climate change in India: Observations and model projections. Clim. Chang. India Issues, Concerns Oppor. Tata McGraw-Hill Publ. Co. Limited, New Delhi.
287. Russo, S., Dosio, A., Sterl, A., Barbosa, P., Vogt, J., 2013. Projection of occurrence of extreme dry-wet years and seasons in Europe with stationary and nonstationary Standardized Precipitation Indices. J. Geophys. Res. Atmos. 118, 7628–7639. https://doi.org/10.1002/jgrd.50571
288. Sachindra, D.A., Huang, F., Barton, A., Perera, B.J.C., 2013. Least square support vector and multi-linear regression for statistically downscaling general circulation model outputs to catchment streamflows. Int. J. Climatol. 33, 1087–1106. https://doi.org/10.1002/joc.3493
289. Saidi, H., Dresti, C., Manca, D., Ciampittiello, M., 2018. Quantifying impacts of climate variability and human activities on the streamflow of an Alpine river. Environ. Earth Sci. 77. https://doi.org/10.1007/s12665-018-7870-z
290. Saini, S., Gulati, A., 2014. El Niño and Indian droughts: A scoping exercise. Working Paper.
291. Saji, N.H., Goswami, B.N., Vinayachandran, P.N., Yamagata, T., 1999. A dipole mode in the tropical Indian Ocean. Nature 401, 360–363. https://doi.org/10.1038/43854
292. Salas, J.D., Obeysekera, J., 2014. Revisiting the Concepts of Return Period and Risk for Nonstationary Hydrologic Extreme Events. J. Hydrol. Eng. 19, 554–568. https://doi.org/10.1061/(ASCE)HE.1943-5584.0000820
293. Salvi, K., Ghosh, S., 2016. Projections of Extreme Dry and Wet Spells in the 21st Century India Using Stationary and Non-stationary Standardized Precipitation Indices. Clim. Change 139, 667–681. https://doi.org/10.1007/s10584-016-1824-9
294. Santos, J.F., Pulido-Calvo, I., Portela, M.M., 2010. Spatial and temporal variability of droughts in Portugal. Water Resour. Res. 46. https://doi.org/10.1029/2009WR008071
295. Sapriza-Azuri, G., Jódar, J., Navarro, V., Slooten, L.J., Carrera, J., Gupta, H. V., 2015. Impacts of rainfall spatial variability on hydrogeological response. Water Resour. Res. 51, 1300–1314. https://doi.org/10.1002/2014WR016168
296. Satish Kumar, K., AnandRaj, P., Sreelatha, K., Sridhar, V., 2021. Regional analysis

of drought severity-duration-frequency and severity-area-frequency curves in the Godavari River Basin, India. Int. J. Climatol. 41, 5481–5501. https://doi.org/10.1002/joc.7137

297. Sattar, M.N., Jehanzaib, M., Kim, J.E., Kwon, H.-H., Kim, T.-W., 2020. Application of the Hidden Markov Bayesian Classifier and Propagation Concept for Probabilistic Assessment of Meteorological and Hydrological Droughts in South Korea. Atmosphere (Basel). 11, 1000. https://doi.org/10.3390/atmos11091000
298. Sattar, M.N., Lee, J.Y., Shin, J.Y., Kim, T.W., 2019. Probabilistic Characteristics of Drought Propagation from Meteorological to Hydrological Drought in South Korea. Water Resour. Manag. 33, 2439–2452. https://doi.org/10.1007/s11269-019-02278-9
299. Savari, M., Eskandari Damaneh, Hamed, Eskandari Damaneh, Hadi, 2022. Drought vulnerability assessment: Solution for risk alleviation and drought management among Iranian farmers. Int. J. Disaster Risk Reduct. 67. https://doi.org/10.1016/j.ijdrr.2021.102654
300. Scheff, J., Frierson, D.M.W., 2015. Terrestrial aridity and its response to greenhouse warming across CMIP5 climate models. J. Clim. 28, 5583–5600. https://doi.org/10.1175/JCLI-D-14-00480.1
301. Schumacher, D.L., Keune, J., Dirmeyer, P., Miralles, D.G., 2022. Drought self-propagation in drylands due to land–atmosphere feedbacks. Nat. Geosci. 15, 262–268. https://doi.org/10.1038/s41561-022-00912-7
302. Setti, S., Maheswaran, R., Radha, D., Sridhar, V., Barik, K.K., Narasimham, M.L., 2020. Attribution of Hydrologic Changes in a Tropical River Basin to Rainfall Variability and Land-Use Change: Case Study from India. J. Hydrol. Eng. 25, 05020015. https://doi.org/10.1061/(asce)he.1943-5584.0001937
303. Shabbar, A., Skinner, W., 2004. Summer Drought Patterns in Canada and the Relationship toGlobal Sea Surface Temperatures. J. Clim. 17, 2866–2880. https://doi.org/10.1175/1520-0442(2004)017<2866:SDPICA>2.0.CO;2
304. Shackley, S., Young, P., Parkinson, S., Wynne, B., 1998. Uncertainty, complexity and concepts of good science in climate change modelling: Are GCMs the best tools? Clim. Change 38, 159–205. https://doi.org/10.1023/A:1005310109968
305. Shah, D., Mishra, V., 2020. Integrated Drought Index (IDI) for Drought Monitoring and Assessment in India. Water Resour. Res. 56. https://doi.org/10.1029/2019WR026284

306. Shah, R.D., Mishra, V., 2015. Development of an Experimental Near-Real-Time Drought Monitor for India. J. Hydrometeorol. 16, 327–345. https://doi.org/10.1175/JHM-D-14-0041.1
307. Sharma, A., Goyal, M.K., 2020. Assessment of drought trend and variability in India using wavelet transform. Hydrol. Sci. J. 65, 1539–1554. https://doi.org/10.1080/02626667.2020.1754422
308. Sharma, S., Mujumdar, P., 2017. Increasing frequency and spatial extent of concurrent meteorological droughts and heatwaves in India. Sci. Rep. 7, 15582. https://doi.org/10.1038/s41598-017-15896-3
309. Sheffield, J., Goteti, G., Wen, F., Wood, E.F., 2004. A simulated soil moisture based drought analysis for the United States. J. Geophys. Res. D Atmos. 109, 1–19. https://doi.org/10.1029/2004JD005182
310. Sheffield, J., Goteti, G., Wood, E.F., 2006. Development of a 50-year high-resolution global dataset of meteorological forcings for land surface modeling. J. Clim. 19, 3088–3111. https://doi.org/10.1175/JCLI3790.1
311. Sheffield, J., Wood, E.F., Roderick, M.L., 2012. Little change in global drought over the past 60 years. Nature 491, 435–438. https://doi.org/10.1038/nature11575
312. Shen, Z., Zhang, Q., Singh, V.P., Sun, P., Song, C., Yu, H., 2019. Agricultural drought monitoring across Inner Mongolia, China: Model development, spatiotemporal patterns and impacts. J. Hydrol. 571, 793–804. https://doi.org/10.1016/j.jhydrol.2019.02.028
313. Shivam, Goyal, M.K., Sarma, A.K., 2017. Analysis of the change in temperature trends in Subansiri River basin for RCP scenarios using CMIP5 datasets. Theor. Appl. Climatol. 129, 1175–1187. https://doi.org/10.1007/s00704-016-1842-6
314. Shukla, S., Wood, A.W., 2008. Use of a standardized runoff index for characterizing hydrologic drought. Geophys. Res. Lett. 35, L02405. https://doi.org/10.1029/2007GL032487
315. Singh, D., Ghosh, S., Roxy, M.K., McDermid, S., 2019. Indian summer monsoon: Extreme events, historical changes, and role of anthropogenic forcings. Wiley Interdiscip. Rev. Clim. Chang. 10. https://doi.org/10.1002/wcc.571
316. Sivapalan, M., Samuel, J.M., 2009. Transcending limitations of stationarity and the return period: process-based approach to flood estimation and risk assessment. Hydrol. Process. 23, 1671–1675. https://doi.org/10.1002/hyp.7292

317. Sklar, M., 1959. Fonctions de repartition an dimensions et leurs marges. Publ. Inst. Stat. Univ. Paris 8, 229--231.
318. Song, Z., Xia, J., She, D., Zhang, L., Hu, C., Zhao, L., 2020. The development of a Nonstationary Standardized Precipitation Index using climate covariates: A case study in the middle and lower reaches of Yangtze River Basin, China. J. Hydrol. 588. https://doi.org/10.1016/j.jhydrol.2020.125115
319. Spennemann, P.C., Rivera, J.A., Celeste Saulo, A., Penalba, O.C., 2015. A comparison of GLDAS soil moisture anomalies against standardized precipitation index and multisatellite estimations over South America. J. Hydrometeorol. 16, 158–171. https://doi.org/10.1175/JHM-D-13-0190.1
320. Spinoni, J., Barbosa, P., Bucchignani, E., Cassano, J., Cavazos, T., Christensen, J.H., Christensen, O.B., Coppola, E., Evans, J., Geyer, B., Giorgi, F., Hadjinicolaou, P., Jacob, D., Katzfey, J., Koenigk, T., Laprise, R., Lennard, C.J., Kurnaz, M.L., Delei, L.I., Llopart, M., McCormick, N., Naumann, G., Nikulin, G., Ozturk, T., Panitz, H.J., da Rocha, R.P., Rockel, B., Solman, S.A., Syktus, J., Tangang, F., Teichmann, C., Vautard, R., Vogt, J. V., Winger, K., Zittis, G., Dosio, A., 2020. Future global meteorological drought hot spots: A study based on CORDEX data. J. Clim. https://doi.org/10.1175/JCLI-D-19-0084.1
321. Spinoni, J., Barbosa, P., Bucchignani, E., Cassano, J., Cavazos, T., Christensen, J.H., Christensen, O.B., Coppola, E., Evans, J., Geyer, B., Giorgi, F., Hadjinicolaou, P., Jacob, D., Katzfey, J., Koenigk, T., Laprise, R., Lennard, C.J., Kurnaz, M.L., Li, D., Llopart, M., McCormick, N., Naumann, G., Nikulin, G., Ozturk, T., Panitz, H.-J., Porfirio da Rocha, R., Rockel, B., Solman, S.A., Syktus, J., Tangang, F., Teichmann, C., Vautard, R., Vogt, J. V., Winger, K., Zittis, G., Dosio, A., 2019. Future global meteorological drought hotspots: a study based on CORDEX data. J. Clim. JCLI-D-19-0084.1. https://doi.org/10.1175/JCLI-D-19-0084.1
322. Spinoni, J., Naumann, G., Carrao, H., Barbosa, P., Vogt, J., 2014. World drought frequency, duration, and severity for 1951-2010. Int. J. Climatol. 34, 2792–2804. https://doi.org/10.1002/joc.3875
323. Spinoni, J., Vogt, J. V., Naumann, G., Barbosa, P., Dosio, A., 2018. Will drought events become more frequent and severe in Europe? Int. J. Climatol. 38, 1718–1736. https://doi.org/10.1002/joc.5291
324. Spott, M., 1999. A theory of possibility distributions. Fuzzy Sets Syst. 102, 135–155.

https://doi.org/10.1016/S0165-0114(97)00102-4

325. Srivastava, A.K., Rajeevan, M., Kshirsagar, S.R., 2009. Development of a high resolution daily gridded temperature data set (1969-2005) for the Indian region. Atmos. Sci. Lett. n/a-n/a. https://doi.org/10.1002/asl.232
326. Stasinopoulos, D.M., Rigby, R.A., 2007. Generalized additive models for location scale and shape (GAMLSS) in R. J. Stat. Softw. 23, 1–46. https://doi.org/10.18637/jss.v023.i07
327. Subash, N., Ram Mohan, H.S., Sikka, A.K., 2011. Decadal frequency and trends of extreme excess/deficit rainfall during the monsoon season over different meteorological sub-divisions of India. Hydrol. Sci. J. 56, 1090–1109. https://doi.org/10.1080/02626667.2011.608677
328. Tabari, H., Hosseinzadeh Talaee, P., 2014. Sensitivity of evapotranspiration to climatic change in different climates. Glob. Planet. Change 115, 16–23. https://doi.org/10.1016/j.gloplacha.2014.01.006
329. TERI, 2014. Assessing Climate Change Vulnerability and Adaptation Strategies for Maharashtra: Maharashtra State Adaptation Action Plan on Climate Change (MSAAPC). New Delhi.
330. Thober, S., Kumar, R., Sheffield, J., Mai, J., Schäfer, D., Samaniego, L., 2015. Seasonal Soil Moisture Drought Prediction over Europe Using the North American Multi-Model Ensemble (NMME). J. Hydrometeorol. 16, 2329–2344. https://doi.org/10.1175/JHM-D-15-0053.1
331. Thomas, A.C., Reager, J.T., Famiglietti, J.S., Rodell, M., 2014. A GRACE-based water storage deficit approach for hydrological drought characterization. Geophys. Res. Lett. 41, 1537–1545. https://doi.org/10.1002/2014GL059323
332. Thrasher, B., Xiong, J., Wang, W., Melton, F., Michaelis, A., Nemani, R., 2013. Downscaled Climate Projections Suitable for Resource Management. Eos, Trans. Am. Geophys. Union 94, 321–323. https://doi.org/10.1002/2013EO370002
333. Tigkas, D., Vangelis, H., Tsakiris, G., 2019. Drought characterisation based on an agriculture-oriented standardised precipitation index. Theor. Appl. Climatol. 135, 1435–1447. https://doi.org/10.1007/s00704-018-2451-3
334. Tijdeman, E., Barker, L.J., Svoboda, M.D., Stahl, K., 2018. Natural and Human Influences on the Link Between Meteorological and Hydrological Drought Indices for a Large Set of Catchments in the Contiguous United States. Water Resour. Res.

54, 6005–6023. https://doi.org/10.1029/2017WR022412

335. Toby, R., 2020. On the essentials of drought in a changing climate. Science (80-.). 368, 256–260.
336. Tosunoglu, F., Gürbüz, F., İspirli, M.N., 2020. Multivariate modeling of flood characteristics using Vine copulas. Environ. Earth Sci. 79. https://doi.org/10.1007/s12665-020-09199-6
337. Touma, D., Ashfaq, M., Nayak, M.A., Kao, S.-C., Diffenbaugh, N.S., 2015. A multi-model and multi-index evaluation of drought characteristics in the 21st century. J. Hydrol. 526, 196–207. https://doi.org/10.1016/j.jhydrol.2014.12.011
338. Trenberth, K., 2011. Changes in precipitation with climate change. Clim. Res. 47, 123–138. https://doi.org/10.3354/cr00953
339. Trenberth, K.E., Dai, A., Van Der Schrier, G., Jones, P.D., Barichivich, J., Briffa, K.R., Sheffield, J., 2014. Global warming and changes in drought. Nat. Clim. Chang. 4, 17–22. https://doi.org/10.1038/nclimate2067
340. Tsakiris, G., 2017. Drought Risk Assessment and Management. Water Resour. Manag. 31, 3083–3095. https://doi.org/10.1007/s11269-017-1698-2
341. Tsakiris, G., Loukas, A., Pangalou, D., Vangelis, H., Tigkas, D., Rossi, G., Cancelliere, A., 2007. Drought Characterization. Drought Manag. Guidel. Tech. Annex 58, 85–102.
342. Tsakiris, G., Nalbantis, I., Vangelis, H., Verbeiren, B., Huysmans, M., Tychon, B., Jacquemin, I., Canters, F., Vanderhaegen, S., Engelen, G., Poelmans, L., De Becker, P., Batelaan, O., 2013. A System-based Paradigm of Drought Analysis for Operational Management. Water Resour. Manag. 27, 5281–5297. https://doi.org/10.1007/s11269-013-0471-4
343. Tsakiris, G., Vangelis, H., 2005. Establishing a drought index incorporating evapotranspiration. Eur. Water 9, 3–11.
344. Turner, A.G., Inness, P.M., Slingo, J.M., 2005. The role of the basic state in the ENSO-monsoon relationship and implications for predictability. Q. J. R. Meteorol. Soc. 131, 781–804.
345. Udmale, P., Ichikawa, Y., Manandhar, S., Ishidaira, H., Kiem, A.S., 2014. Farmers′ perception of drought impacts, local adaptation and administrative mitigation measures in Maharashtra State, India. Int. J. Disaster Risk Reduct. 10, 250–269. https://doi.org/10.1016/j.ijdrr.2014.09.011

346. Udmale, P.D., Ichikawa, Y., Kiem, A.S., Panda, S.N., 2014. Drought impacts and adaptation strategies for agriculture and rural livelihood in the Maharashtra State of India. Open Agric. J. 8, 41–47.
347. Ukkola, A.M., Pitman, A.J., De Kauwe, M.G., Abramowitz, G., Herger, N., Evans, J.P., Decker, M., 2018. Evaluating CMIP5 Model Agreement for Multiple Drought Metrics. J. Hydrometeorol. 19, 969–988. https://doi.org/10.1175/JHM-D-17-0099.1
348. Ummenhofer, C.C., Sen Gupta, A., Briggs, P.R., England, M.H., McIntosh, P.C., Meyers, G.A., Pook, M.J., Raupach, M.R., Risbey, J.S., 2011. Indian and Pacific Ocean Influences on Southeast Australian Drought and Soil Moisture. J. Clim. 24, 1313–1336. https://doi.org/10.1175/2010JCLI3475.1
349. Van Lanen, H.A.J., Wanders, N., Tallaksen, L.M., Van Loon, A.F., 2013. Hydrological drought across the world: impact of climate and physical catchment structure. Hydrol. Earth Syst. Sci. 17, 1715–1732. https://doi.org/10.5194/hess-17-1715-2013
350. Van Loon, A.F., 2015. Hydrological drought explained. Wiley Interdiscip. Rev. Water 2, 359–392. https://doi.org/10.1002/wat2.1085
351. Van Loon, A.F., Laaha, G., 2015. Hydrological drought severity explained by climate and catchment characteristics. J. Hydrol. 526, 3–14. https://doi.org/10.1016/j.jhydrol.2014.10.059
352. Van Loon, A.F., Van Huijgevoort, M.H.J., Van Lanen, H.A.J., 2012. Evaluation of drought propagation in an ensemble mean of large-scale hydrological models. Hydrol. Earth Syst. Sci. 16, 4057–4078. https://doi.org/10.5194/hess-16-4057-2012
353. Vasiliades, L., Galiatsatou, P., Loukas, A., 2015. Nonstationary Frequency Analysis of Annual Maximum Rainfall Using Climate Covariates. Water Resour. Manag. 29, 339–358. https://doi.org/10.1007/s11269-014-0761-5
354. Vergni, L., Todisco, F., Mannocchi, F., 2015. Analysis of agricultural drought characteristics through a two-dimensional copula. Water Resour. Manag. 29, 2819–2835. https://doi.org/10.1007/s11269-015-0972-4
355. Vicente-Serrano, S.M., Beguería, S., López-Moreno, J.I., 2010. A multiscalar drought index sensitive to global warming: The standardized precipitation evapotranspiration index. J. Clim. 23, 1696–1718. https://doi.org/10.1175/2009JCLI2909.1
356. Villarini, G., Smith, J.A., Napolitano, F., 2010. Nonstationary modeling of a long

record of rainfall and temperature over Rome. Adv. Water Resour. 33, 1256–1267. https://doi.org/10.1016/j.advwatres.2010.03.013

357. Villarini, G., Smith, J.A., Serinaldi, F., Ntelekos, A.A., 2011. Analyses of seasonal and annual maximum daily discharge records for central Europe. J. Hydrol. 399, 299–312. https://doi.org/10.1016/j.jhydrol.2011.01.007
358. Vogel, E., Donat, M.G., Alexander, L. V., Meinshausen, M., Ray, D.K., Karoly, D., Meinshausen, N., Frieler, K., 2019. The effects of climate extremes on global agricultural yields. Environ. Res. Lett. 14. https://doi.org/10.1088/1748-9326/ab154b
359. Wang, B., 2000. commentary and analysis: Comments on "Choice of South Asian Summer Monsoon Indices." Bull. Am. Meteorol. Soc. 81, 821–822. https://doi.org/10.1175/1520-0477(2000)081<0821:CAA>2.3.CO;2
360. Wang, B., Wu, R., Lau, K.-M., 2001. Interannual Variability of the Asian Summer Monsoon: Contrasts between the Indian and the Western North Pacific–East Asian Monsoons*. J. Clim. 14, 4073–4090. https://doi.org/10.1175/1520-0442(2001)014<4073:IVOTAS>2.0.CO;2
361. Wang, F., Lai, H., Li, Y., Feng, K., Zhang, Z., Tian, Q., Zhu, X., Yang, H., 2021. Dynamic variation of meteorological drought and its relationships with agricultural drought across China. Agric. Water Manag. https://doi.org/10.1016/j.agwat.2021.107301
362. Wang, Y., Duan, L., Liu, T., Li, J., Feng, P., 2020a. A Non-stationary Standardized Streamflow Index for hydrological drought using climate and human-induced indices as covariates. Sci. Total Environ. 699, 134278. https://doi.org/10.1016/j.scitotenv.2019.134278
363. Wang, Y., Duan, L., Liu, T., Li, J., Feng, P., 2020b. A Non-stationary Standardized Streamflow Index for hydrological drought using climate and human-induced indices as covariates. Sci. Total Environ. 699, 134278. https://doi.org/10.1016/j.scitotenv.2019.134278
364. Wang, Y., Li, J., Feng, P., Chen, F., 2015a. Effects of large-scale climate patterns and human activities on hydrological drought: a case study in the Luanhe River basin, China. Nat. Hazards 76, 1687–1710. https://doi.org/10.1007/s11069-014-1564-y
365. Wang, Y., Li, J., Feng, P., Hu, R., 2015b. A Time-Dependent Drought Index for Non-Stationary Precipitation Series. Water Resour. Manag. 29, 5631–5647.

https://doi.org/10.1007/s11269-015-1138-0

366. Wang, Y., Peng, T., Lin, Q., Singh, V.P., Dong, X., Chen, C., Liu, J., Chang, W., Wang, G., 2022. A New Non-stationary Hydrological Drought Index Encompassing Climate Indices and Modified Reservoir Index as Covariates. Water Resour. Manag. https://doi.org/10.1007/s11269-022-03151-y
367. Wilhite, D.A., 2017. National drought management policy guidelines: A template for action. Drought Water Cris. Integr. Sci. Manag. Policy, Second Ed. 55–94. https://doi.org/10.1201/b22009
368. Wilhite, D.A., 2016. Droughts: A Global Assesment. Routledge.
369. Wilhite, D.A., Glantz, M.H., 1985. Understanding: the Drought Phenomenon: The Role of Definitions. Water Int. 10, 111–120. https://doi.org/10.1080/02508068508686328
370. Wilhite, D.A., Sivakumar, M.V.K., Pulwarty, R., 2014. Managing drought risk in a changing climate: The role of national drought policy. Weather Clim. Extrem. 3, 4–13. https://doi.org/10.1016/j.wace.2014.01.002
371. Willett, K.M., Gillett, N.P., Jones, P.D., Thorne, P.W., 2007. Attribution of observed surface humidity changes to human influence. Nature 449, 710–712. https://doi.org/10.1038/nature06207
372. WMO, 2021. WMO ATLAS OF MORTALITY AND ECONOMIC LOSSES FROM WEATHER, CLIMATE AND WATER EXTREMES (1970–2019).
373. WMO, 1999. NOTE World Meteorological Organization.
374. WMO, GWP, 2016. Handbook of Drought Indicators and Indices. Geneva.
375. Wu, H., Su, X., Singh, V.P., Feng, K., Niu, J., 2021. Agricultural Drought Prediction Based on Conditional Distributions of Vine Copulas. Water Resour. Res. 57. https://doi.org/10.1029/2021WR029562
376. Wu, H., Wilhite, D.A., 2004. An Operational Agricultural Drought Risk Assessment Model for Nebraska, USA. Nat. Hazards 33, 1–21. https://doi.org/10.1023/B:NHAZ.0000034994.44357.75
377. Wu, Jiefeng, Chen, X., Yao, H., Liu, Z., Zhang, D., 2018. Hydrological Drought Instantaneous Propagation Speed Based on the Variable Motion Relationship of Speed-Time Process. Water Resour. Res. 54, 9549–9565. https://doi.org/10.1029/2018WR023120
378. Wu, J., Chen, X., Yuan, X., Yao, H., Zhao, Y., AghaKouchak, A., 2021. The

interactions between hydrological drought evolution and precipitation-streamflow relationship. J. Hydrol. 597. https://doi.org/10.1016/j.jhydrol.2021.126210

379. Wu, J., Chen, Xingwei, Love, C.A., Yao, H., Chen, Xiaohong, AghaKouchak, A., 2020. Determination of water required to recover from hydrological drought: Perspective from drought propagation and non-standardized indices. J. Hydrol. 590. https://doi.org/10.1016/j.jhydrol.2020.125227
380. Wu, Jingwen, Miao, C., Zheng, H., Duan, Q., Lei, X., Li, H., 2018. Meteorological and Hydrological Drought on the Loess Plateau, China: Evolutionary Characteristics, Impact, and Propagation. J. Geophys. Res. Atmos. 123, 11,569-11,584. https://doi.org/10.1029/2018JD029145
381. Wu, T., Bai, J., Han, H., 2022. Short-Term Agricultural Drought Prediction based on D-vine copula quantile regression in snow-free unfrozen surface area, China. Geocarto Int. 1–16. https://doi.org/10.1080/10106049.2021.2017015
382. Wu, W.Y., Lo, M.H., Wada, Y., Famiglietti, J.S., Reager, J.T., Yeh, P.J.F., Ducharne, A., Yang, Z.L., 2020. Divergent effects of climate change on future groundwater availability in key mid-latitude aquifers. Nat. Commun. 11. https://doi.org/10.1038/s41467-020-17581-y
383. Xiao, M., Zhang, Q., Singh, V.P., Liu, L., 2016. Transitional properties of droughts and related impacts of climate indices in the Pearl River basin, China. J. Hydrol. 534, 397–406. https://doi.org/10.1016/j.jhydrol.2016.01.012
384. Xie, W., Xiong, W., Pan, J., Ali, T., Cui, Q., Guan, D., Meng, J., Mueller, N.D., Lin, E., Davis, S.J., 2018. Decreases in global beer supply due to extreme drought and heat. Nat. Plants 4, 964–973. https://doi.org/10.1038/s41477-018-0263-1
385. Xu, R., Chen, Y., Chen, Z., 2019. Future changes of precipitation over the Han River basin using NEX-GDDP dataset and the SVR_QM method. Atmosphere (Basel). 10. https://doi.org/10.3390/atmos10110688
386. Xu, Y., Zhang, X., Hao, Z., Singh, V.P., Hao, F., 2021. Characterization of agricultural drought propagation over China based on bivariate probabilistic quantification. J. Hydrol. 598. https://doi.org/10.1016/j.jhydrol.2021.126194
387. Xu, Y., Zhang, X., Wang, X., Hao, Z., Singh, V.P., Hao, F., 2019. Propagation from meteorological drought to hydrological drought under the impact of human activities: A case study in northern China. J. Hydrol. 579. https://doi.org/10.1016/j.jhydrol.2019.124147

388. Yaduvanshi, A., Zaroug, M., Bendapudi, R., New, M., 2019. Impacts of 1.5 °C and 2 °C global warming on regional rainfall and temperature change across India. Environ. Res. Commun. 1, 125002. https://doi.org/10.1088/2515-7620/ab4ee2
389. Yang, Q., Li, M.X., Zheng, Z.Y., Ma, Z.G., 2017a. Regional applicability of seven meteorological drought indices in China. Sci. China Earth Sci. 60, 745–760. https://doi.org/10.1007/s11430-016-5133-5
390. Yang, Q., Ma, Z., Fan, X., Yang, Z.-L., Xu, Z., Wu, P., 2017b. Decadal Modulation of Precipitation Patterns over Eastern China by Sea Surface Temperature Anomalies. J. Clim. 30, 7017–7033. https://doi.org/10.1175/JCLI-D-16-0793.1
391. Yao, N., Li, L., Feng, P., Feng, H., Li Liu, D., Liu, Y., Jiang, K., Hu, X., Li, Y., 2020. Projections of drought characteristics in China based on a standardized precipitation and evapotranspiration index and multiple GCMs. Sci. Total Environ. 704, 135245. https://doi.org/10.1016/j.scitotenv.2019.135245
392. Yevjevich, V.M., 1967. Objective approach to definitions and investigations of continental hydrologic droughts, An. Hydrol. Pap. (Colorado State Univ. no. 23.
393. Yirdaw, S.Z., Snelgrove, K.R., Agboma, C.O., 2008. GRACE satellite observations of terrestrial moisture changes for drought characterization in the Canadian Prairie. J. Hydrol. 356, 84–92. https://doi.org/10.1016/j.jhydrol.2008.04.004
394. Zadeh, L.A., 1999. Fuzzy sets as a basis for a theory of possibility. Fuzzy Sets Syst. 100, 9–34. https://doi.org/10.1016/S0165-0114(99)80004-9
395. Zampieri, M., Ceglar, A., Dentener, F., Toreti, A., 2017. Wheat yield loss attributable to heat waves, drought and water excess at the global, national and subnational scales. Environ. Res. Lett. 12. https://doi.org/10.1088/1748-9326/aa723b
396. Zarch, M.A.A., Sivakumar, B., Sharma, A., 2015a. Droughts in a warming climate: A global assessment of Standardized precipitation index (SPI) and Reconnaissance drought index (RDI). J. Hydrol. 526, 183–195. https://doi.org/10.1016/j.jhydrol.2014.09.071
397. Zarch, M.A.A., Sivakumar, B., Sharma, A., 2015b. Droughts in a warming climate: A global assessment of Standardized precipitation index (SPI) and Reconnaissance drought index (RDI). J. Hydrol. 526, 183–195. https://doi.org/10.1016/j.jhydrol.2014.09.071
398. Zargar, A., Sadiq, R., Naser, B., Khan, F.I., 2011. A review of drought indices. Environ. Rev. 19, 333–349. https://doi.org/10.1139/a11-013

399. Zaussinger, F., Dorigo, W., Gruber, A., Tarpanelli, A., Filippucci, P., Brocca, L., 2018. Estimating irrigation water use over the contiguous United States by combining satellite and reanalysis soil moisture data. Hydrol. Earth Syst. Sci. Discuss. 1–42. https://doi.org/10.5194/hess-2018-388
400. Zeng, X., Zhao, N., Sun, H., Ye, L., Zhai, J., 2015. Changes and relationships of climatic and hydrological droughts in the Jialing River basin, China. PLoS One 10. https://doi.org/10.1371/journal.pone.0141648
401. Zhang, A., Zhang, C., Fu, G., Wang, B., Bao, Z., Zheng, H., 2012. Assessments of Impacts of Climate Change and Human Activities on Runoff with SWAT for the Huifa River Basin, Northeast China. Water Resour. Manag. 26, 2199–2217. https://doi.org/10.1007/s11269-012-0010-8
402. Zhang, B., Xia, Y., Huning, L.S., Wei, J., Wang, G., AghaKouchak, A., 2019. A Framework for Global Multicategory and Multiscalar Drought Characterization Accounting for Snow Processes. Water Resour. Res. 55, 9258–9278. https://doi.org/10.1029/2019WR025529
403. Zhang, D., Chen, P., Zhang, Q., Li, X., 2017. Copula-based probability of concurrent hydrological drought in the Poyang lake-catchment-river system (China) from 1960 to 2013. J. Hydrol. 553, 773–784. https://doi.org/10.1016/j.jhydrol.2017.08.046
404. Zhang, H., Ding, J., Wang, Y., Zhou, D., Zhu, Q., 2021. Investigation about the correlation and propagation among meteorological, agricultural and groundwater droughts over humid and arid/semi-arid basins in China. J. Hydrol. 603. https://doi.org/10.1016/j.jhydrol.2021.127007
405. Zhang, J., Mu, Q., Huang, J., 2016. Assessing the remotely sensed Drought Severity Index for agricultural drought monitoring and impact analysis in North China. Ecol. Indic. 63, 296–309. https://doi.org/10.1016/j.ecolind.2015.11.062
406. Zhang, Q., Xiao, M., Singh, V.P., 2015. Uncertainty evaluation of copula analysis of hydrological droughts in the East River basin, China. Glob. Planet. Change 129, 1–9. https://doi.org/10.1016/j.gloplacha.2015.03.001
407. Zhang, T., Su, X., Feng, K., 2021. The development of a novel nonstationary meteorological and hydrological drought index using the climatic and anthropogenic indices as covariates. Sci. Total Environ. 786. https://doi.org/10.1016/j.scitotenv.2021.147385
408. Zhang, X., Obringer, R., Wei, C., Chen, N., Niyogi, D., 2017. Droughts in India from

1981 to 2013 and Implications to Wheat Production. Sci. Rep. 7. https://doi.org/10.1038/srep44552

409. Zhang, Y., Keenan, T.F., Zhou, S., 2021. Exacerbated drought impacts on global ecosystems due to structural overshoot. Nat. Ecol. Evol. 2021 1–9.
410. Zhao, M., Huang, S., Huang, Q., Wang, H., Leng, G., Xie, Y., 2019. Assessing socio-economic drought evolution characteristics and their possible meteorological driving force. Geomatics, Nat. Hazards Risk 10, 1084–1101. https://doi.org/10.1080/19475705.2018.1564706
411. Zhou, K., Li, J., Zhang, T., Kang, A., 2021. The use of combined soil moisture data to characterize agricultural drought conditions and the relationship among different drought types in China. Agric. Water Manag. 243. https://doi.org/10.1016/j.agwat.2020.106479
412. Zhu, Y., Liu, ·Yi, Wang, W., Singh, V.P., Ren, L., 2021. A global perspective on the probability of propagation of drought: From meteorological to soil moisture. J. Hydrol. 603. https://doi.org/10.1016/j.jhydrol.2021.126907
413. Zou, L., Xia, J., She, D., 2018. Analysis of Impacts of Climate Change and Human Activities on Hydrological Drought: a Case Study in the Wei River Basin, China. Water Resour. Manag. 32, 1421–1438. https://doi.org/10.1007/s11269-017-1877-1
414. Zscheischler, J., Seneviratne, S.I., 2017. Dependence of drivers affects risks associated with compound events. Sci. Adv. 3, e1700263. https://doi.org/10.1126/sciadv.1700263

Acknowledgement

The research work during my PhD years at NITW has been the most fulfilling of my life. I would like to thank my supervisor **Prof. N.V. Umamahesh** with deepest gratitude for providing me with an opportunity to work in his lab. I had this luxury of unlimited freedom in exploring new ideas and directions. This thesis would not have materialized had it not been for his constant guidance.

I would specifically like to thank **Prof. M. Chandrasekhar**, **Sri. V.N. Kameswara Rao** and **Prof. K. Venkata Reddy** for their insights. I am also thankful to **Prof. P. Anandraj** and **Prof. R.B.V. Subramaanyam** for their encouragement and guidance during the progress review in each semester throughout my Ph.D. I also want to thank all the faculty, student and staff members of the Water and Environment Division for building a synergistic environment to work in.

My deepest thank to **Dr. Jew Das** for his excellent guidance, enthusiastic discussion, good company and active involvement in all phases of this work. I was lucky to be around a sincere group of people as my lab mates, each one of them was very helpful and understanding. I thank all my lab members Nikhil, Manikanta, Rudraswami, Shrikant.

I wouldn't have been able to complete this thesis without the support of my parents **Mr. Ashok Das** and **Mrs. Mamata Sahu**, my younger brother **Niladri**, and my husband **Dr. Tuhin Chakrabortty**. They made sure that I need not worry about any stuff and could focus entirely on my research. I am extremely lucky to have a loving extended family where my grandma, uncles, aunts, cousins and my entire family take pride in the smallest of my achievements.

It is my privilege to thank the authority of National Institute of Technology (Department of Civil Engineering) for providing necessary facilities for education and research. I am also thankful to the office and technical staff for their co-operation.

Thank you very much.

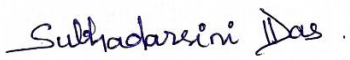

Subhadarsini Das

Date: 14/10/2022